T-3637

COMPUTER AND PHYSICAL VSP MODELING OF YUCCA MOUNTAIN, NEVADA

by

David A. Cunningham

9212170138 921005
PDR WASTE
WM-11 PDR

8.3.1.2.2.3

T-3637

A thesis submitted to the Faculty and the Board of Trustees of the Colorado School of Mines in partial fulfillment of the requirements for the degree of Master of Science (Geophysics).

Golden, Colorado

Date Nov. 7, 1988

Signed: David A. Cunningham
David A. Cunningham

Approved: Alfred H. Balch
Dr. Alfred H. Balch
Thesis Advisor

Golden, Colorado

Date 11/7/88

P R Romig
Dr. Phillip R. Romig, Head,
Department of Geophysics

ABSTRACT

The U. S. Geological Survey is currently characterizing Yucca Mountain in southern Nevada as a potential storage site for high-level radioactive waste. Vertical Seismic Profiling will be conducted as one phase of the investigations. In order to better understand the results of these surveys, a preliminary modeling study was conducted to simulate VSPs at Yucca Mountain.

Both computer and physical modeling studies were performed to study the imaging of key subsurface horizons at Yucca Mountain. Data sets were generated to illustrate the effects of source offset and topography on the quality of the VSP record, as recorded at two different receiver boreholes. All modeling was conducted on two-dimensional models simulating the cross section of Yucca Mountain between the two receiver boreholes, USW UZ-6 and UE25 UZ-9.

The modeling experiments provided insight into how the vital subsurface horizons, such as high-angle fault planes, will appear on the VSP records at various source offsets. The horizons surrounding the potential repository unit and the high-angle faults were best imaged on VSP records with source offsets within 4000 feet of borehole USW UZ-6.

The data sets also showed that special care must be taken during the processing of the records, so that the key

horizons can best be enhanced. In particular, it is necessary to be cautious during the separation of the up-going and downgoing wavefields on the VSP record. The modeling experiments showed that reflections from fault planes can have upgoing, downgoing, or near-vertical slopes on the record. A median filter of sufficiently high fold must be used to separate wavefields so that the fault plane reflections are not damaged when removing direct arrivals from the record. A muting step may be necessary to improve the median filtering process. It is also necessary to recognize the slopes of the fault plane reflections when applying FK filters to the records, so that the events are not damaged during filtering.

TABLE OF CONTENTS

	Page
ABSTRACT	iii
LIST OF FIGURES	vii
LIST OF TABLES	xvii
ACKNOWLEDGEMENTS	xviii
Chapter 1: INTRODUCTION	1
1.1 Yucca Mountain as a Potential Repository Site	1
1.2 Vertical Seismic Profiling at Yucca Mountain	2
1.3 Yucca Mountain Geology	4
1.4 Purpose of Thesis Work	10
Chapter 2: COMPUTER VSP MODELING	13
2.1 Introduction	13
2.2 Zero-offset VSP	21
2.3 1000-foot source offset VSP	51
2.4 2000-foot source offset VSP	61
2.5 3000-foot source offset VSP	70
2.6 4000-foot source offset VSP	80
2.7 5000-foot source offset VSP	89
2.8 6000-foot source offset VSP	99
2.9 7000-foot source offset VSP	108
2.10 8000-foot source offset VSP	117
2.11 UE25 UZ-9: Zero-offset VSP	126
2.12 UE25 UZ-9: 1000-foot source offset VSP	132
2.13 UE25 UZ-9: 2000-foot source offset VSP	137
2.14 UE25 UZ-9: 3000-foot source offset VSP	143
2.15 Conclusions	148
Chapter 3: PHYSICAL VSP MODELING PART I	153
3.1 Introduction	153
3.2 1000-foot source offset VSP	160
3.3 2000-foot source offset VSP	176
3.4 3000-foot source offset VSP	182
3.5 4000-foot source offset VSP	188
3.6 5000-foot source offset VSP	193
3.7 6000-foot source offset VSP	197
3.8 7000-foot source offset VSP	199

Page

3.9 8000-foot source offset VSP 208
3.10 Conclusions 212

Chapter 4: PHYSICAL VSP MODELING PART II 214

4.1 Introduction 214
4.2 1000-foot source offset VSP 220
4.3 2000-foot source offset VSP 233
4.4 3000-foot source offset VSP 241
4.5 4000-foot source offset VSP 247
4.6 5000-foot source offset VSP 253
4.7 6000-foot source offset VSP 257
4.8 7000-foot source offset VSP 261
4.9 8000-foot source offset VSP 264
4.10 An Additional Recording Configuration 267
4.11 1000-foot source offset VSP 269
4.12 2000-foot source offset VSP 281
4.13 Conclusions 289

Chapter 5: CONCLUSIONS 292

5.1 Introduction 292
5.2 Yucca Mountain Recommendations 293
5.3 Future Modeling Work 300
5.4 Closing Remarks 303

REFERENCES CITED 304

SELECTED READINGS 305

APPENDIX: BATCH FILE USED TO GENERATE THE
YUCCA MOUNTAIN COMPUTER MODEL IN AIMS 306

LIST OF FIGURES

Figure		Page
1.1	Map of Yucca Mountain and Existing Boreholes	3
1.2	Yucca Mountain Cross Section Between Boreholes USW UZ-6 and UE25 UZ-9	6
2.1	Raypath Diagram for Zero-offset VSP	22
2.2	Synthetic Record for Zero-offset Source	25
2.3	Raypath Diagram for Zero-offset VSP, Tptw Fault Planes Imaged	28
2.4	Synthetic Record for Zero-offset Source, Tptw Fault Planes Imaged	29
2.5	Raypath Diagram for Zero-offset VSP, n2 Fault Planes Imaged	31
2.6	Synthetic Record for Zero-offset Source, n2 Fault Planes Imaged	32
2.7	Raypath Diagram for Zero-offset VSP, Segment of Fault Plane 1 Imaged	33
2.8	Synthetic Record for Zero-offset Source, Segment of Fault Plane 1 Imaged	35
2.9	Synthetic Record for Zero-offset Source, Direct Arrivals Aligned	37
2.10	Synthetic Record for Zero-offset Source, After Application of 7-fold Median Filter	39
2.11	Synthetic Record for Zero-offset Source, After Application of 9-fold Median Filter	41
2.12	Synthetic Record for Zero-offset Source, After Application of 11-fold Median Filter	42
2.13	Synthetic Record for Zero-offset Source, Direct Arrivals Removed	44

Figure | Page

2.14 Raypath Diagram for Zero-offset VSP, Fault Planes Excluded 46

2.15 Synthetic Record for Zero-offset Source, Fault Planes Excluded 47

2.16 Synthetic Record for Zero-offset Source, Fault Planes Excluded, After AGC 48

2.17 Synthetic Record for Zero-offset Source, Fault Planes Excluded, Direct Arrivals Removed 49

2.18 Raypath Diagram for 1000-foot Source Offset VSP .. 52

2.19 Synthetic Record for 1000-foot Source Offset 53

2.20 Synthetic Record for 1000-foot Source Offset, Direct Arrivals Removed 55

2.21 Raypath Diagram for 1000-foot Source Offset VSP, Fault Planes Excluded 57

2.22 Synthetic Record for 1000-foot Source Offset, Fault Planes Excluded, After AGC 59

2.23 Synthetic Record for 1000-foot Source Offset, Fault Planes Excluded, Direct Arrivals Removed . 60

2.24 Raypath Diagram for 2000-foot Source Offset VSP .. 62

2.25 Synthetic Record for 2000-foot Source Offset 63

2.26 Synthetic Record for 2000-foot Source Offset, Direct Arrivals Removed 65

2.27 Raypath Diagram for 2000-foot Source Offset VSP, Fault Planes Excluded 67

2.28 Synthetic Record for 2000-foot Source Offset, Fault Planes Excluded, After AGC 68

2.29 Synthetic Record for 2000-foot Source Offset, Fault Planes Excluded, Direct Arrivals Removed . 69

2.30 Raypath Diagram for 3000-foot Source Offset VSP .. 71

2.31 Synthetic Record for 3000-foot Source Offset 73

Figure Page

2.32 Synthetic Record for 3000-foot Source Offset, Direct Arrivals Removed 74

2.33 Raypath Diagram for 3000-foot Source Offset VSP, Fault Planes Excluded 77

2.34 Synthetic Record for 3000-foot Source Offset, Fault Planes Excluded, After AGC 78

2.35 Synthetic Record for 3000-foot Source Offset, Fault Planes Excluded, Direct Arrivals Removed . 79

2.36 Raypath Diagram for 4000-foot Source Offset VSP .. 81

2.37 Synthetic Record for 4000-foot Source Offset 82

2.38 Synthetic Record for 4000-foot Source Offset, Direct Arrivals Removed 84

2.39 Raypath Diagram for 4000-foot Source Offset VSP, Fault Planes Excluded 86

2.40 Synthetic Record for 4000-foot Source Offset, Fault Planes Excluded, After AGC 87

2.41 Synthetic Record for 4000-foot Source Offset, Fault Planes Excluded, Direct Arrivals Removed . 88

2.42 Raypath Diagram for 5000-foot Source Offset VSP .. 90

2.43 Synthetic Record for 5000-foot Source Offset 92

2.44 Synthetic Record for 5000-foot Source Offset, Direct Arrivals Removed 94

2.45 Raypath Diagram for 5000-foot Source Offset VSP, Fault Planes Excluded 95

2.46 Synthetic Record for 5000-foot Source Offset, Fault Planes Excluded, After AGC 97

2.47 Synthetic Record for 5000-foot Source Offset, Fault Planes Excluded, Direct Arrivals Removed . 98

2.48 Raypath Diagram for 6000-foot Source Offset VSP .. 100

2.49 Synthetic Record for 6000-foot Source Offset 101

Figure Page

2.50 Synthetic Record for 6000-foot Source Offset, Direct Arrivals Removed 102

2.51 Raypath Diagram for 6000-foot Source Offset VSP, Fault Planes Excluded 105

2.52 Synthetic Record for 6000-foot Source Offset, Fault Planes Excluded, After AGC 106

2.53 Synthetic Record for 6000-foot Source Offset, Fault Planes Excluded, Direct Arrivals Removed . 107

2.54 Raypath Diagram for 7000-foot Source Offset VSP .. 109

2.55 Synthetic Record for 7000-foot Source Offset 110

2.56 Synthetic Record for 7000-foot Source Offset, Direct Arrivals Removed 112

2.57 Raypath Diagram for 7000-foot Source Offset VSP, Fault Planes Excluded 114

2.58 Synthetic Record for 7000-foot Source Offset, Fault Planes Excluded, After AGC 115

2.59 Synthetic Record for 7000-foot Source Offset, Fault Planes Excluded, Direct Arrivals Removed . 116

2.60 Raypath Diagram for 8000-foot Source Offset VSP .. 118

2.61 Synthetic Record for 8000-foot Source Offset 119

2.62 Synthetic Record for 8000-foot Source Offset, Direct Arrivals Removed 121

2.63 Synthetic Record for 8000-foot Source Offset, Fault Planes Excluded 124

2.64 Synthetic Record for 8000-foot Source Offset, Fault Planes Excluded, Direct Arrivals Removed . 125

2.65 Raypath Diagram for Zero-offset VSP at Borehole UE25 UZ-9 128

2.66 Synthetic Record for Zero-offset Source, after AGC 129

Figure Page

2.67 Synthetic Record for Zero-offset Source, Direct Arrivals Removed 131

2.68 Raypath Diagram for 1000-foot Source Offset VSP at Borehole UE25 UZ-9 133

2.69 Synthetic Record for 1000-foot Source Offset, after AGC 134

2.70 Synthetic Record for 1000-foot Source Offset, Direct Arrivals Removed 135

2.71 Raypath Diagram for 2000-foot Source Offset VSP at Borehole UE25 UZ-9 138

2.72 Synthetic Record for 2000-foot Source Offset, after AGC 140

2.73 Synthetic Record for 2000-foot Source Offset, Direct Arrivals Removed 141

2.74 Raypath Diagram for 3000-foot Source Offset VSP at Borehole UE25 UZ-9 144

2.75 Synthetic Record for 3000-foot Source Offset, after AGC 145

2.76 Synthetic Record for 3000-foot Source Offset, Direct Arrivals Removed 146

3.1 Schematic Diagram of Laboratory Equipment used to Record Data from the Uniform Velocity Model . 154

3.2 Data Set Recorded for 1000-foot Source Offset 161

3.3 1000-foot Source Offset Data Set, Direct P-wave Aligned 164

3.4 1000-foot Source Offset Data Set, Direct P-wave Removed 165

3.5 1000-foot Source Offset Data Set, Surface Wave Aligned 167

3.6 1000-foot Source Offset Data Set, Surface Wave Removed 168

Figure Page

3.7 FK Spectrum, 1000-foot Source Offset Data Set 169

3.8 FK Spectrum of 1000-foot Source Offset Data Set, After FK Filtering 170

3.9 1000-foot Source Offset Data Set, After FK Filtering 171

3.10 Synthetic AIMS Data Set Simulating the 1000-foot Source Offset Data Set from the Physical Model . 175

3.11 Data Set Recorded for 2000-foot Source Offset 177

3.12 2000-foot Source Offset Data Set, Direct P-wave and Surface Wave Removed 179

3.13 2000-foot Source Offset Data Set, After FK Filtering 181

3.14 Synthetic AIMS Data Set Simulating the 2000-foot Source Offset Data Set from the Physical Model . 183

3.15 Data Set Recorded for 3000-foot Source Offset 184

3.16 3000-foot Source Offset Data Set, Direct P-wave and Surface Wave Removed 186

3.17 3000-foot Source Offset Data Set, After FK Filtering 187

3.18 Data Set Recorded for 4000-foot Source Offset 189

3.19 4000-foot Source Offset Data Set, Direct P-wave and Surface Wave Removed 190

3.20 4000-foot Source Offset Data Set, After FK Filtering 192

3.21 Data Set Recorded for 5000-foot Source Offset 194

3.22 5000-foot Source Offset Data Set, Direct P-wave and Surface Wave Removed 195

3.23 5000-foot Source Offset Data Set, After FK Filtering 196

3.24 Data Set Recorded for 6000-foot Source Offset 198

Figure Page

3.25 6000-foot Source Offset Data Set, Direct P-wave and Surface Wave Removed 200

3.26 6000-foot Source Offset Data Set, After FK Filtering 201

3.27 Data Set Recorded for 7000-foot Source Offset 202

3.28 7000-foot Source Offset Data Set, After Using an 11-fold Median Filter to Remove the Direct P-wave 204

3.29 7000-foot Source Offset Data Set, After Using a 15-fold Median Filter to Remove the Direct P-wave 205

3.30 7000-foot Source Offset Data Set, Direct P-wave and Surface Wave Removed 206

3.31 7000-foot Source Offset Data Set, After FK Filtering 207

3.32 Data Set Recorded for 8000-foot Source Offset 209

3.33 8000-foot Source Offset Data Set, Direct P-wave and Surface Wave Removed 210

3.34 8000-foot Source Offset Data Set, After FK Filtering 211

4.1 Schematic Diagram of the Laboratory Equipment used to Record Data from Variable Velocity Model 216

4.2 Data Set Recorded for 1000-foot Source Offset 221

4.3 1000-foot Source Offset Data Set, Downgoing Events Removed 223

4.4 1000-foot Source Offset Data Set, After 100/12 Low Pass Filtering 224

4.5 FK Spectrum, 1000-foot Source Offset Data Set 226

4.6 FK Filter used to Remove Downgoing Energy from the Data Sets in Chapter 4 227

Figure | Page

4.7 FK Spectrum, 1000-foot Source Offset Data Set After FK Filtering 228

4.8 1000-foot Source Offset Data Set, After FK Filtering 230

4.9 Synthetic AIMS Data Set Simulating a 1000-foot Source Offset Data Set from the Physical Model . 231

4.10 Data Set Recorded for 2000-foot Source Offset 234

4.11 2000-foot Source Offset Data Set, Downgoing Events Removed 235

4.12 2000-foot Source Offset Data Set, After 100/12 Low Pass Filtering 237

4.13 2000-foot Source Offset Data Set, After FK Filtering 238

4.14 Synthetic AIMS Data Set Simulating a 2000-foot Source Offset Data Set from the Physical Model . 240

4.15 Data Set Recorded for 3000-foot Source Offset 242

4.16 3000-foot Source Offset Data Set, Downgoing Events Removed 244

4.17 3000-foot Source Offset Data Set, After 100/12 Low Pass Filtering 245

4.18 3000-foot Source Offset Data Set, After FK Filtering 246

4.19 Data Set Recorded for 4000-foot Source Offset 248

4.20 4000-foot Source Offset Data Set, Downgoing Events Removed 249

4.21 4000-foot Source Offset Data Set, After 100/12 Low Pass Filtering 251

4.22 4000-foot Source Offset Data Set, After FK Filtering 252

4.23 Synthetic AIMS Data Set Simulating Fault Plane Reflections for a 4000-foot Source Offset 254

Figure Page

4.24 Data Set Recorded for 5000-foot Source Offset 255

4.25 5000-foot Source Offset Data Set,
Downgoing Events Removed 256

4.26 5000-foot Source Offset Data Set,
After 100/12 Low Pass Filtering 258

4.27 5000-foot Source Offset Data Set,
After FK Filtering 259

4.28 Data Set Recorded for 6000-foot Source Offset 260

4.29 6000-foot Source Offset Data Set,
After Low Pass and FK Filtering 262

4.30 Data Set Recorded for 7000-foot Source Offset 263

4.31 7000-foot Source Offset Data Set,
After Low Pass and FK Filtering 265

4.32 Data Set Recorded for 8000-foot Source Offset 266

4.33 8000-foot Source Offset Data Set,
After Low Pass and FK Filtering 268

4.34 Data Set Recorded for 1000-foot Source Offset,
Using the V133 Transducers 270

4.35 1000-foot Source Offset Data Set,
Noise Burst Removed 272

4.36 1000-foot Source Offset Data Set,
After 100/12 Low Pass Filtering 273

4.37 1000-foot Source Offset Data Set,
Direct P-wave Removed 275

4.38 1000-foot Source Offset Data Set,
Surface Wave Removed 276

4.39 1000-foot Source Offset Data Set,
Direct S-wave Removed 277

4.40 FK Spectrum, 1000-foot Source Offset Data Set 278

Figure Page

4.41 FK Spectrum, 1000-foot Source Offset Data Set After FK Filtering 279

4.42 1000-foot Source Offset Data Set, After FK Filtering 280

4.43 Data Set Recorded for 2000-foot Source Offset, Using the V133 Transducers 282

4.44 2000-foot Source Offset Data Set, Noise Burst Removed 284

4.45 2000-foot Source Offset Data Set, After 100/12 Low Pass Filtering 285

4.46 2000-foot Source Offset Data Set, Downgoing Events Removed 286

4.47 2000-foot Source Offset Data Set, After FK Filtering 288

LIST OF TABLES

Table		Page
1.1	Geologic Summary of the Volcanic Units	7
2.1	Velocity Information for Computer Modeling	15
2.2	Density Information for the Volcanic Units	17
3.1	Recording Parameters for Physical Modeling, Part I	160
4.1	Recording Parameters for Physical Modeling, Part II	219

ACKNOWLEDGEMENTS

I would like to thank the U. S. Geological Survey for providing the funding for this project. In particular, I would like to thank Joe Rousseau for securing the laboratory equipment for the physical modeling experiments, as well as for providing the funding for the computer time necessary to process the VSP data sets.

I would like to thank my advisor, Dr. Al Balch for allowing me to participate in this very interesting project and for all of his guidance during my stay at CSM. I would also like to thank Drs. Ron Knoshaug and Tom Davis for serving on my thesis committee. I am also grateful to Bob Benson for his help on this project.

I also thank my fellow laboratory slaves Gregg Hofland, Kurt Ranzinger, and Garon Reeves, whose contributions to this project have been extensive.

My deepest thanks go to my father, H. D. Cunningham, whose skills as a craftsman made the entire physical modeling portion of this thesis possible. I would also like to thank my father, and my mother Patricia, for their endless support over the past 24 years.

Finally, I would like to thank my dear wife Yvette for all of her help during my stay at CSM.

Chapter 1

INTRODUCTION

1.1 Yucca Mountain as a Potential Repository Site

By the end of the century, there will exist approximately 50,000 metric tons of highly radioactive spent uranium fuel stored in water pools at the 106 licensed nuclear power plants in the United States (Monastersky, 1988). At the end of 1987, Congress amended the Nuclear Waste Policy Act of 1983, abandoning the simultaneous characterization of three possible locations for the subsurface burial of the high-level waste. Congress authorized the U.S. Department of Energy (DOE) to work with the U.S. Geological Survey (USGS) and other national and private laboratories in the study of Yucca Mountain in southern Nevada, which is considered to be the most promising potential waste storage site (Monastersky, 1988).

Yucca Mountain consists of a gently-dipping sequence of fine-grained ash-flow tuffs, which are mostly welded and fractured. Some of the ash-flow and air-fall tuffs are non-welded and sparsely fractured, however. The tuffs which comprise and surround the location of the proposed radioactive waste repository are unsaturated. The water table ranges from 1650 to 2450 feet below the sloping surface of Yucca Mountain. This places the water table approximately

750 feet below the proposed repository level. The fact that the repository level at Yucca Mountain is above the water table was one of the considerations leading to the selection of Yucca Mountain for the site characterization study.

Several studies are planned by the USGS to characterize flow processes in the unsaturated zone at Yucca Mountain. One of these studies, the characterization of percolation in the unsaturated zone-surface based borehole investigations, has two primary objectives. The first objective is the definition of the multi-phase liquid and gas fluid flow within the unsaturated zone. The second objective is the determination of in-situ bulk permeability and bulk hydrologic properties of units in the unsaturated zone. The characterization of percolation in the unsaturated zone-surface based borehole investigations is divided into many areas of research. A Vertical Seismic Profiling (VSP) investigation will be conducted at Yucca Mountain under this program.

1.2 Vertical Seismic Profiling at Yucca Mountain

Figure 1.1 shows a map of Yucca Mountain and the location of the test site in southern Nevada. Vertical Seismic Profiling will be conducted in boreholes at the USW UZ-6 and the UE25 UZ-9 sites. Hydrologic properties such as fracture permeability, porosity, and bulk permeability will be

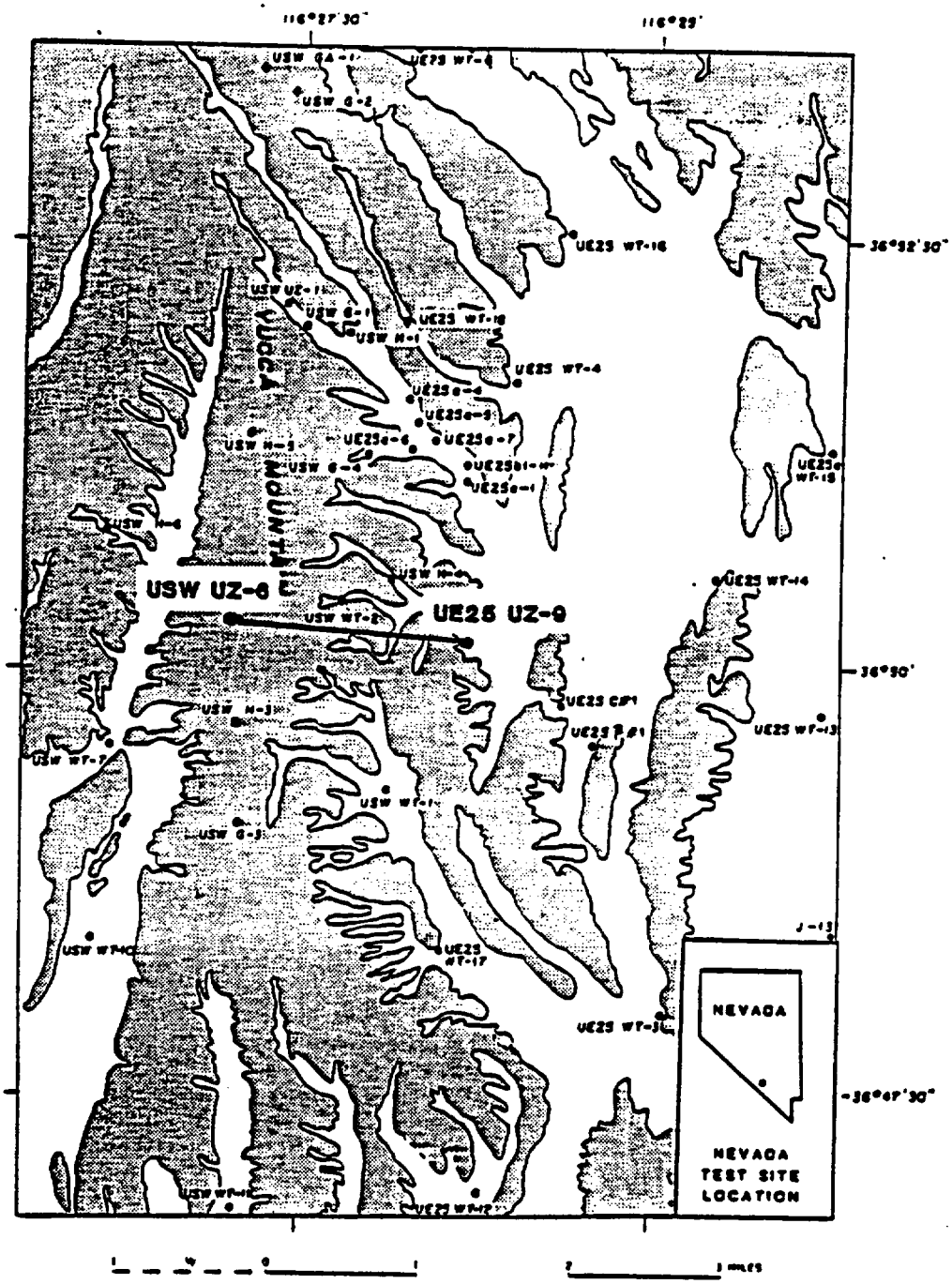

Figure 1.1. Map of southern Nevada showing the location of Yucca Mountain with proposed and existing boreholes. The proposed initial line of vertical seismic profiling will occur between boreholes at the USW UZ-6 and UE25 UZ-9 sites (from Muller and Kibler, 1985).

correlated to reflectivity and acoustic velocity. Zero-offset VSP data will be utilized to make these correlations.

The VSP surveys will use three-component geophones permanently cemented into boreholes at the UZ-6 and UZ-9 sites. The geophones will be placed at 100 depth levels in the boreholes, with a receiver spacing of approximately 20 feet. The use of three-component sources and receivers will allow the study of acoustic phenomena which can be associated with permeability zones. These phenomena include acoustic birefringence, scattering, and converted wave reflections.

Since the receivers will be permanently emplaced in the borehole, VSP surveys will be taken from multiple offsets and along multiple azimuths. Profiles which produce interesting results can be repeated at a later date with the geophones at identical locations with identical mechanical coupling to the earth. Profiles which produce poor data can also be repeated with varying parameters in an attempt to improve the quality of the data.

1.3 Yucca Mountain Geology

The proposed initial line of Vertical Seismic Profiling at Yucca Mountain, shown on Figure 1.1, is between boreholes UZ-6 and UZ-9. A cross section along this line was created based on USGS Open File Report 84-494, a Preliminary Geologic Map of Yucca Mountain Nye County, Nevada and Geologic

Sections by Robert Scott and Jerry Bonk. The cross section is shown in Figure 1.2. The volcanic units of Yucca Mountain have been divided into ten layers in this cross section, using divisions consistent with Scott and Bonk. Units whose abbreviations end with "w" are considered to be welded tuffs, while units whose abbreviations begin with "n" are considered non-welded tuffs. The numbering scheme of the non-welded units is introduced in this thesis to help differentiate between events on the data sets created by the computer and physical modeling experiments. This numbering scheme is not consistent with Scott and Bonk, who did not assign specific names to the non-welded units on their cross sections.

The lithology of the volcanic units along the cross section in Figure 1.2 are briefly summarized in Table 1.1.

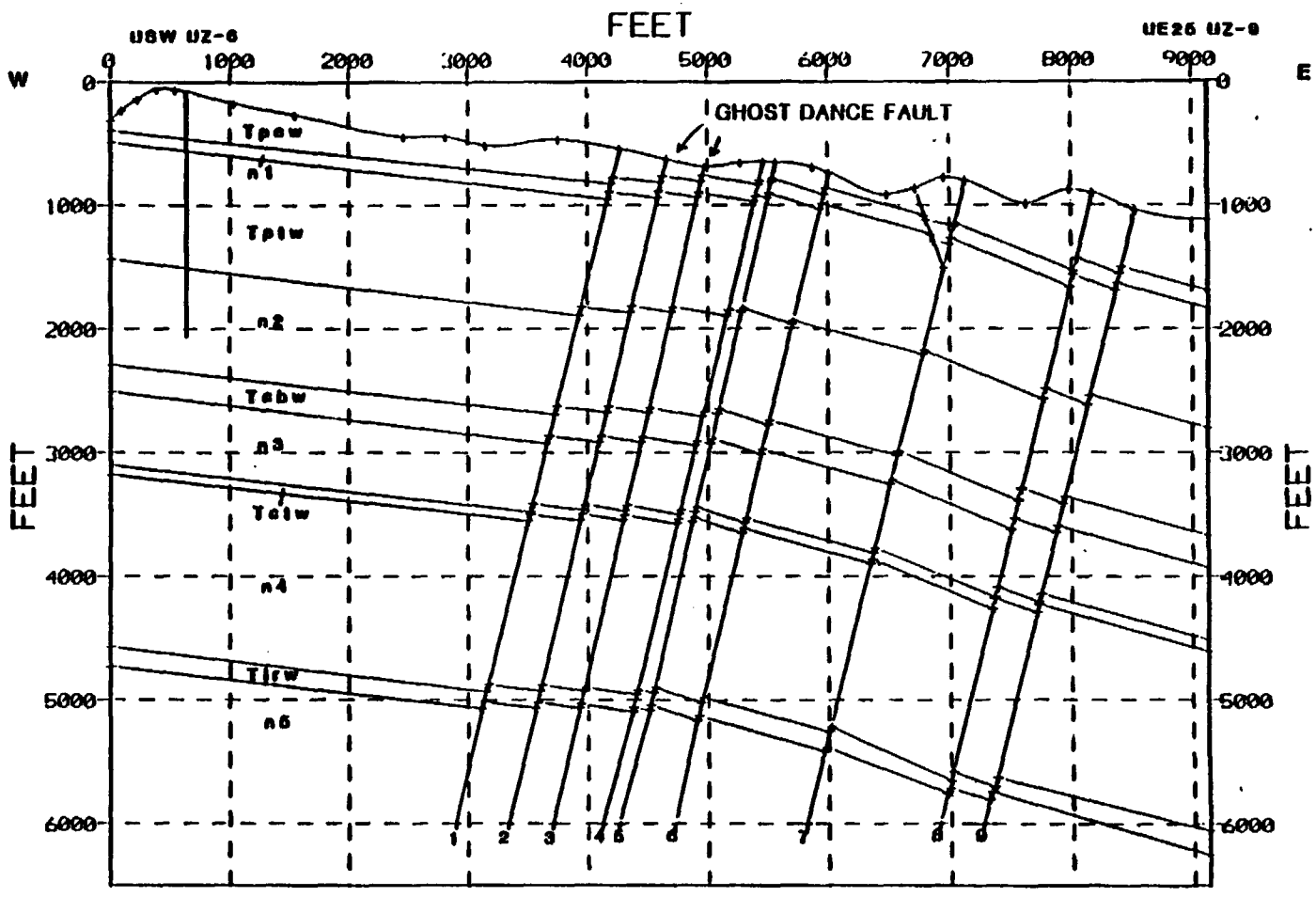

Figure 1.2. Cross section of Yucca Mountain along the line between boreholes UZ-6 and UZ-9. The volcanic units dip to the east at 7 degrees at the crest of the mountain. The high-angle faults have been numbered 1 through 9 for identification purposes. The faults are assumed to dip to the west at 75 degrees (based on Scott & Bonk, 1984).

Table 1.1 Geologic Summary of the Volcanic Units

Unit	Description
Tpcw	Tiva Canyon Member, Paintbrush Tuff. This member consists of six units, which range from moderately to densely welded. The uppermost layer is a quartz-latitic Caprock Zone which is welded. Underlying the caprock is the Upper Lithophysal Zone which is moderately welded, devitrified, and rhyolitic. Lithophysae are abundant. A Clinkstone layer underlies the Upper Lithophysal Zone. The Clinkstone is moderately-welded, devitrified, rhyolitic, and contains numerous concoidal fractures. The Lower Lithophysal Zone underlies the Clinkstone. This unit is moderately to densely welded, devitrified, and rhyolitic. Lithophysae are abundant. A Hackly Zone underlies the Lower Lithophysal Zone. This unit is densely welded, devitrified, rhyolitic, and contains hackly fracture surfaces. The Hackly Zone overlies the Columnar Zone, which is non-welded to densely-welded and rhyolitic. Fractures in the Tiva Canyon are primarily within the units and near the faults. Horizontal partings exist between some of the units. The units of the Tiva Canyon have been generalized into one unit, Tpcw, in this thesis.
nl	Shardy Base. This is an informal name given to the non-welded unit between the Tiva Canyon and Topopah Spring Members of the Paintbrush Tuff. This unit consists of vitric pumice clasts and glass shards. The Shardy Base is an ash-fall tuff and is very porous.
Tptw	Topopah Spring Member, Paintbrush Tuff. This unit consists of a non-welded to partially-welded top vitrophyre which grades downward into 1000 feet of moderately-welded to densely-welded tuff which contains abundant

(Continued)

Table 1.1 (Continued)

Unit	Description
Tptw	pumice fragments. This densely-welded unit is underlain by a glassy vitrophyric layer which grades downward into a less-welded unit. There are three lithophysal zones between the upper and lower vitrophyres. The zone between the lowermost lithophysal zone and the basal vitrophyre contains few or no lithophysal cavities. This zone is being considered by the DOE as the potential host rock for emplacement of the nuclear waste. This unit is a devitrified, densely-welded and highly fractured tuff. The VSP activity at Yucca Mountain will attempt to delineate the permeability zones within this unit.
n2	Calico Hills Tuff. This is an informal name given to the tuff beds that occupy the stratigraphic position between the Paintbrush Tuff and the Crater Flat tuff. This unit consists of non-welded ash-flow tuffs and isolated ash-fall tuffs. The unit is rhyolitic and zeolitized.
Tcbw	Bullfrog Member, Crater Flat Tuff. This unit is a moderately-welded to densely-welded, devitrified tuff. The contact with the Calico Hills Tuff is somewhat gradational. This unit shows large variations in the degree of welding, but induration increases significantly with depth.
n3	This unit occupies the stratigraphic interval between the Bullfrog and Tram Members of the Crater Flat Tuff. It is a reworked, ash-fall tuff which contains numerous zeolitic pumice clasts. The pumice clasts, along with clinoptilolite and mordenite constitute 30% of the rock.

(Continued)

Table 1.1 (Continued)

Unit	Description
Tctw	Tram Member, Crater Flat Tuff. This unit is partially-welded to moderately-welded. The unit has a high content of lithic fragments.
n4	This unit occupies the stratigraphic interval between the Tram Member of the Crater Flat Tuff and the Lithic Ridge Tuff. This unit is a non-welded, quartz-latitic ash-flow tuff.
Tlrw	Lithic Ridge Tuff. This unit is moderately-welded and vitric in some instances. The unit contains a small percentage of lithic fragments and phenocrysts.
n5	This unit occupies the stratigraphic interval below the Lithic Ridge Tuff. The unit is a non-welded, quartz-latitic, ash-flow tuff.

Sources: Carr, W. J., F. M. Byers, Jr., and P. P. Orklid. 1984. Stratigraphic and volcano-tectonic relations of Crater Flat Tuff and some older volcanic units, Nye County, Nevada: U. S. Geological Survey Open-File Report 84-114.

Spengler, R. W. and M. P. Chornack. 1984. Stratigraphic and structural characteristics of volcanic rocks in core hole USW G-4, Yucca Mountain, Nye County, Nevada: U. S. Geological Survey Open-File Report 84-789.

The cross section shows that the volcanic units dip to the east at approximately 7 degrees at the crest of Yucca Mountain. The layers are assumed to be cut by nine high-angle (75 degrees) normal faults which dip to the west. These faults may or may not sole into one major fault at depth, but their representation in this cross section is consistent with the cross sections of Scott and Bonk. Displacement across these faults is assumed to range from 30 to 120 feet in this cross section. Approximately 6700 feet from the west edge of the cross section is a single high-angle normal fault dipping to the east. This fault forms the west boundary of a small graben.

1.4 Purpose of Thesis Work

The VSP experiments conducted at Yucca Mountain will produce an enormous amount of data. Since the geophones will be permanently emplaced in the receiver boreholes, a complete VSP record will be obtained in a matter of minutes. In order to make the most efficient use of the VSP receivers and the data that they will provide, we decided to conduct modeling experiments in a laboratory. The modeling experiments were designed to test how well subsurface horizons at Yucca Mountain will be imaged by VSP surveys. Of particular importance is the determination of advantages and disadvantages of various source positions on the sloping surface

of Yucca Mountain. Certain source offsets will provide good reflections from key horizons, such as fault planes, while other source offsets will not provide good reflections. The creation of synthetic data sets will provide a useful reference guide to aid in the interpretation of the field records, as well.

Software that will aid in the processing of the field data is being developed and tested before the actual field data are acquired. Tests of some of the programs were performed on the model data sets. The processing of the model data sets also provided valuable information that can be used later to improve the processing of the field data.

Two types of modeling experiments were performed in this thesis. The first type of modeling was done on a VAX 8600 computer. A computer model of the cross section in Figure 1.2 was used to generate 22 synthetic VSP data sets. Receivers were user-specified in boreholes UZ-6 and UZ-9. The advantages of the computer model were numerous. The modeling could be done using appropriate seismic velocities and densities. The interpretation of these synthetic data sets could be done exactly, in contrast to the physical model data sets, since the horizon producing a given reflection could be uniquely tracked down. Fault planes could be designated as reflecting or non-reflecting surfaces. One disadvantage of the computer models was the cost. A

complete ray tracing through the computer model ran from one to eight hours of CPU time on the VAX for each computer generated data set.

The second type of modeling was done on physical models of Yucca Mountain. The laboratory equipment used to generate the VSP data sets with the physical models will be discussed in Chapter 3. The advantages of the physical modeling experiments were also numerous. Since the data from Yucca Mountain will not be in the pristine condition of the computer model data, the testing of the processing software is best accomplished using data of moderate quality. Coupling of the source and receivers at Yucca Mountain will not be perfectly constant and this may produce anomalies on the data. This is also true for the physical modeling experiments. The disadvantage of the physical modeling was that obtaining the laboratory equipment necessary to do a thorough job of modeling was very expensive, initially.

Chapter 2

COMPUTER VSP MODELING

2.1 Introduction

The cross section in Figure 1.2 was digitized as a model containing 269 separate horizons. Each horizon is a line segment defined by its beginning and ending points. The sole exception is the surface topography, which was defined by thirty points from left to right. The horizon definition module of the AIMS modeling package, SUBSRF, fits a third order polynomial to the interval between adjacent points on the horizon. In this way the surface topography was defined continuously across the model.

Each horizon is assigned a horizon number, a pressure wave velocity, and a density. The velocity and density extend from the horizon down to the top of the next underlying horizon. Subsurface horizons in AIMS must be carefully numbered such that a higher-numbered horizon does not overlap a lower-numbered horizon. Due to the complexity of this model, several numbering schemes for the horizons were tested until an appropriate system was found.

As noted above, in order to conduct a VSP modeling experiment with AIMS it is necessary to define interval velocities for each of the units in the model. In addition to the interval velocities, inserting a density for each

unit allows AIMS to calculate appropriate reflection coefficients at each boundary.

Interval velocities were calculated by examining sonic logs from ten boreholes and velocity surveys from two additional boreholes in the vicinity of Yucca Mountain (Muller and Kibler, 1985). Sonic logs were obtained from boreholes: USW WT#2, USW WT#7, USW WT#10, USW WT#11, UE-25 WT#12, UE-25 WT#17, USW G-1, USW G-2, USW G-3, and USW P-1. Velocity surveys were obtained for boreholes USW UZ-6 and USW G-3. The locations of these boreholes can be seen on Figure 1.1. The boreholes are of various depths and only USW G-3 penetrates every unit in the model cross section. Therefore, most of the sonic logs provided velocities for only four or five of the volcanic units. Table 2.1 shows interval velocity values calculated from the logs for each of the units. Where the borehole did not penetrate a unit, or the velocity estimate could not be made from the log, a dash appears in the table.

Table 2.1 Velocity Information used to Derive Interval Velocities for the Computer Models in Feet/Second

	SONIC LOGS						
Unit	WT-2	WT-7	WT-10	WT-11	WT-12	WT-17	G-1
Tpcw	8,800	8,200	9,000	9,840	7,216	7,216	--
n1	6,900	6,527	7,000	6,560	7,000	5,900	--
Tptw	11,550	10,700	12,136	10,000	10,500	10,500	--
n2	8,200	9,800	--	10,500	--	8,500	10,200
Tcbw	13,120	--	--	--	--	12,500	12,904
n3	--	--	--	--	--	--	11,045
Tctw	--	--	--	--	--	--	12,740
n4	--	--	--	--	--	--	12,029
Tlrw	--	--	--	--	--	--	--
n5	--	--	--	--	--	--	--

	SONIC LOGS			VEL. SURVEYS		AVERAGE	ROUNDED
Unit	G-2	G-3	P-1	UZ-6	G-3		
Tpcw	--	11,024	--	8,900	7,073	8,685	8,700
n1	--	6,173	--	5,494	6,525	6,448	6,400
Tptw	--	11,818	--	9,917	9,673	10,755	10,800
n2	10,279	7,408	10,957	8,612	8,441	9,289	9,300
Tcbw	12,413	12,876	13,648	--	12,516	12,854	12,900
n3	11,264	--	12,073	--	10,015	11,099	11,100
Tctw	12,248	--	12,926	--	12,933	12,711	12,700
n4	11,592	--	--	--	11,482	11,701	11,700
Tlrw	--	--	--	--	13,056	13,056	13,100
n5	--	--	--	--	12,536	12,536	12,500

Source: Values calculated from Muller, D. C. and J. E. Kibler. 1985. Preliminary analysis of geophysical logs from the WT series of drill holes, Yucca Mountain, Nye County, Nevada: U. S. Geological Survey Open-File Report 86-46.

The values in Table 2.1 were averaged and rounded to the nearest hundred. The rounded values, also shown in Table 2.1, were used as the interval velocities for the model horizons in every synthetic data set created by AIMS in this chapter.

Density values for the units were calculated from core sample measurements from boreholes USW GU-3/G-3 and USW G-4 (Anderson, 1984). Two density values were examined, the natural bulk density (NBD) of the core sample and the saturated bulk density (SBD) of the core sample. Several samples were tested for each volcanic unit, so the values in Table 2.2 show the average NBD and the average SBD for a given unit in each borehole. Density values from each borehole were averaged to produce a single density value for each horizon in the model.

The static water table at USW UZ-6 is roughly 2000 to 2200 feet below the surface. For units below n2, the Calico Hills Tuff, the saturated bulk density values were used to calculate a density for the model layers which are below the static water table. Units above Tcbw, the Bullfrog Member, were given density values calculated from NBD figures. This provided a means for incorporating the effect of the water table into the model without specifically designating the water table as a real horizon with reflectivity.

Once the model had been defined by AIMS, the file

containing the model was left unchanged for the duration of the modeling experiments.

Table 2.2 Density Values (gm/cc) for the Volcanic Units

	BOREHOLE USW GU-3/G-3		BOREHOLE USW G-4		
Unit	NBD	SBD	NBD	SBD	MODEL VALUE
Tptw	2.36	2.37	2.38	2.40	2.37
n1	1.66	1.80	--	1.68	1.66
Tpcw	2.31	2.32	2.30	2.34	2.30
n2	1.84	1.88	1.88	1.88	1.88
--STATIC WATER TABLE--					
Tcbw	2.36	2.39	2.24	2.25	2.32
n3	2.09	2.12	2.03	2.03	2.07
Tctw	2.22	2.24	2.29	2.31	2.27
n4	2.21	2.21	--	--	2.21
Tlrw	2.22	2.23	--	--	2.23
n5	2.26	2.26	--	--	2.26

Source: The density values were calculated from Anderson, Lennart A. 1984. USGS Open-File Report 84-552.

The AIMS module VSPRAY is used to trace rays for a VSP configuration. Three items of information are needed for this module to generate the raypaths. The first necessary parameter is the location and deviation of the borehole containing receivers. For the data sets in this phase of the modeling, the boreholes were defined at two locations. The first section of computer modeling took place with the borehole defined 626 feet from the west edge of the model. This is the location of borehole USW UZ-6. The borehole was defined in the model to be 2000 feet deep, with a surface elevation of 4920 feet above sea level. The borehole was defined to be perfectly vertical, although AIMS allows the user to define a deviated borehole as well. The second borehole used in the computer modeling was defined 8500 feet east of USW UZ-6. This is the proposed location of borehole UE25 UZ-9. This borehole was also defined to be 2000 feet deep and perfectly vertical. The surface elevation at UE25 UZ-9 is 3800 feet above sea level.

The second item of information necessary for VSPRAY is the location of the receivers. For every synthetic VSP created, the number of receivers was set at 100 with a receiver spacing of 20 feet. The shallowest receiver location was defined at 20 feet below the datum. The deepest receiver location was defined at 2000 feet below the datum. These parameters were selected to emulate the expected parameters

of the field survey that will be carried out later.

The third item of information is the location of the source on the surface. The source locations used for generating the synthetic VSPs were selected at multiples of 1000 feet from the receiving boreholes.

During the running of VSPRAY, rays are traced from the source, through the model, and into the receiving borehole. Travel times are calculated for each ray, as well as amplitude loss due to inelastic attenuation, reflection and transmission, and geometric divergence. For downgoing raypaths, successive rays are traced at increasing angles from the vertical at the location of the seismic source. When a pair of rays are found to intersect the borehole both above and below a given receiver location, the module searches for an intermediate angle which allows the ray to intersect the borehole at the receiver location, within a small margin of error. The tracing scheme for upgoing reflections is similar, but rays are first traced from the source to the reflecting horizon. The angle of reflection is determined from geometric optics and the ray tracing continues until an intersection with the borehole is found or is determined to be impossible.

The ray trace information is sorted into trace sequential order by the AIMS module RPSORT. Synthetic seismic traces are then generated by the module SPGENR. Parameters

such as sample interval, trace length, and amplitude loss mechanisms are specified in this module. For the data sets used in this modeling, a 4 millisecond sample interval was used with a trace length of 2.5 seconds. The effect of spreading losses was excluded from all data sets, as were the effects of inelastic attenuation. For data sets in which reflections from the fault planes were desired, the effect of the reflection coefficient had to be excluded. Since the densities and p-wave velocities were identical across most of the fault planes in the model, these horizons would not normally produce a reflection on a seismic data set. Excluding the effect of the reflection coefficient allowed AIMS to produce events on the VSP records.

The synthetic traces were generated by SPGENR. "Spike-sections," were then convolved with a wavelet in the module WAVLET. For most of the data sets, a zero-phase Butterworth bandpass wavelet was used. The low-pass half amplitude point was 10 hz and the high-pass half amplitude point was 100 hz. Roll-off slope on both ends of the wavelet was 12 db/octave. The frequency content was selected as a conservative estimate of the possible frequency range of the data to be recorded at Yucca Mountain. All spike-sections were written to magnetic tape so that alternate wavelets could be convolved with the traces at a later date, if desired. In this way, new synthetic traces could be

generated without having to run the computer-intensive ray tracing module again.

The synthetic traces were then converted into SEGY format by the AIMS module RFMT. These traces were written to magnetic tape and transferred to the GOULD 9750. The VSEIS VSP processing package, created by SPECTRUM GEOPHYSICAL SERVICES, resides on the GOULD. All additional processing of the synthetic data was accomplished using VSEIS.

2.2 Zero-offset VSP

Figure 2.1 shows zero-offset VSP raypaths generated by AIMS for borehole USW UZ-6. The borehole has a surface elevation of 4920 feet and extends down 2000 feet, into the Calico Hills Tuff. The level of the static water table is several hundred feet below the bottom of the borehole.

The ray trace diagram in Figure 2.1 shows raypaths which intersect the borehole at every fifteenth receiver location. By selecting every fifteenth receiver for ray plotting, it is possible to discern individual raypaths. Plotting every raypath that intersects the borehole creates a confusing diagram. From Figure 2.1, it is observed that the subsurface horizons are being imaged updip from the borehole. Since the horizons are dipping to the east, this result was expected. In fact, the model was designed with the UZ-6 borehole 626 feet east of the left boundary of the model so

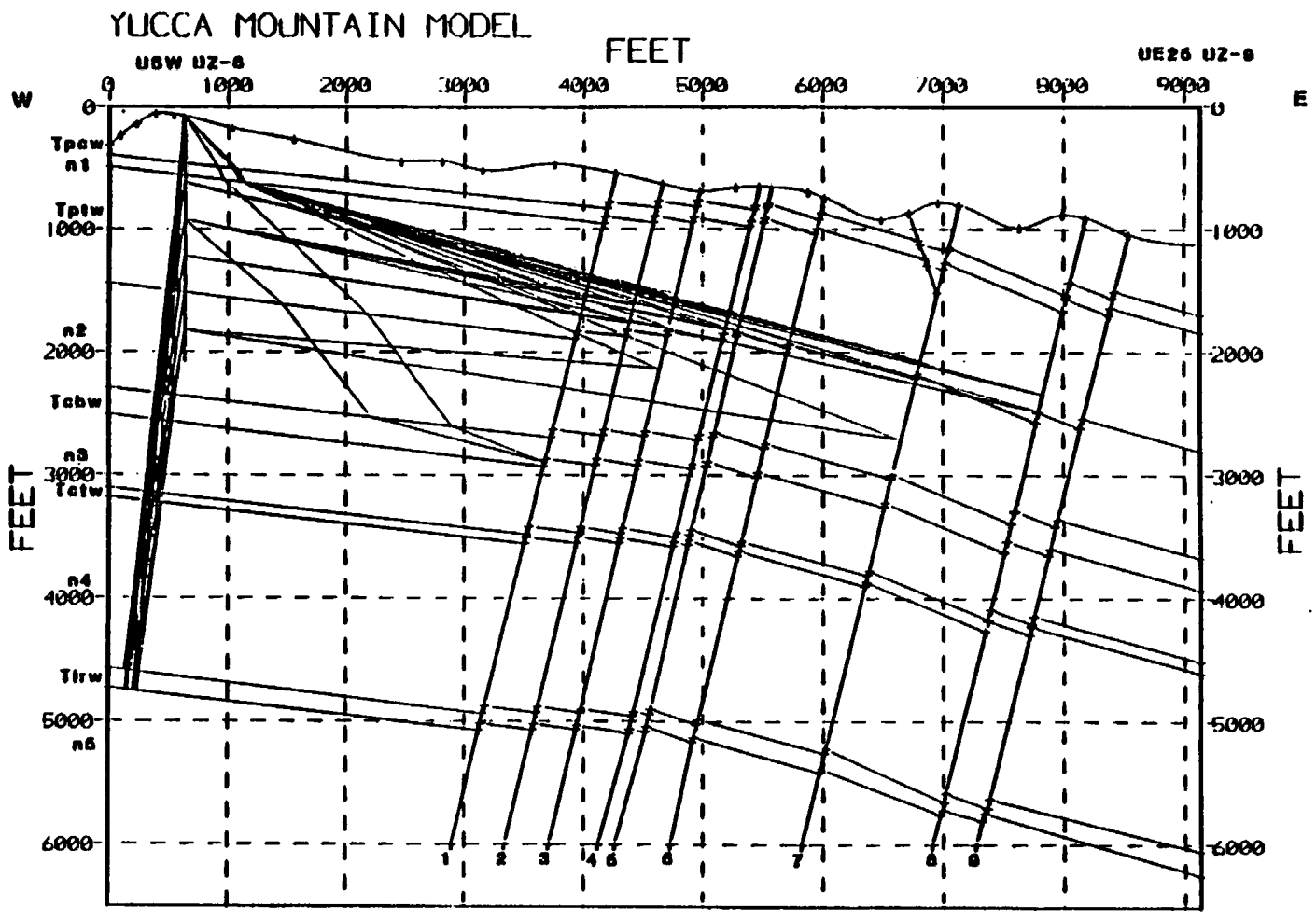

Figure 2.1. Raypath diagram for zero-offset VSP at USW UZ-6.

that the updip reflections could be generated during the zero-offset VSP.

For each of the synthetic VSPs generated for the UZ-6 borehole, the high-angle faults were treated as both reflecting and non-reflecting interfaces. Since the faults have only small offsets, the geologic units on each side of the faults are usually the same, except at the very top and very bottom of each unit. Near the top and bottom of a given unit, different units will be faulted against one another, and reflections can be generated due to velocity and density contrasts across the fault. In most cases, however, AIMS sees the fault planes as boundaries which have the same velocity and the same density on both sides of the boundary. A ray is reflected off of the boundary and back to the borehole during the ray tracing, but a reflection coefficient of zero is assigned to the event and it can not be seen on the synthetic VSP. At Yucca Mountain, it is possible that the fault planes serve as conduits for groundwater and that mineralization has occurred along the fault (Chornack, 1988. Interview with author, 4 May). This could cause the reflection of seismic energy from the fault planes. Brecciated zones may also exist along the faults (Chornack, 1988. Interview with author, 4 May) and this may cause the reflection of seismic energy. The imaging of the high-angle faults is a major goal of the VSP experiments at Yucca

Mountain, so the computer modeling was carried out to accomodate the presence or absence of fault plane reflections.

In order to generate reflections from the fault planes with AIMS, it is necessary to eliminate the effect of the reflection coefficient during the creation of the spike section in the module SPGENR. This will create a fault plane reflection on the synthetic VSP, but it will also give all other reflections on the VSP the same polarity and similar amplitudes. This destroys the effect of the density information contained in the model, but seeing the locations of the fault planes is a reasonable trade-off for the loss of the amplitude information.

On Figure 2.1, the raypaths can be seen reflecting off the high-angle fault planes, primarily within the Tptw (Topopah Spring) and the n2 (Calico Hills) Tuffs. For ease of identification, the fault planes have been numbered one through nine. This numbering scheme is used throughout the remaining models in this paper. Fault planes 2 and 3 represent the Ghost Dance Fault. This fault is thought to be a major fault farther to the north, but it has split into two branches at the location of the model cross section.

Figure 2.2 is the raw synthetic data set generated with the zero-offset source and 100 receivers in borehole UZ-6. The receivers are spaced at 20 foot intervals. The depth annotations represent depth, in feet, below the zero

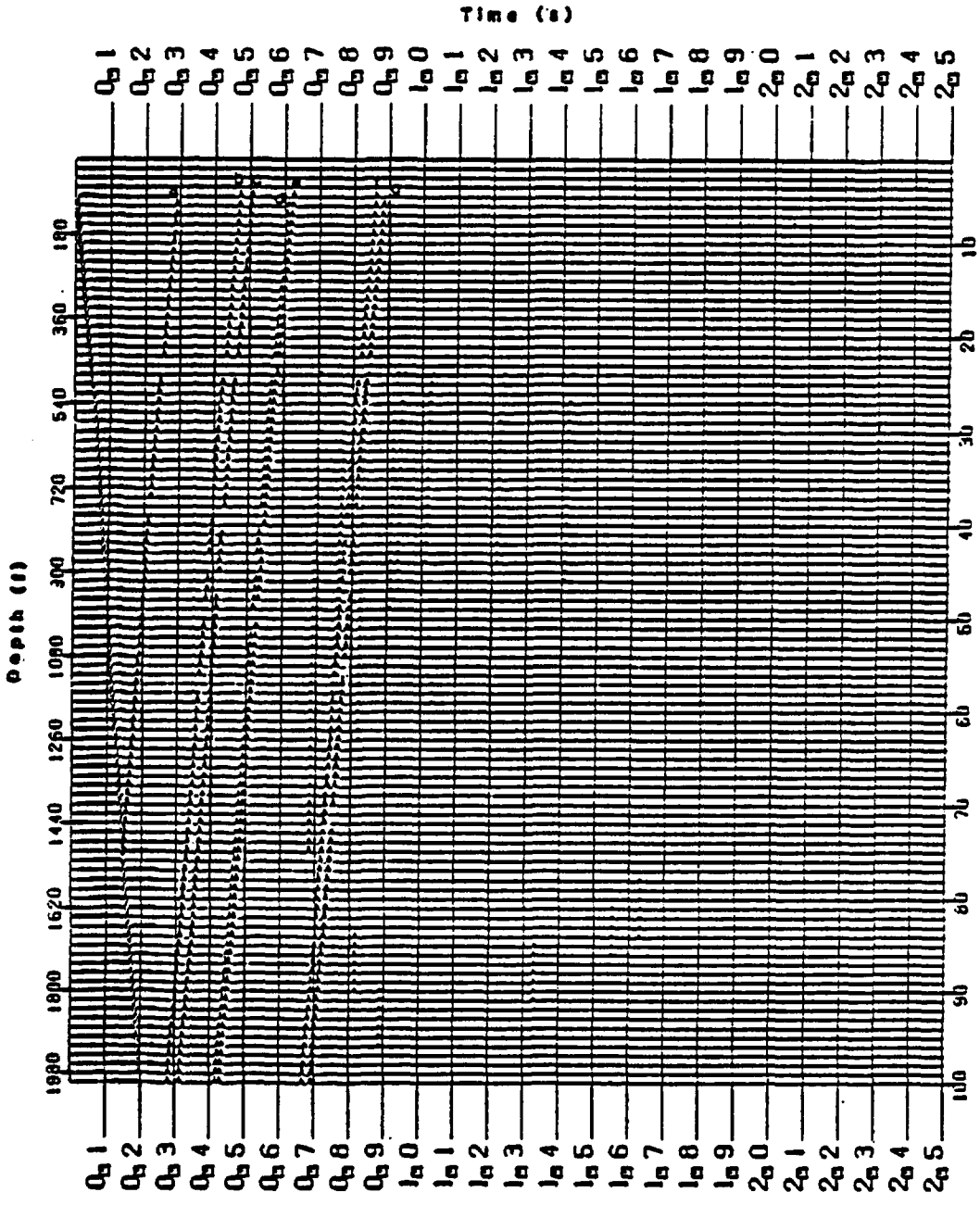

Figure 2.2. Synthetic VSP record for zero-offset source. Reflections are seen from n2(a), Tcbw(b), n3(c), Tctw(d), n4(e), Tlrw(f), and n5(g).

foot horizontal datum at the top of the model. Time is annotated in seconds and increases to the right. All reflected events are shown with positive amplitude. The downgoing first arrivals are seen to have negative amplitude on the data set.

The reflections from boundaries between geologic units are identified on Figure 2.2. The n2 reflection (a) represents the upgoing reflection generated by the boundary between Tptw and n2, for example. The reflections from the seven deepest unit boundaries are clearly seen on this data set. Horizons which intersect the borehole produce reflections which merge with the direct arrival on the VSP at the depth level of the intersection. The n2 reflection can be seen to merge with the direct arrival at 1480 feet below datum in Figure 2.2

An interesting feature of this data set is that reflections from horizons n1 and Tptw do not appear on this data set or on the ray trace diagram in Figure 2.1. Physically, there does not appear to be a reason why these horizons wouldn't produce reflected events on the seismic record. The aperture of ray tracing from the source is restricted to 86 degrees from the vertical in the AIMS ray tracing algorithm. Due to this restriction, computer generated raypaths at this source offset can not reflect off n1 or Tptw and intersect the borehole so that reflected events can appear

on the synthetic data set.

In order to positively identify the remaining events on the data set in Figure 2.2, additional ray tracings were performed using selected horizons in the model. Figure 2.3 shows the zero-offset profile with only fault planes within Tptw designated as reflectors. Other horizons in the model still affect the path of the rays. This is clearly seen by the refraction that takes place early in the path of the rays as they enter and exit n1. n1 is a low-velocity, non-welded tuff sandwiched by the higher-velocity, welded tuffs of Tpcw and Tptw. Once again, this ray diagram shows only rays which converge at every fifteenth receiver location in the borehole in order to make the diagram easier to comprehend.

Figure 2.4 is the VSP data set obtained from the preceding ray tracing. It is not surprising that the high-angle fault planes produce near-vertical reflections on the synthetic data set. Eight of the nine fault planes have produced reflections, with only fault plane 9 not producing an event on the data set. Apparently, rays reflecting off of fault plane 9 are refracted in such a way that none of the rays intersect borehole receivers. The near-vertical appearance of the fault plane reflections on the synthetic data set and the spacing of the events (particularly the reflections from fault planes 4 and 5) make the identification

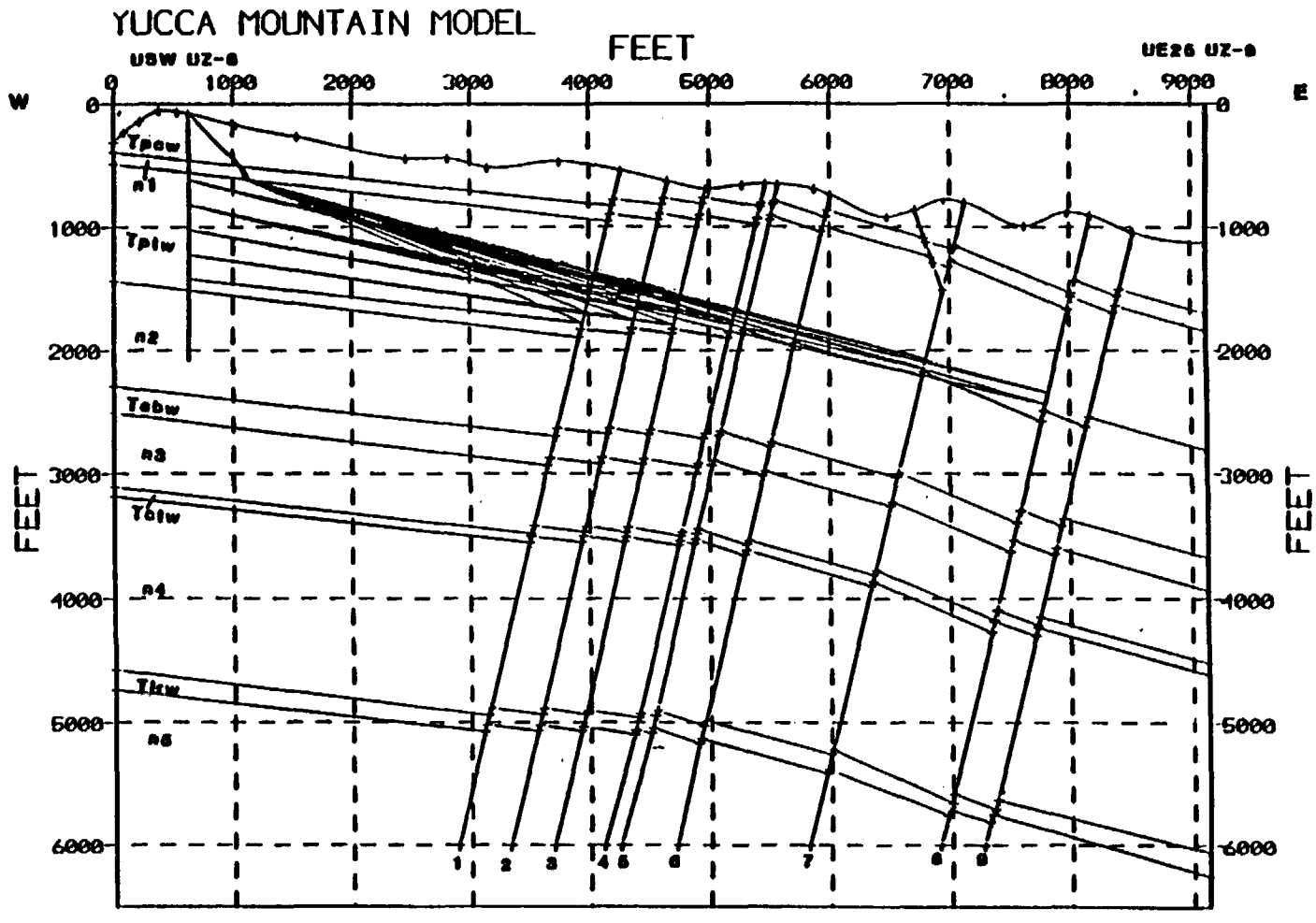

Figure 2.3. Raypath diagram for zero-offset VSP, using only fault plane segments within Tptw as reflecting horizons.

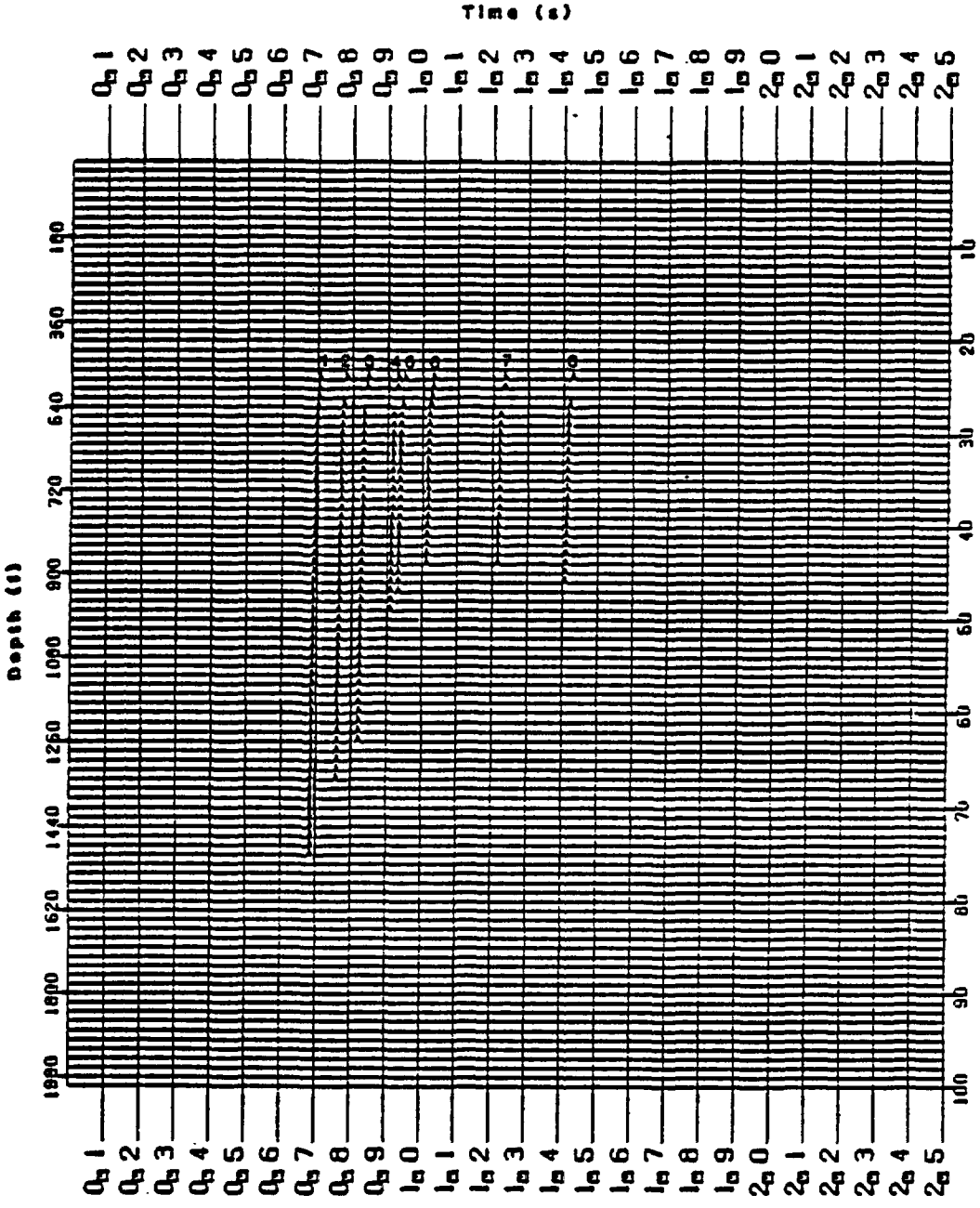

Figure 2.4. Synthetic VSP record created by the ray tracing in Figure 2.3. Eight of the nine high-angle faults produced a reflection on this record. The reflections are characterized by their near-vertical slopes.

of the fault plane reflections obvious on this and on following data sets.

Continuing with the identification of events on the data set in Figure 2.2, a ray tracing was performed using only fault planes within n2 as reflecting interfaces. Figure 2.5 shows a complete diagram of every ray which reflects off of a fault within n2 and arrives at UZ-6. The synthetic data set created by this ray tracing is shown in Figure 2.6. Identifying fault plane reflections from faults below the level of Tptw will be quite difficult. The depth of the borehole and the high angle of the fault planes suggest that only segments of the fault planes contained within Tpcw, n1, and Tptw will be identifiable and important on the remaining data sets. There is not an obvious pattern that can be used to identify all of the small events which are produced from the fault planes within n2.

One additional horizon produced an event on the data set in Figure 2.2. A small segment of fault plane 1, where the top of n3 is offset by 50 feet, produced a large reflection on the data set in Figure 2.2. Figure 2.7 shows a partial ray tracing (every 15th receiver) with only the small segment of fault plane 1 designated as a reflecting horizon. The pattern of velocity changes in the model produces an interesting set of refractions in the upgoing and downgoing segments of the raypaths as they travel down from the source

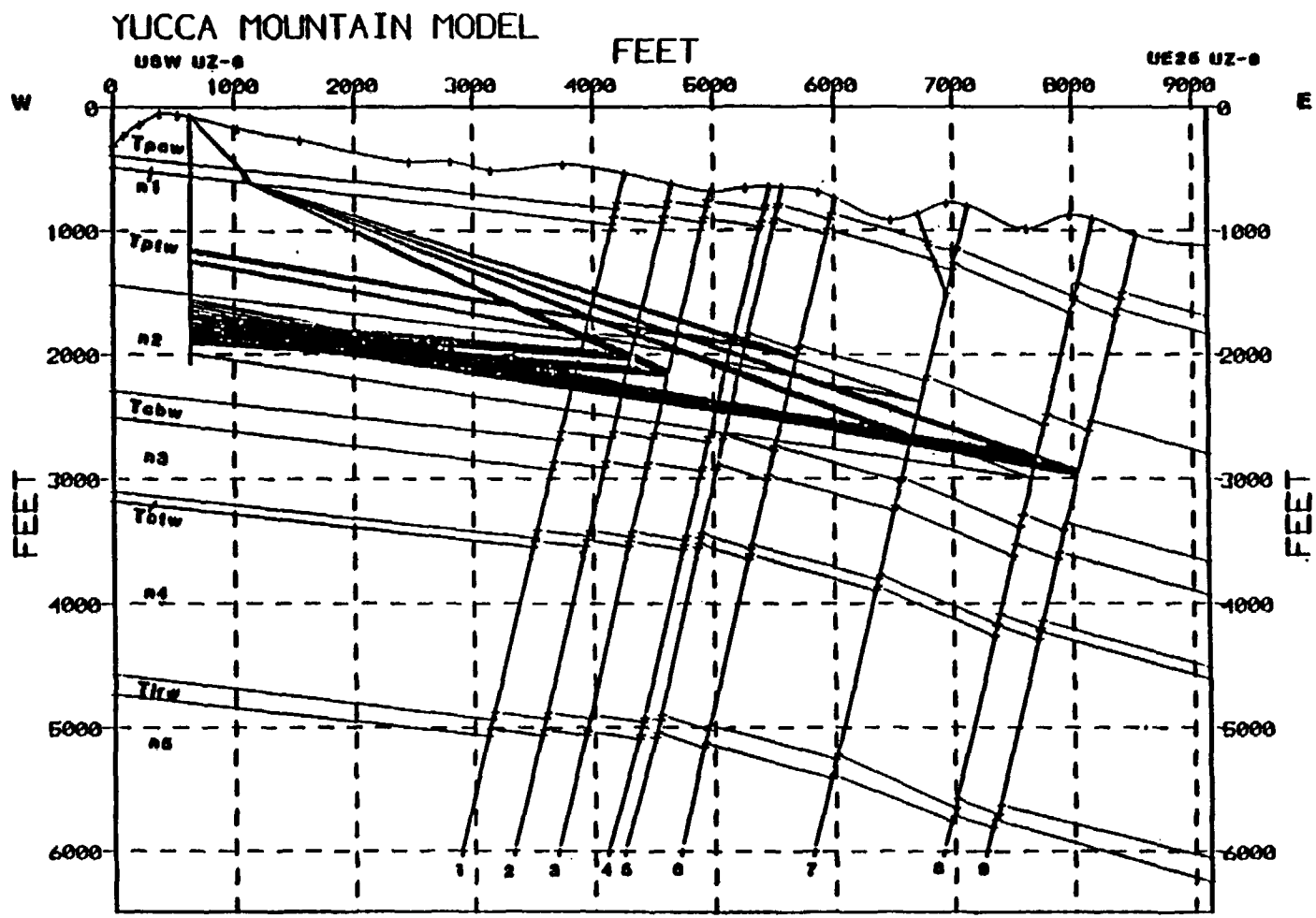

Figure 2.5. Raypath diagram for zero-offset VSP, using only fault plane segments within n2 as reflecting horizons.

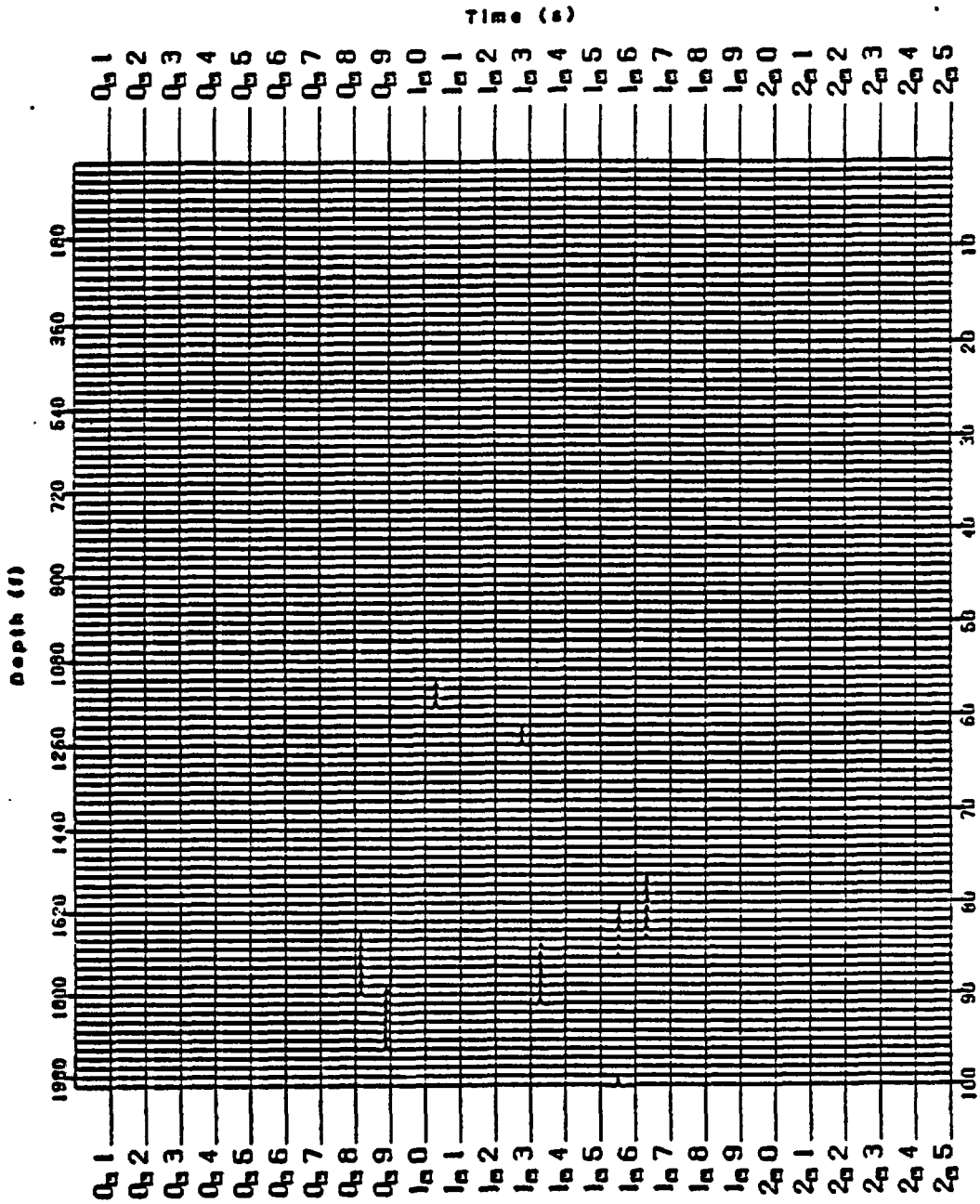

Figure 2.6. Synthetic VSP record created by the ray tracing in Figure 2.5. The reflected events do not show a recognizeable pattern, as did the fault reflections in Figure 2.4.

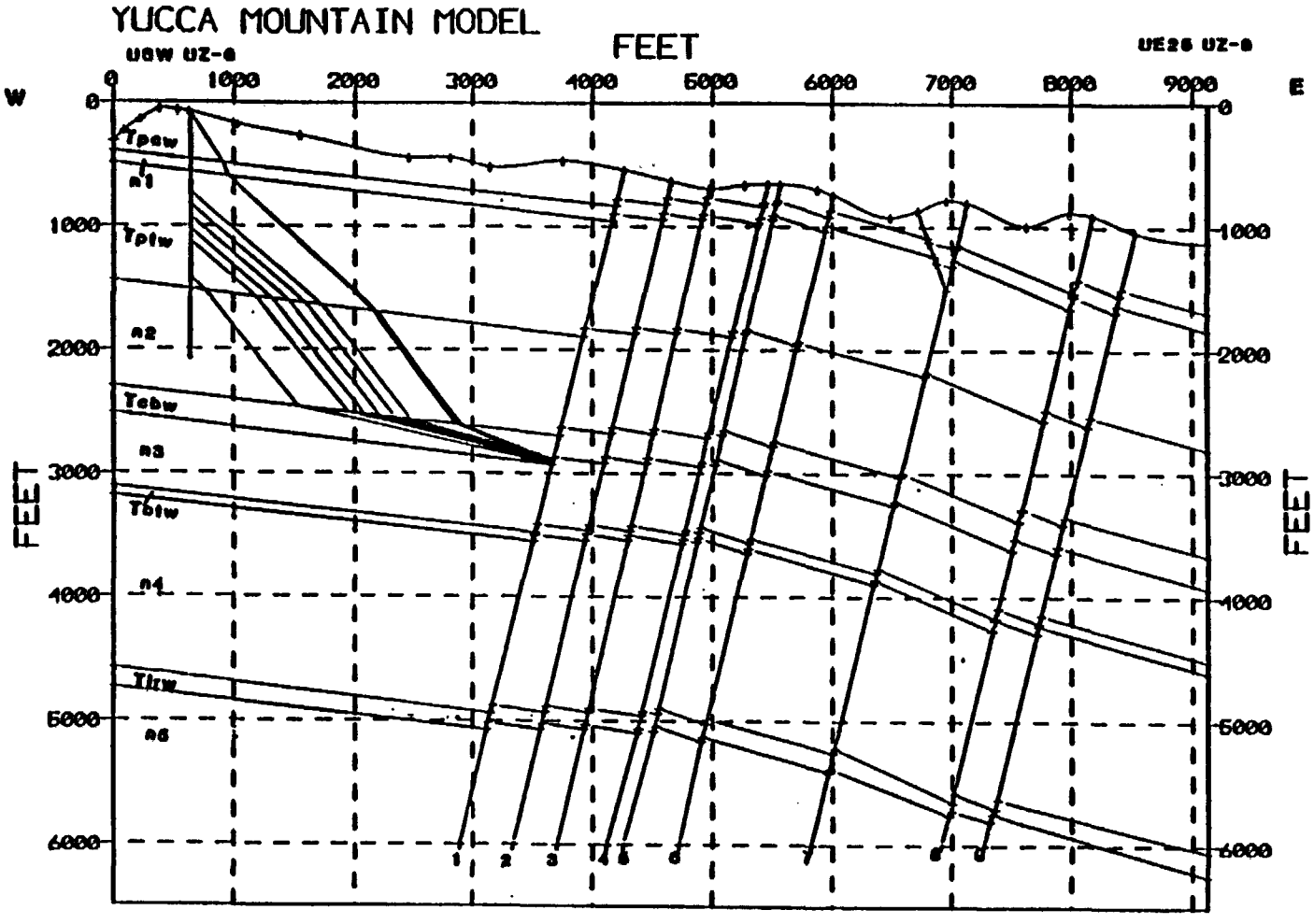

Figure 2.7. Raypath diagram for zero-offset VSP, using only a small segment of fault plane 1 as a reflecting horizon. Refraction at the Tcbw/n2 boundary allows this reflection to reach many receiver locations.

and back up to the borehole. The synthetic data set created by this ray tracing is shown in Figure 2.8. This event is hard to discern from the reflections from fault plane 2 and from horizon Tlrw (f) on the data set in Figure 2.2.

On a VSP data set, it is the reflected energy (upgoing) which is of primary interest for imaging the subsurface. Quite often the direct arrivals (downgoing) do not provide any useful information and are removed from the data set. One of two methods is generally used to separate the upgoing and downgoing wavefields. The first is the application of an FK filter to the data set. When plotted in FK space, selected events can be eliminated using either pie-slice or trapezoidal velocity filters. This method was found to work better for removing residual downgoing energy than for separating wavefields. The second and preferred method of separating the upgoing and downgoing energy is the use of the median filter.

The median filter works by preserving events which lie along lines of equal time in a VSP data set. For example, a 5-fold median filter works by finding the median value of the first sample from each of the first five traces in the data set. This median value becomes the first sample value for a brand-new trace one. Next, the second sample value from each of the first five traces is analyzed and a second median value is determined. This value becomes the second

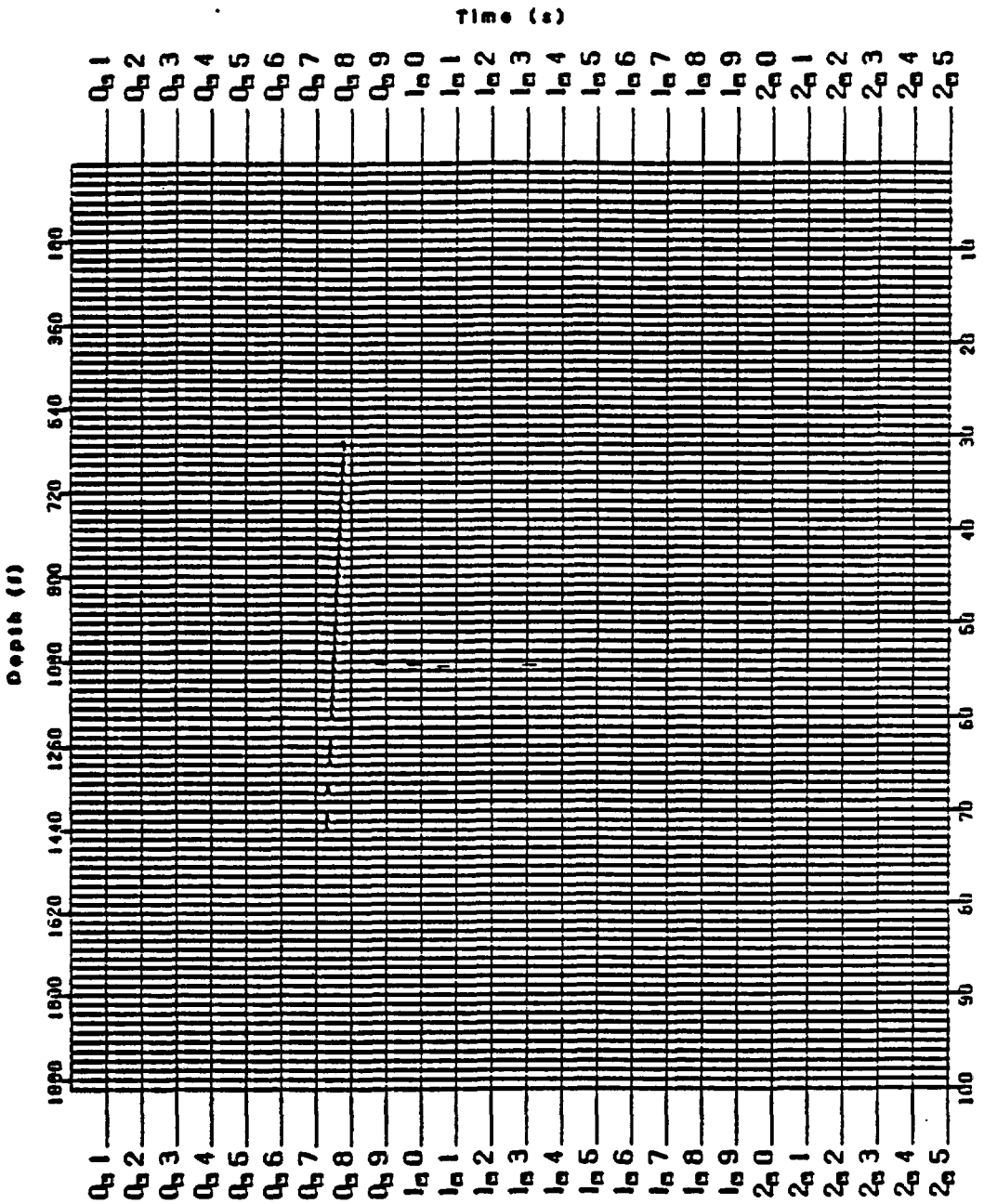

Figure 2.8. Synthetic VSP record created by the ray tracing in Figure 2.7. This event interferes with the Tlrw and fault plane 2 reflections on the data set in Figure 2.2.

sample value for the brand-new trace one. The process continues until the end of the trace is reached. The window then shifts to traces two through six, and another new trace two is created in the same manner. The filtering continues until an entire new data set has been created.

The median filter preserves events which lie along lines of equal time since each of the five samples will have roughly the same value. Events which do not lie along lines of equal time will tend to be canceled during the filtering.

In order to use the median filter to separate the upgoing and downgoing wavefields, it is necessary to have the direct arrivals aligned along a line of equal time. As seen in Figure 2.2, the first arrivals clearly do not lie along a line of equal time. The VSP processing package VSEIS, residing on the GOULD 9750 at the Colorado School of Mines, was used for all data processing in this thesis. VSEIS contains a processing module named GTIM, which allows a user to interactively pick times of events from individual traces. By picking the first arrival time from each trace in the data set, it is possible to shift each of the traces so that the first arrivals lie along a line of equal time. Figure 2.9 shows the data set shifted such that the direct arrivals lie along the 0.1 second time line. The reflected events have a pronounced slope and do not line up along lines of equal time.

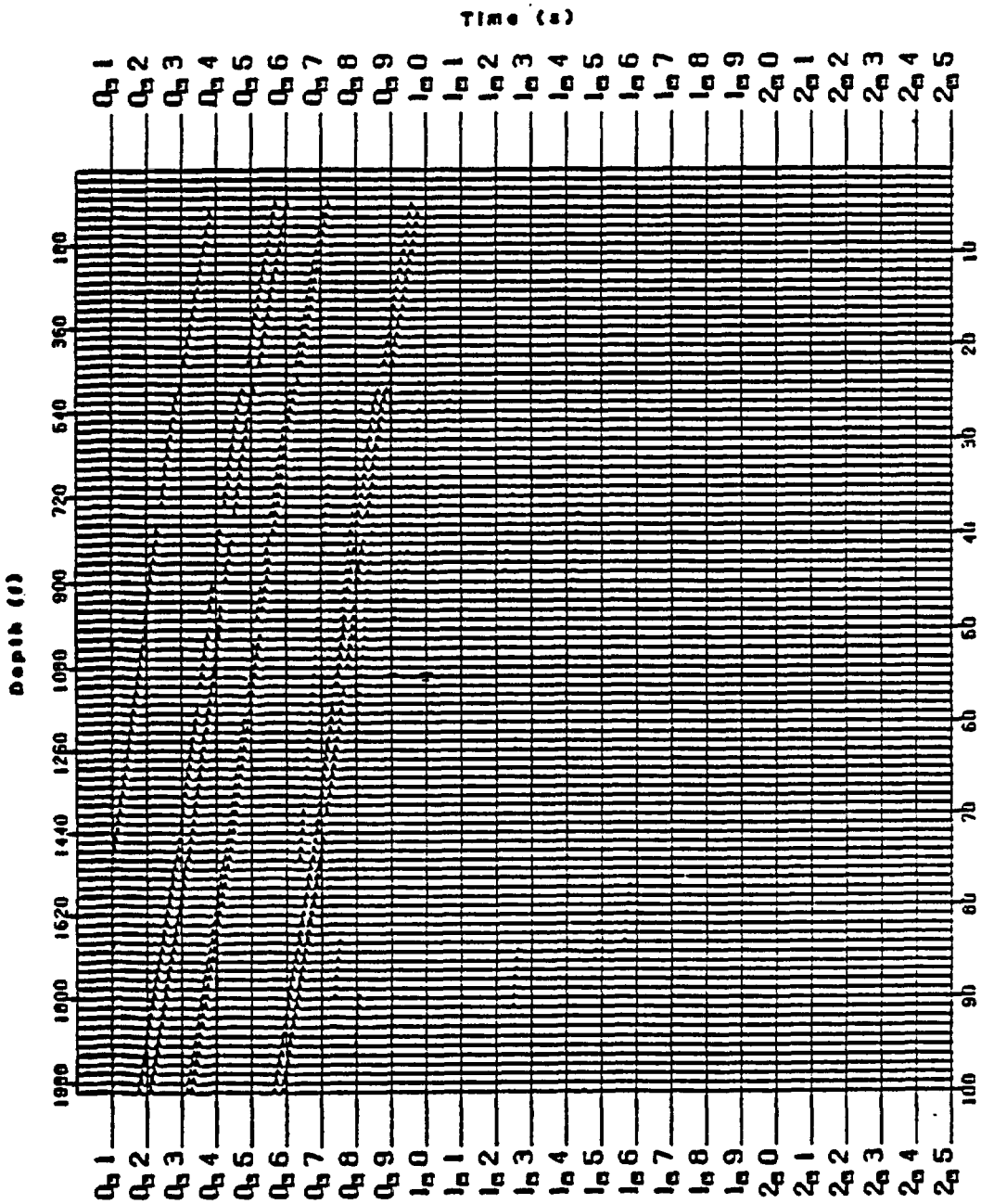

Figure 2.9. Synthetic VSP record for zero-offset source, with the direct arrivals aligned at 0.1 second in preparation for spatial median filtering.

The effectiveness of the spatial median filter is increased by scaling the events aligned along the 0.1 second time line so that the amplitudes of the aligned events are consistent from trace to trace. Figure 2.10 shows a data set created by applying a 7-fold median filter to the data set in Figure 2.9. The first arrivals clearly have been preserved along the 0.1 second time line. Unfortunately, this data set also contains a fair amount of reflected energy in addition to the first arrivals. In order to obtain the upgoing wavefield, it is necessary to subtract the output from the median filter from the original shifted data set. In this way, all events preserved by the median filter (such as direct arrivals) are removed from the original data set. Since the output from the median filter preserved more than just the first arrivals, subtracting the output from the original data set would cause a loss of valuable signal.

The reflections from Tctw and n4 are very close together on Figure 2.9, as are the reflections from Tlrw and n5. The median filter operates because the upgoing reflections have a pronounced slope and do not lie along lines of equal time. Since the reflections from these horizons are close together, the cancellation of the dipping events during filtering is not as effective and, unfortunately, a portion of the two reflections is preserved as one event on the median filter output. More unfortunate is the observation that portions

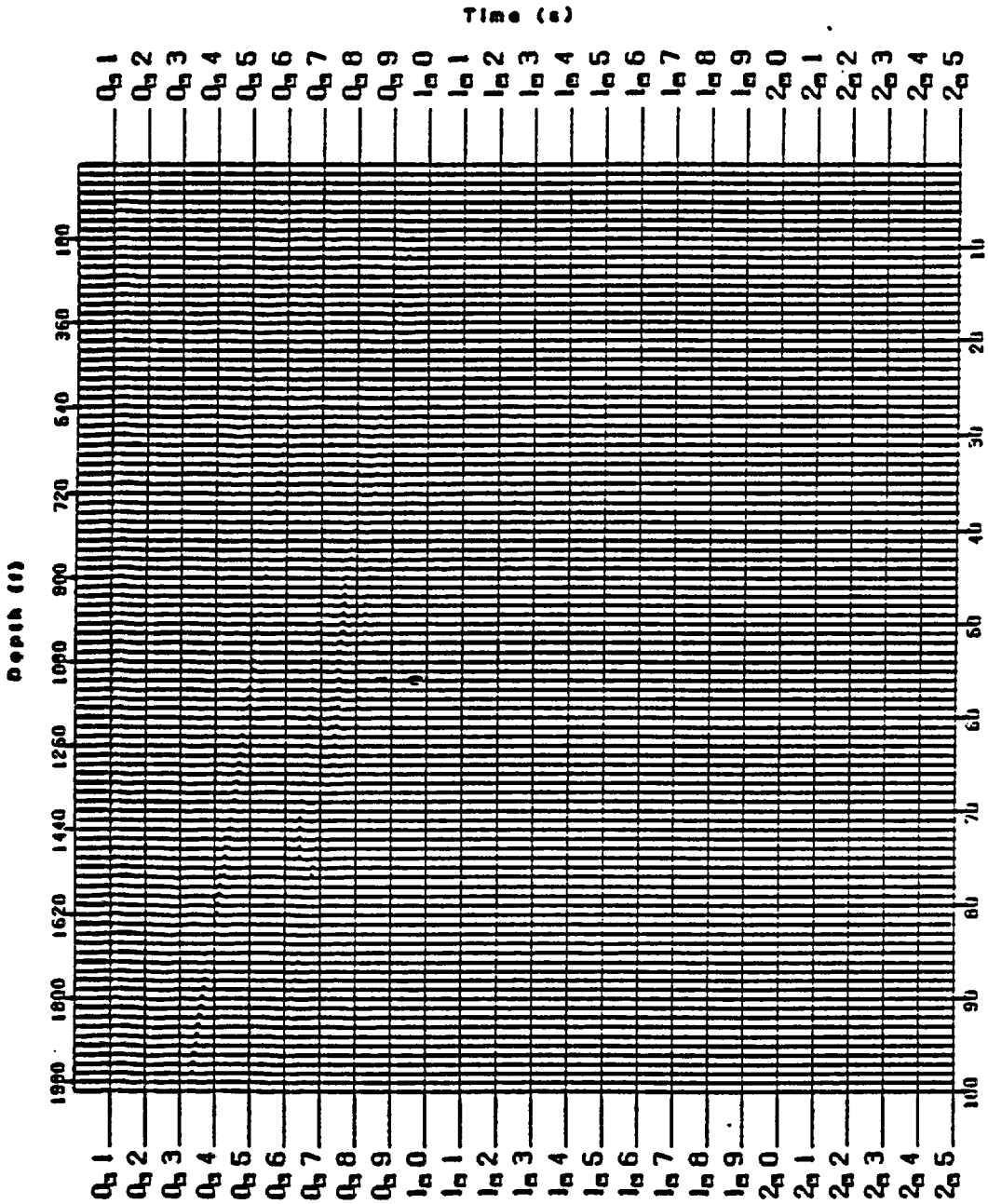

Figure 2.10. Synthetic VSP record for zero-offset source after applying a 7-fold median filter. The first arrivals have been preserved along the 0.1 second time line. Energy from other events can also be seen. Since this record is subtracted from the original record, any energy present (other than the direct arrival) will cause a loss of signal quality.

of the fault plane reflections were also preserved by the filter. These reflections are particularly vulnerable, since their slopes fall in between the slope of the direct arrivals and the slope of the other reflections. The fault plane reflections are already weak, and losing additional information during median filtering could hamper interpretation.

In order to combat the loss of fault plane energy from the data, a higher fold median filter is necessary. As the fold of the median filter increases, only events which are very carefully aligned are preserved. Figure 2.11 shows the output from a 9-fold median filter. Once again, the direct arrival has been preserved very well. The amount of reflected energy has been significantly reduced compared to the output of the 7-fold median filter in Figure 2.10. Still, a small amount of upgoing energy exists in this data set, energy that would be lost if this data set were subtracted from the original data set to obtain the upgoing wavefield.

Figure 2.12 shows the output from an 11-fold median filter. This data set contains very little information, other than the first arrivals aligned along the 0.1 second time line. Only a small amount of the T1rw/n5 reflections was preserved by the median filter. The 11-fold filter was selected as satisfactory for the separation of the upgoing and downgoing wavefields.

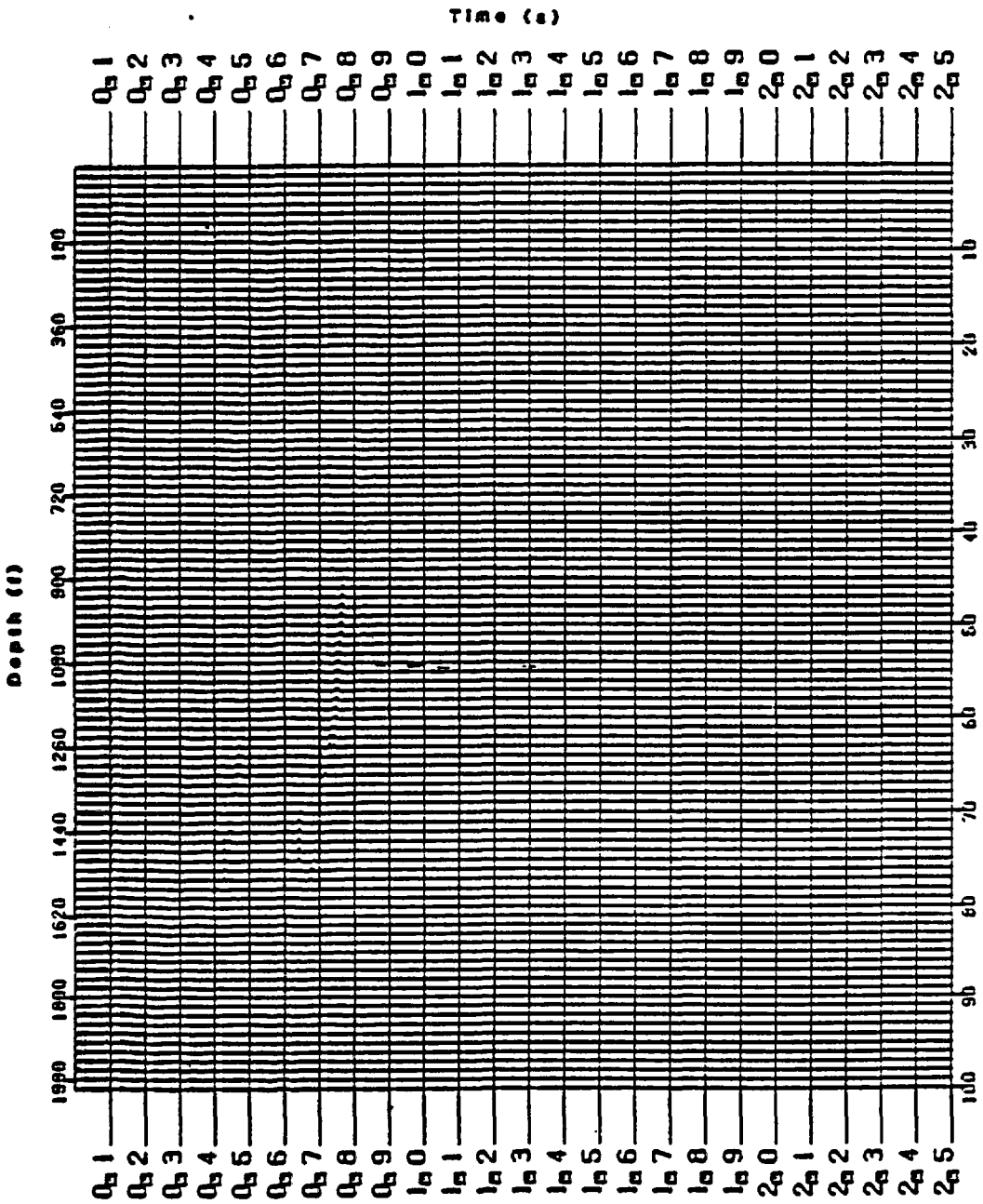

Figure 2.11. Synthetic VSP record for zero-offset source, after applying a 9-fold median filter. The direct arrivals have been preserved along the 0.1 second time line. Energy from reflected events can still be seen on this record.

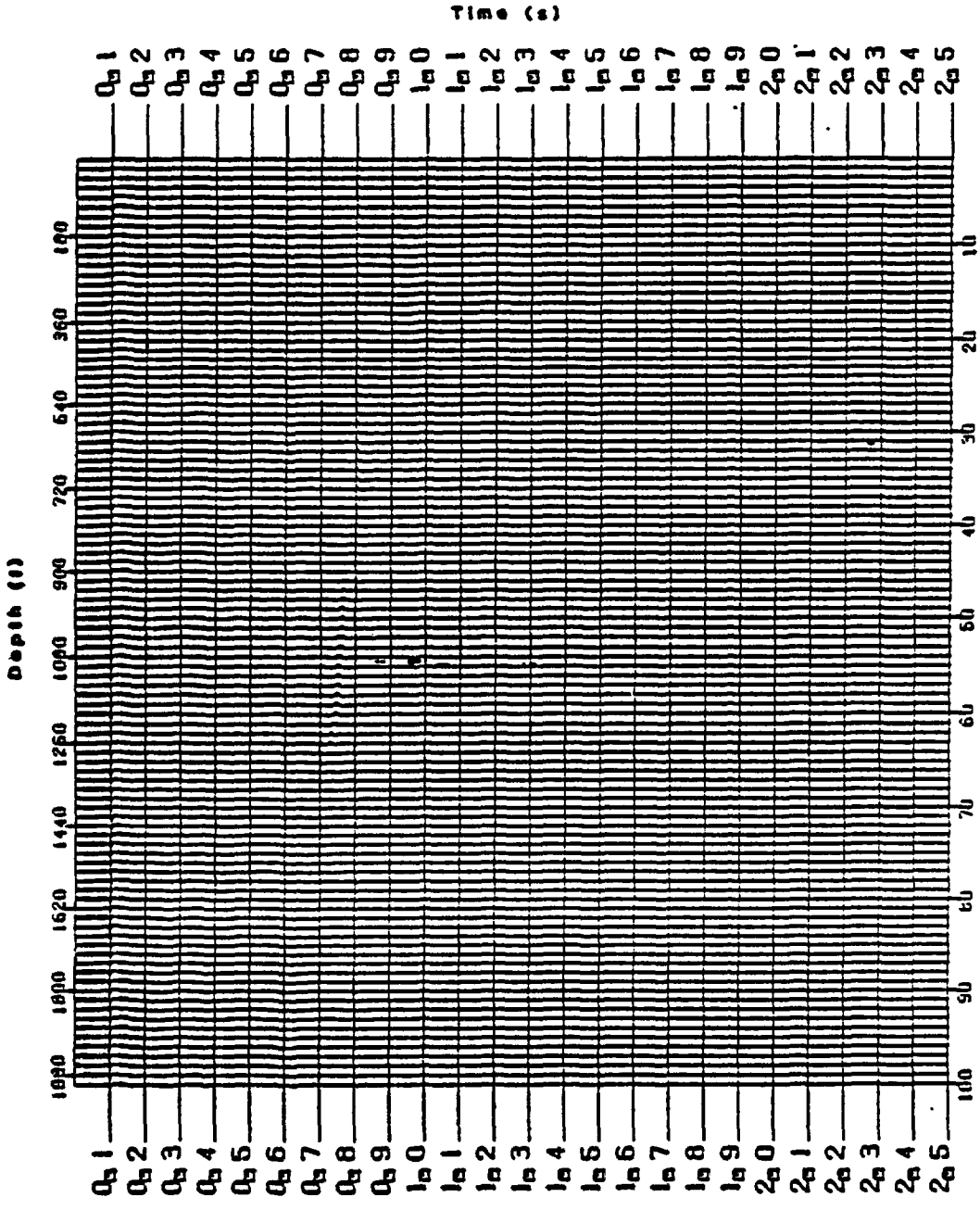

Figure 2.12. Synthetic VSP record for zero-offset source after applying an 11-fold median filter. Very little energy appears on this record, other than the direct arrivals. An 11-fold filter was chosen as adequate for separating the wavefields.

Figure 2.13 shows the original data set shifted back to its proper time base after subtracting the output of the 11-fold median filter. The strong first arrivals have lost most of their amplitude, and the data set contains primarily reflected information. Reflected events have survived the wavefield separation with only minor losses.

Since the identification of fault plane reflections is a major goal of the VSP experiments at Yucca Mountain, it is suggested here that great care be taken to choose the proper median filter fold when separating wavefields. The near-vertical slope of the fault plane reflections on the VSP records requires that the median filter be of sufficiently high fold. A median filter fold of 11 is used throughout the rest of this paper, except where a different filter fold has been specified.

It is entirely possible that the fault planes at Yucca Mountain will not act as reflecting horizons which can be imaged by a vertical seismic profile. The ray tracing for the zero-offset VSP at UZ-6 was repeated with the exclusion of the zero reflection coefficient fault segments as reflecting horizons. In addition to removing these fault plane segments from the ray tracing, the program card which controls the effect of the reflection coefficient was turned on in the AIMS module SPGENR. This allowed the effects of density contrasts between horizons to be incorporated into the

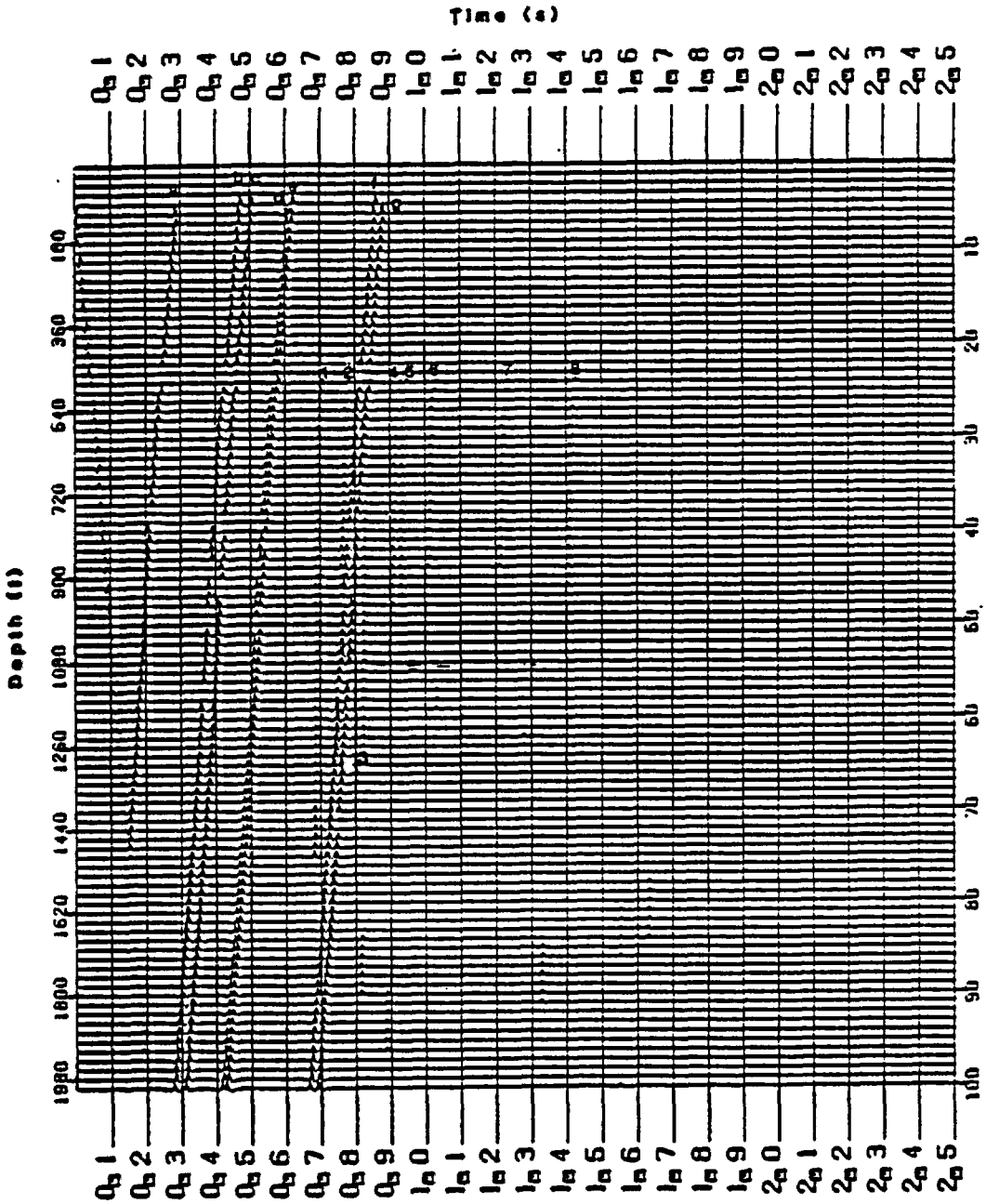

Figure 2.13. Synthetic VSP record for zero-offset source after removing the direct arrivals. Reflections are seen from n2(a), Tcbw(b), n3(c), Tctw(d), n4(e), Tlrw(f), n5(g), and from fault planes 1 through 8.

model. Figure 2.14 shows a ray trace diagram, excluding the zero reflection coefficient fault planes. Only the small segment of fault plane 1 which has different units across the fault plane was included during this ray tracing.

The synthetic data set created by the preceding ray tracing is shown in Figure 2.15. The direct arrival dominates the data set, with only a hint of the upgoing energy appearing on the traces. To overcome the low amplitudes of the reflections, an AGC (automatic gain control) was applied to the data set. The data set, after applying the AGC, appears in Figure 2.16. The reflected events in Figure 2.16 are much more prominent than those in Figure 2.15.

Since the traces are scaled by the highest amplitude event on the trace, the direct arrivals still dominate. The first arrivals were aligned along the 0.1 second time line and removed from the data set with an 11-fold median filter. The upgoing wavefield is shown in Figure 2.17. The effect of the reflection coefficient gives this data set a decidedly different appearance from the data set in Figure 2.13. In Figure 2.17, reflections have their polarities represented properly, instead of every event having a positive amplitude. Reflections from the tops of welded units are seen as peaks on this data set. Reflections from the tops of non-welded units are seen as troughs.

An important boundary to identify on the VSP records

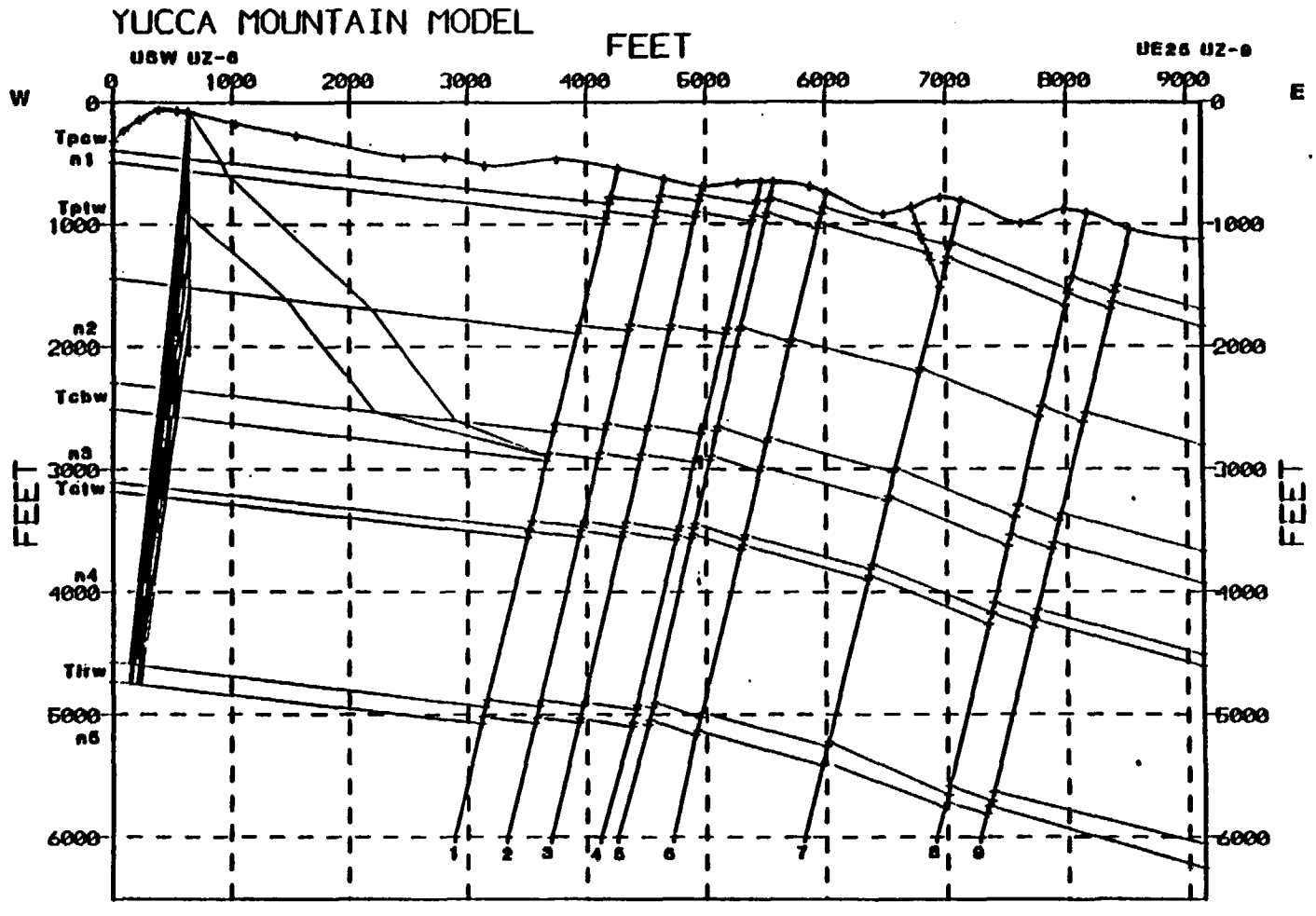

Figure 2.14. Raypath diagram for zero-offset VSP, excluding reflections from zero reflection coefficient fault planes.

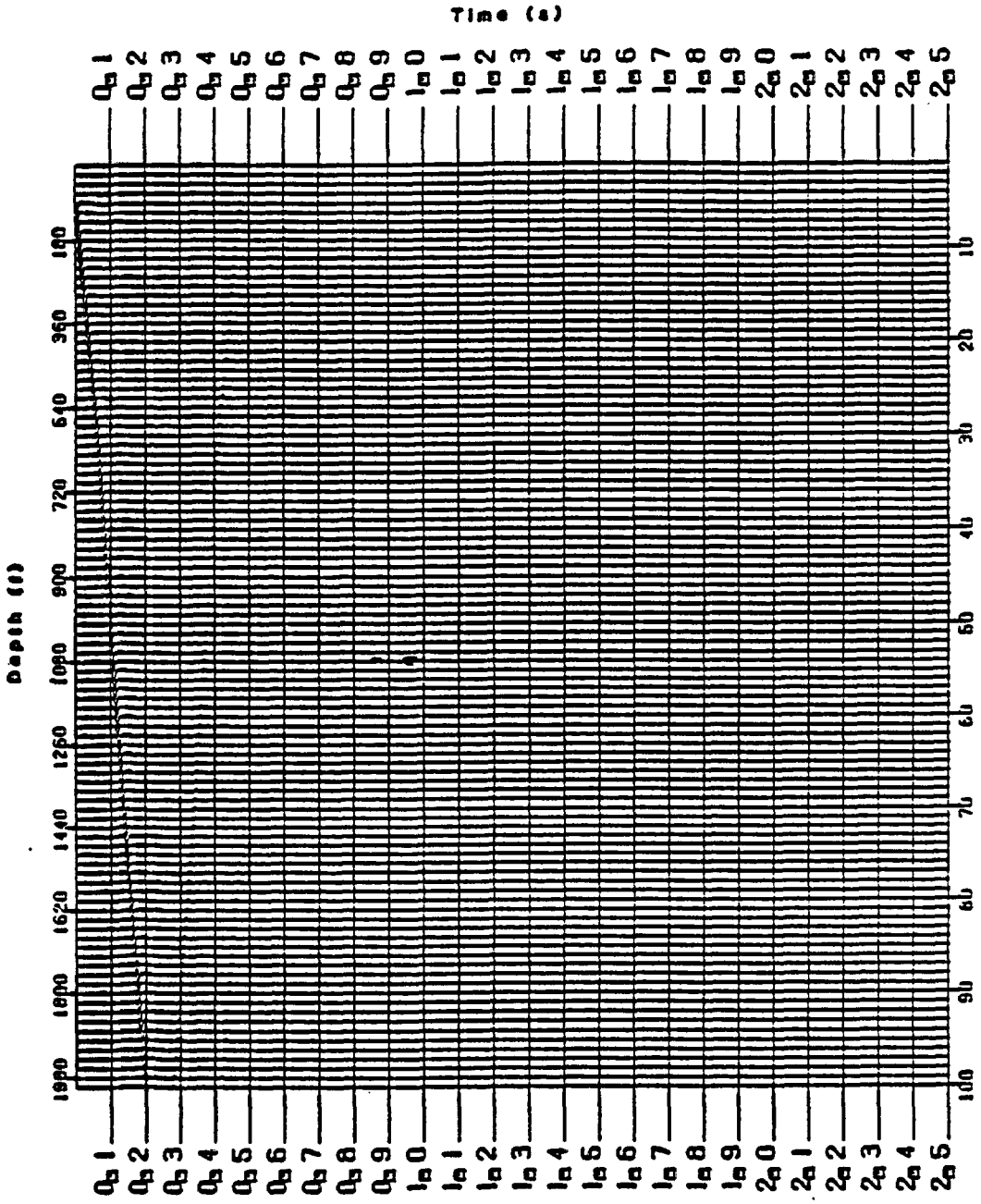

Figure 2.15. Synthetic VSP record generated by the ray tracing in Figure 2.14. The first arrival trough dominates the record. Upgoing reflections are very faint.

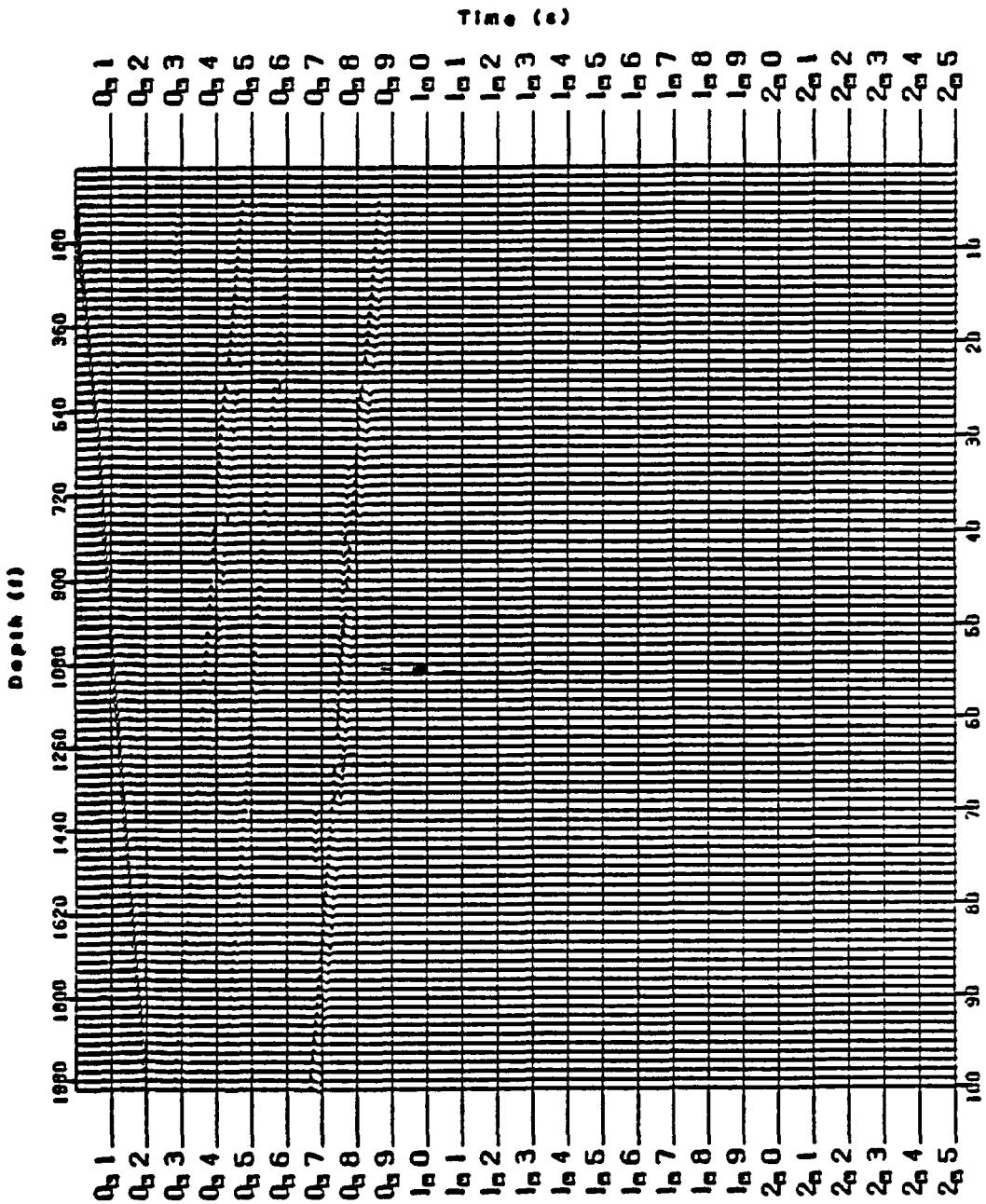

Figure 2.16. Synthetic VSP record for zero-offset source after applying AGC. The upgoing reflections are now visible. Welded tuffs are represented by peaks. Non-welded tuffs are represented by troughs.

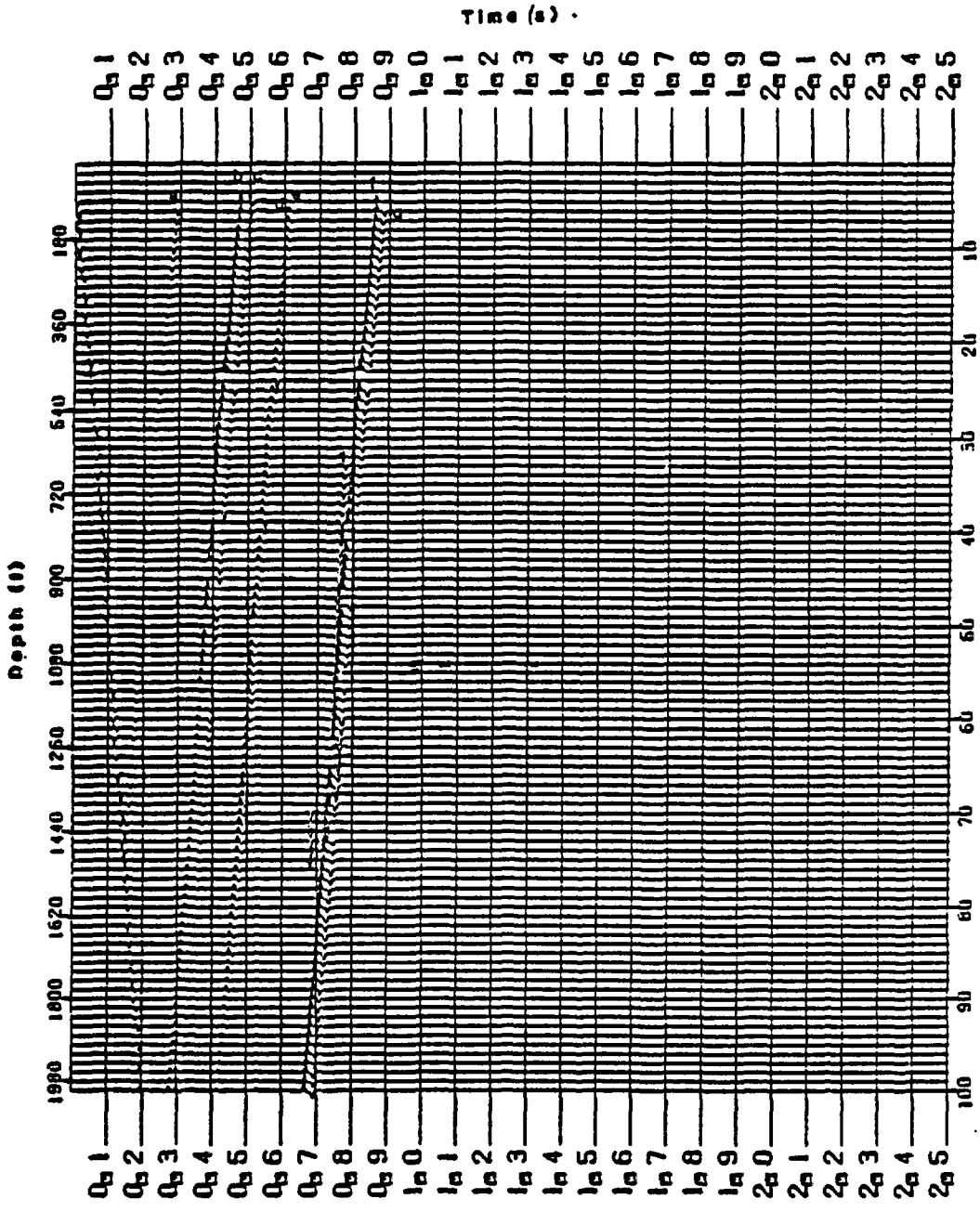

Figure 2.17. Synthetic VSP record for zero-offset source after removing the direct arrivals. Reflections are seen from n2(a), Tcbw(b), n3(c), Tctw(d), n4(e), Tlrw(f), and n5(g). A small segment of fault plane 1 is visible to the left of the Tlrw reflection.

from Yucca Mountain will be the interface between Tptw and n2 (a). This interface represents the bottom of the potential waste repository unit at Yucca Mountain. On the data set in Figure 2.17, this boundary produces a weak reflection. The velocity and density contrasts across the horizon produce a reflection coefficient of -0.173, which is one of the smaller reflection coefficients contained in this model. By tailoring the AGC window to suit this problem, the amplitude of this important reflection could be increased if the event was so small that the reflection could not be clearly seen.

Since the Tram Member of the Crater Flat Tuff (Tctw) is thin, the source wavelet would need to contain 150 hz for events (d) and (e) to appear separately. A gap can be seen between the top (b) and bottom (c) of the Bullfrog Tuff and the top (f) and bottom (g) of the Lithic Ridge Tuff. Increasing the frequency content of the source wavelet would increase the resolution of all boundaries in this model. To increase the frequency content, the sampling interval would have to be changed from 4 ms to 2 ms, however.

The reflection from the small segment of fault plane 1 is easy to identify as the trough arriving slightly before the Tlrw peak on the data set.

2.3 1000-foot source offset VSP

The VSP activity at Yucca Mountain will consist of multiple offsets along several azimuths. The modeling in this thesis is performed only along the line between boreholes USW UZ-6 and UE25 UZ-9. Figure 2.18 shows the raypath diagram for a source 1000 feet east of borehole UZ-6. The rays which intersect every fifteenth receiver location are shown. Reflections off horizons n1 and Tptw can be seen, unlike the zero-offset ray tracing (Figure 2.1) where AIMS was unable to overcome the aperture problem and produce the reflected raypaths. Reflected raypaths are not seen from horizons Tlrw and n5. This is partially due to the aforementioned aperture problem, and to the fact that only raypaths for every fifteenth receiver location are included in this diagram. A few reflected rays actually do bounce off these two horizons and intersect the borehole.

All nine of the vertical faults are producing reflected rays in Figure 2.18. Small segments of the fault planes within Tcbw produce many reflections which are refracted strongly as they leave Tcbw and enter n2.

Figure 2.19 is the synthetic data set produced by the preceding ray tracing. The strong direct arrival appears as the initial trough on the entire data set. The trough does not appear on every trace, however. The trough is not seen until the nineteenth trace in the data set. This is due

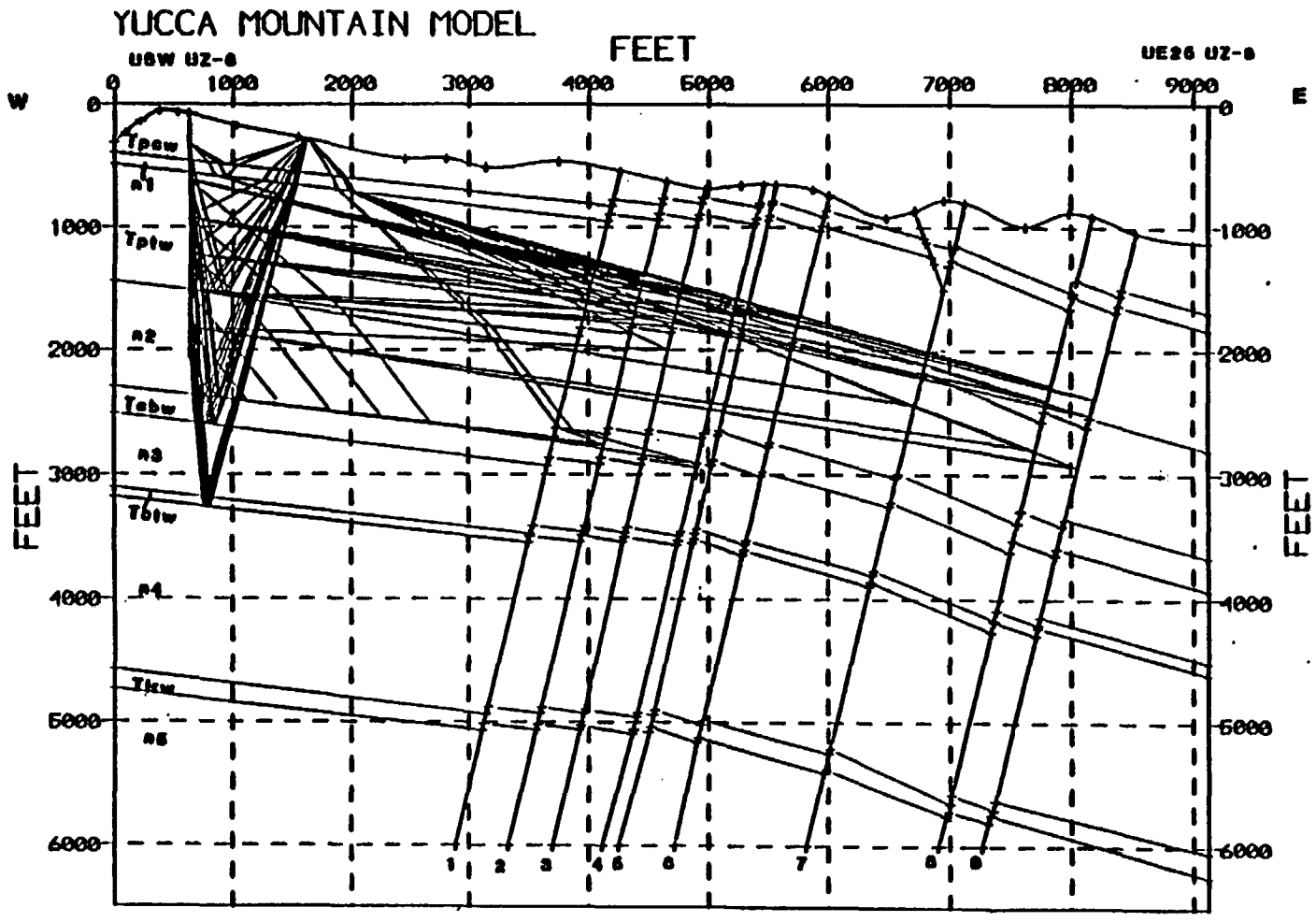

Figure 2.18. Raypath diagram for a 1000-foot source offset VSP.

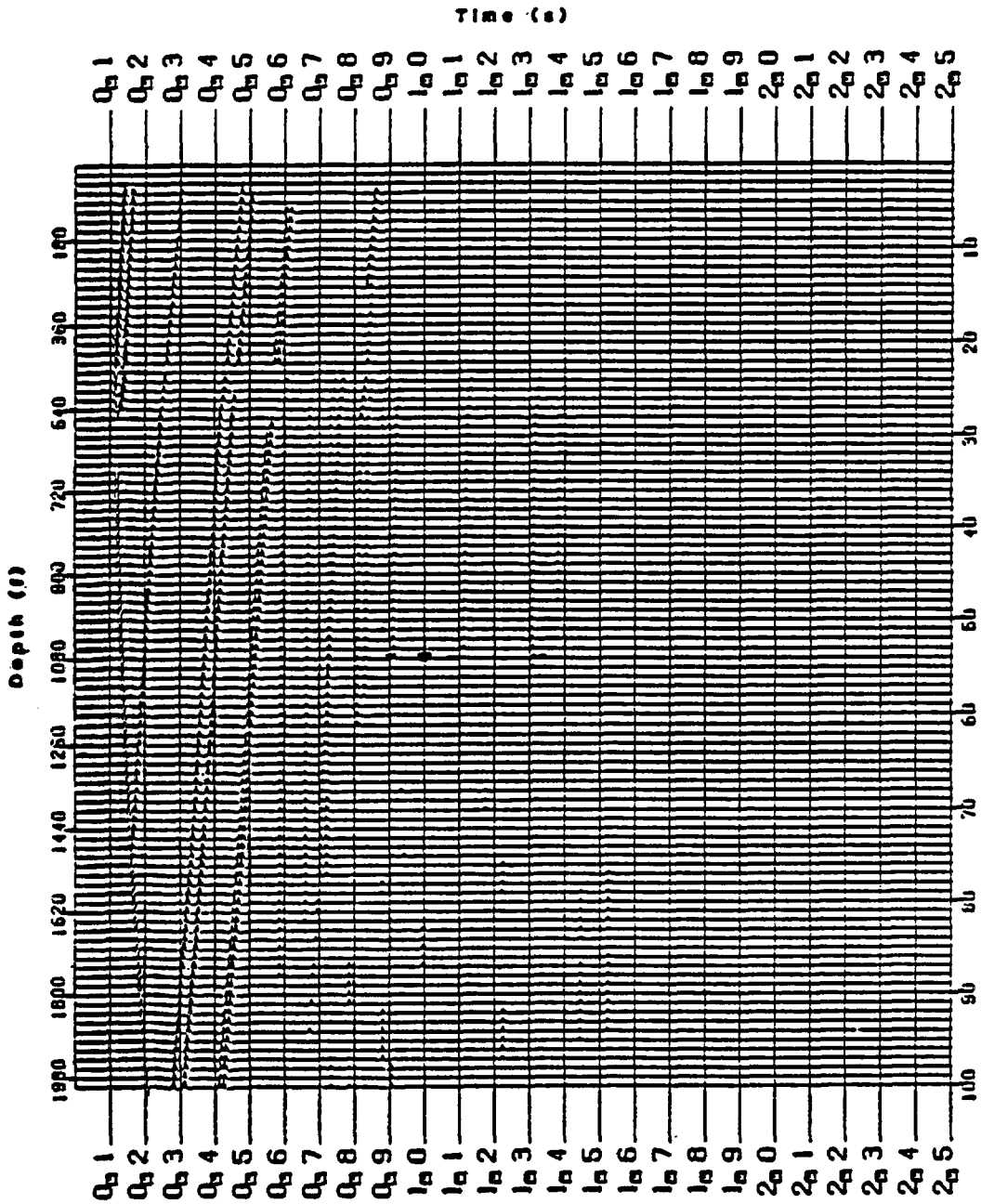

Figure 2.19. Synthetic VSP record generated by the ray tracing in Figure 2.18. The direct arrival trough is seen on traces 19 through 28 and traces 34 through 100.

to the decrease in the source elevation with respect to the surface elevation of the borehole. The AIMS ray tracing algorithm makes a distinction between upgoing and downgoing raypaths. For this reason, first arrival raypaths cannot travel to a receiver higher than the elevation of the source. The second gap in the string of first arrival troughs occurs between traces 28 and 33. This gap results from a critical refraction of the direct arrival at the Tptw horizon. Refraction at this interface prevents rays from intersecting the borehole throughout this 120 foot interval.

The downgoing trough was removed from the data set with a median filter. In order to keep the data set as unaltered as possible, the traces were broken into groups before filtering. Only groups which contained the first arrival trough were filtered. Traces 19 through 28 were isolated and filtered with a 7-fold median filter. Traces 34 through 100 were filtered with an 11-fold median filter. The resulting traces were recombined with the unfiltered traces to produce a data set with the first arrivals removed. This data set is shown in Figure 2.20. This technique of filtering only traces containing the first arrival was employed throughout this thesis.

The upgoing wavefield in Figure 2.20 shows reflections from each of the nine unit boundaries. Reflected events from n1 (a) and Tptw (b) are apparent on this data set,

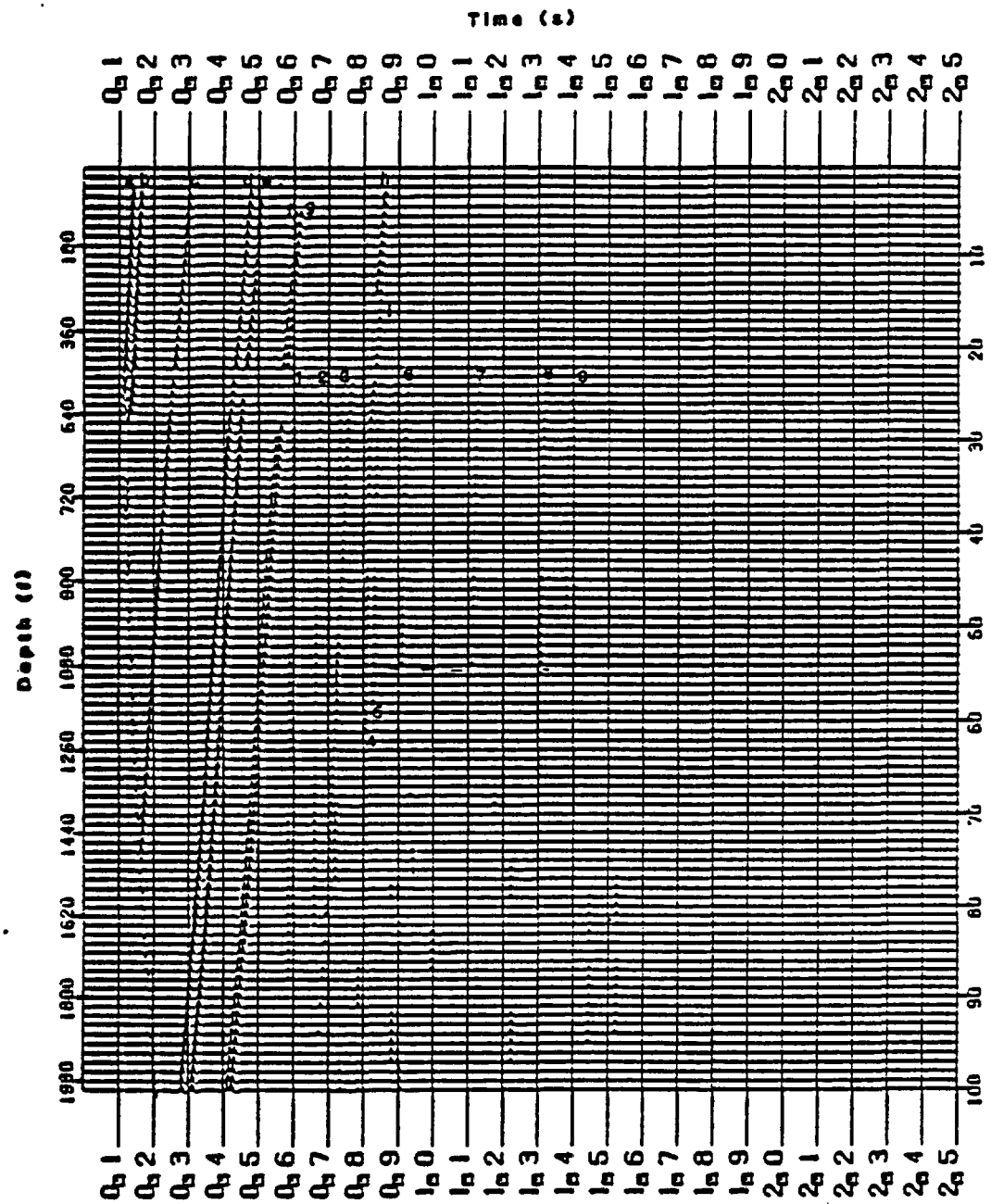

Figure 2.20. Synthetic VSP record for 1000-foot source offset with the direct arrivals removed. Reflections are seen from n1(a), Tptw(b), n2(c), Tcbw(d), n3(e), Tctw(f), n4(g), Tlrw(h), n5(i), and from fault planes 1 through 9. The faults are identified by their near-vertical slopes.

unlike the zero-offset traces. The events from Tlrw (h) and n5 (i) are recorded only by the highest receivers in the borehole. As seen previously, this is due to the restricted aperture of the AIMS seismic source. Physically, there does not appear to be a reason why the two horizons would not produce a reflection at most of the receiver locations.

The reflections from the nine vertical fault segments within Tptw are easily identified on this data set. The spacing of the reflections and their near-vertical slopes are a consistent indicator on every data set that the fault planes are the source of these events. Small segments of fault planes 2 and 4 within Tcbw produce events at many receiver locations on the data set. Segments of the fault planes within n2 produce scattered events on the lower traces in the data set. These events are much more difficult to identify, although fault planes 8 and 9 within n2 produce very coherent events on traces 77 through 94.

The ray tracing for the 1000-foot source offset was repeated with the zero reflection coefficient fault planes turned off. Once again, segments of fault planes which possessed non-zero reflection coefficients were left to produce reflections. Figure 2.21 shows the raypath diagram for this model. In addition to the reflections coming from the gently dipping unit boundaries near the borehole, three small segments of fault planes are producing reflections. It is

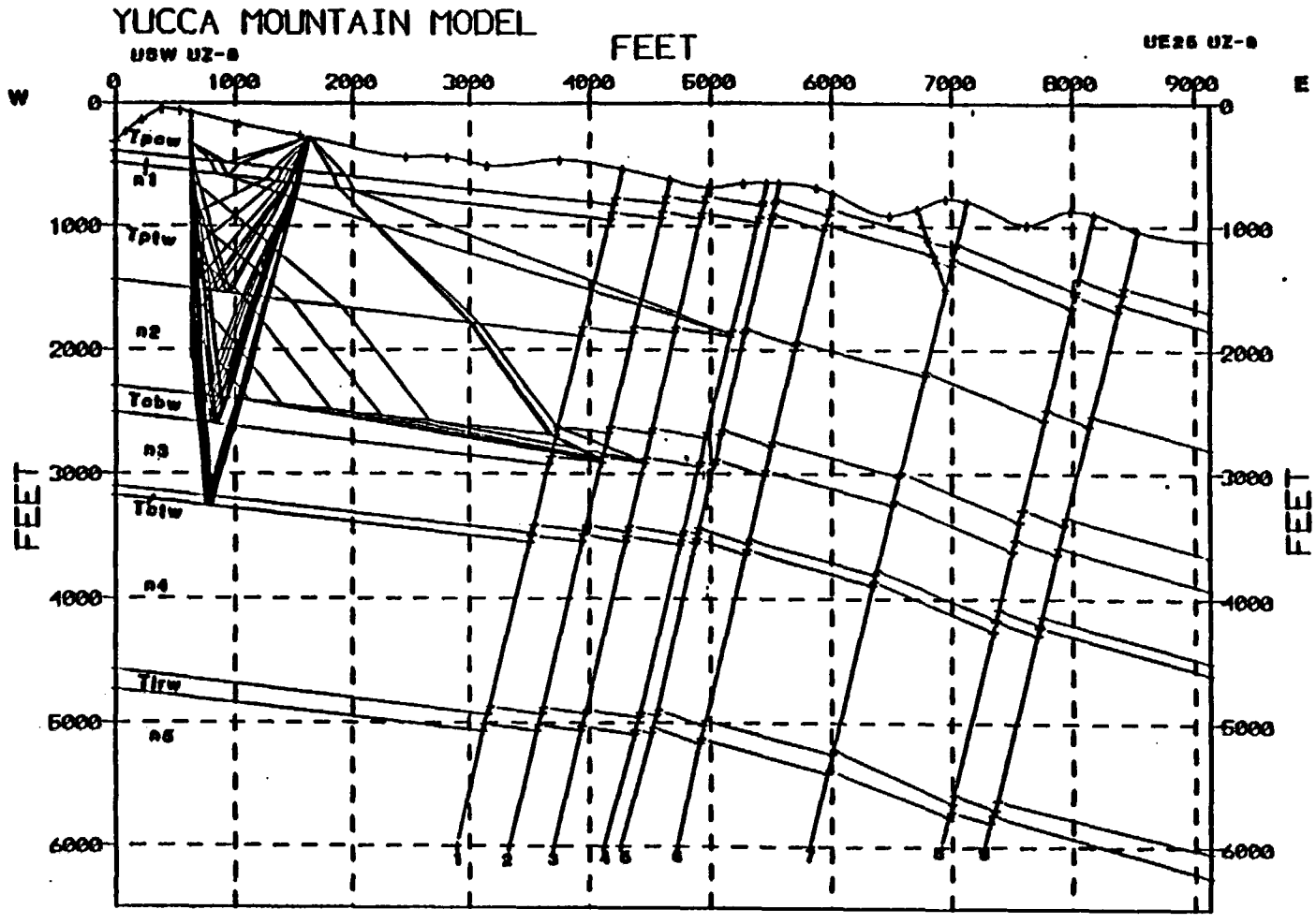

Figure 2.21. Raypath diagram for 1000-foot source offset VSP, excluding reflections from zero reflection coefficient fault planes.

possible that other fault segments produce reflections as well, since this diagram shows only rays that intersect every fifteenth receiver location in the borehole.

Figure 2.22 shows the synthetic data set created by the preceding ray tracing after an AGC had been applied. The technique of splitting the data set into sections containing the first arrival trough and median filtering each section separately was applied, as was done for the data set in Figure 2.19. After the traces were recombined, the data set minus the direct arrivals is displayed in Figure 2.23. As seen in Figure 2.17, the non-welded tuffs produce a trough while welded tuffs produce a peak. The thickness of the units controls the interpreter's ability to distinguish between reflections from the top and bottom. An identifiable spacing occurs between the top of n1 (a) and the top of Tptw (b). The same is true for Tcbw (d) and n3 (e). The peak-trough pair that represents the top (f) and bottom (g) of Tctw once again shows destructive interference. Using a finer sampling interval and increasing the bandwidth of the source wavelet would alleviate much of the interference.

The fault plane reflections from within Tcbw are seen as large troughs (j) on this data set from trace 36 to trace 100. Since the reflected rays are refracted at the top of Tcbw, the rays bend upward. The result is an event which has a slope similar to the slope of the unit boundary

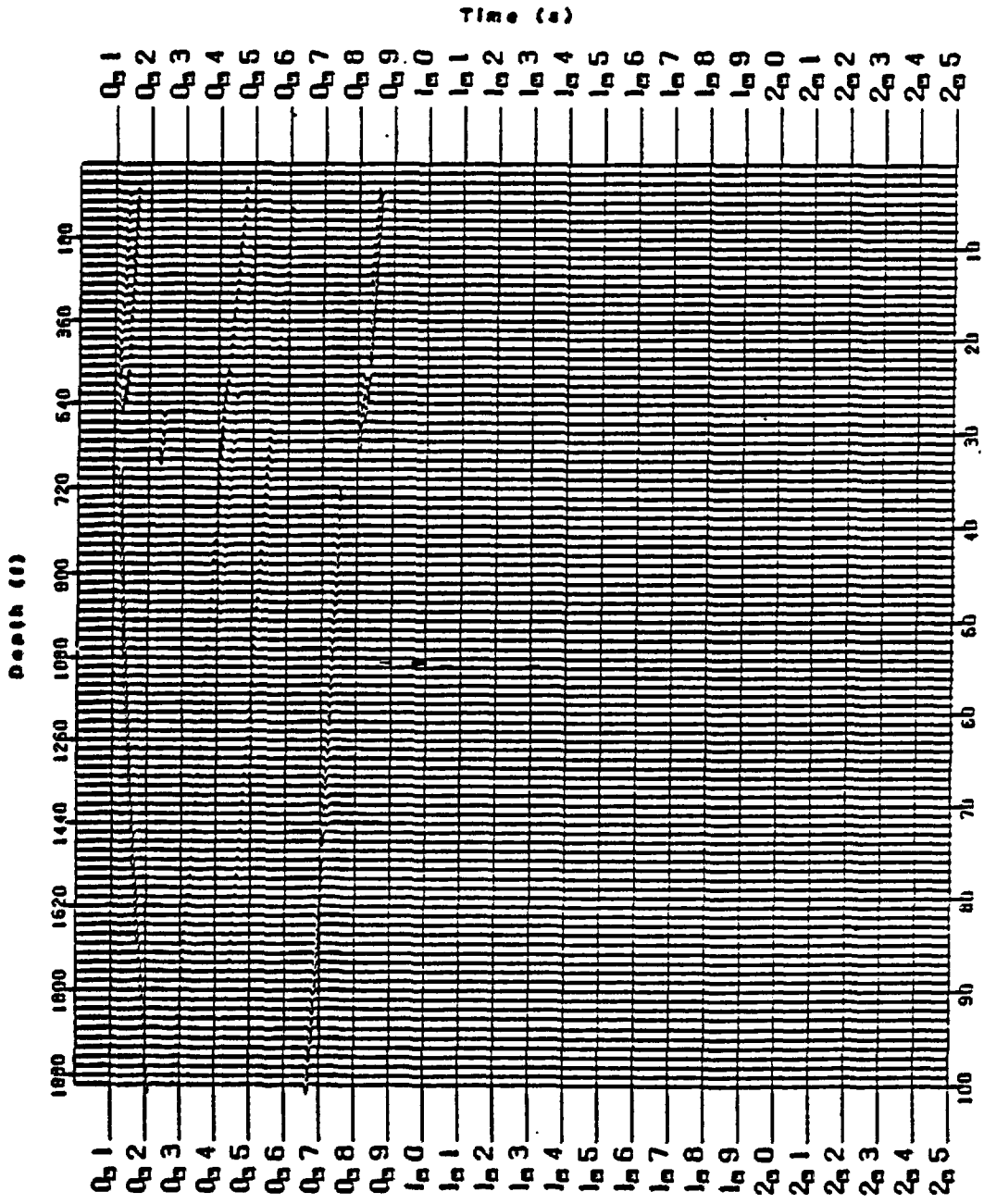

Figure 2.22. Synthetic VSP record generated by the ray tracing in Figure 2.21, after applying AGC.

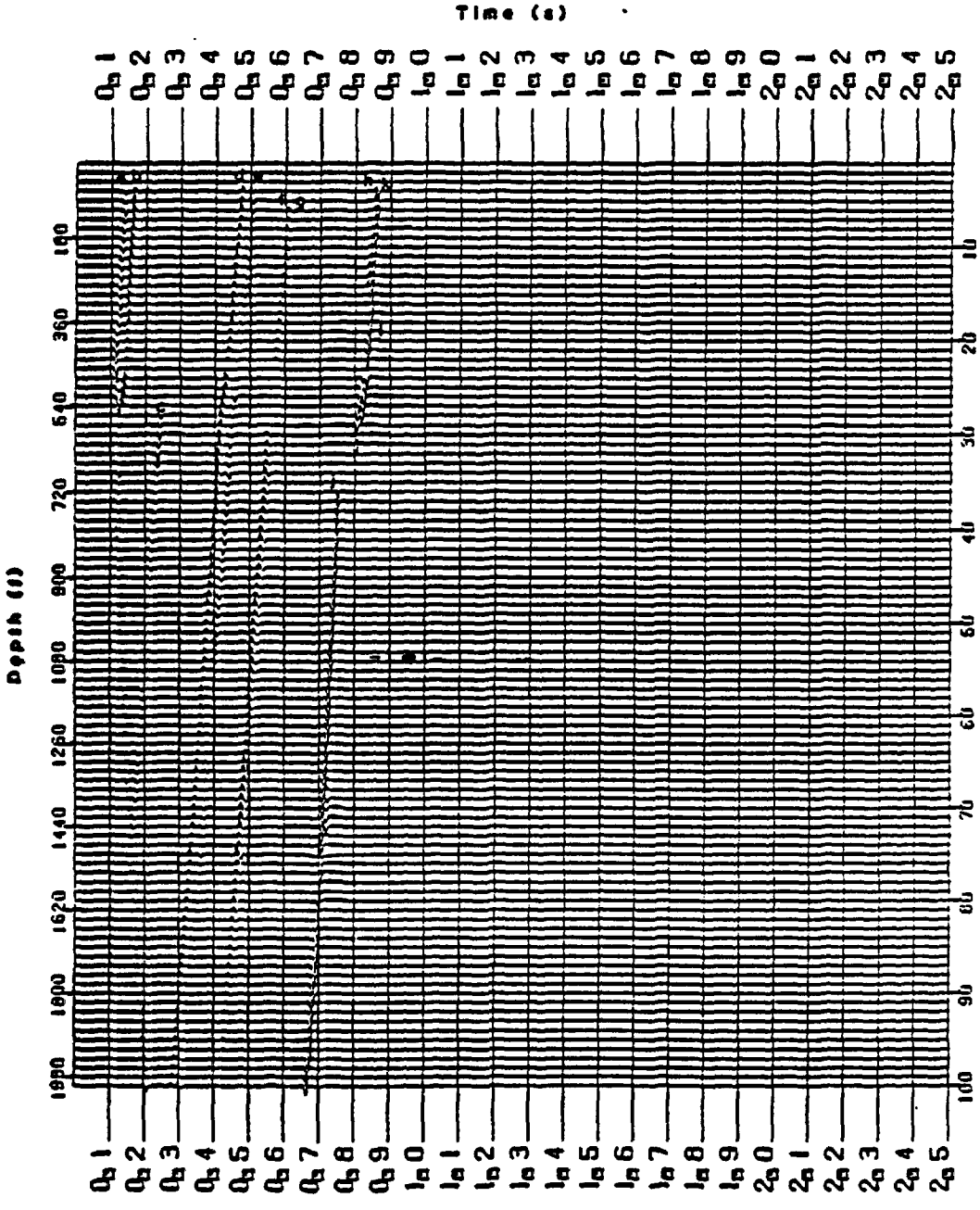

Figure 2.23. Synthetic VSP record for 1000-foot source offset after removing the direct arrivals. Reflections are seen from n1(a), Tptw(b), n2(c), Tcbw(d), n3(e), Tctw(f), n4(g), Tlrw(h), and n5(i). Fault plane reflections from within Tcbw (j) are seen as large troughs on traces 36 through 100. Event (k) is a reflection from fault plane 4.

reflections on the same data set. This is a contrast to the near-vertical slope of fault plane reflections seen earlier in this thesis.

The segment of fault plane 4 at the top of n2 (see Figure 2.21) produces an event which can be seen on Figure 2.23. The trough (k) directly below the Tlrw peak was generated by this fault segment.

2.4 2000-foot source offset VSP

Figure 2.24 is a ray trace diagram for a source offset of 2000 feet east of borehole USW UZ-6. Reflections from the seven lowest unit boundaries are clearly visible. Since only rays which intersect every fifteenth borehole receiver are shown, no rays are seen reflecting off the two highest horizons (n1 and Tptw) in the section. The nine near-vertical fault planes produce a reflection from the Tptw segment of each fault. Isolated reflections can be seen to originate along the n2 segment of fault plane 6.

The synthetic data set created by the preceding ray tracing is shown in Figure 2.25. The strong first arrival is represented by the trough on traces 45 through 100. In addition to the aperture problem, refraction occurs as the downgoing raypaths enter and exit n1. Both factors contribute to the absence of direct arrivals on traces 1 through 44. The absence of the direct arrivals on the computer

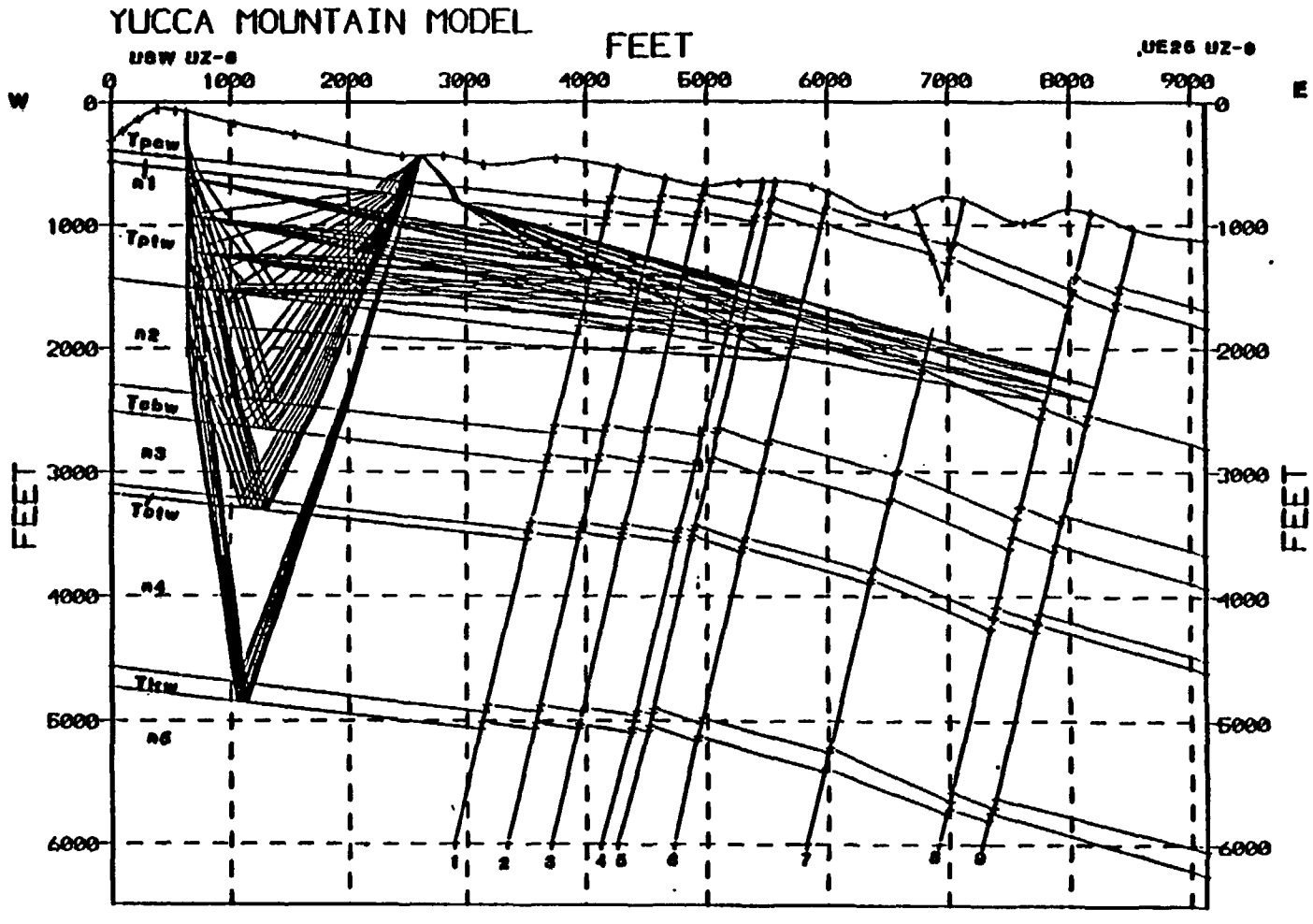

Figure 2.24. Raypath diagram for 2000-foot source offset VSP. No reflections are seen from n1 or Tptw.

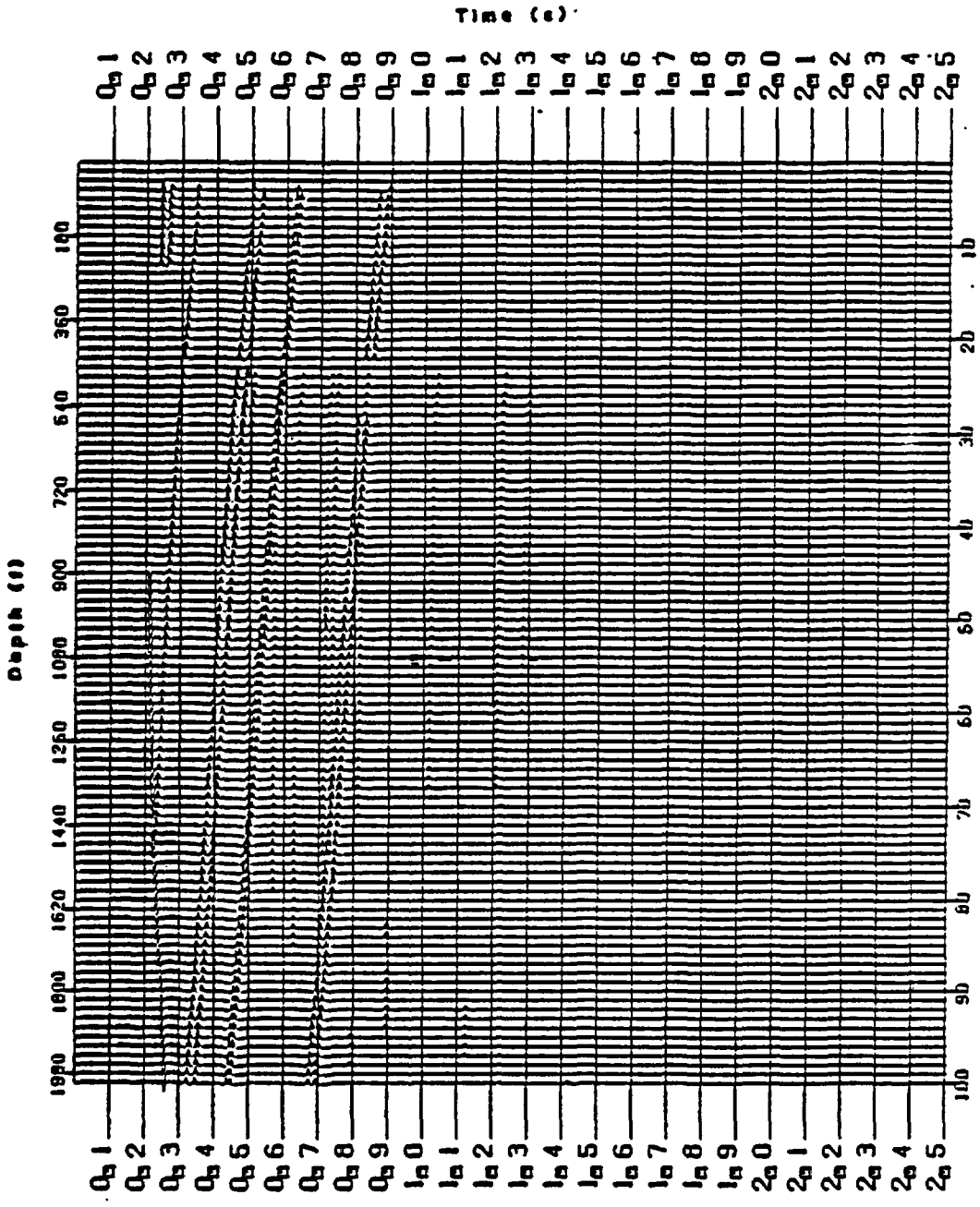

Figure 2.25. Synthetic VSP record generated by the ray tracing in Figure 2.24. The direct arrival trough can be seen on traces 45 through 100.

generated data does not imply that direct arrivals will not be seen on the field data. It only indicates that this ray tracing program has some modeling limitations.

The direct arrival is a good indicator of velocity change in the subsurface. The slope of the direct arrival is constant until the first break merges with the n2 reflection at 1480 feet. Below the 1480 foot level, the slope of the direct arrival decreases. This indicates that n2 has a lower velocity than Tptw, which is known to be true.

The direct arrival on traces 45 through 100 was removed by median filtering. The data set after median filtering is shown in Figure 2.26. Strong reflections are seen from all nine of the tuff units, including n1 (a) and Tptw (b) which did not show reflecting raypaths on Figure 2.24. The reflections from n1 and Tptw appear only on traces 4 through 12. The raypath diagram shows rays which converge at receiver locations 1 and 16.

Reflections from all nine fault plane segments within Tptw can be identified. The reflection from fault plane 2 is obscured by the Tctw (f) and n4 (g) reflections between traces 24 and 40, but it is visible on traces 69 through 79. A few isolated events from lower fault plane segments can be seen below the n5 reflection (i) on traces 82 through 98.

The ray tracing for the source 2000 feet east of UZ-6 was repeated with the zero reflection coefficient fault

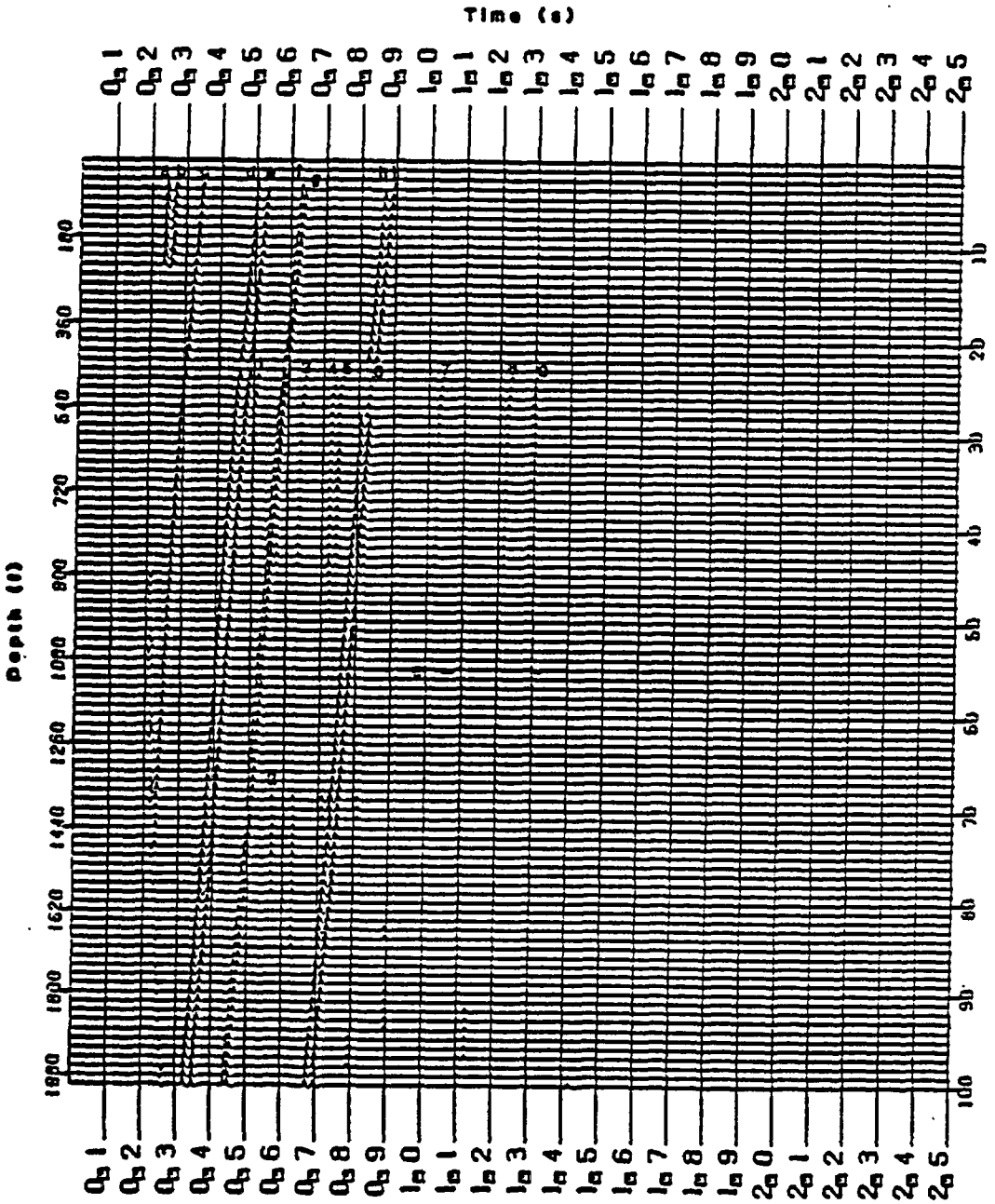

Figure 2.26. Synthetic VSP record for 2000-foot source offset after applying the median filter. Reflections are seen from n1(a) and Tptw(b), although they were not seen on Figure 2.24. Reflections are seen from n2(c), Tcbw(d), n3(e), Tctw(f), n4(g), Tlrw(h), and n5(i). The nine near-vertical fault plane reflections are labeled 1 through 9.

planes excluded. Figure 2.27 shows the raypath diagram for the model. A small segment of fault plane 4 at the top of n2 provides a reflected ray which intersects the borehole at receiver location 46. If any other fault plane segment is being imaged, it is not visible on this diagram.

Figure 2.28 shows the synthetic data set created by the preceding ray tracing after an AGC has been applied to the traces. The strong first arrival trough was suppressed on the data set by applying an 11-fold median filter to traces 45 through 100. The upgoing wavefield appears in Figure 2.29. All nine unit boundaries are identifiable, with the welded tuffs appearing as peaks and the non-welded tuffs appearing as troughs. The tops and the bottoms of each of the volcanic units are still identifiable. As seen with the data sets from zero and 1000-foot offsets, however, the top (f) and bottom (g) of the Tram Member (Tctw) interfere destructively. The resulting peak-trough pair appears as a low amplitude event on many of the traces.

The pair of trough sets (4) to the left of the Tlrw reflection (h) represents energy from the small segment of fault plane 4 that was pointed out in Figure 2.27. The position of the reflecting segment of the fault plane would be very difficult to ascertain from this data set alone, without the computer generated raypath diagram to consult. The same is true for the set of troughs to the right of the n5

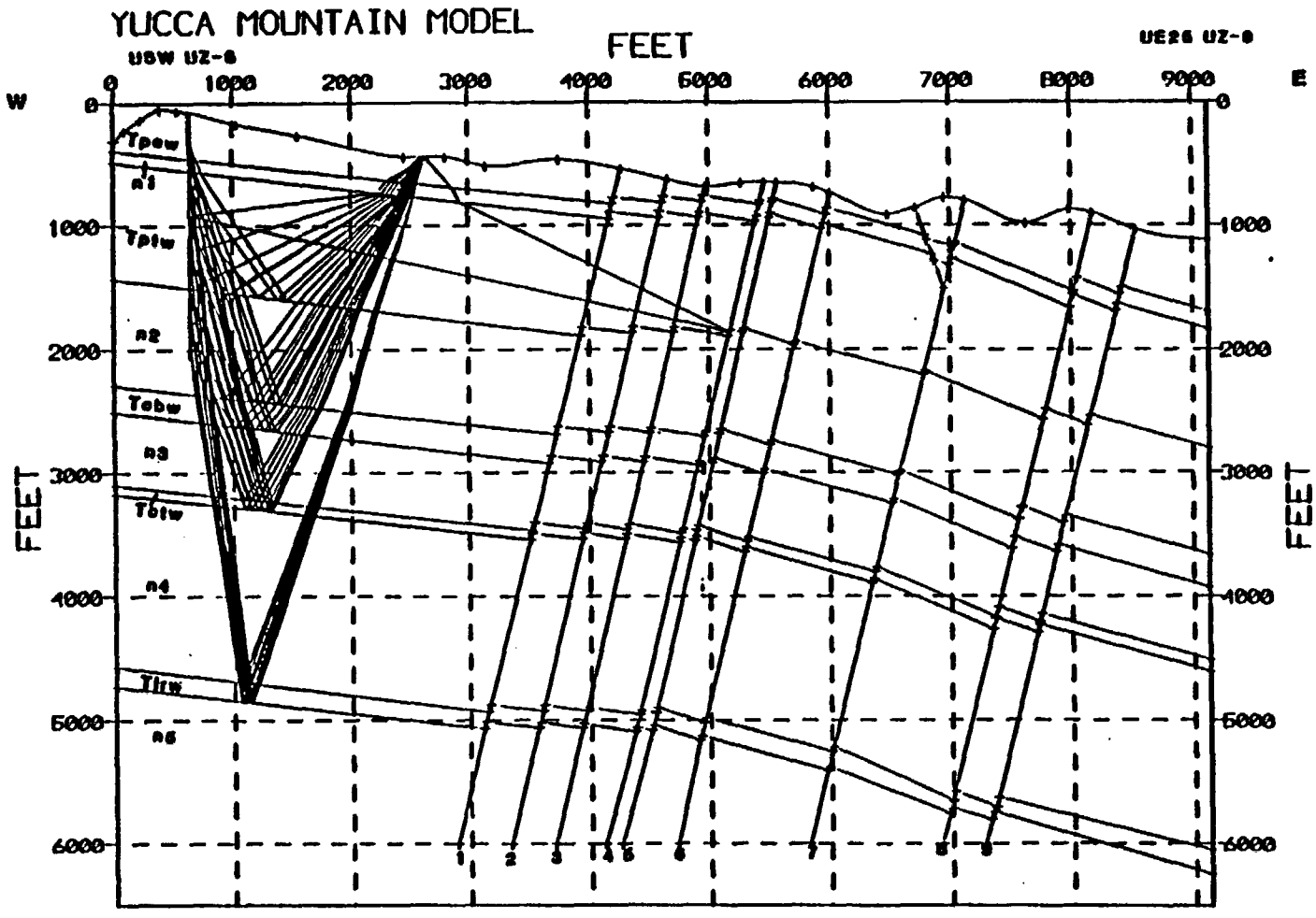

Figure 2.27. Raypath diagram for 2000-foot source offset VSP, excluding reflections from zero reflection coefficient fault planes.

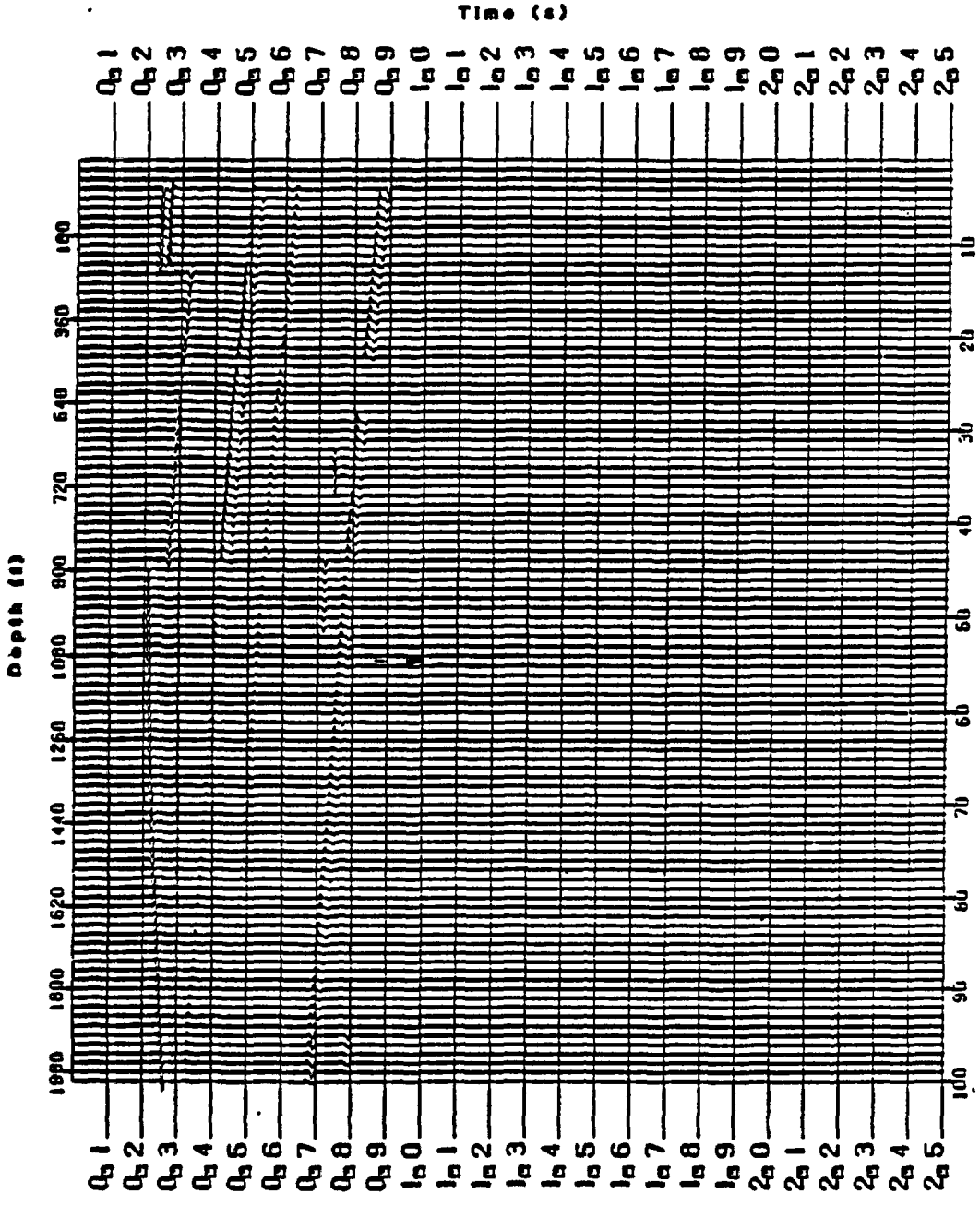

Figure 2.28. Synthetic VSP record generated by the ray tracing in Figure 2.27. The direct arrival trough can be seen on traces 45 through 100.

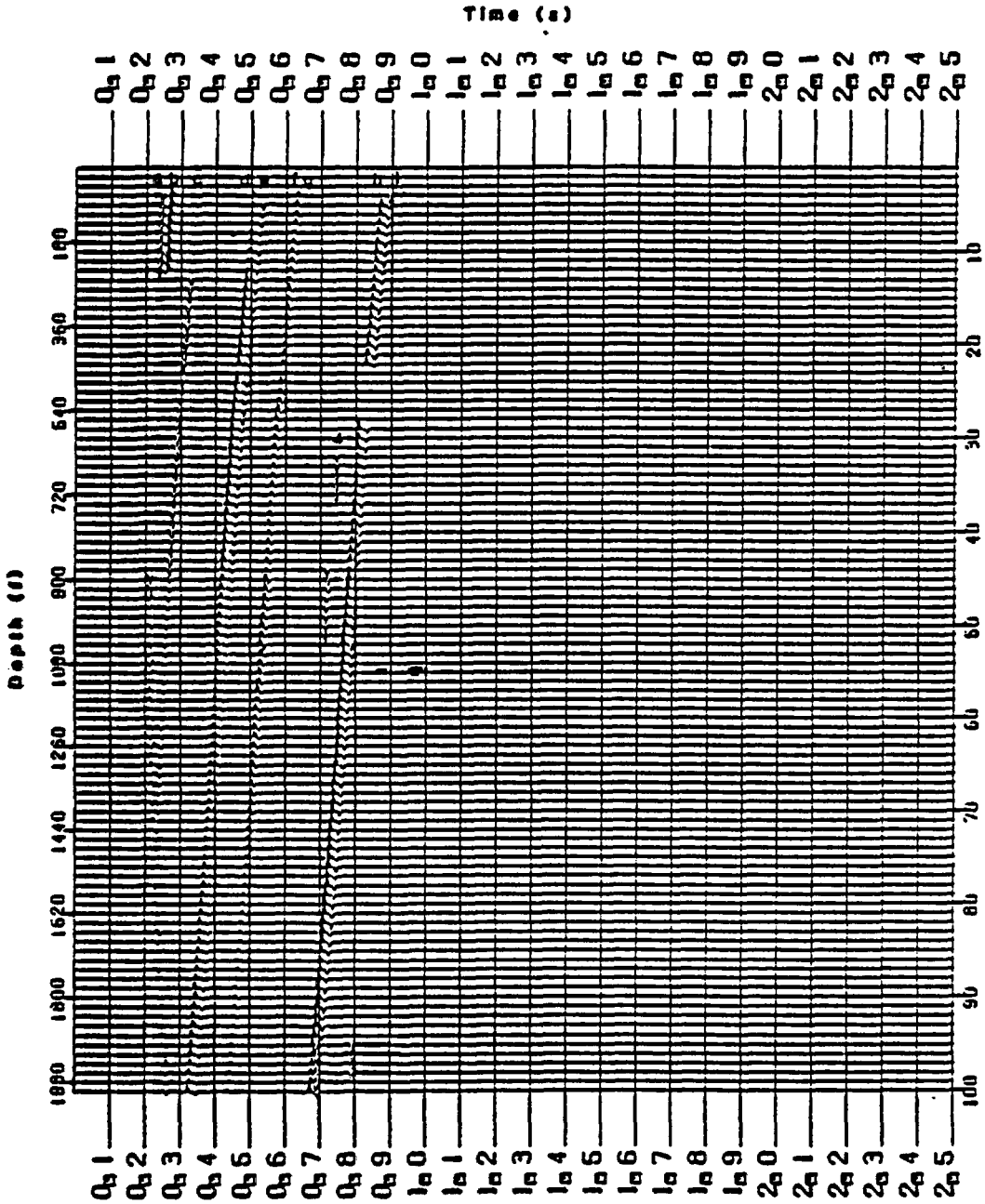

Figure 2.29. Synthetic VSP record for 2000-foot source offset after removing the direct arrivals. Reflections are seen from n1(a), Tptw(b), n2(c), Tcbw(d), n3(e), Tctw(f), n4(g), Tlrw(h), and n5(i). Reflections from a small segment of fault plane 4 appear to the left of the Tlrw event.

reflection (i) on traces 94 through 98. The troughs are reflections from a fault plane, but without a raypath to consult on Figure 2.27, it is impossible to positively identify the source of the reflection.

2.5 3000-foot source offset VSP

The source was next positioned 3000 feet to the east of borehole UZ-6. From the raypath diagram in Figure 2.30, it appears that no rays are reflecting off of n1 and Tptw and intersecting the borehole due to the aperture problem. The seven lowest unit boundaries provide reflections, however. As the source moves away from the borehole to the east, the reflecting segments of the unit boundaries continue to move downdip away from the borehole. For the zero-offset source in Figure 2.1, the reflecting segments of the unit boundaries were updip to the west of the borehole. The reflecting segments of Tlrw and n5 are now at least 1000 feet downdip to the east of the borehole. The importance of multiple offsets in VSP work lies in the observation that different portions of reflectors are imaged for each source location. Hence, more information about the subsurface can be obtained with multiple offsets.

The nine fault plane segments within Tptw all show rays reflecting and intersecting the borehole. Also, the highest segment of fault plane 1 (within Tpcw) is seen to be a

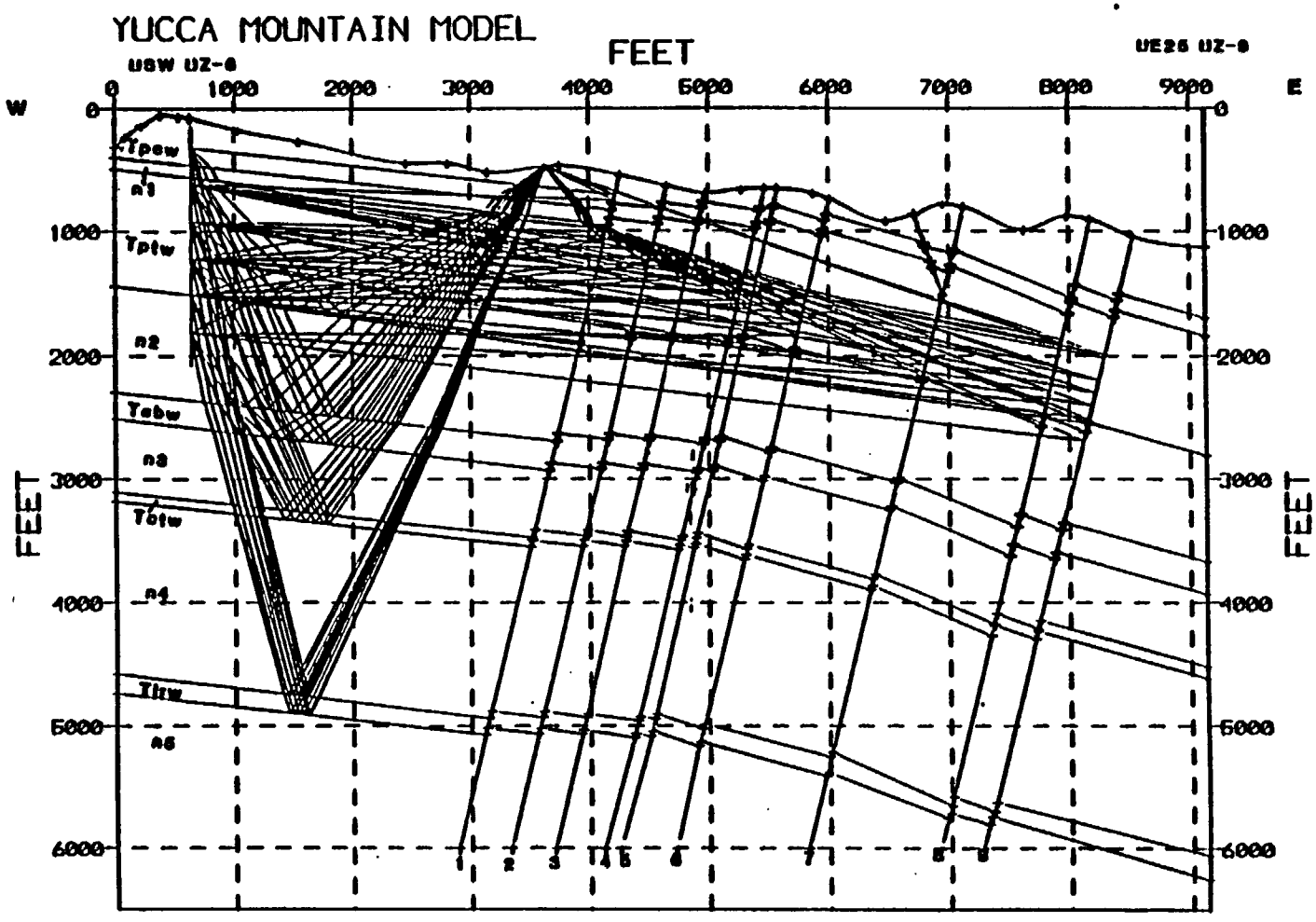

Figure 2.30. Raypath diagram for 3000-foot source offset VSP. No rays appear to be reflecting off n1 or Tptw.

reflecting horizon. This is the first occurrence of a fault plane segment above Tptw providing reflecting raypaths.

The synthetic data set created by the preceding ray tracing is shown in Figure 2.31. The first arrival is not seen until trace 55. Again, this is due to the aperture of the AIMS ray tracing algorithm and refraction of the downgoing rays as they enter and exit horizon n1. Also, the topography suggests that a downgoing first arrival would be physically shielded from a receiver high in the borehole, even if the AIMS aperture were wider.

The first arrival troughs were removed from the data set by median filtering traces 55 through 100. The resulting upgoing wavefield is shown in Figure 2.32. The seven lowest unit boundaries are identifiable. As expected, horizons n1 and Tptw did not produce reflections for this offset.

All nine of the fault plane segments within Tptw produced identifiable reflections on the data set, with the exception of fault plane 2. This reflection is obscured by the Tcbw (b) and n3 (c) reflections. It appears that the amplitude of the fault plane reflections was diminished by median filtering in the trace range 55 through 73. This problem was addressed earlier in the paper, but it appears that even an 11-fold median filter may be insufficient on some data sets.

The highest segment of fault plane 1 (within Tpcw)

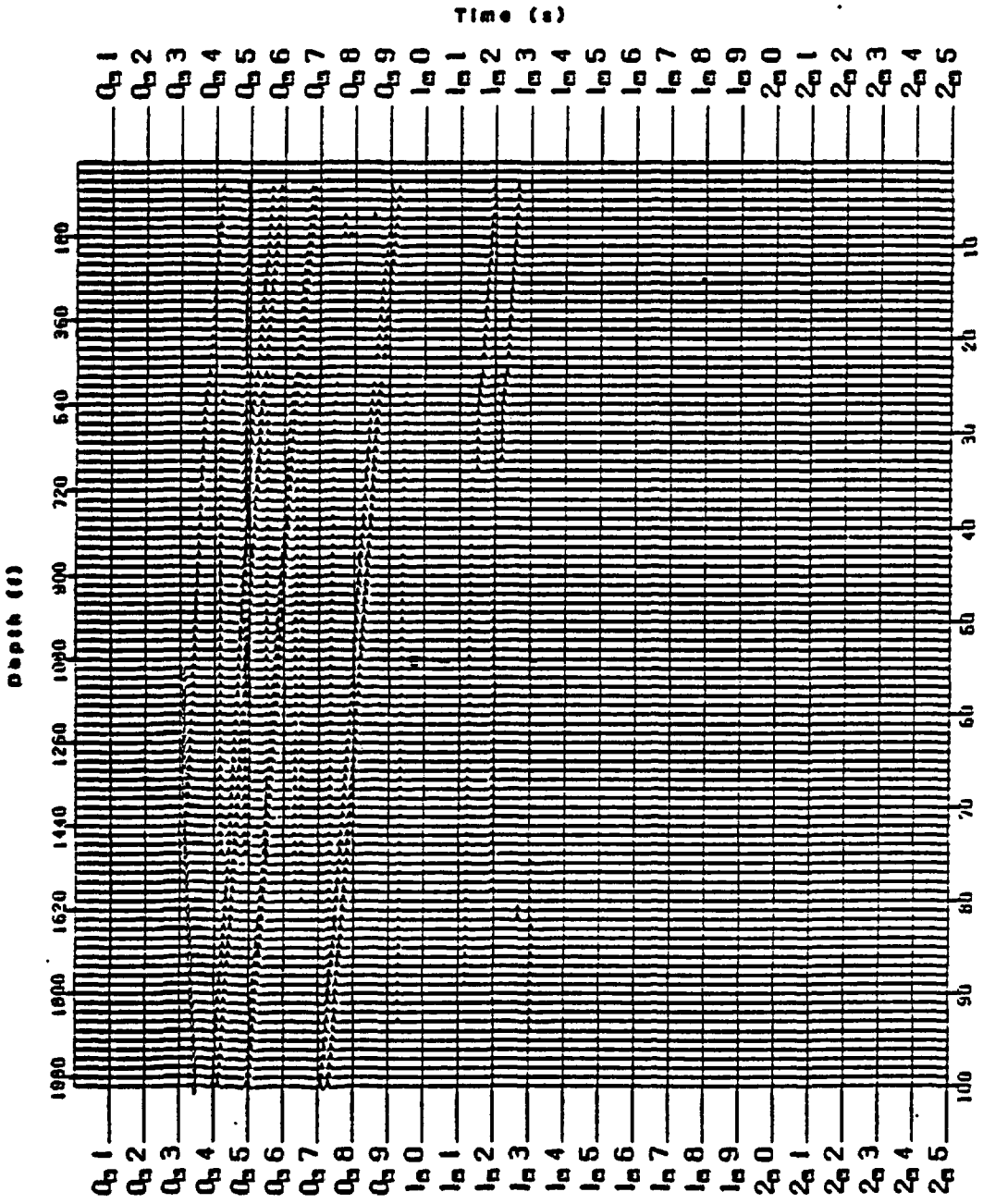

Figure 2.31. Synthetic VSP record generated by the ray tracing in Figure 2.30. The direct arrival trough appears on traces 55 through 100.

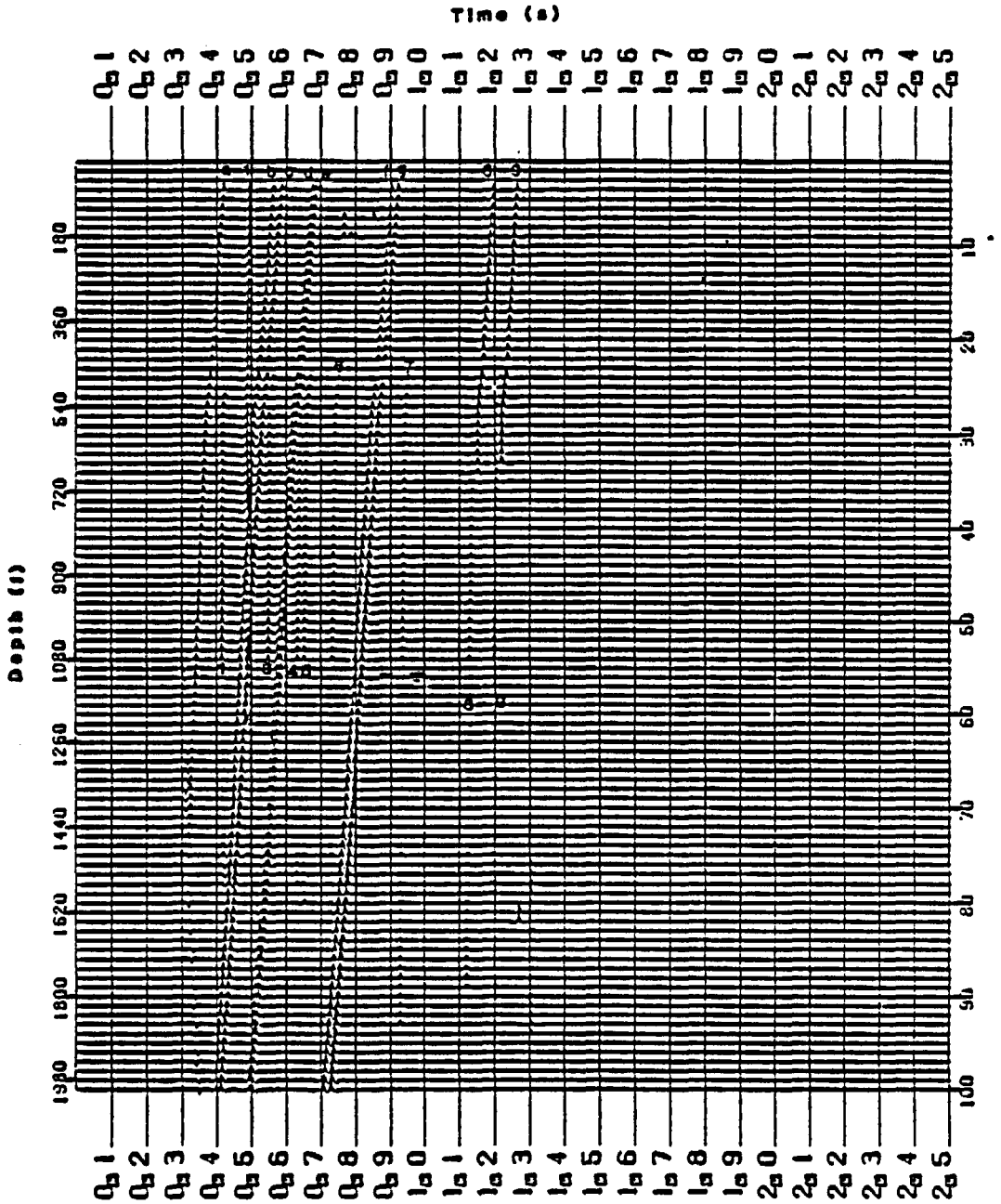

Figure 2.32. Synthetic VSP record for 3000-foot source offset after removing the direct arrivals. Reflections are seen from n2(a), Tcbw(b), n3(c), Tctw(d), n4(e), Tlrw(f), and n5(g). Reflections from the fault planes 1 and 3 through 9 are identifiable. The reflection from fault 2 interferes with events (b) and (c). Fault planes 1, 8, and 9 produce additional events on the shallow traces.

produced a strong downgoing event on the data set. The event (1) can be seen along the 0.5 second time line in the trace range 4 to 40.

Two other events appear on this data set that have not been seen previously. The upgoing events lie far to the right of the n5 reflection on traces 4 through 33. The events are reflections off fault planes 8 and 9 which are refracted by the n1 unit along the path from the source. An additional fault plane reflection from fault plane 1 also appears on this data set. This result shows that a fault plane reflection can have a slight upgoing slope, similar to the slope of a reflection from one of the unit boundaries. The fault plane reflection can also have a near-vertical slope as has been the case with most of the fault plane reflections seen up to this point.

As the source moves closer to the fault planes, the data sets become more complicated. The fault plane reflections become superimposed on the unit boundary reflections with the source 3000 feet from the borehole. For the zero-offset data set (Figure 2.2), only the reflections from fault planes 1 and 2 interfered with the T1rw and n5 reflections. Since the modeling in this thesis is being done with a zero phase wavelet on a noise-free trace, it is possible to identify each of the reflections on the 3000-foot offset data set even though interference occurs. The interference could

cause considerable interpretation difficulties on noisy field data, however.

The ray tracing was repeated for the source offset of 3000 feet, excluding the zero reflection coefficient fault planes. The raypath diagram is shown in Figure 2.33. It is interesting that not a single segment of any fault plane produced a reflection. Although the raypath diagram shows only rays which intersect at every fifteenth receiver location, the synthetic traces generated by this ray tracing confirm that no fault segment produced a reflection.

The synthetic data set generated by the preceding ray tracing after applying an AGC is shown in Figure 2.34. The first arrival trough was suppressed by an 11-fold median filter. The resulting upgoing wavefield is shown in Figure 2.35. The seven reflections are easy to identify without the fault plane reflections in the data set. The Tctw peak (d) and the n4 trough (e) interfere destructively and produce a small event. The gap between the Tlrw peak (f) and the n5 trough (g) has narrowed as source offset has increased. Interference has caused a noticeable decrease in amplitude of the n5 trough on this data set compared to the amplitude of the n5 trough on the zero-offset data set.

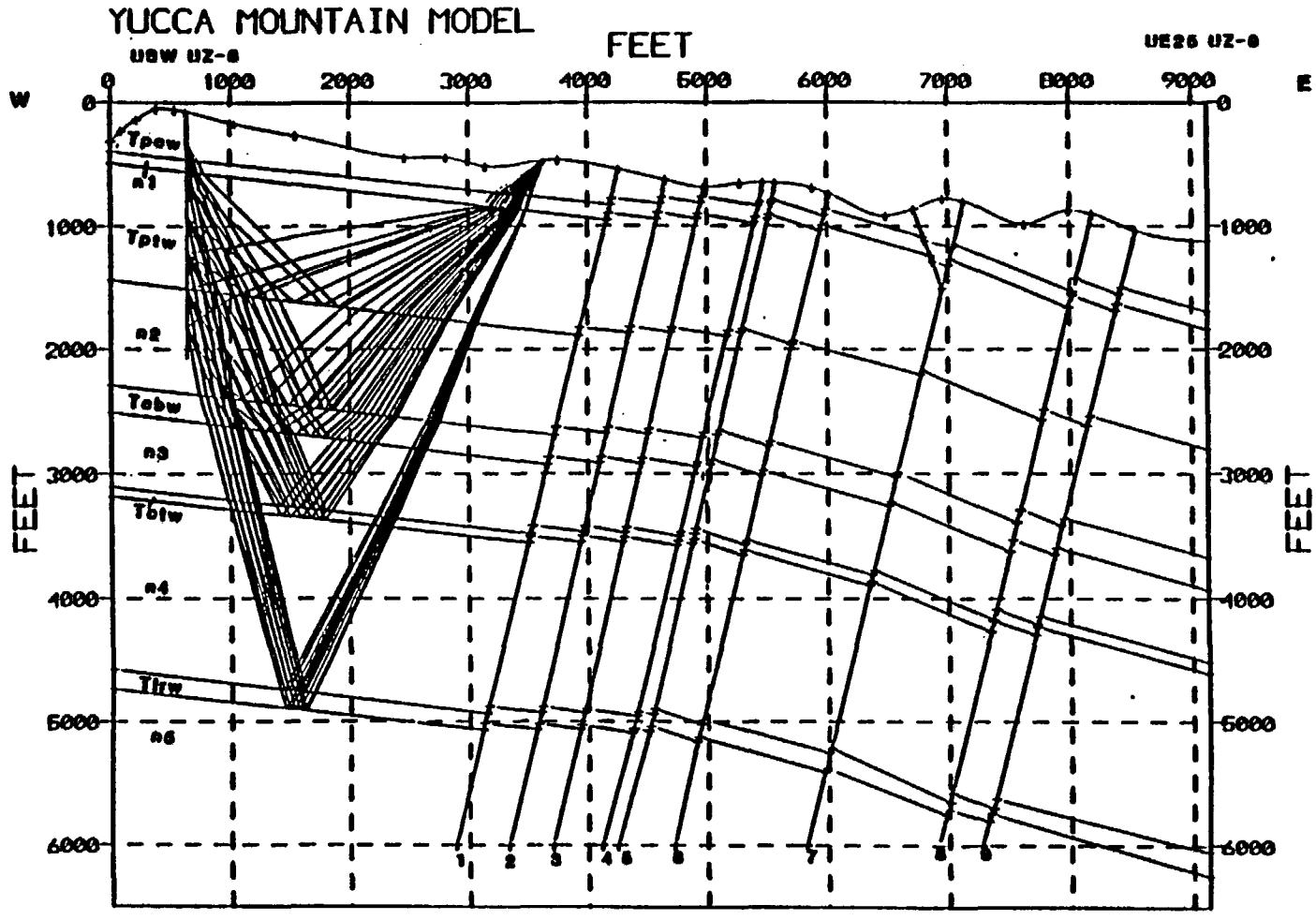

Figure 2.33. Raypath diagram for 3000-foot source offset VSP, excluding reflections from zero reflection coefficient fault planes.

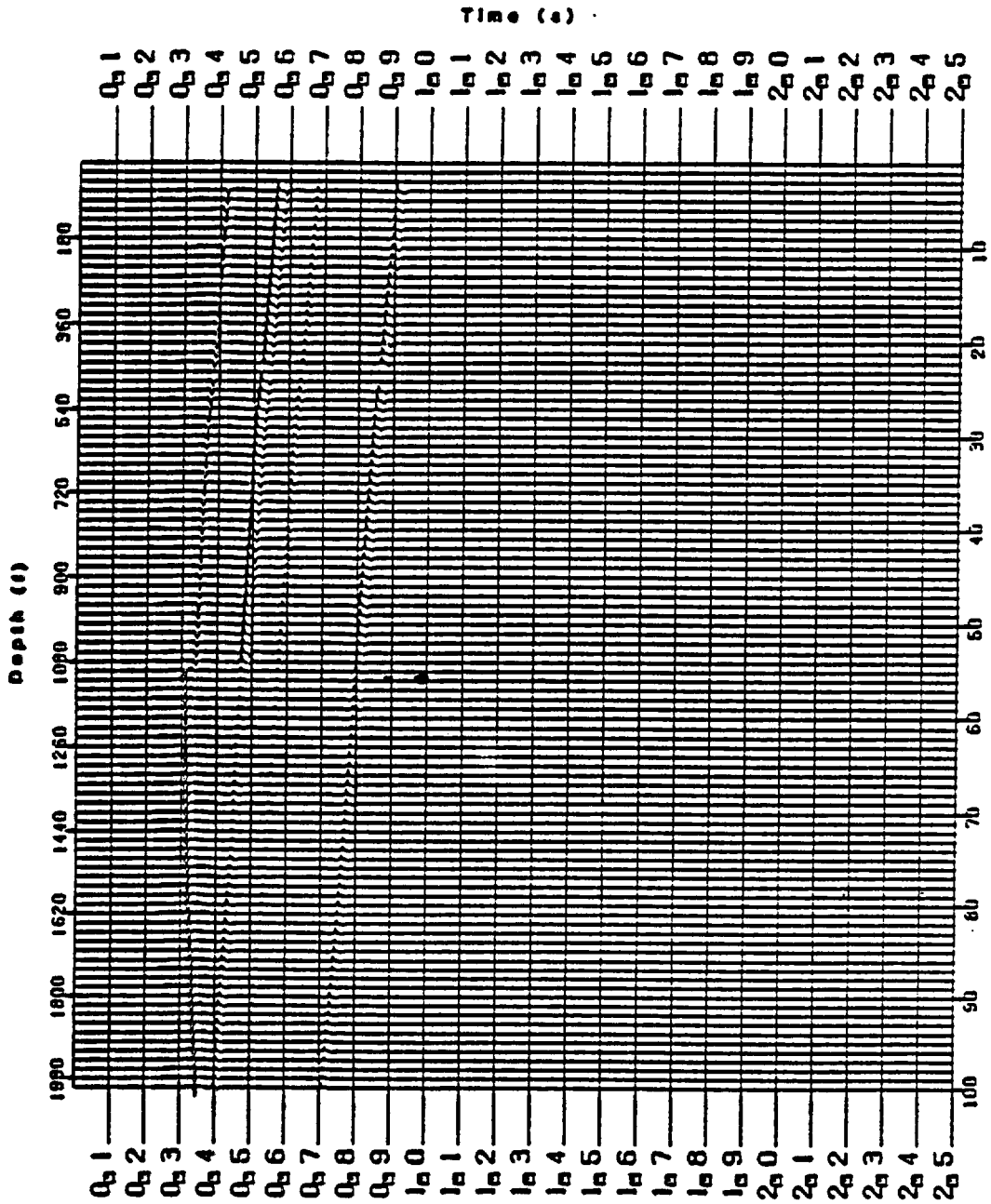

Figure 2.34. Synthetic VSP record generated by the ray tracing in Figure 2.33, after applying AGC. The direct arrival trough appears on traces 55 through 100.

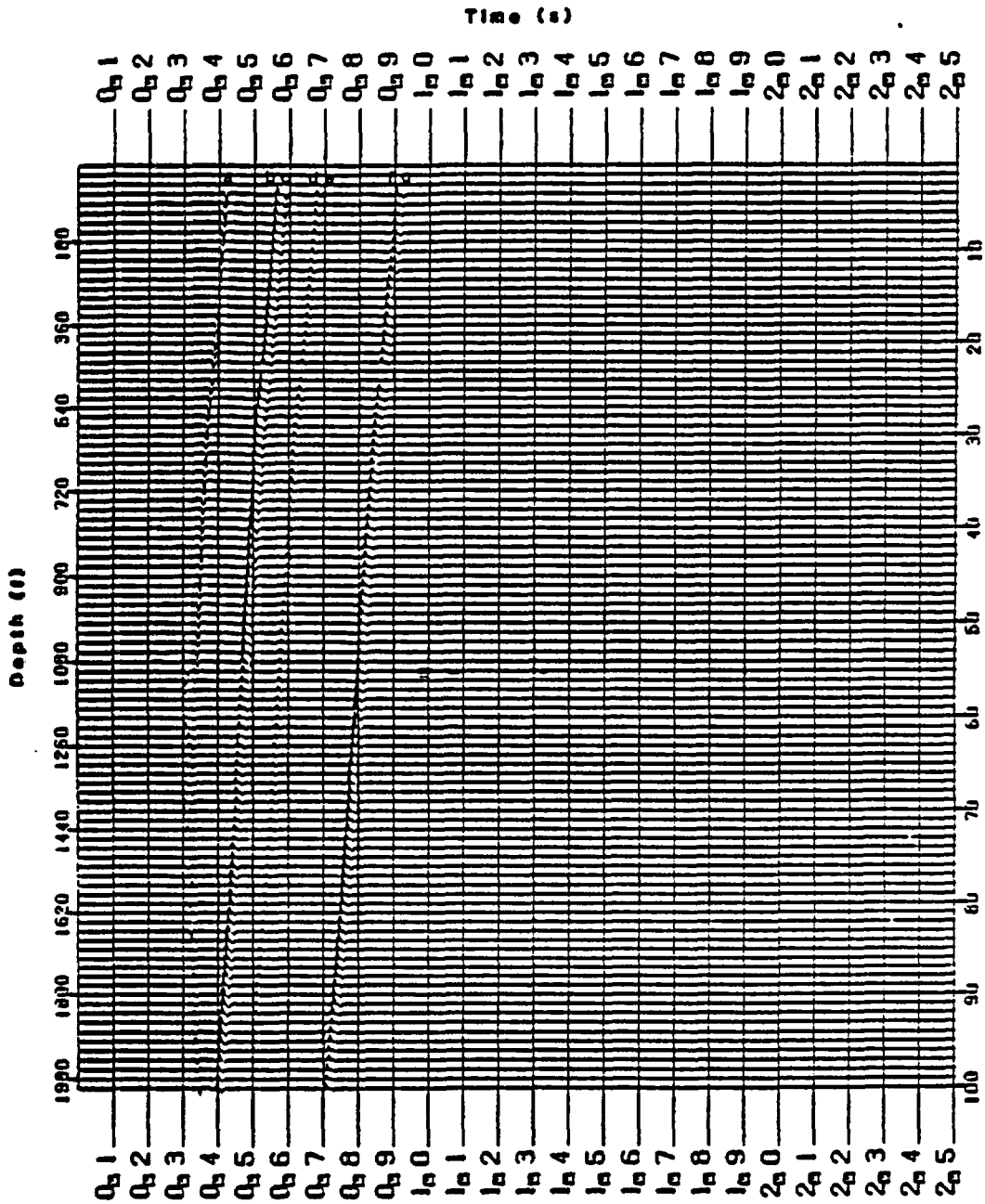

Figure 2.35. Synthetic VSP record for 3000-foot source offset with the direct arrivals removed. Reflections from n2(a), Tcbw(b), n3(c), Tctw(d), n4(e), Tlrw(f), and n5(g) are seen. No fault plane segment produced an event.

2.6 4000-foot source offset VSP

With the source offset 4000 feet to the east of UZ-6, fault plane 1 is to the west of the source and can no longer be imaged. Figure 2.36 shows a raypath diagram for the 4000 foot offset model. The seven lowest unit boundaries in the section provide reflections at this offset, as do fault planes 3 through 9 within Tptw. A segment of fault plane 8 within n2 also provides a reflected ray which converges at the borehole.

The Shardy Base (n1) provides an interesting refraction pattern on this diagram that has not been seen on previous models. Rays traveling through Tpcw are refracted strongly downward upon entering n1. This creates multiple downgoing arrivals. The set of first arrivals enters the ground at a steep angle and is refracted sideways through the higher velocity units in the section. The other set of downgoing raypaths travels nearly horizontal to the surface, before being refracted downward.

The synthetic data set created by the preceding ray tracing is shown in Figure 2.37. The first arrival trough can be seen on traces 64 through 100. This arrival represents the rays which entered the ground at a steep angle and were refracted sideways. Two other downgoing arrivals appear on this data set. Between the 0.5 and 0.6 second time lines, a strong peak occurs on traces 5 through 42 (3) with

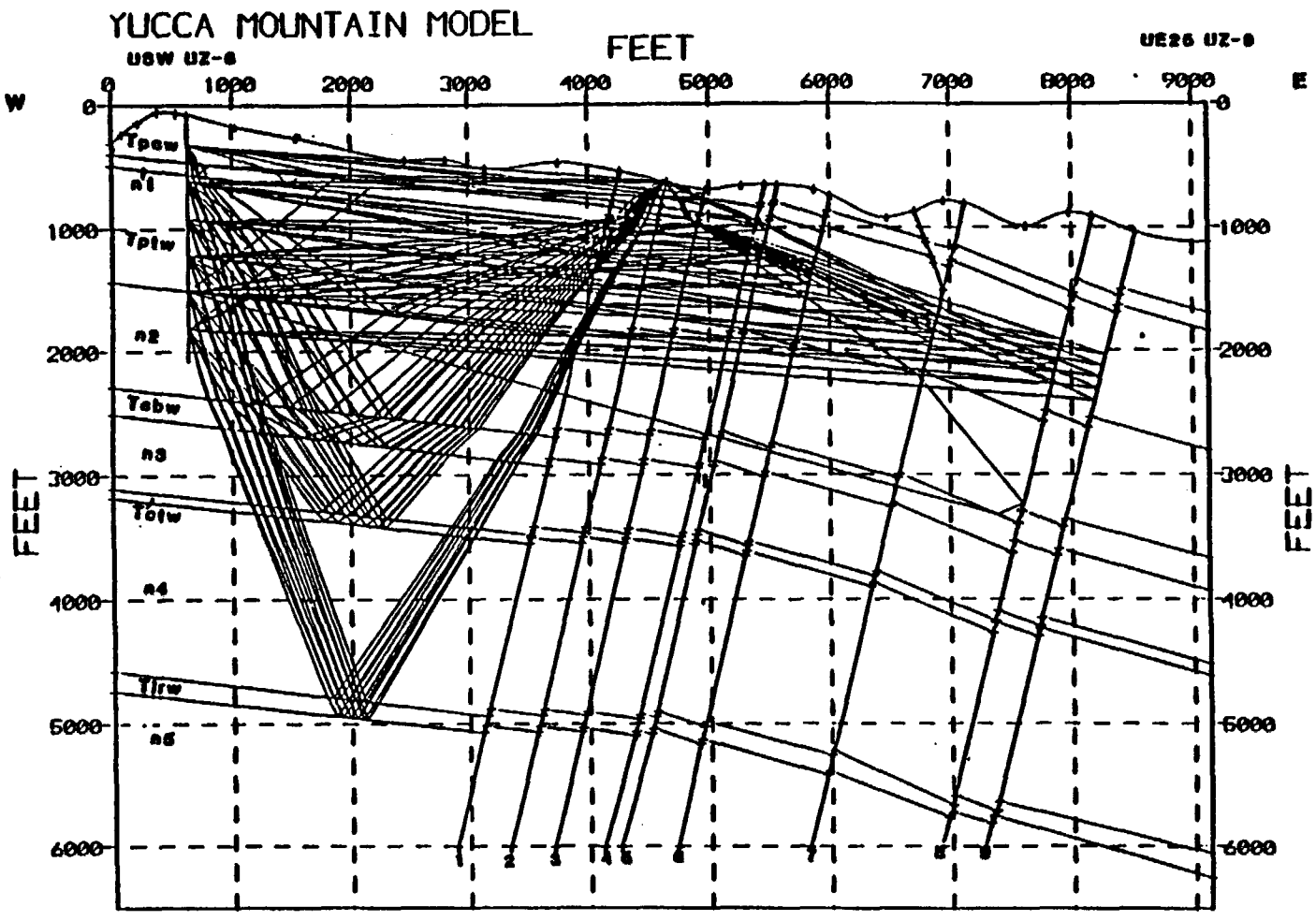

Figure 2.36. Raypath diagram for 4000-foot source offset VSP.

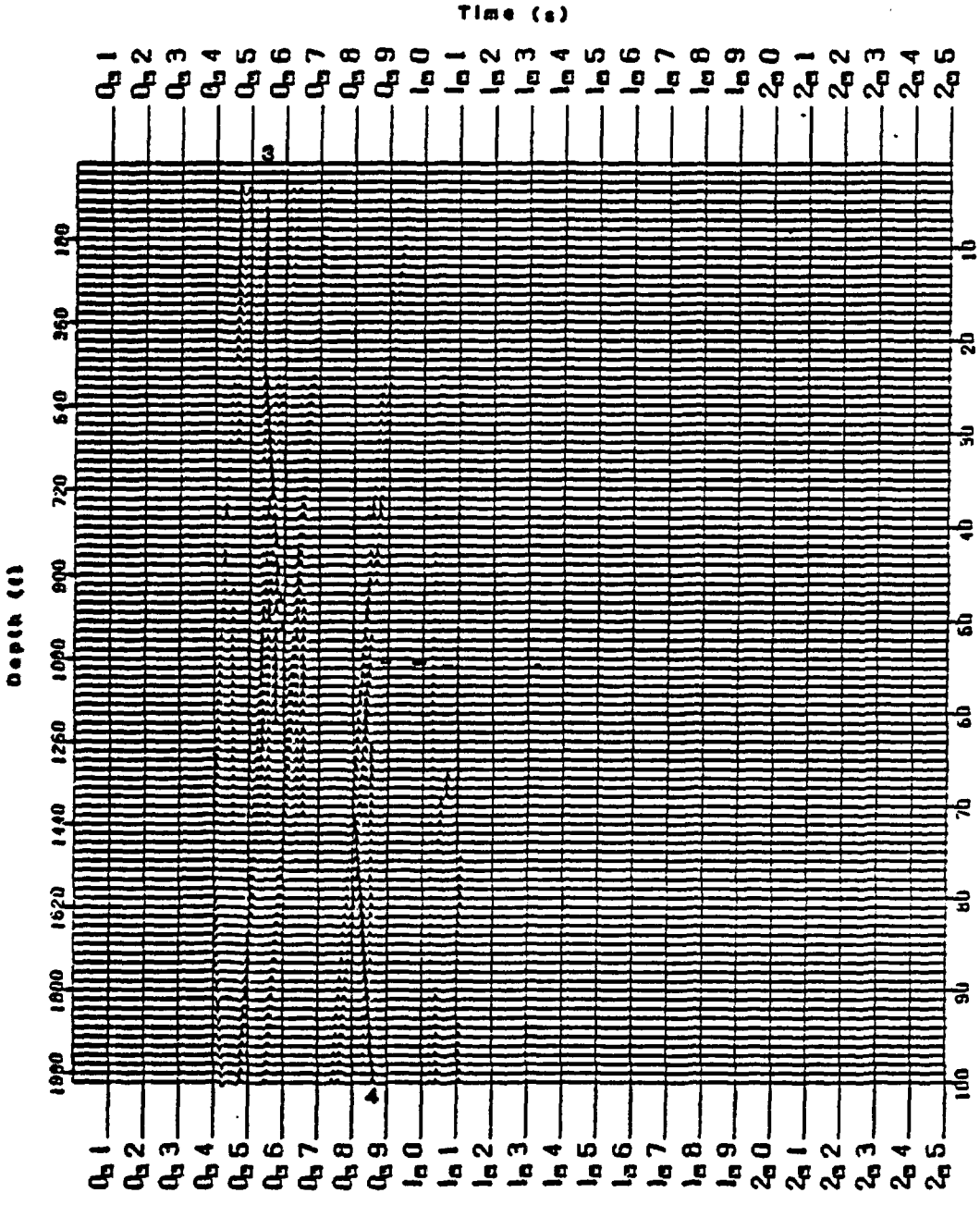

Figure 2.37. Synthetic VSP record generated by the ray tracing in Figure 2.36. The direct arrival trough appears on traces 64 through 100. Event (3) is a fault plane reflection from fault plane 3 which is refracted downward at n1. Event (4) is a fault plane reflection from fault plane 4, near the top of Tptw.

additional peaks on traces 44, 45, 48, and 52. This event represents a fault plane reflection which travels through Tpcw and is refracted downward by n1. This event arrives after the reflection from n2, due to higher velocities along the the n2 reflection's travel path. The remaining downgoing event occurs on traces 72 through 100 between the 0.8 and 0.9 second time lines (4). This peak is a reflection off fault plane 4, near the top of Tptw.

The first arrival was removed by median filtering. The resulting upgoing wavefield is shown in Figure 2.38. The downgoing reflection from fault plane 4 was partially destroyed by the median filtering, since its slope was very similar to the slope of the first arrival trough. The other downgoing fault plane reflection was left in the data set by choice. The slope of this event is very similar to the slope of the n1 reflection (a) on the shallow receivers, and filtering out the downgoing event would have destroyed the n1 reflection.

Each of the nine unit boundaries can be identified on at least a portion of the traces. On the deep traces, the Tcbw (d) and n3 (e) reflections merge into one peak. The same is true for the Tctw (f) and n4 (g) reflections.

The fault plane reflections from within Tptw have become considerably more difficult to identify on this data set. Reflections from fault planes 3, 6, 7, 8, and 9 can be

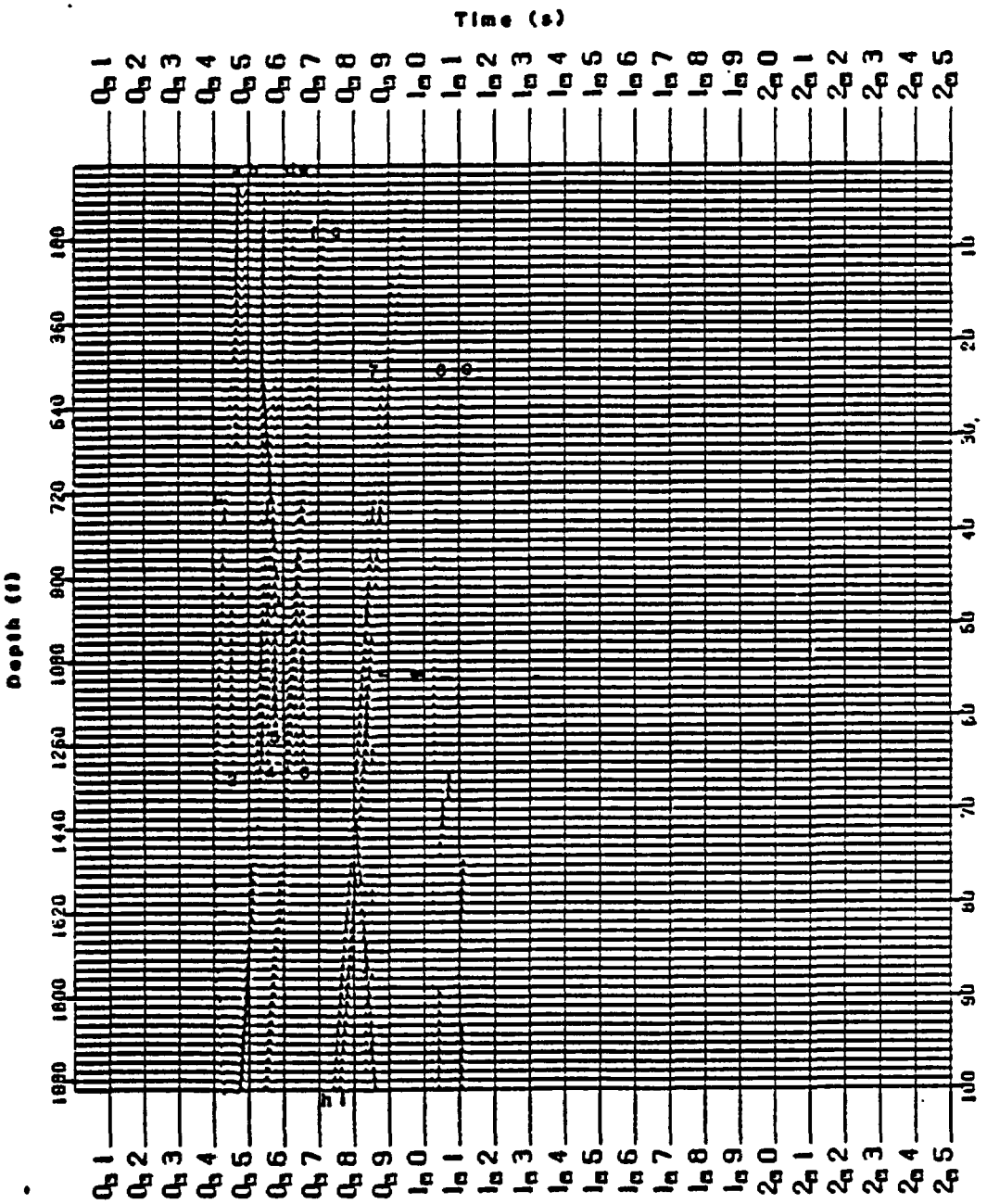

Figure 2.38. Synthetic VSP record for 4000-foot source offset, after removing the direct arrivals. Reflections are seen from n1(a), Tptw(b), n2(c), Tcbw(d), n3(e), Tctw(f), n4(g), Tlrw(h), and n5(i). Reflections can also be seen from fault planes 3 through 9.

identified on certain traces, but reflections from fault planes 4 and 5 are not easily picked. These reflections can be seen on traces 50 through 60 to the right of the n3 reflection at 0.55 second. Isolated reflections from various fault planes can be seen between 1.0 and 1.1 seconds on traces 70 through 100.

The ray tracing was repeated for the source offset of 4000 feet, excluding the zero reflection coefficient fault planes. Figure 2.39 is a raypath diagram for this model. Reflections can be followed from all nine layers. A segment of fault plane 3 at the top of n1 acts as the only fault reflector in the model. The synthetic data set created from the preceding ray tracing (after AGC) is shown in Figure 2.40.

The first arrival trough was removed by median filtering. The resulting data set is shown in Figure 2.41. The trough representing the reflection from n1 (a) is quite prominent on traces 4 through 22, as is the peak from Tptw (b). A reason for the prominence of the n1 trough is that the reflection from n2 (c) constructively interferes with the n1 reflection on the shallower traces. The higher velocity of the lower horizons causes the n2 reflections to arrive at roughly the same time as the n1 reflections, which travel a shorter distance through a lower velocity medium.

On the shallower traces, the Tcbw (d) peak and the n3

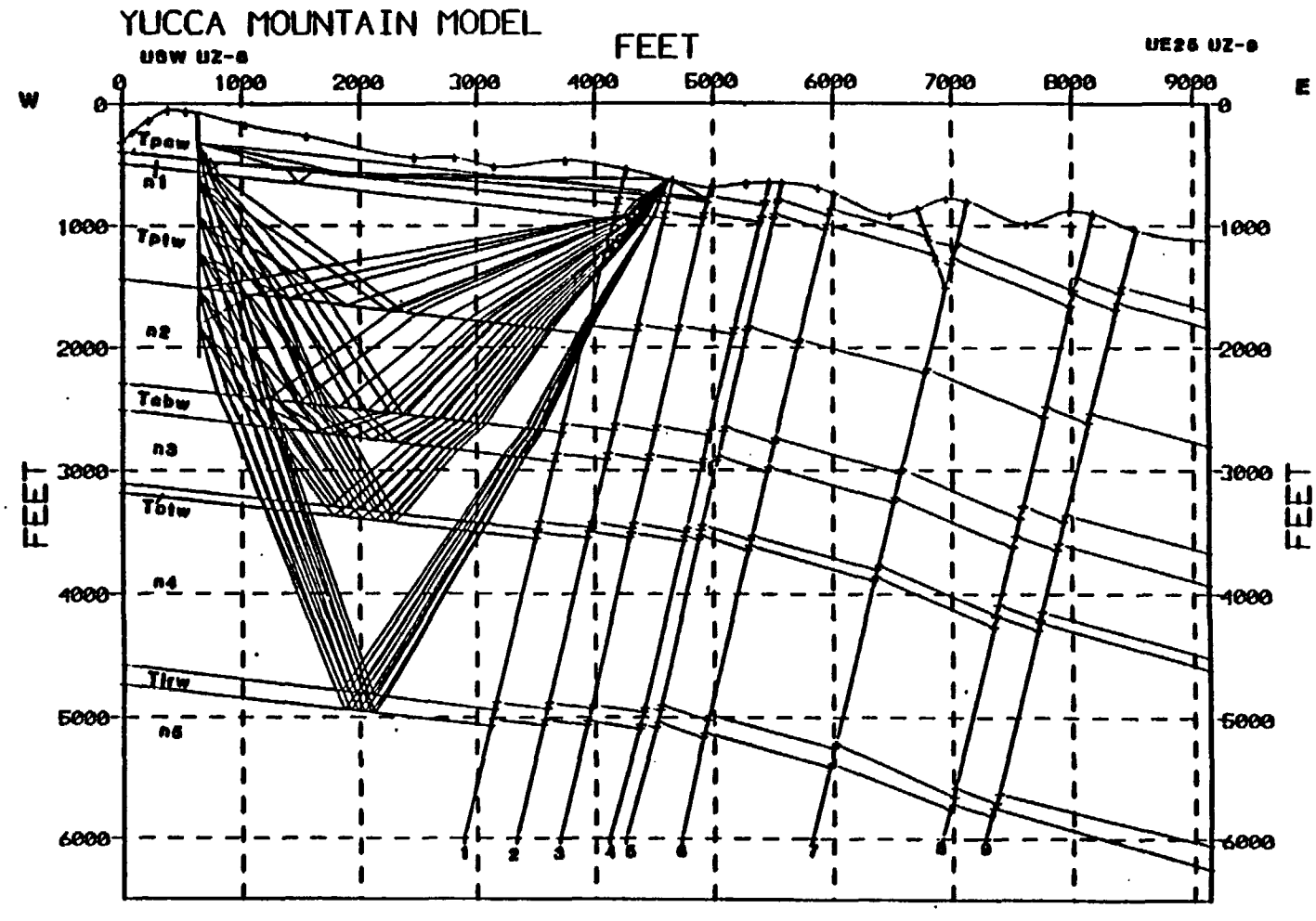

Figure 2.39. Raypath diagram for 4000-foot source offset VSP, excluding reflections from zero reflection coefficient fault planes.

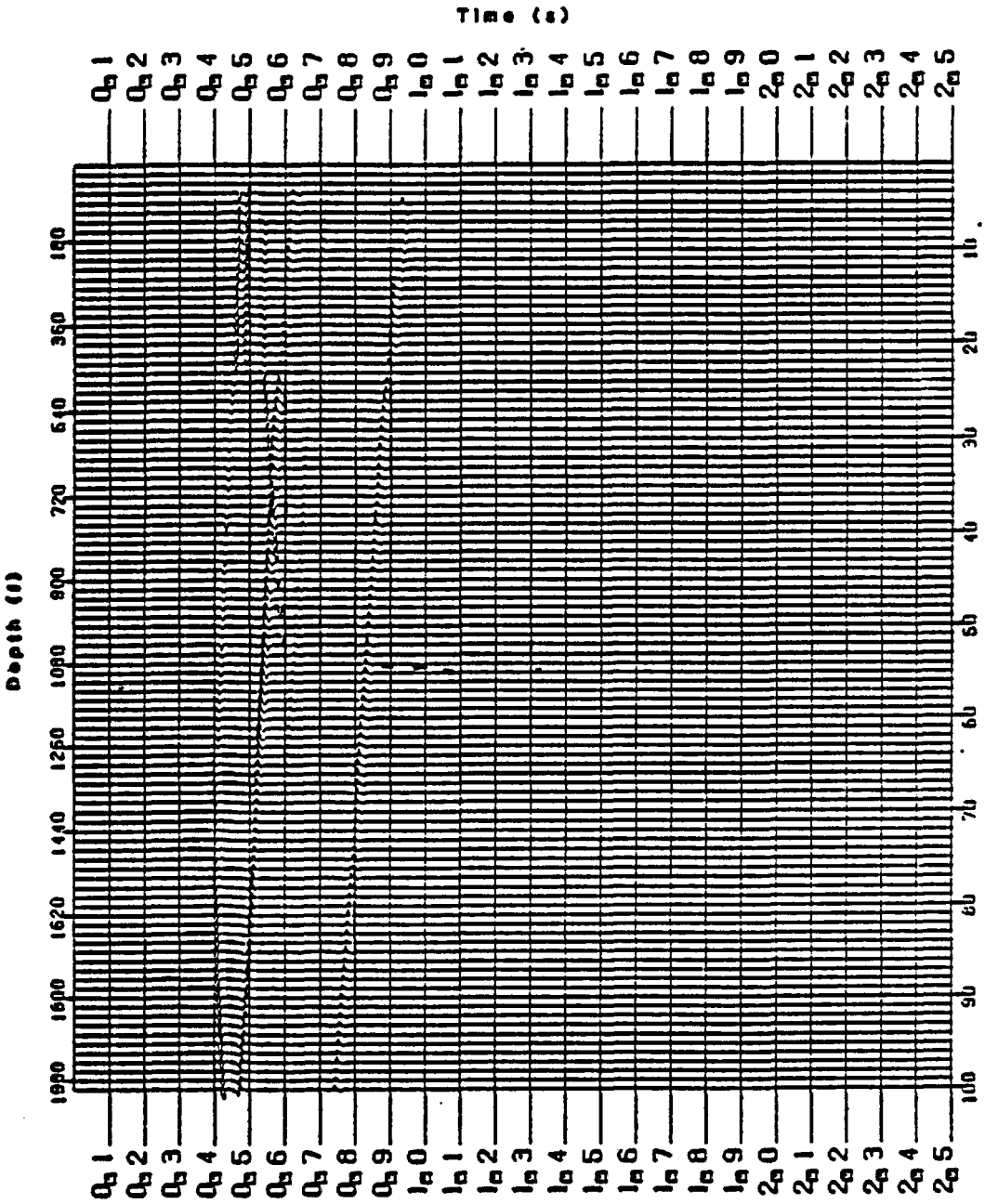

Figure 2.40. Synthetic VSP record generated by the ray tracing in Figure 2.39, after applying AGC. The direct arrival trough is seen on traces 64 through 100.

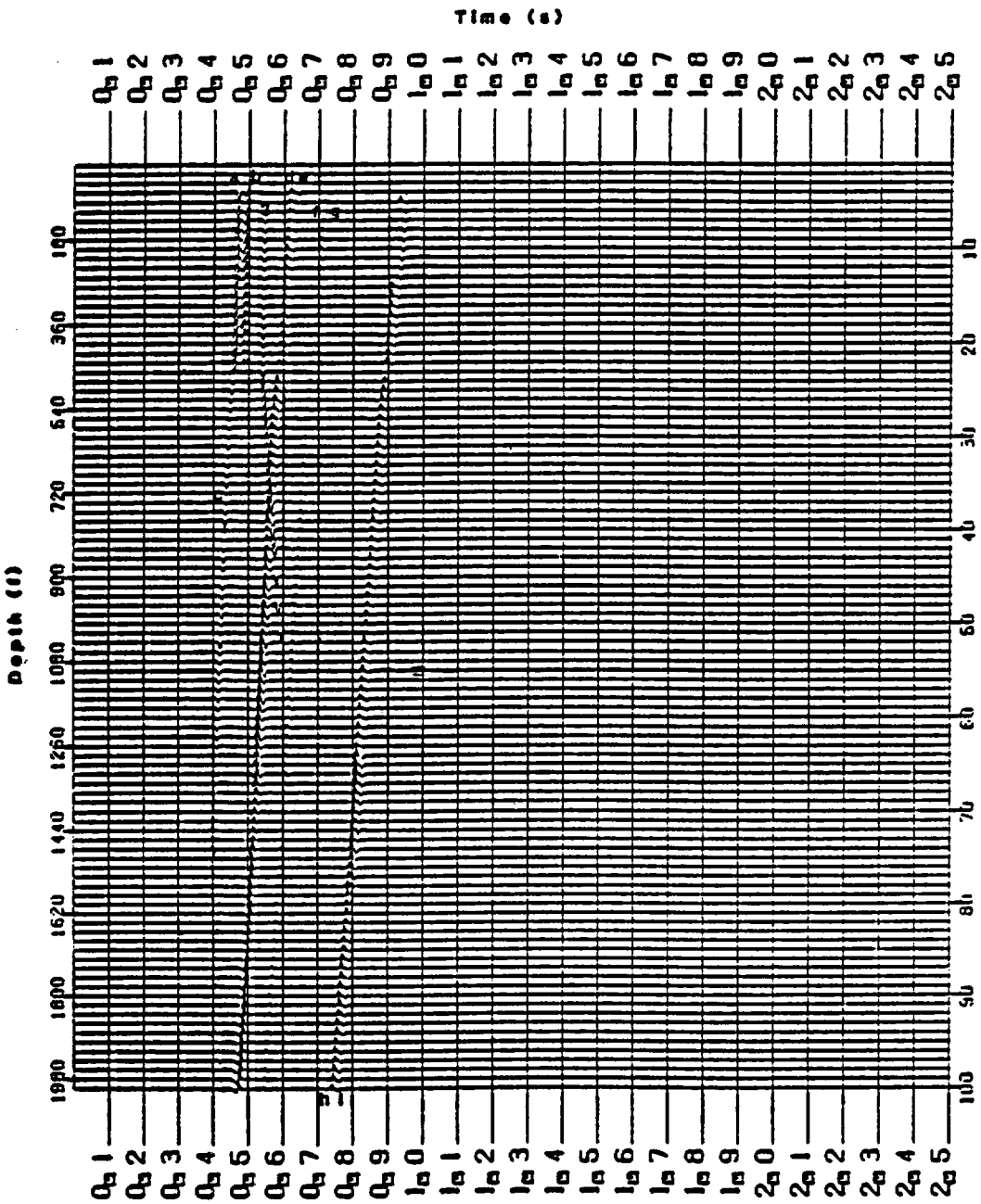

Figure 2.41. Synthetic VSP record for 4000-foot source offset after removing the direct arrivals. Reflections can be identified from n1(a), Tptw(b), n2(c), Tcbw(d), n3(e), Tctw(f), n4(g), Tlrw(h), and n5(i).

trough (e) can be identified as separate events, although destructive interference is occurring. On the deepest traces, however, the two events have merged into a single peak. Identifying the n3 reflection is impossible. The Tlrw reflection (h) and the n5 reflection (i) show a similar pattern, but an identifiable hint of the n5 trough does exist on the deeper traces.

Destructive interference is most apparent on the Tctw (f) and n4 (g) reflections. Only a faint hint of a peak-trough pair can be seen on Figure 2.41. This event could easily be obscured if the traces weren't free from noise.

The reflection from the n2 segment of fault plane 3 is seen as a trough on traces 5 through 42 and traces 44, 45, 48, and 52 between 0.5 and 0.6 second (3). As noted on Figure 2.38, a fault plane reflection can have a downgoing slope. Earlier, fault plane reflections with near-vertical and upgoing slopes were identified. This observation may have important ramifications when the field data from Yucca Mountain is collected, processed, and interpreted.

2.7 5000-foot source offset VSP

The sixth synthetic data set was created by moving the source 5000 feet to the east of borehole UZ-6. Five of the nine near-vertical faults lie to the west of the source and can not be imaged by reflecting raypaths. Figure 2.42 shows

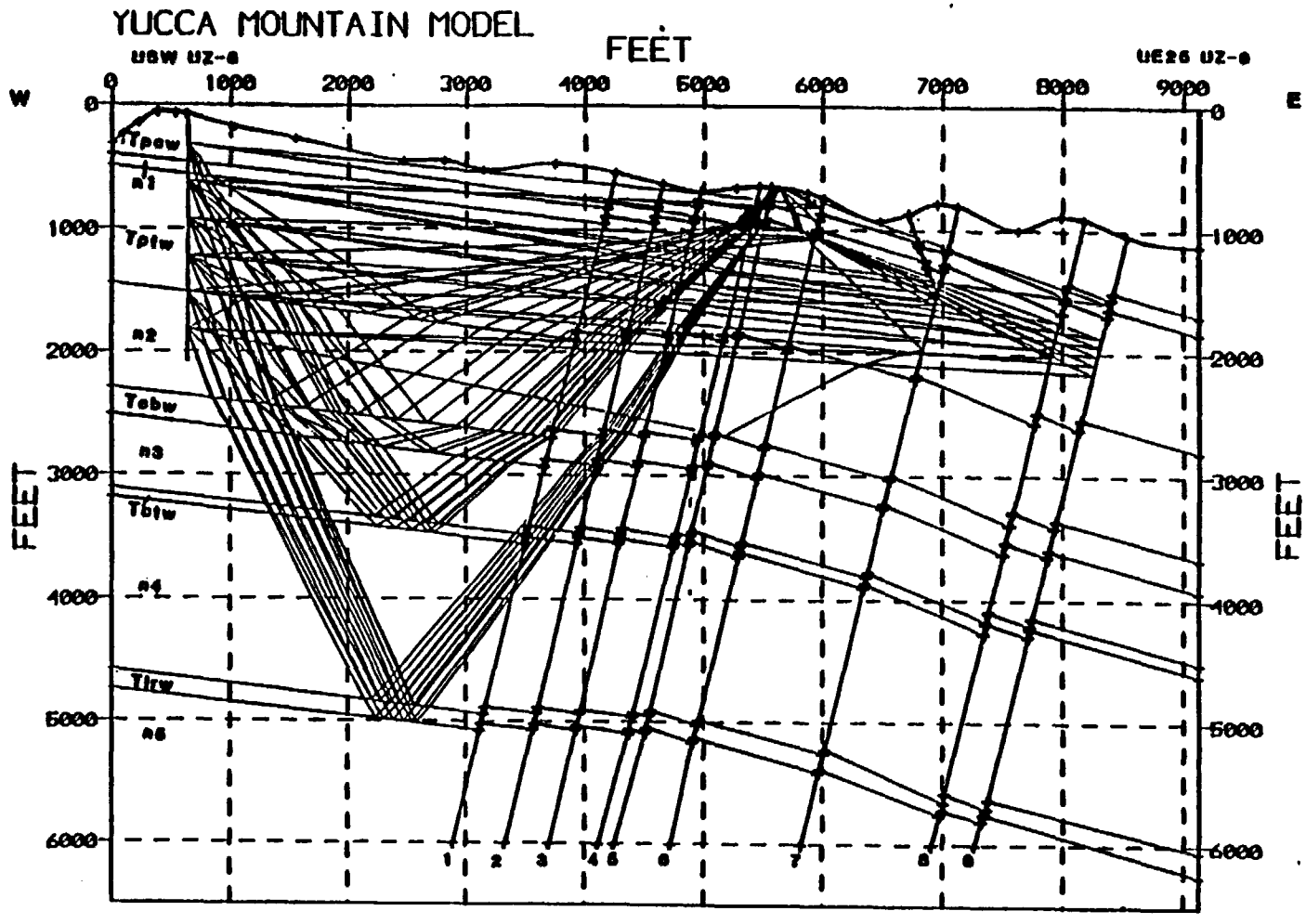

Figure 2.42. Raypath diagram for 5000-foot source offset VSP.

a raypath diagram for the 5000 foot offset model. The seven lowest unit boundaries are imaged in this diagram. As noted earlier, the reflective portions of the gently dipping horizons continue to move farther downdip to the east as the source offset increases. Horizons n1 and Tptw do not appear to be imaged in this diagram, although only rays which intersect at every fifteenth receiver are shown.

Rays which reflect off fault planes 6, 7, 8, and 9 within Tptw are seen in this diagram. Also, the highest segment of fault plane 6 (within Tpcw) provides many reflected rays which intersect borehole UZ-6.

The synthetic data set generated by the preceding ray tracing is shown in Figure 2.43. The first arrival can be seen as the trough which appears (with two gaps) on traces 70 through 100. The direct arrival also can be seen on traces 24 through 27 to the right of the n2 reflection.

A slightly different technique of median filtering was used to remove the first arrival in this data set. First arrival times were picked to align the first breaks at 0.1 second for traces 70 through 100. The first arrival does not appear on traces 76, 89, 90, and 91 so estimates of the arrival time (if a first break existed) were made and the traces were shifted accordingly. An 11-fold median filter was used to preserve the first arrivals on traces 70 through 100. Then traces 76, 89, 90, and 91 were muted on the data

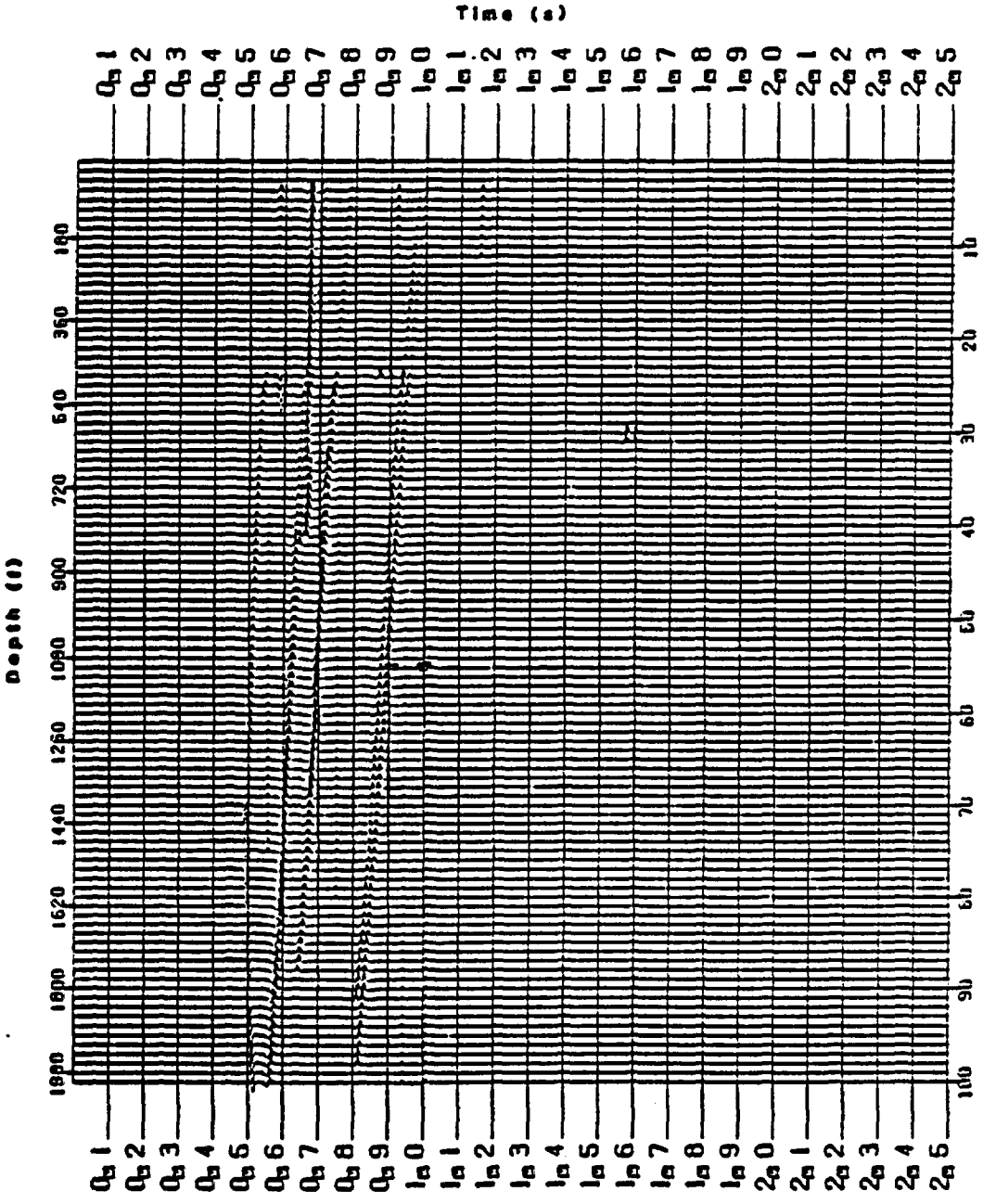

Figure 2.43. Synthetic VSP record generated by the ray tracing in Figure 2.42. The direct arrival trough appears on traces 24 through 27 at 0.59 second and again on traces 70 through 100.

set output by the median filter. The data set containing the first arrivals and the four muted traces was subtracted from the original data set. This effectively removed the first arrivals from the original data without altering the traces on which the first arrivals did not appear. This data set appears in Figure 2.44.

The reflections from fault planes 6, 7, 8, and 9 within Tptw are easily identified as the faint events with near-vertical slopes. Fortunately, the fault plane reflections are spaced such that no interference with the other reflections occurs.

The highest segments of fault plane 6 produce a reflection which can be seen at 0.675 second on traces 4 through 41 as a strong peak. This event arrives later than the reflection from the lower portion of the same fault plane due to the higher velocities at depth.

Reflections from seven of the nine unit boundaries are identifiable (excluding n1 and Tptw) on the shallow traces. On the deeper traces, Tcbw (b) and n3 (c) merge into one peak, as do Tctw (d) and n4 (e).

The ray tracing for the 5000-foot offset was repeated with the zero reflection coefficient fault segments excluded from the modeling. The raypath diagram for this model is shown in Figure 2.45. Rays can be seen reflecting off the seven lowest unit boundaries in the section, but not from

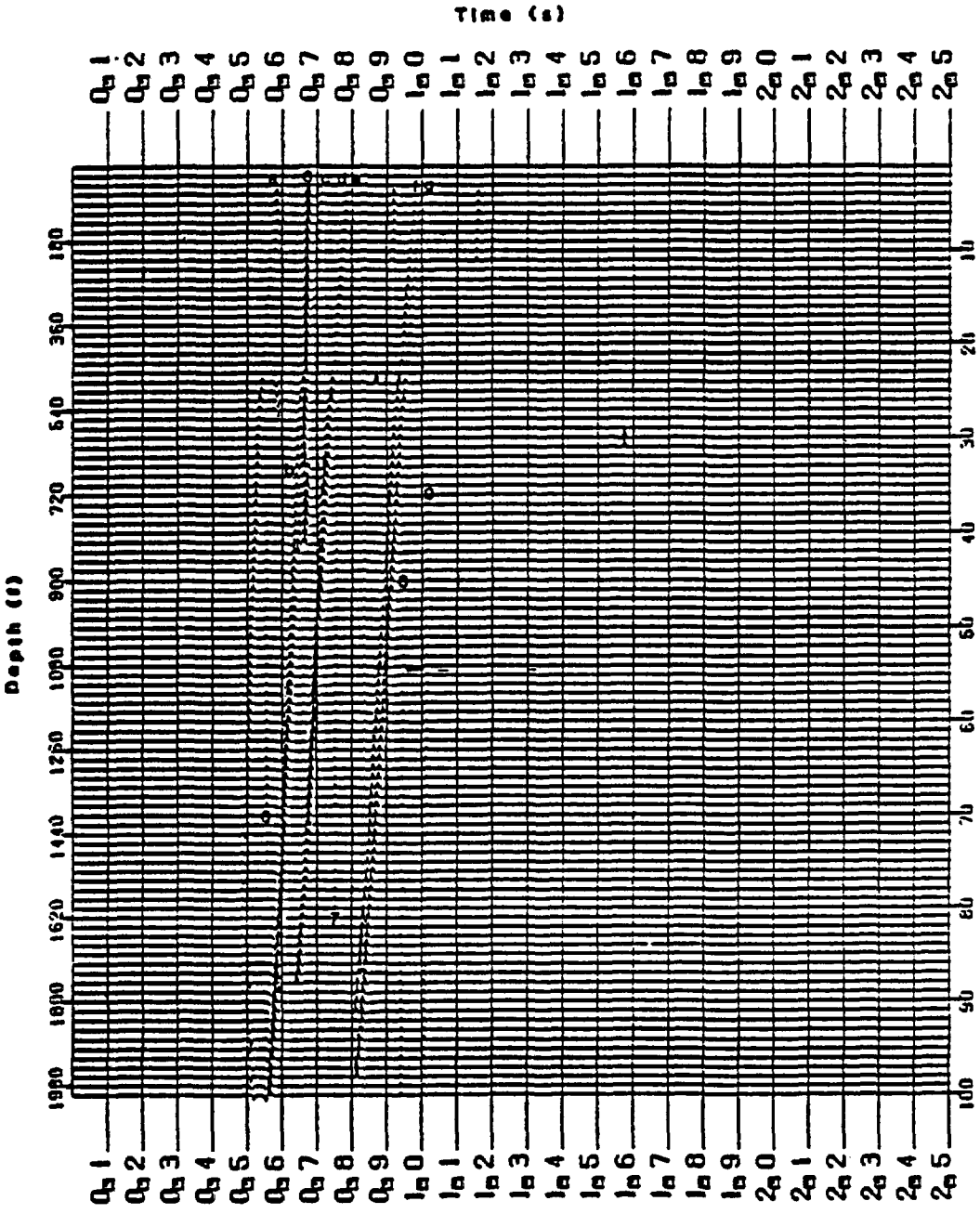

Figure 2.44. Synthetic VSP record for 5000-foot source offset after removing the direct arrivals. Reflections can be identified from n2(a), Tcbw(b), n3(c), Tctw(d), n4(e), Tlrw(f) and n5(g). Reflections from fault planes 6 through 9 can also be identified.

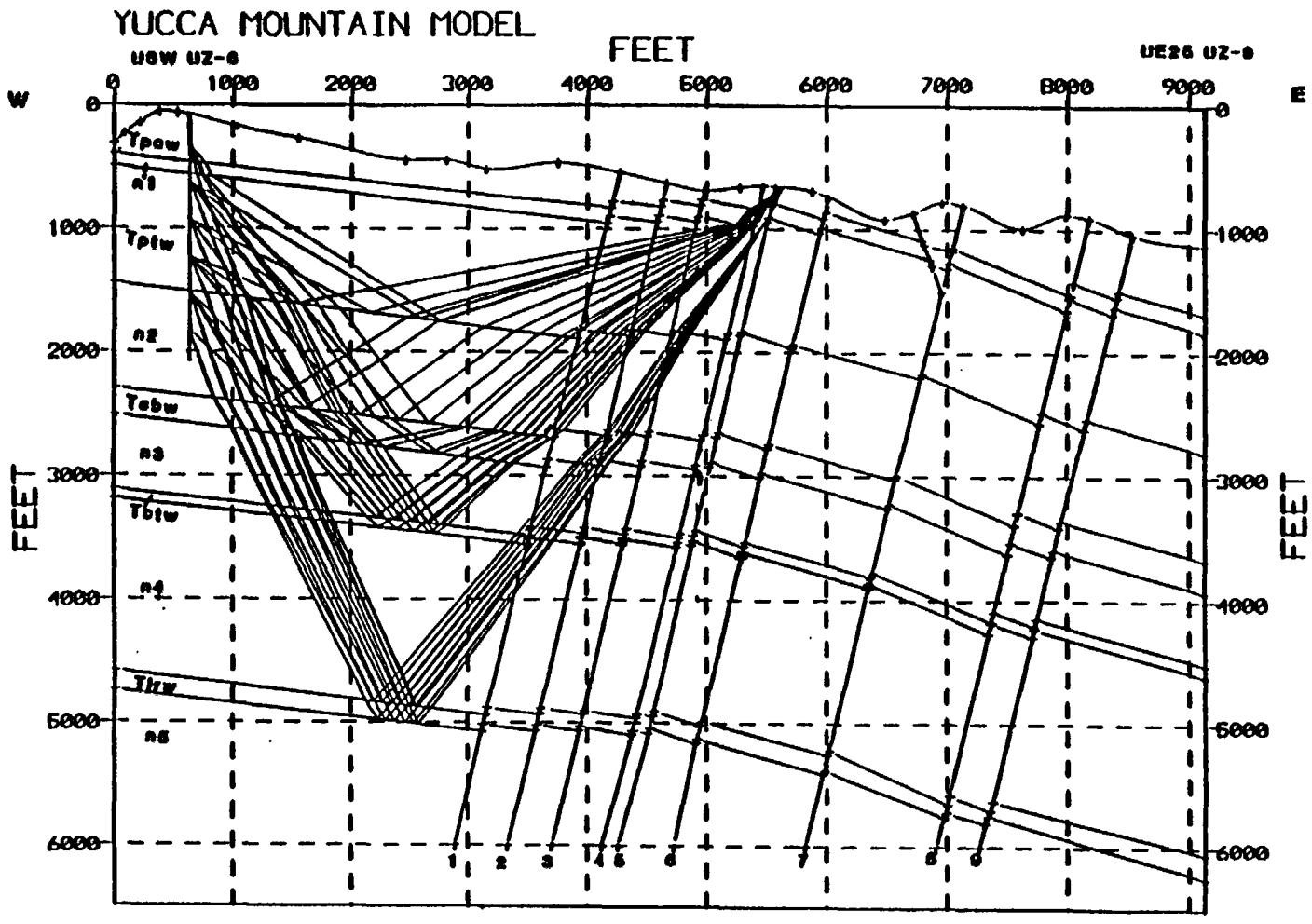

Figure 2.45. Raypath diagram for 5000-foot source offset VSP, excluding reflections from zero reflection coefficient fault planes.

any small segment of the high-angle fault planes. The data set from this ray tracing, after applying an AGC, is shown in Figure 2.46. The strong first arrival trough was removed in the same manner as described for the 5000-foot offset data set that contained fault plane reflections.

The data set with the first arrivals removed is shown in Figure 2.47. The n2 (a) reflection is of moderate amplitude and is easily identified. The Tcbw (b) and n3 (c) reflections interfere such that the n3 trough is almost completely obscured on traces 43 through 100. It is possible to distinguish the Tcbw peak from the n3 trough on the shallower traces, however.

The Tctw (d) and n4 (e) reflections interfere destructively again, resulting in a very small event on the data set. Interference of the Tlrw peak (f) and the n5 trough (g) decreases the amplitude of both of these events as well. It is difficult to distinguish the top of Tlrw from the top of n5, but it is slightly more distinct than the situation for Tctw and n4.

The data sets for the source offset of 5000 feet begin to show that the interpretation of the records will be increasingly difficult with increased offset. Reflections are beginning to interfere, and the identification of major events is becoming less obvious.

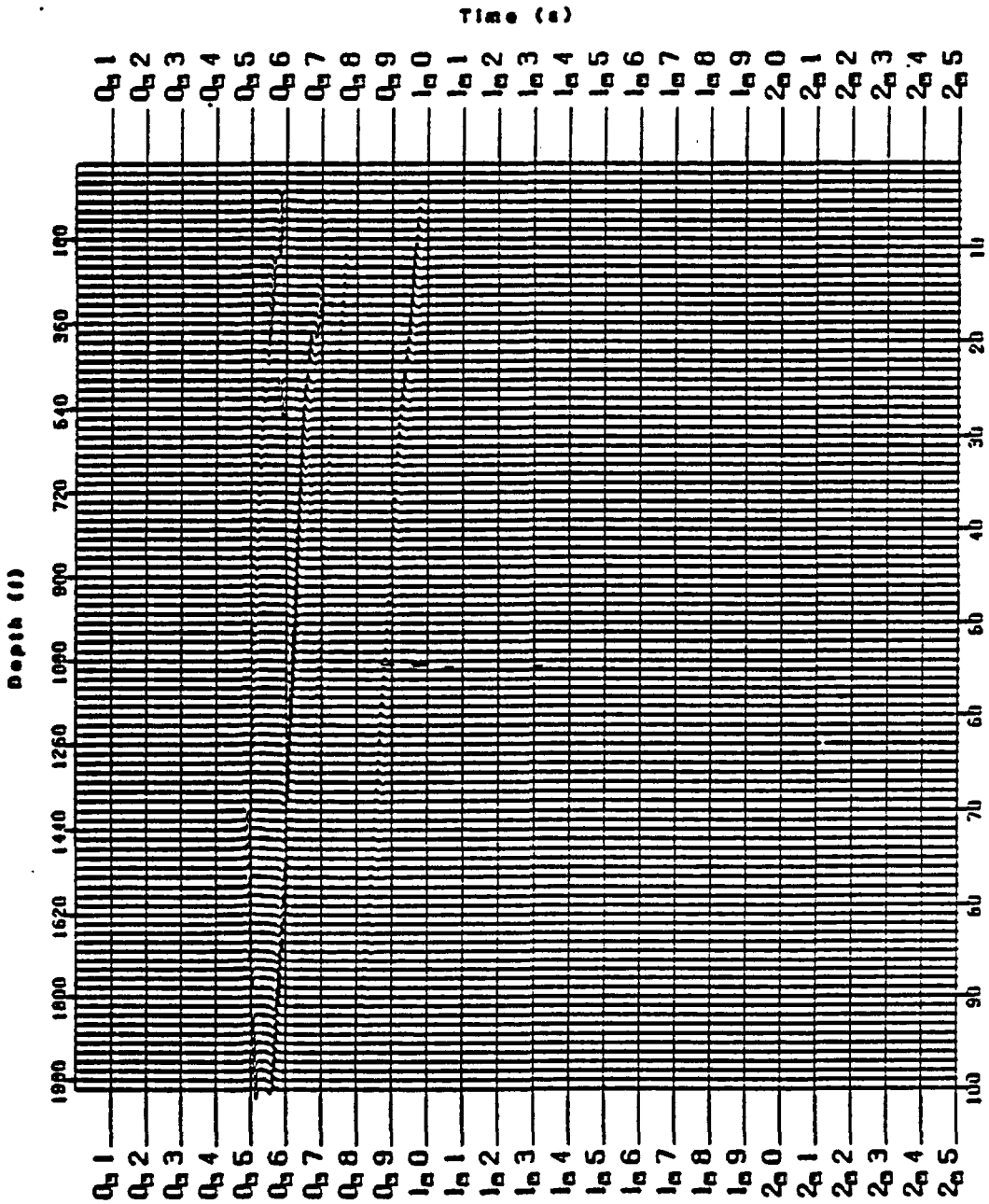

Figure 2.46. Synthetic VSP record generated by the ray tracing in Figure 2.45, after applying AGC. The first arrival trough appears on traces 24 through 27 and again on traces 70 through 100.

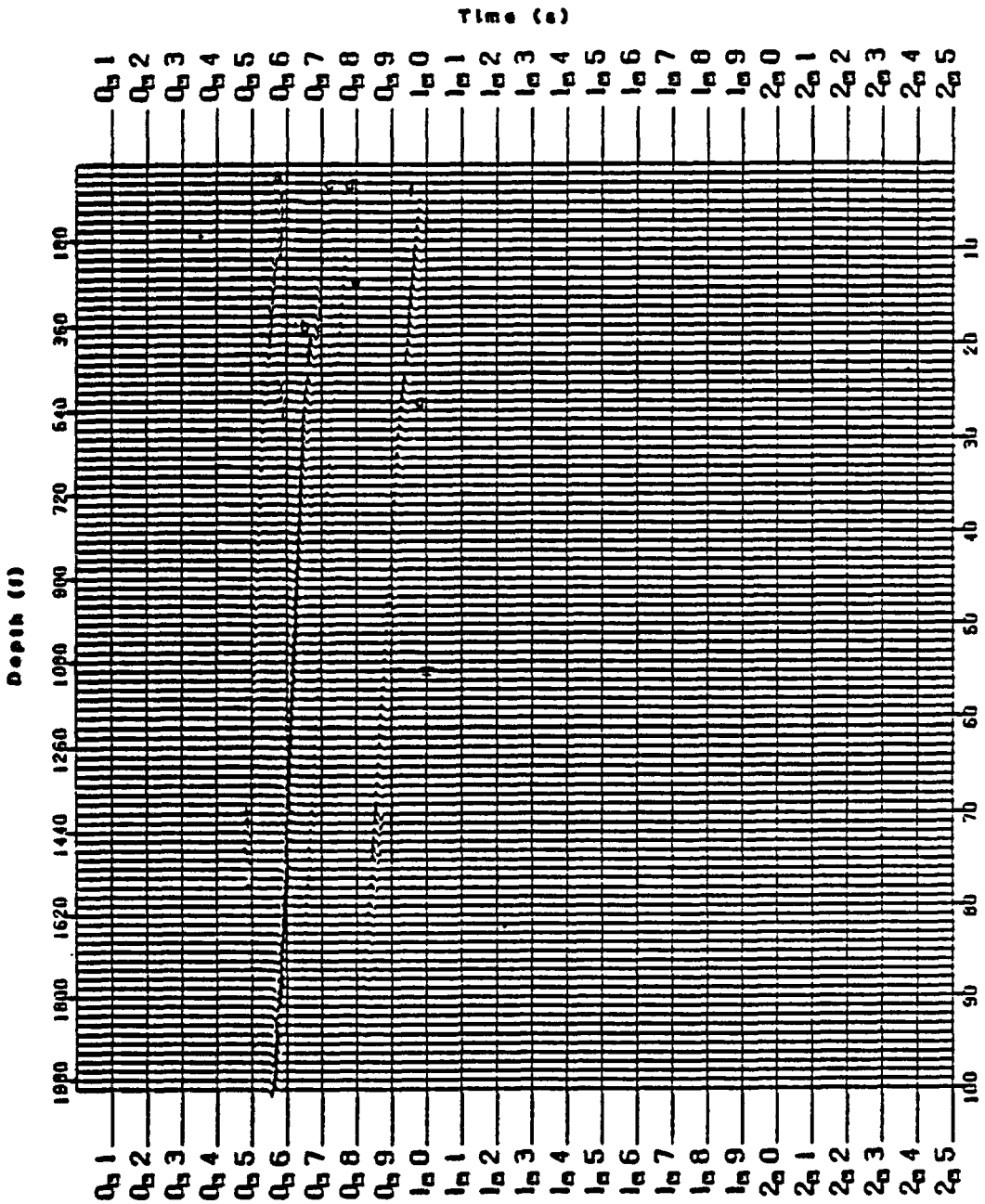

Figure 2.47. Synthetic VSP record for 5000-foot source offset after removing the direct arrivals. Reflections can be identified from n2(a), Tcbw(b), n3(c), Tctw(d), n4(e), Tlrw(f), and n5(g).

2.8 6000-foot source offset VSP

The raypath diagram for a seismic source 6000 feet east of borehole USW UZ-6 is shown in Figure 2.48. Only fault planes 7, 8, and 9 lie to the east of the source and have a chance of being imaged. From the diagram, it is apparent that many rays are indeed being reflected off the fault planes and intersecting the borehole.

For the first time, rays are reflecting off horizons on upthrown fault blocks. On the diagram, rays can be seen reflecting off horizons n3, n4, and n5 on at least one upthrown fault block.

The synthetic data set generated by the preceding ray tracing is shown in Figure 2.49. Interestingly, only four traces contain the first arrival trough. Traces 81 through 84 show the trough at 0.590 second. The source is located on the east side of a stream channel, and this seems to have had an effect on AIMS' ability to trace a downgoing ray from the source to UZ-6. The aforementioned aperture problems also may have helped limit the appearances of the direct arrival. In any event, a 3-fold median filter was used on the four traces containing the direct arrivals to separate the upgoing and downgoing wavefields.

The data set after removing the direct arrivals is shown in Figure 2.50. It is possible to identify five of the seven unit boundaries individually. The n2 (a) reflection

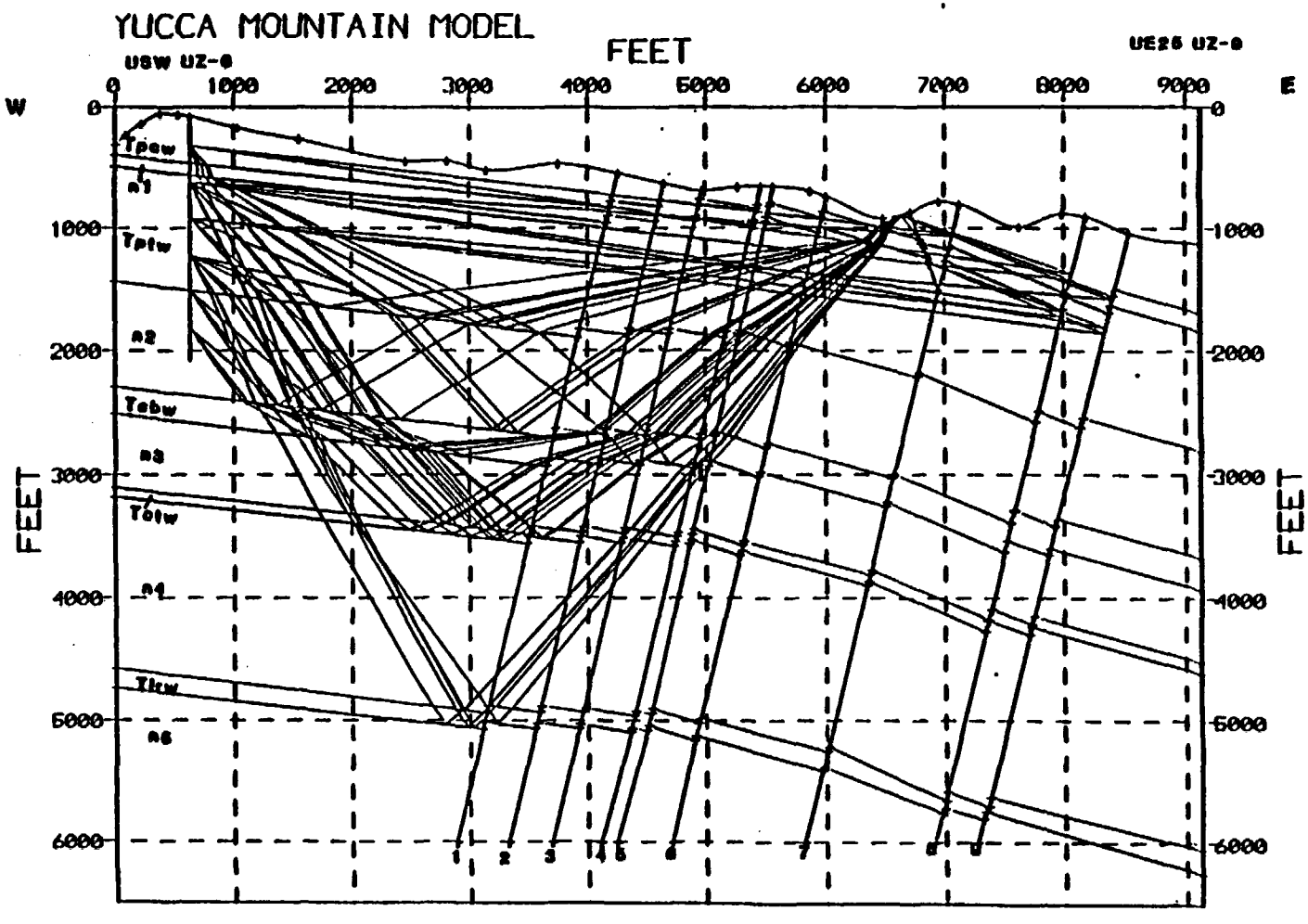

Figure 2.48. Raypath diagram for 6000-foot source offset VSP. Reflections from horizons on upthrown fault blocks can be seen.

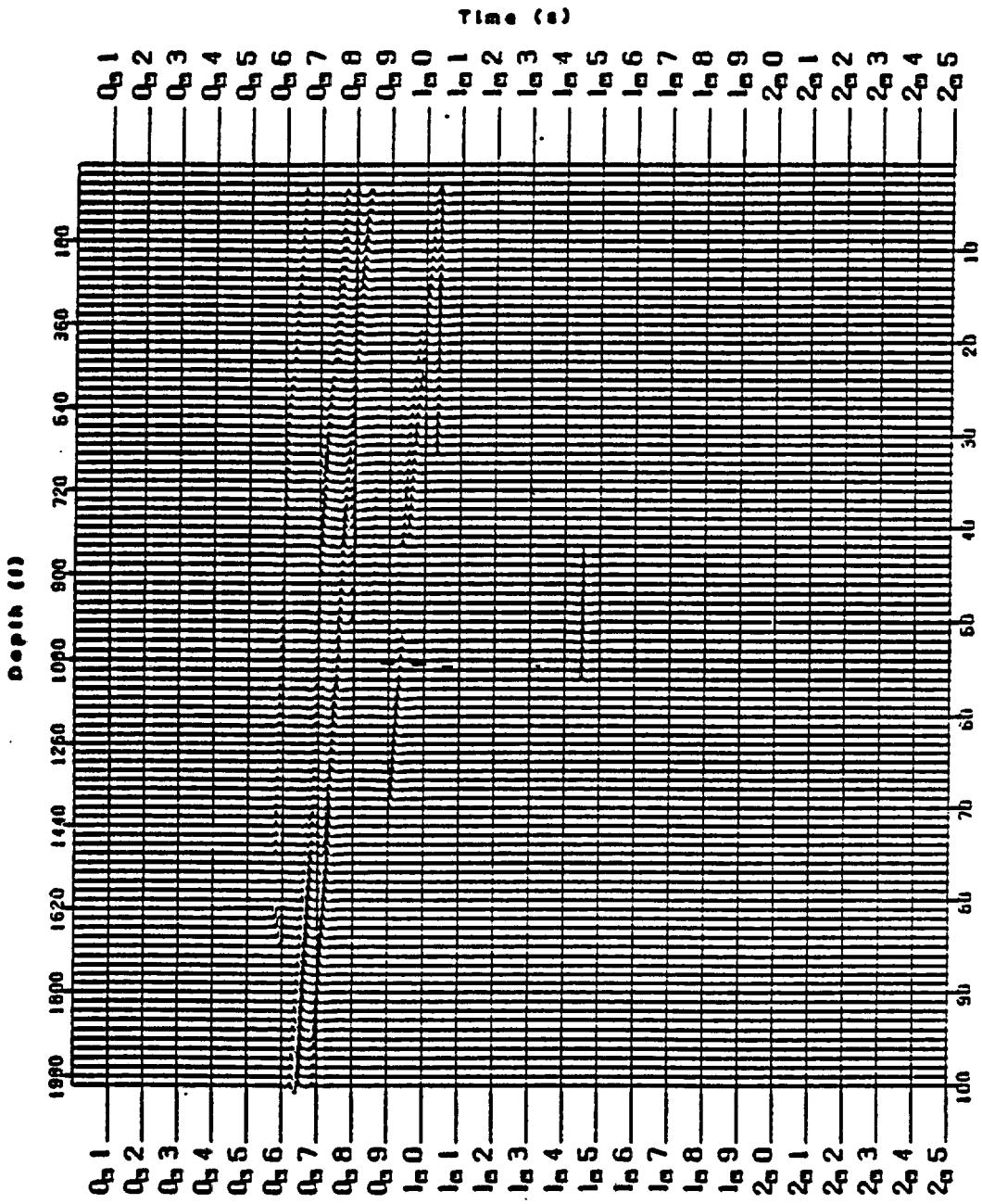

Figure 2.49. Synthetic VSP record generated by the ray tracing in Figure 2.48. The direct arrival trough can be seen only on traces 81 through 84.

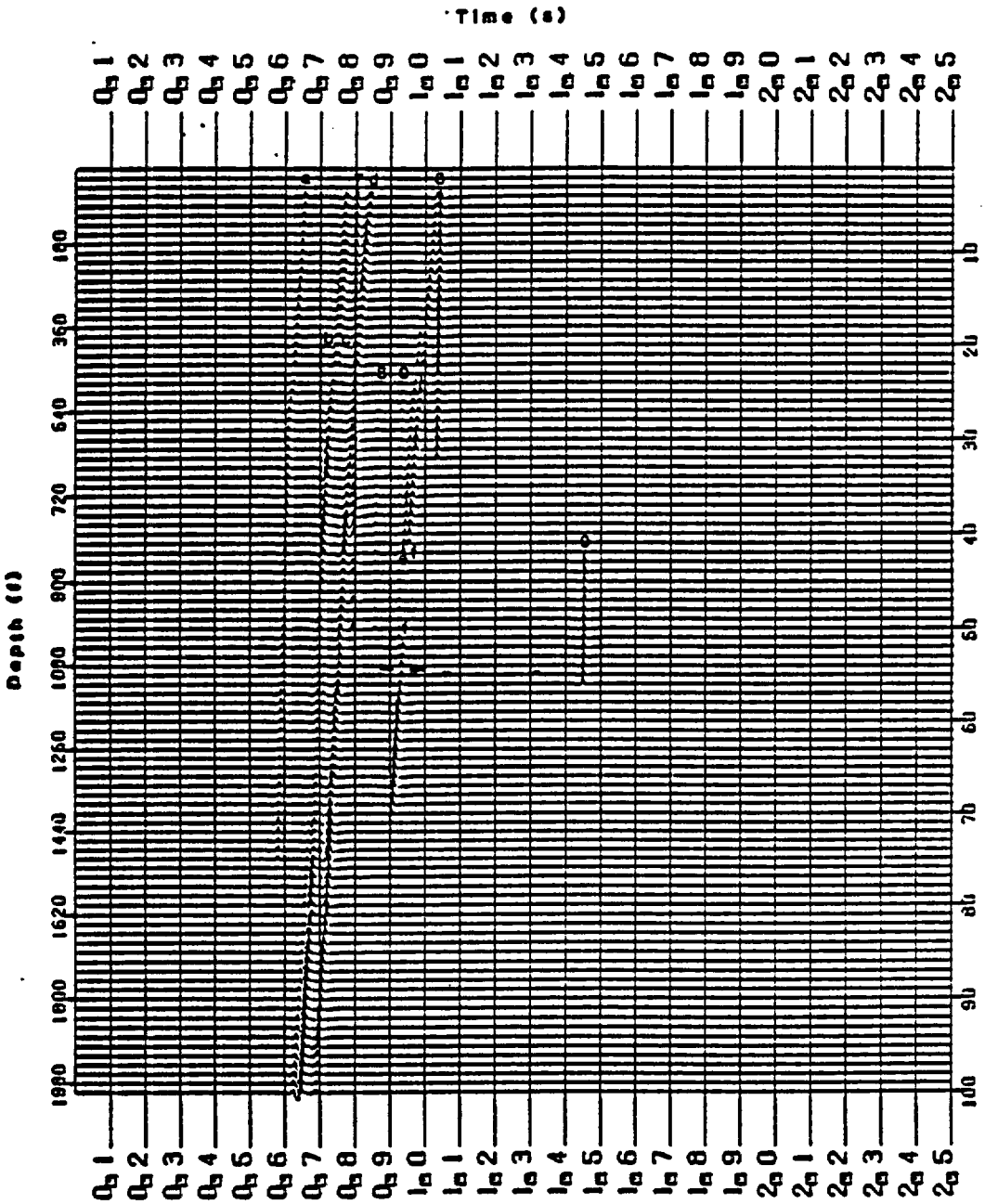

Figure 2.50. Synthetic VSP record for 6000-foot source offset after removing the direct arrivals. Reflections can be identified from n2(a), Tcbw(b), n3(c), Tctw and n4(d), Tlrw(e), and n5(f). Fault plane reflections from 8 and 9 can be identified in two separate locations.

is distinct, as it was on most of the previous data sets. The Tcbw (b) and n3 (c) reflections can be seen as separate peaks on traces 9 through 22. Lower in the borehole, only one peak is seen until trace 54, where two peaks can be seen down to trace 100. The Tlrw (e) and n5 (f) reflections can be identified as distinctly separate events on traces 19 through 41, between 0.9 and 1.0 second.

The Tctw and n4 reflections can not be identified uniquely, other than the hint of two peaks seen on traces 16, 17, and 18. On all other traces, only one peak (d) can be seen for the two events.

Reflections from fault planes 8 and 9 can be seen as the near-vertical events at 0.860 and 0.930 second on traces 24 through 50. The reflection from the highest segment of fault plane 7 (within Tpcw) appears as the peak which lies along the 0.8 second time line on traces 4 through 40 and on traces 43, 44, 47, and 50. This event is difficult to identify due to interference with the Tctw and n4 reflections. A reflection from the highest segment of fault plane 8 can be seen on traces 4 through 32 at 1.05 seconds. Finally, a segment of fault plane 9 within the Shardy Base (n1) produces a reflection on traces 46 through 56 at 1.450 seconds.

The gap in the n5 (f) reflection between traces 43 and 52 is due to offset across fault plane 1. The n5 events on traces 4 through 42 are events reflecting off the downthrown

block. The n5 reflection on traces 52 through 70 are events reflecting off the upthrown fault block. Gaps in the n3 and n4 reflections are not obvious on this data set, making it difficult to distinguish separate n3 and n4 reflections from the upthrown and downthrown blocks.

The ray tracing was repeated for a source offset of 6000 feet, excluding the zero reflection coefficient fault planes. The raypath diagram from this ray tracing appears in Figure 2.51. No segment of any fault plane appears to be generating reflections. The synthetic data set created by this ray tracing is shown in Figure 2.52. As in the previous data set, the four traces containing the first arrivals were median filtered. The upgoing wavefield appears in Figure 2.53.

The n2 reflection (a) appears as a strong, consistent trough which is easily identified. A strong peak (b) occurs from Tcbw, but the underlying n3 trough is completely obscured. The Tctw peak and the n4 trough interfere destructively and the result is a small peak (c) on most traces. At trace 76, the small peak changes polarity and becomes a small trough. Selective ray tracing experiments showed that this indicates a change in fault block. The string of small peaks on traces 4 through 75 were generated on the downthrown block from Tctw. The troughs on traces 76 through 100 (d) are n4 reflections from the upthrown fault block.

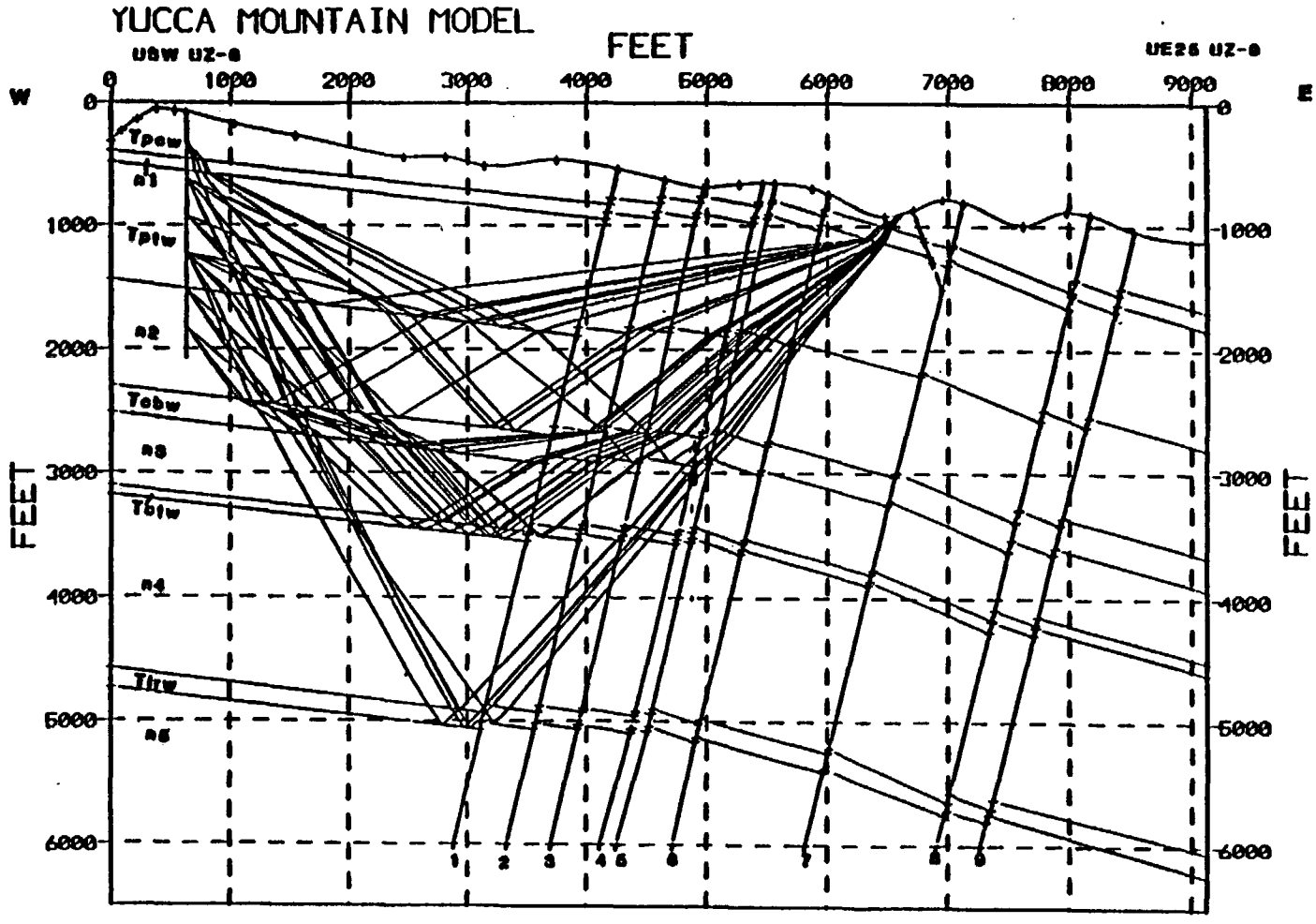

Figure 2.51. Raypath diagram for 6000-foot source offset VSP, excluding reflections from zero reflection coefficient fault planes.

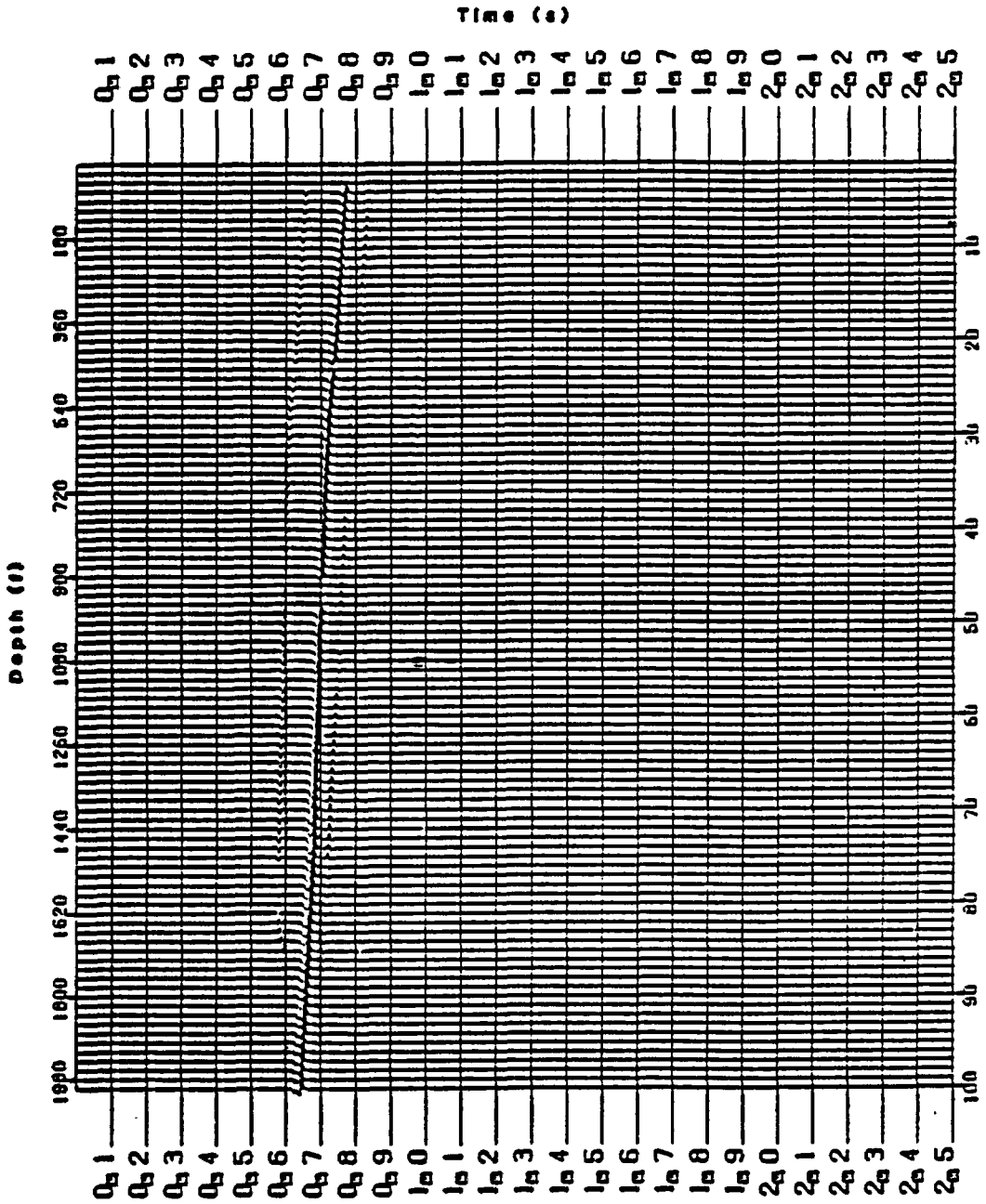

Figure 2.52. Synthetic VSP record generated by the ray tracing in Figure 2.51, after applying AGC. The direct arrival trough appears on traces 81 through 84.

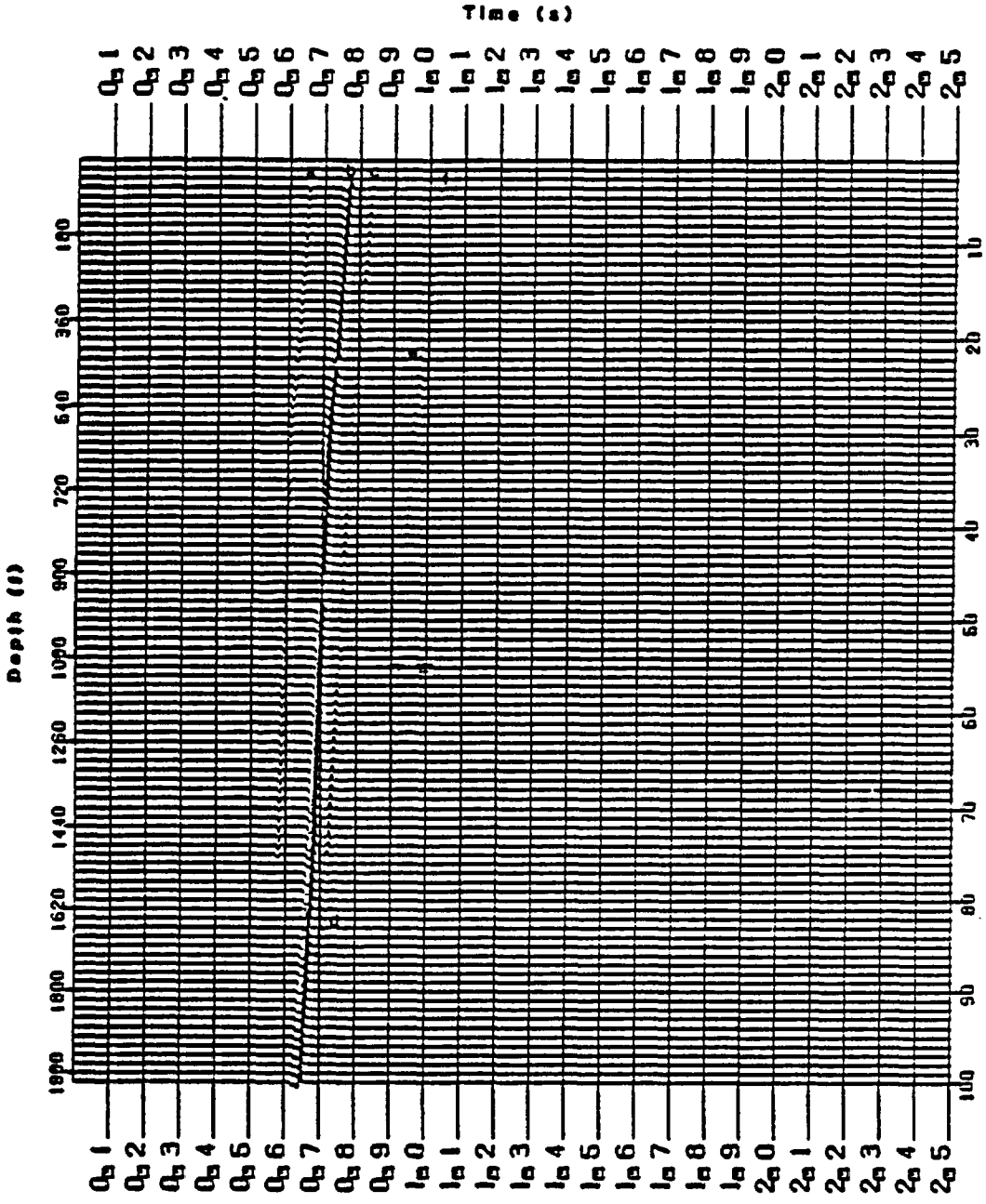

Figure 2.53. Synthetic VSP record for 6000-foot source offset after removing the direct arrivals. Reflections can be identified from n2(a), Tcbw and n3(b), Tctw and n4(c), n4(d), Tlrw(e), and n5(f). Interpretation is becoming increasingly difficult with increasing offset.

The Tlrw and n5 reflections are very weak on this data set. It is possible to identify the Tlrw peak (e) and the n5 trough (f) on selected traces high in the borehole.

2.9 7000-foot source offset VSP

With the source offset 7000 feet to the east of UZ-6, the seismic source is located at the center of a dry stream bed. The model does not contain any alluvium, so coupling of the computer source to the ground is probably considerably better than an actual source would have at the same location at Yucca Mountain.

Only fault planes 8 and 9 lie to the east of the source for a 7000 foot offset. Figure 2.54 shows a raypath diagram for the model. Fault planes 8 and 9 are seen to generate reflections. As for the model with a 6000 foot offset, reflections are generated by horizons on both the upthrown and downthrown sides of fault planes. As seen on the diagram, horizons n2 and n5 produce reflections from multiple fault blocks.

The synthetic data set created by the preceding ray tracing is shown in Figure 2.55. The AIMS ray tracing algorithm was only able to find a single downgoing direct arrival which intersected borehole UZ-6. The solitary direct arrival trough appears on trace 88 and 0.695 second. In a real physical situation, it is difficult to imagine that a

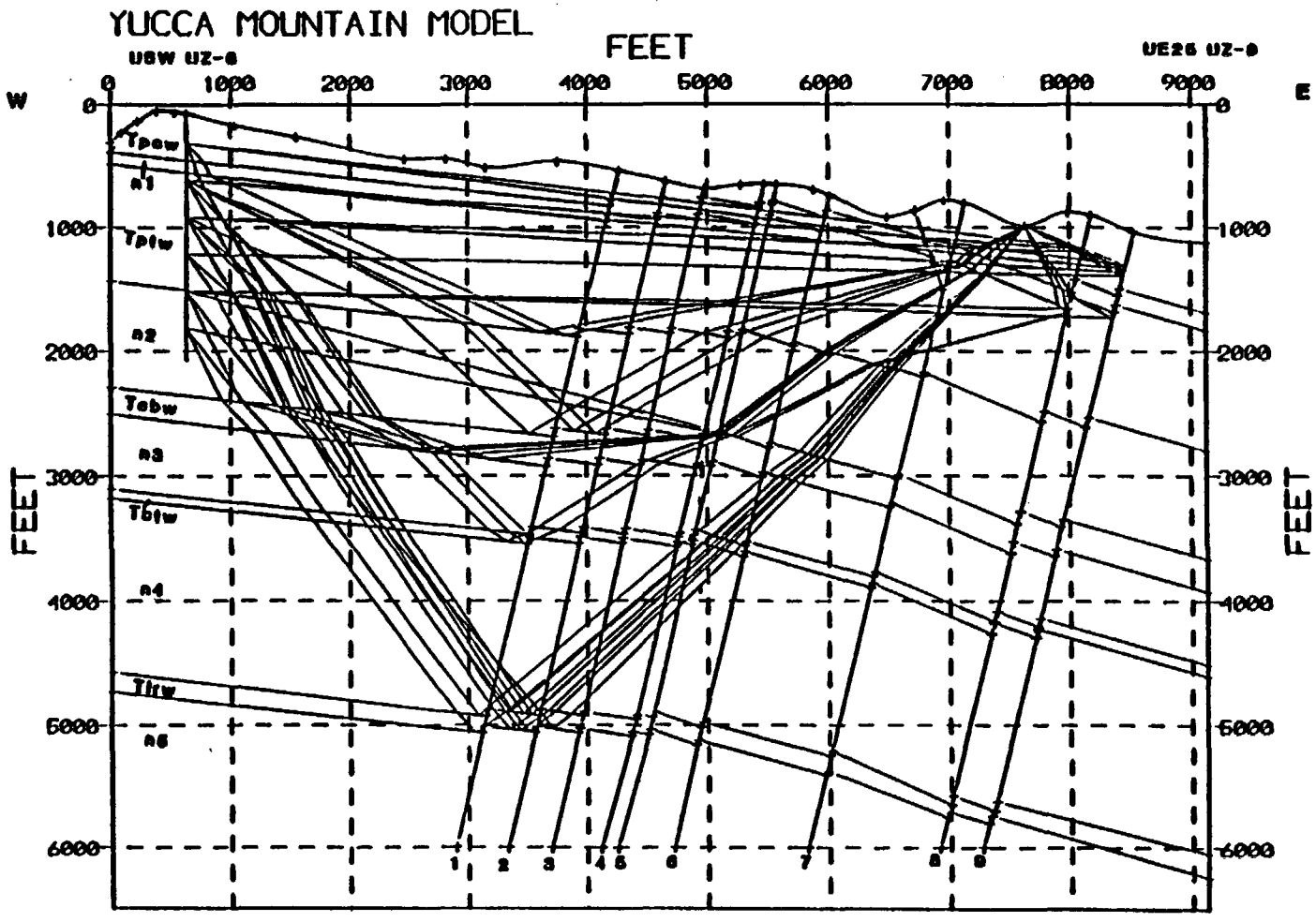

Figure 2.54. Raypath diagram for 7000-foot source offset VSP. Reflections from horizons on upthrown fault blocks can be seen.

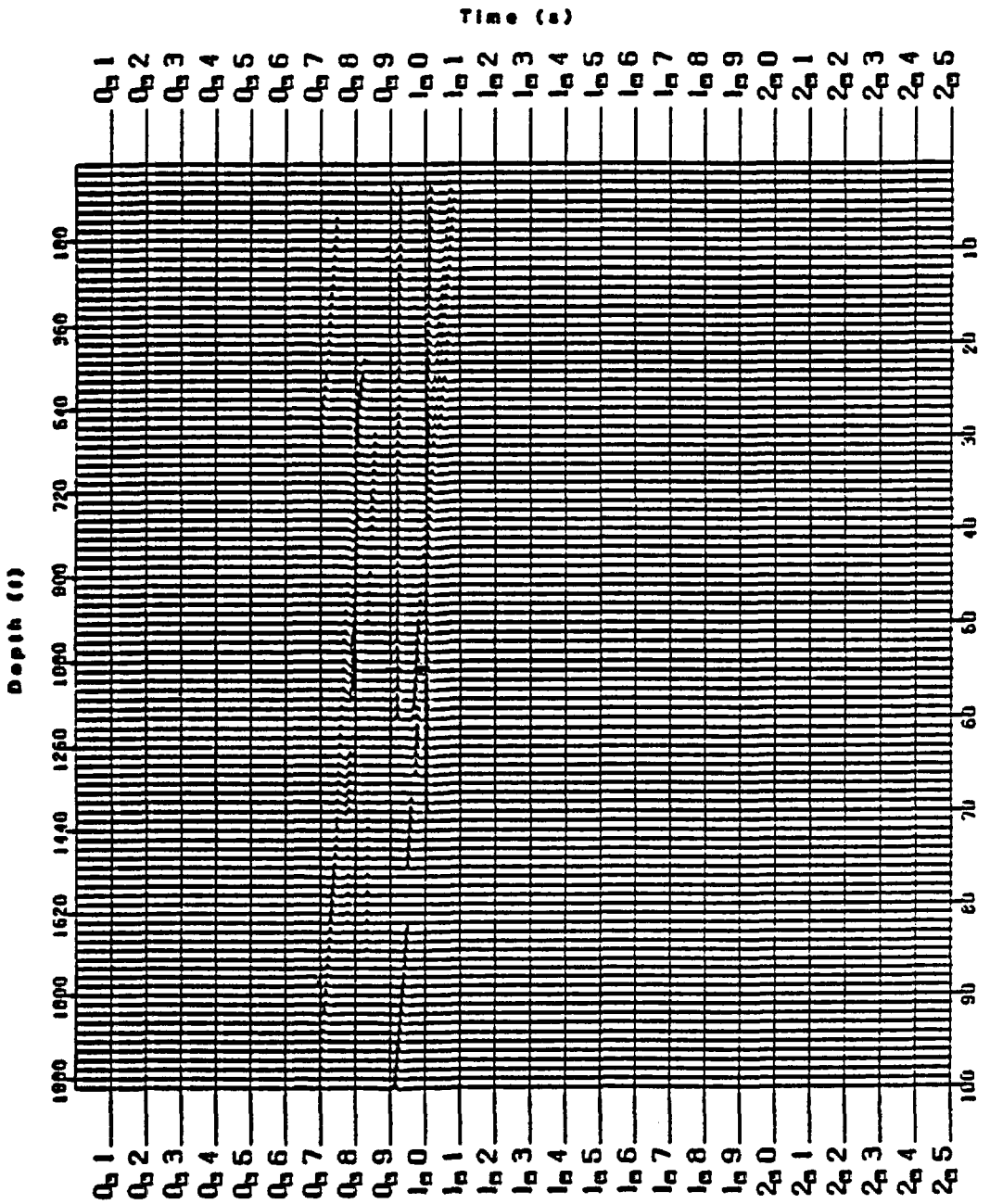

Figure 2.55. Synthetic VSP record generated by the ray tracing in Figure 2.54. The direct arrival trough appears only on trace 88, at 0.695 second.

direct arrival would only be able to intersect one of the one hundred geophones in the borehole. It is possible that the orientation of the fault blocks near the source makes it impossible for the direct arrivals to reach the borehole in this model. The single first arrival trough was muted out of the data set. The upgoing wavefield appears in Figure 2.56.

The reflections in Figure 2.56 have become difficult to interpret. The peak which arrives at 0.925 second on traces 4 through 60 is a reflection from the highest segments of fault plane 8. The peak which arrives at 1.0 second on traces 4 through 70 is a reflection from the highest segments of fault plane 9.

The reflection from n2 (a) is easy to identify as the peak between 0.7 and 0.8 second on traces 7 through 32. The remaining reflections required additional ray tracings with selected horizons in order to identify the events.

The event on traces 46 through 100 between 0.7 and 0.8 second (c) is a reflection from n3. The event on traces 22 through 58 and on traces 64 through 70 near 0.8 second (b) are reflections from two sections of Tcbw. The events on traces 64 through 70 come from the downthrown block west of fault plane 1. The events on traces 22 through 58 come from both the upthrown and downthrown blocks. It is difficult to discern the break between the upthrown block events and the

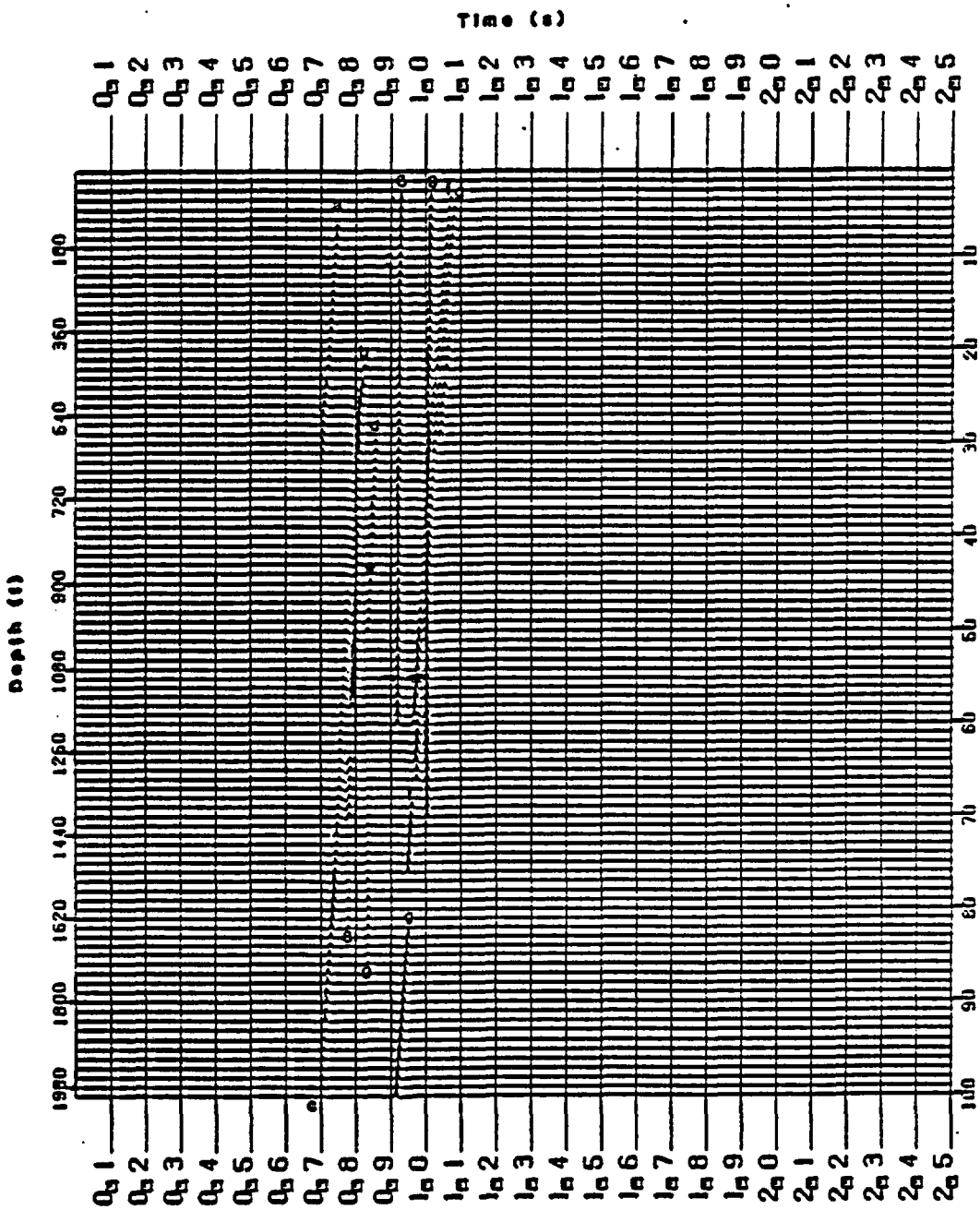

Figure 2.56. Synthetic VSP record for 7000-foot source offset after removing the direct arrival. Reflections can be identified from n2(a), Tcbw(b), n3(c), Tctw(d), n4(e), Tlrw(f), and n5(g). Fault plane reflections from faults 8 and 9 can be identified at two locations.

downthrown block events.

The peaks on traces 30 through 41 at 0.850 second (d) are reflections from Tctw. The peaks on traces 45 through 50 (e) are reflections from n4.

The remaining events are reflections from Tlrw (f) and n5 (g). Since the reflections are coming from both upthrown and downthrown fault blocks, gaps appear in the events. The source of these events is seen more clearly on the next data sets.

Figure 2.57 is a raypath diagram for a 7000-foot source offset with the zero reflection coefficient fault planes excluded. No reflections are generated from any segment of fault plane 8 or 9. The synthetic data set created by this ray tracing is shown in Figure 2.58. The single first arrival on trace 88 was muted. The upgoing wavefield is shown in Figure 2.59.

The identification of the events is slightly easier in this data set since events have their proper polarities. The n2 trough (a) between 0.7 and 0.8 second is easily identified once again. The strong peaks (b) at 0.8 second are from Tcbw. The string of troughs on traces 46 through 100 (c) come from n3. Referring to the raypath diagram in Figure 2.57, it is seen that the reflections from n3 travel a great distance through Tcbw, which has a high velocity. The result is a unit, Tcbw, whose bottom reflection

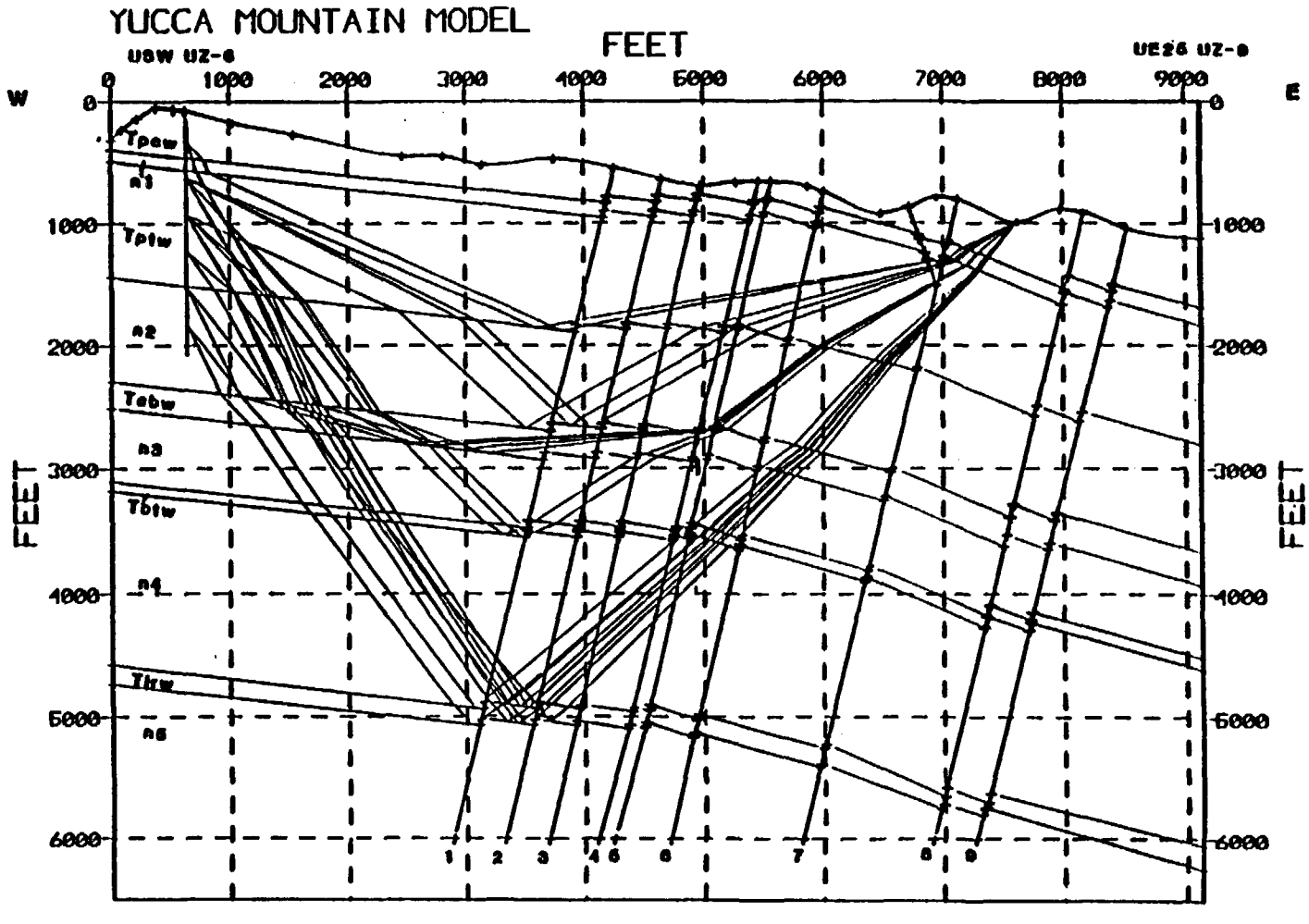

Figure 2.57. Raypath diagram for 7000-foot source offset VSP, excluding reflections from zero reflection coefficient fault planes.

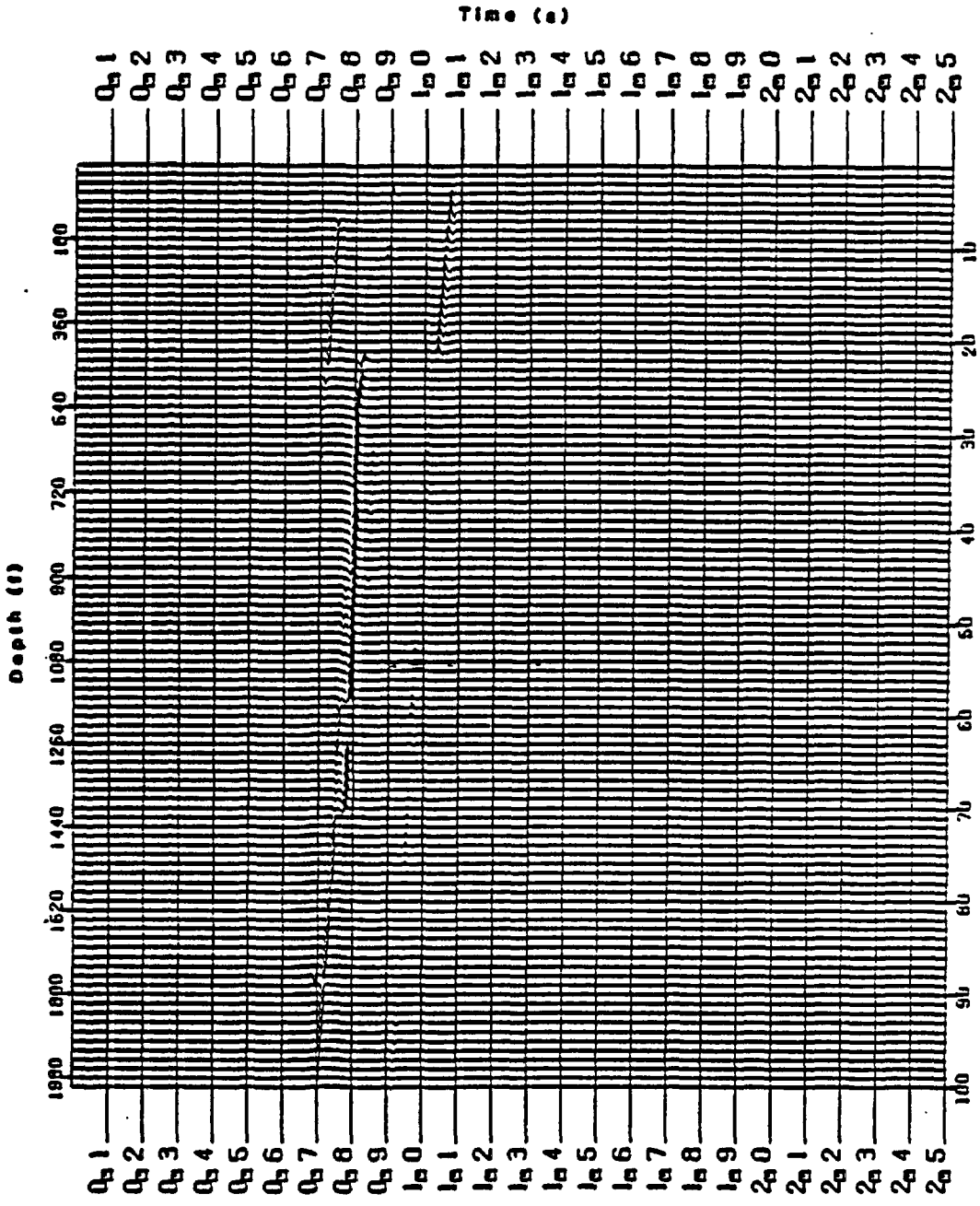

Figure 2.58. Synthetic VSP record generated by the ray tracing in Figure 2.57, after applying AGC. The sole first arrival trough appears on trace 88 at 0.695 second.

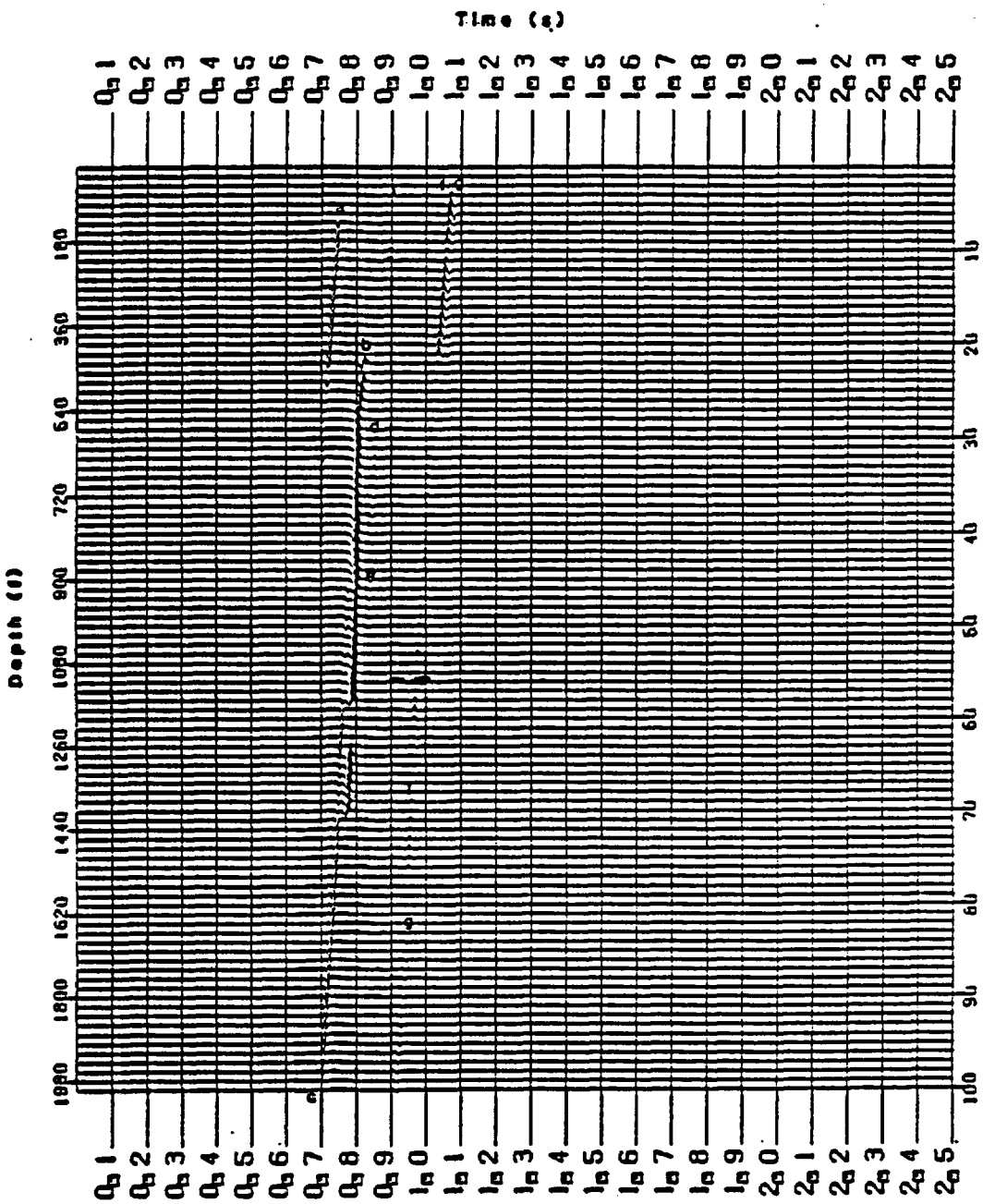

Figure 2.59. Synthetic VSP record for 7000-foot source offset after removing the direct arrival. Reflections can be identified from n2(a), Tcbw(b), n3(c), Tctw(d), n4(e), Tlrw(f), and n5(g). Polarity reversals are critical for identifying these events.

arrives before its top reflection on the deeper traces.

The small string of events on traces 30 through 41 at 0.85 second (d) come from Tctw. The string of troughs on traces 45 through 50 (e) are generated from n4.

The reflections from Tlrw (f) and n5 (g) are seen between 1.0 and 1.1 seconds on the shallow traces. On the deeper traces, these reflection are fragmented. The peaks on traces 69 through 76 at 0.95 second (f) are generated from Tlrw on the downthrown block west of fault plane 1. The troughs on traces 83 through 100 at 0.925 second (g) are reflections from n5 on the same fault block.

2.10 8000-foot source offset VSP

The final modeling experiment for the UZ-6 borehole was conducted using a source offset of 8000 feet to the east of the borehole. All nine of the high-angle fault planes lie to the west of the source, and can not be imaged by the reflection of seismic rays. Figure 2.60 is a raypath diagram for this model. Several of the rays have very complicated paths, such as the reflections from Tcbw and the reflections from the n3 horizons on fault blocks 5000 feet from the borehole. The synthetic data set generated by this ray tracing is shown in Figure 2.61.

The first arrival trough is seen at 0.790 second on traces 76 through 93. This event was removed by median

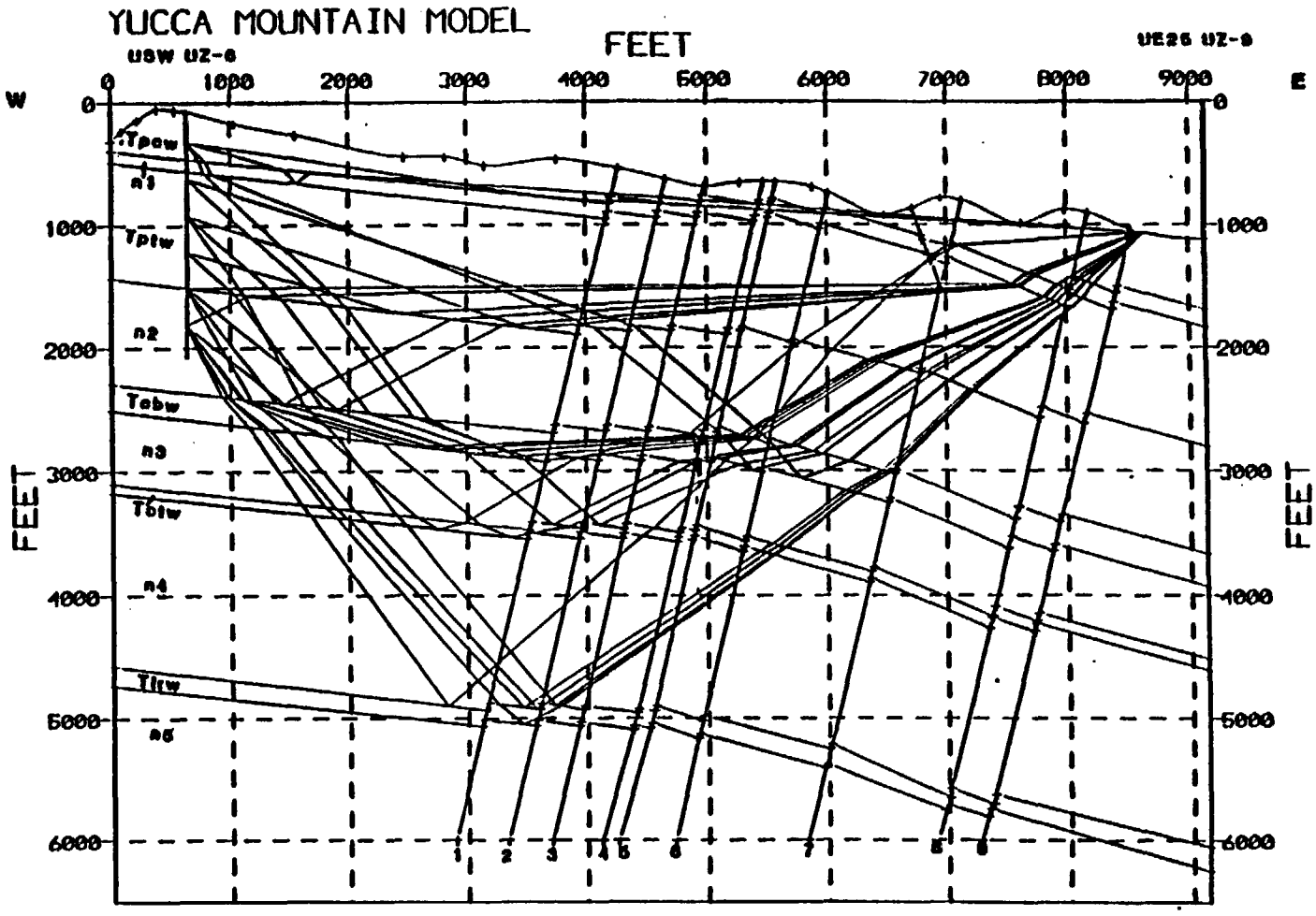

Figure 2.60. Raypath diagram for 8000-foot source offset VSP. Reflections from horizons on upthrown fault blocks can be seen. Since no fault planes are imaged, this diagram shows the raypaths for both data sets generated at this offset.

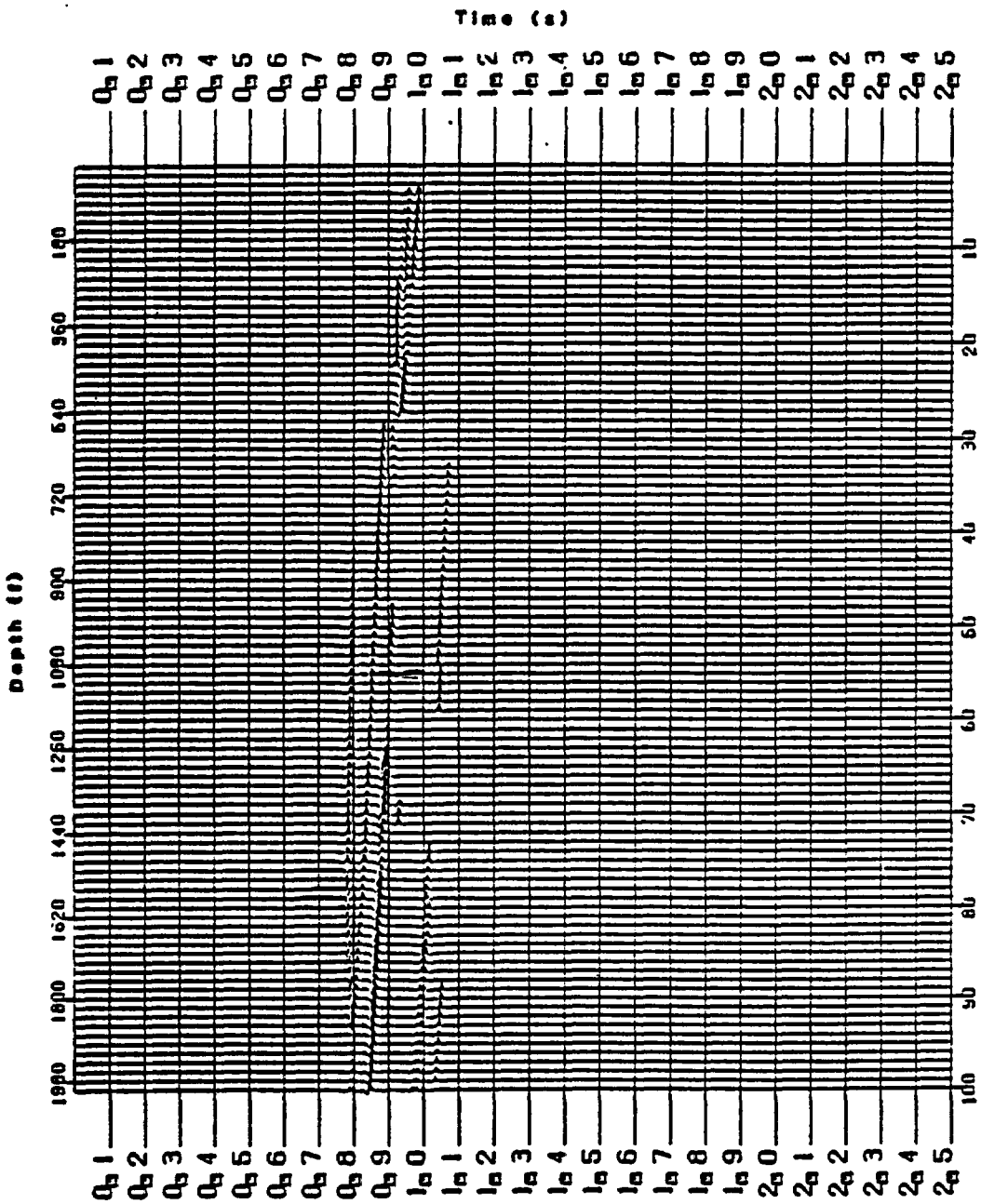

Figure 2.61. Synthetic VSP record generated by the ray tracing in Figure 2.60. The direct arrival trough is seen on traces 76 through 93.

filtering. The resulting upgoing wavefield is shown in Figure 2.62.

In order to identify the events in Figure 2.62, it was necessary to repeat the 8000-foot offset ray tracing using only one or two reflecting horizons at a time. The reflection from n2 (a) is fairly easy to identify at 0.8 second. The reflection from n3 on traces 30 through 100 (b) comes from the fault block west of fault plane 1. The peaks on traces 4 through 23 (b) also come from n3, but from fault blocks 5000 feet to the east of UZ-6.

The peaks between 0.9 and 1.0 second on traces 4 through 27 (c) are reflected events from Tptw. Due to the lower velocities along the travel paths for these events, the events arrive later than reflections from deeper horizons. The peaks on traces 14 through 22 at 0.920 second (d) are reflections from n1. These events reflect at a very low angle off the downthrown fault block west of fault plane 1.

Reflections from Tctw (e) appear in three segments. Several peaks at 0.950 second between events (b) and (c) on traces 4 through 15 are reflections from Tctw on the fault block between fault planes 2 and 3. On traces 48 through 70 at 0.9 second are reflections from Tctw on the fault block between fault planes 1 and 2. Finally, the peaks on traces 94 through 100 at 0.850 second are Tctw reflections from

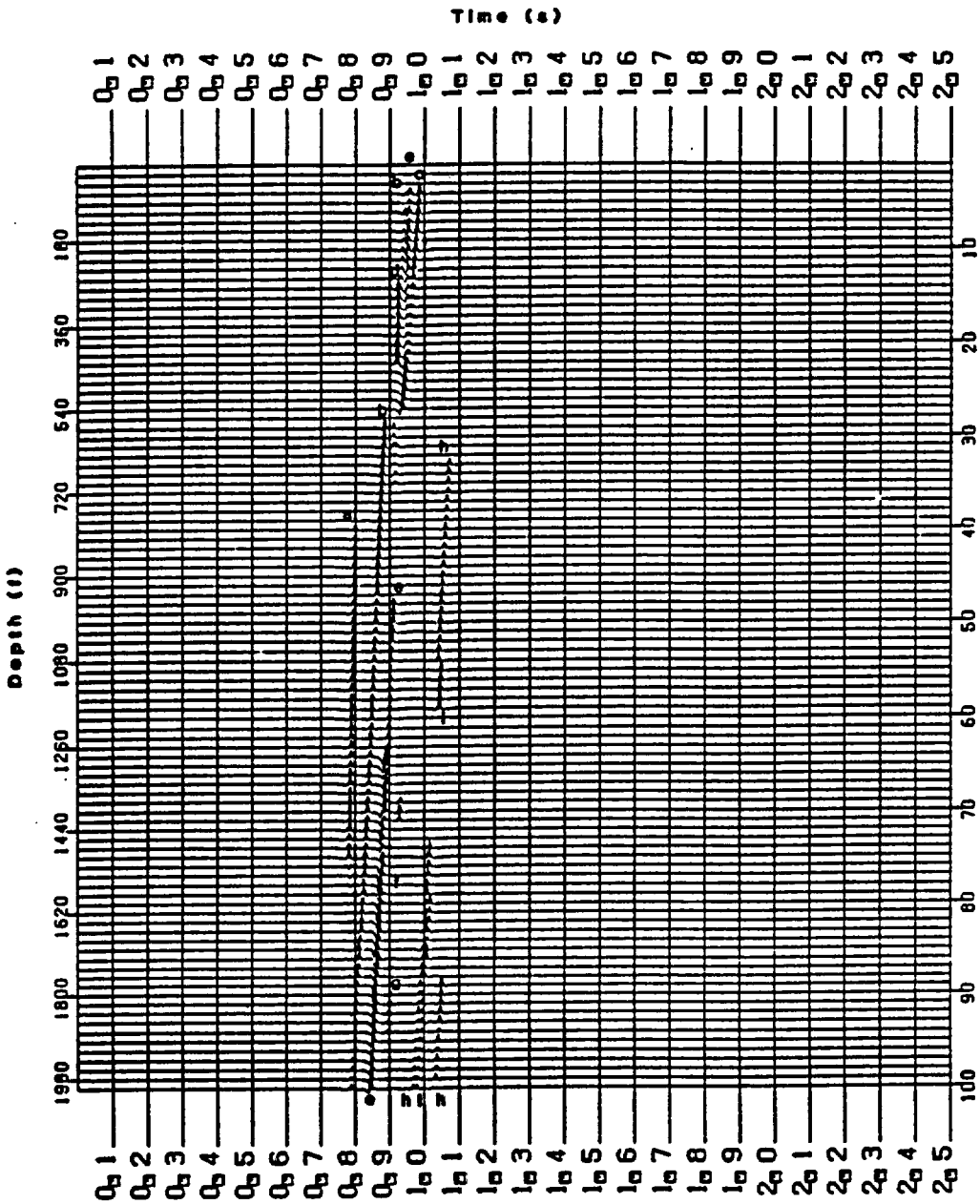

Figure 2.62. Synthetic VSP record for 8000-foot source offset after removing the direct arrivals. Reflections can be identified from n2(a), n3(b), Tptw(c), n1(d), Tctw(e), Tcbw(f), n4(g), Tlrw(h), and n5(i). Interpretation of this record required repeated ray tracings using only selected horizons.

the fault block west of fault plane 1.

Reflections from Tcbw (f) interfere with reflections from Tctw on traces 64 through 90 at 0.875 second. As seen with the 7000-foot offset data sets, reflections from deeper horizons can arrive before or at the same time as reflections from shallower horizons.

The reflections from n4 (g) appear as the peaks on traces 90 through 94 at 0.9 second. Another small set of peaks from this horizon is hidden by the Tctw peaks at 0.850 second.

Finally, the reflections from Tlrw (h) and n5 (i) appear between 1.0 and 1.1 seconds. The Tlrw peaks on traces 33 through 53 at 1.05 seconds are reflections from the fault block between fault planes 2 and 3. The peaks on traces 74 through 100 are reflections from Tlrw on the fault block between fault planes 1 and 2. The third set of Tlrw reflections appears at 1.04 seconds on traces 89 through 99 (h). These events are generated from the fault block west of fault plane 1. Two segments of n5 reflections can be identified. The peaks on traces 53 through 58 (i) at 1.04 seconds come from the n5 horizon on the fault block between fault planes 1 and 2. The n5 peaks on traces 80 through 100 (i) are reflected from the fault block west of fault plane 1.

The ray tracing for the 8000 foot source offset was

repeated excluding fault plane reflections. Since no fault planes provide reflections, the raypath diagram in Figure 2.60 is also the raypath diagram for this model. The data set generated by this ray tracing is shown in Figure 2.63.

Since fault planes were excluded, the program card controlling reflection coefficients was turned on, giving the events proper amplitudes and polarities. Although no reflections appear in Figure 2.61 that do not appear in Figure 2.63, the polarities of the events give this data set a much different appearance. The direct arrival troughs on traces 76 through 93 were removed by median filtering.

The upgoing wavefield appears in Figure 2.64. The n2 trough (a) appears on traces 39 through 75 at 0.8 second. The n3 trough (b) is seen on traces 30 through 100.

The other reflections require close comparison with Figure 2.62 in order to determine their sources. A set of peaks on traces 4 through 20 at 0.98 second (c) can be identified as reflections from Tptw. The peaks marked (d) correspond to two segments of reflections from Tctw. Peaks on traces 48 through 70 come from the fault block between fault planes 1 and 2. Peaks on traces 94 through 100 come from the fault block west of fault plane 1.

Reflections from Tcbw (e) are indistinguishable from Tctw reflections, but appear on traces 64 through 90 at 0.875 second. This was determined by selective ray tracing

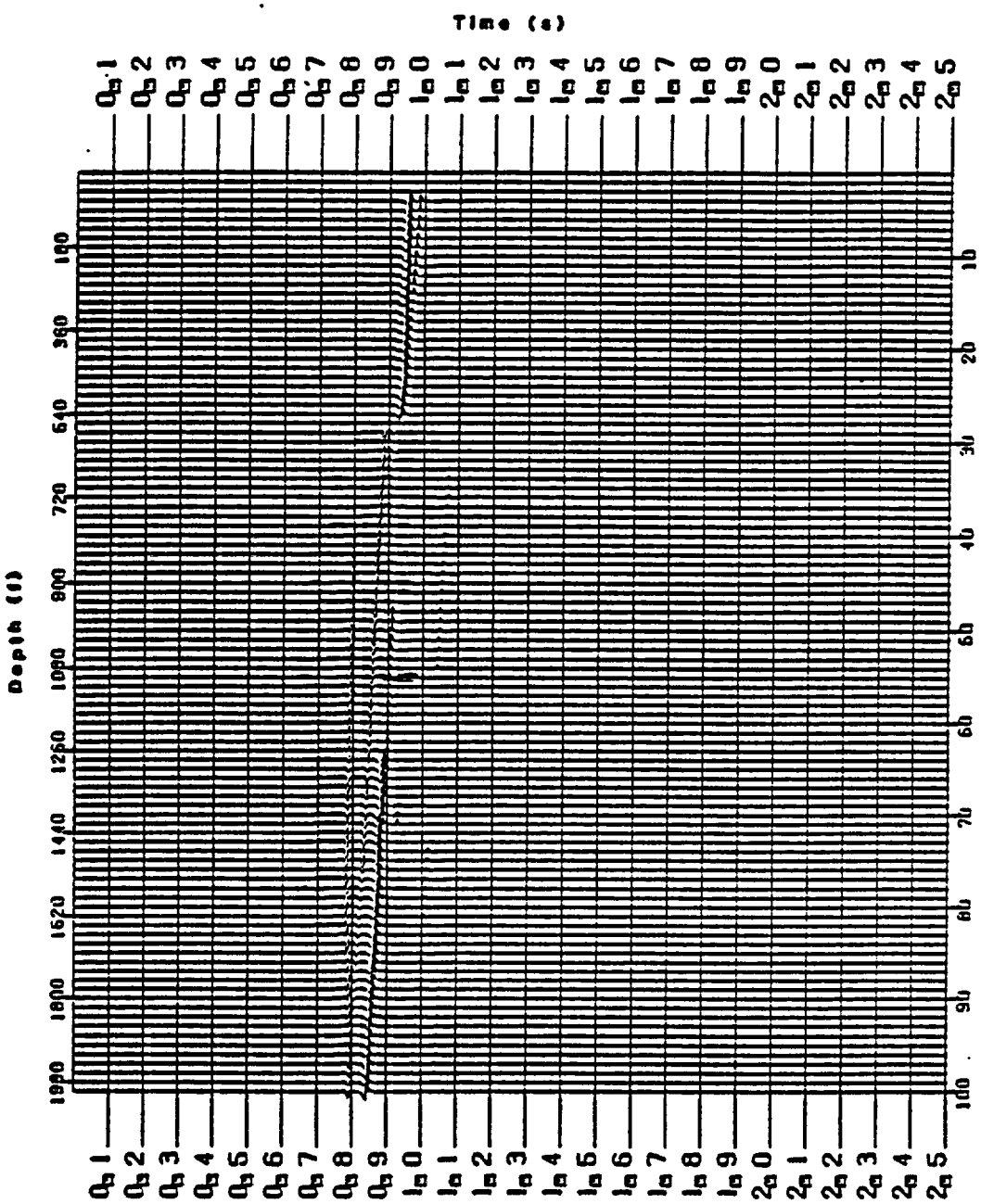

Figure 2.63. Synthetic VSP record generated by the ray tracing in Figure 2.60, including the effect of the reflection coefficient. The direct arrival appears on traces 76 through 93.

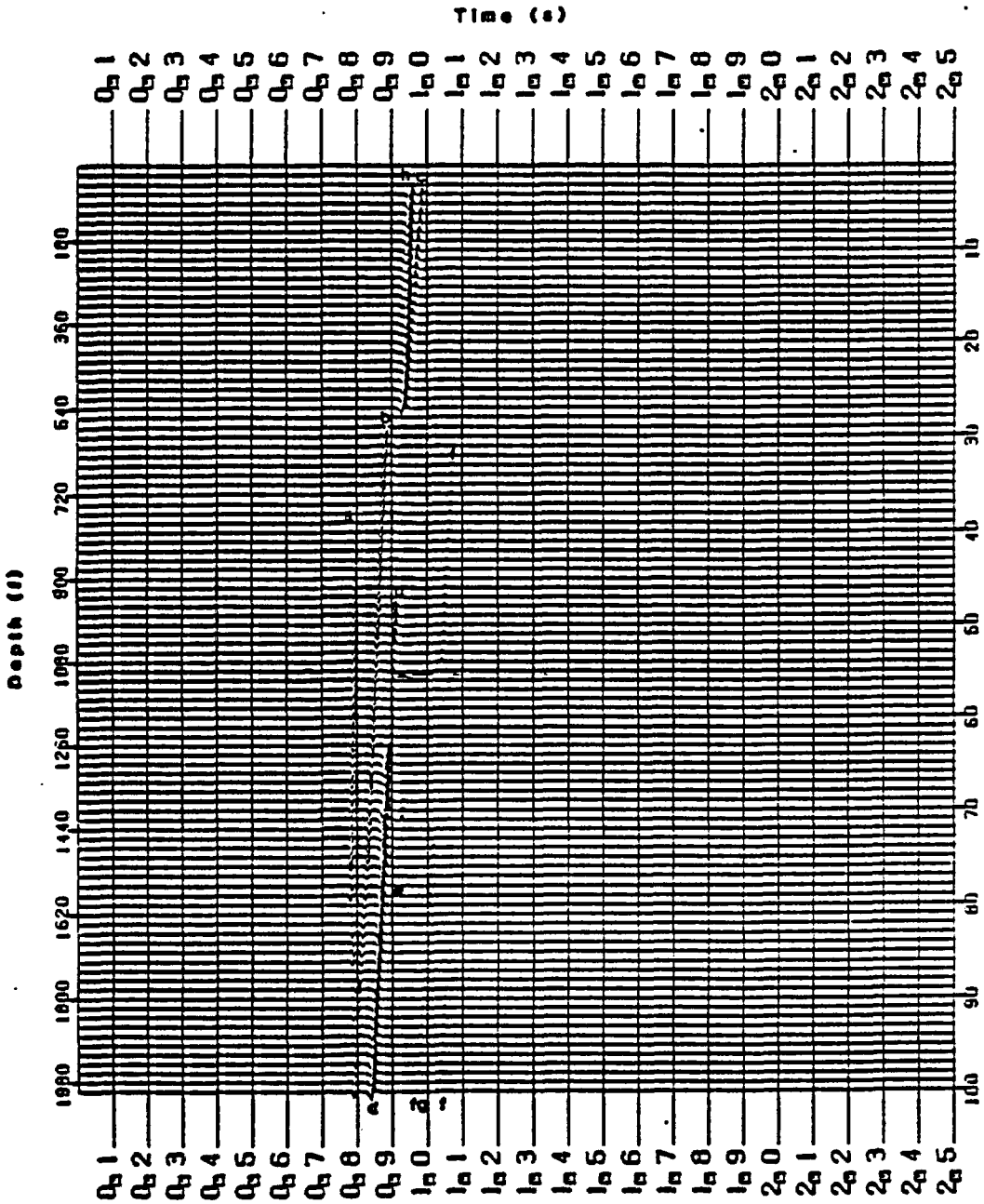

Figure 2.64. Synthetic VSP record for 8000-foot source offset after removing the direct arrivals. Reflections can be identified from n2(a), n3(b), Tptw(c), Tctw(d), Tcbw (e), Tlrw(f), and n5(g). The event labeled (h) results from the interference of n1, Tptw, n3, and Tctw reflections. Selective ray tracings were performed to aid in the identification of the events.

on Tcbw horizons. The three segments of Tlrw reflections are denoted by (f). The events on traces 33 through 53 are reflections from the fault block between fault planes 2 and 3. The peaks on traces 74 through 100 are reflections from the fault block between fault planes 1 and 2. The peaks on traces 89 through 99 at 1.05 seconds are from the fault block west of fault plane 1. The troughs from n5 (g) can be seen at two locations. On traces 53 through 58 are reflections from the fault block between fault planes 1 and 2. The troughs on traces 88 through 100 were generated from the fault block west of fault plane 1.

The remaining event on this data set is denoted (h). This set of peaks appears on traces 4 through 27 at 0.950 second. The events are a result of the interference of several reflections. Comprising these events are reflections from n1, Tptw, n3, and Tctw. None of these reflections can be identified uniquely on this data set.

2.11 UE25 UZ-9: Zero offset VSP

The computer model created for the previous modeling experiments is not restricted to a single borehole location. It is possible to move the borehole anywhere on the model. It is also possible to define a non-vertical trajectory for the borehole, if desired. For the following modeling experiments, a vertical borehole extending 2000 feet below the

surface was defined at the right boundary of the model. This corresponds to the proposed location of the UE25 UZ-9 borehole at Yucca Mountain. As was the case for all model studies using the UZ-6 borehole, the UZ-9 borehole data sets all contain 100 traces spaced 20 feet apart.

Figure 2.65 shows a zero-offset ray tracing for the UZ-9 borehole. The raypaths plotted intersect every fifteenth receiver location in the borehole. Rays can be seen reflecting off six of the nine unit boundaries. Horizons n4, Tlrw, and n5 do not appear to be sending reflections back to the borehole, although this diagram does not show every ray which converges at UZ-9.

Since AIMS can only recognize the top of a subsurface horizon (unless multiple reflections are desired), there is no way for any of the nine near-vertical faults to be imaged at the UZ-9 borehole for any offset. AIMS horizons are defined by points whose x-coordinates must increase from left to right. Primary reflections can be generated only from the top side of a horizon using AIMS, not the bottom side.

Figure 2.66 shows the synthetic data set created by the preceding ray tracing, after applying an AGC. The first arrival trough appears only on traces 1 through 28. The direct arrivals don't appear on lower traces due to refraction at the n1 horizon. The downgoing ray can not pass straight through n1, it must refract to the left (west). After the

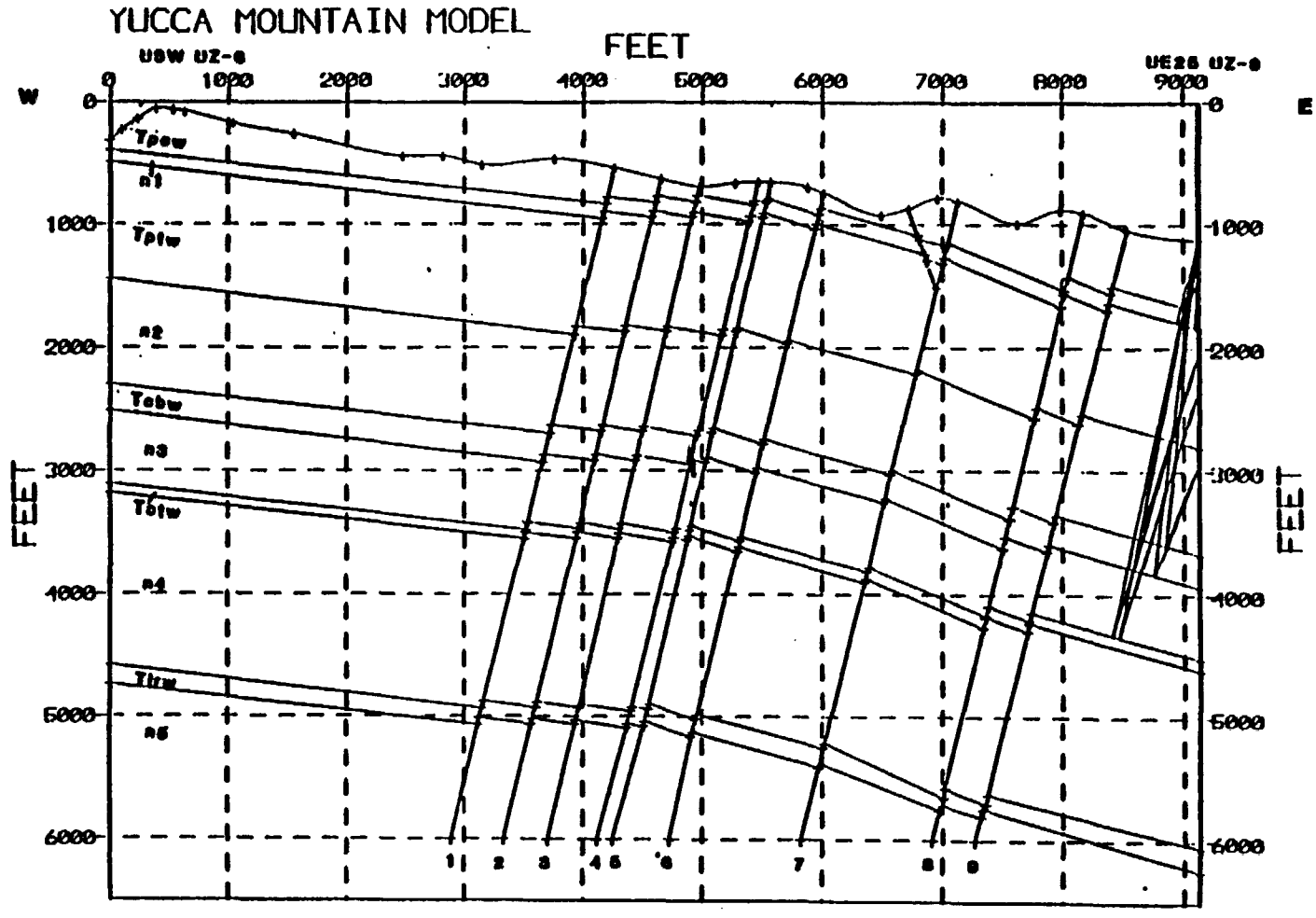

Figure 2.65. Raypath diagram for zero-offset VSP at borehole UE25 UZ-9.

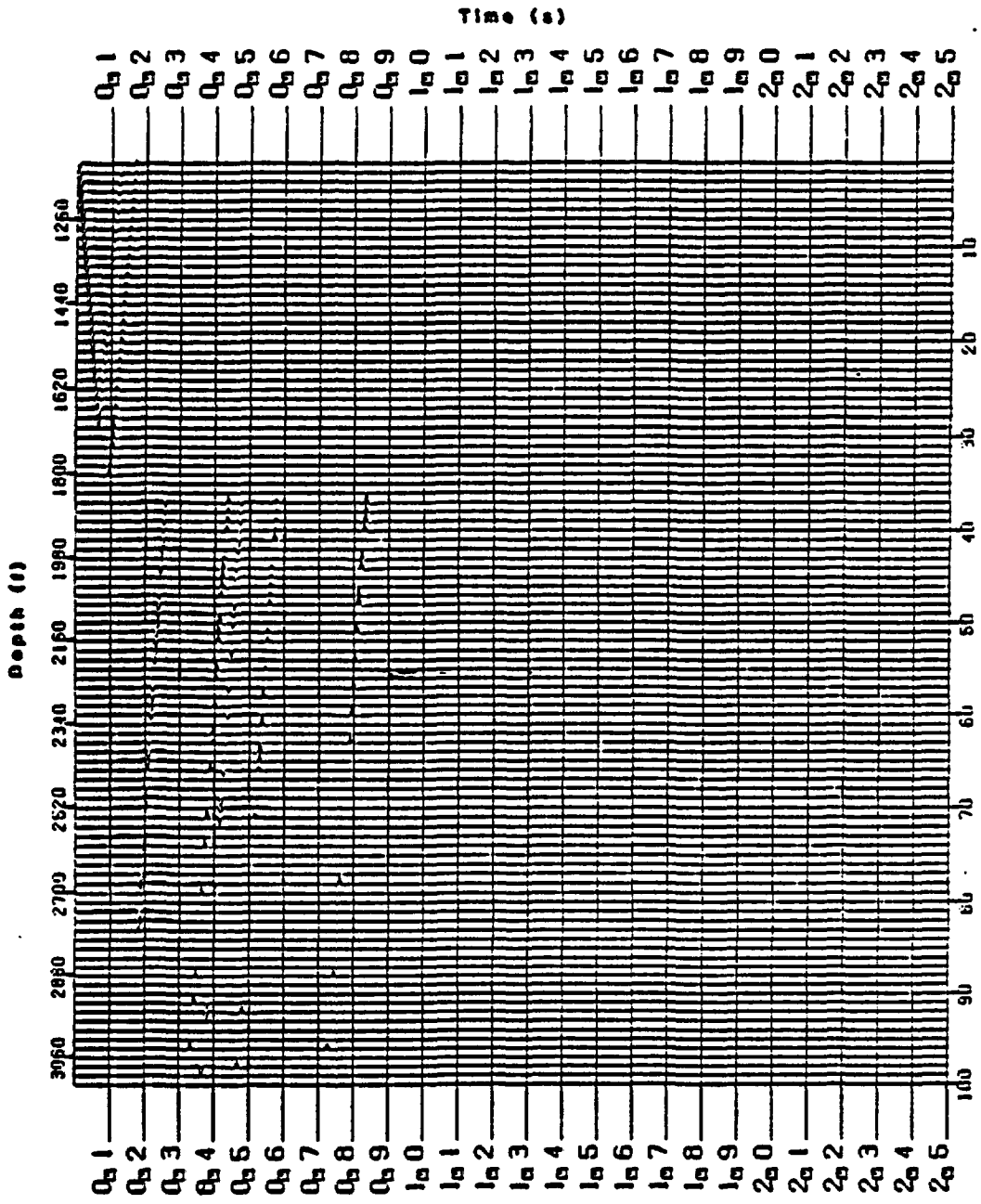

Figure 2.66. Synthetic VSP record generated by the ray tracing in Figure 2.65, after applying AGC. The direct arrival appears on traces 1 through 28.

refraction occurs, there is no chance of the ray ever intersecting the borehole. For a direct arrival to occur on the deeper traces, the model would have to be extended to the east slightly.

The first arrival trough was removed by applying an 11-fold median filter to traces 1 through 28. The resulting upgoing wavefield is shown in Figure 2.67. Reflections from seven of the nine unit boundaries can be positively identified. The n1 horizon produces a strong trough on traces 2 through 28. The strong peak on traces 1 through 34 corresponds to Tptw.

The other five reflected events have a more interesting character. The events lack continuity from trace to trace. Identification, however, is not a problem. The string of troughs which appear intermittently on traces 37 through 82 between 0.2 and 0.3 second are reflections from n2. The n3 horizon produces a string of troughs on several of the traces between traces 37 and 71. The three remaining reflections are peaks generated by Tcbw, Tctw, and Tlrw.

The appearance of the reflections may be related to the source aperture problems mentioned in earlier sections of this paper. Also, refraction at the interfaces may contribute to the odd, sparse appearance of the reflections on this data set.

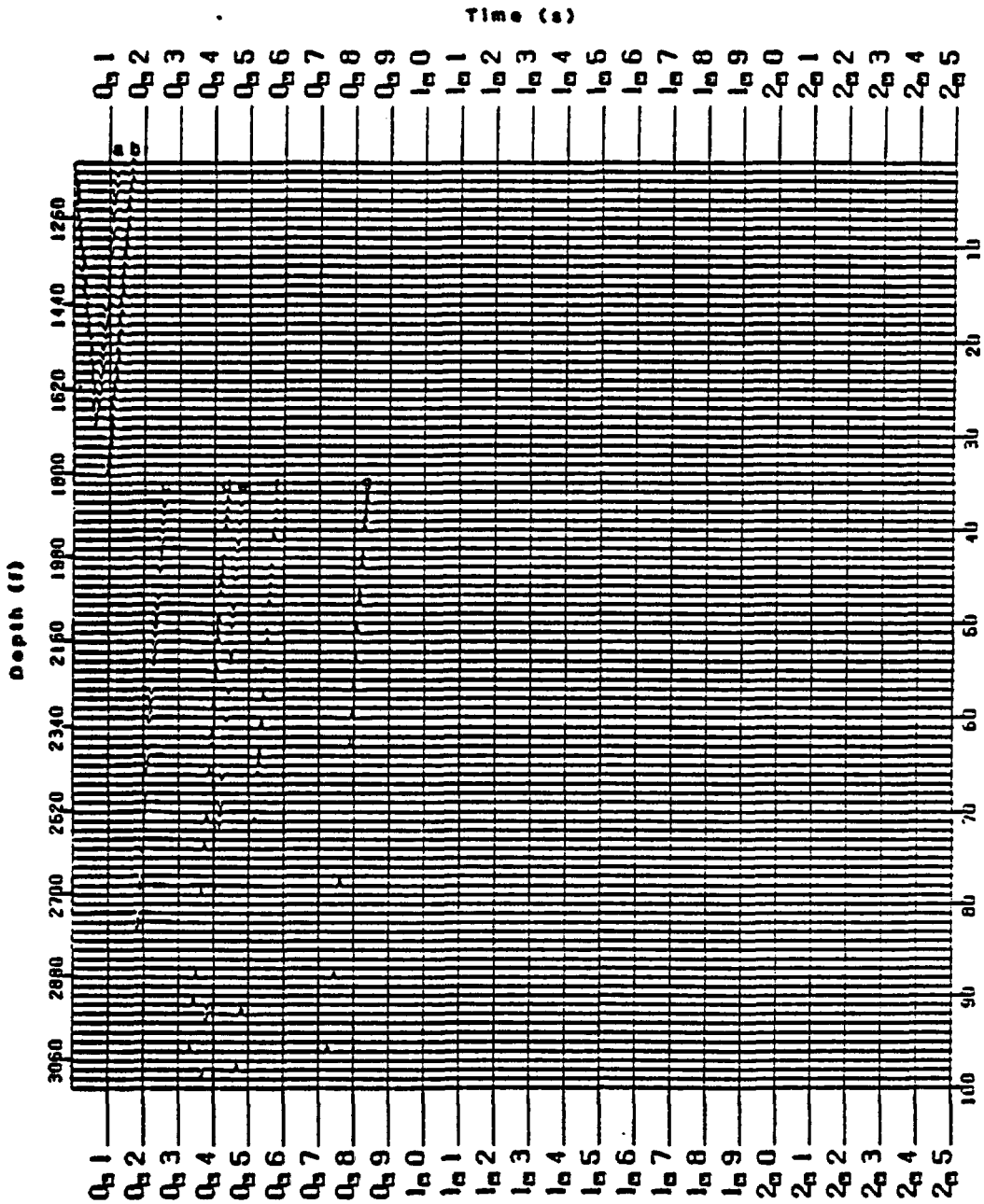

Figure 2.67. Synthetic VSP record for zero-offset VSP after removing the direct arrivals. Reflections can be identified from n1(a), Tptw(b), n2(c), Tcbw(d), n3(e), Tctw(f), Tlrw(g).

2.12 UE25 UZ-9: 1000-foot source offset VSP

The second experiment using the UZ-9 borehole was carried out with a source offset of 1000 feet to the west of the borehole. The raypath diagram for this model is shown in Figure 2.68. Rays which intersect every fifteenth borehole receiver are shown. Reflections from all nine unit boundaries can be seen on this diagram. In fact, some horizons produce reflections from three fault blocks.

A surprising feature of this diagram is that AIMS has ignored the surface topography while tracing direct arrivals. A ray can be seen traveling above the surface of the mountain between the source and the shallowest receiver. Apparently, AIMS assigns the "air" above the topography a velocity and a density equal to that of Tpcw, the shallowest unit. Fortunately, the direct arrivals are not important to the modeling, and this inconsistency does not affect the character of the reflected events.

The synthetic data set generated by the preceding ray tracing, after applying an AGC, is shown in Figure 2.69. The direct arrival trough can be seen on the first 70 traces and again on traces 88 through 100. The first arrival was removed by breaking the traces into two groups containing the event and applying a median filter to each group. The results were recombined to form the data set in Figure 2.70.

All nine of the unit boundaries can be seen in Figure

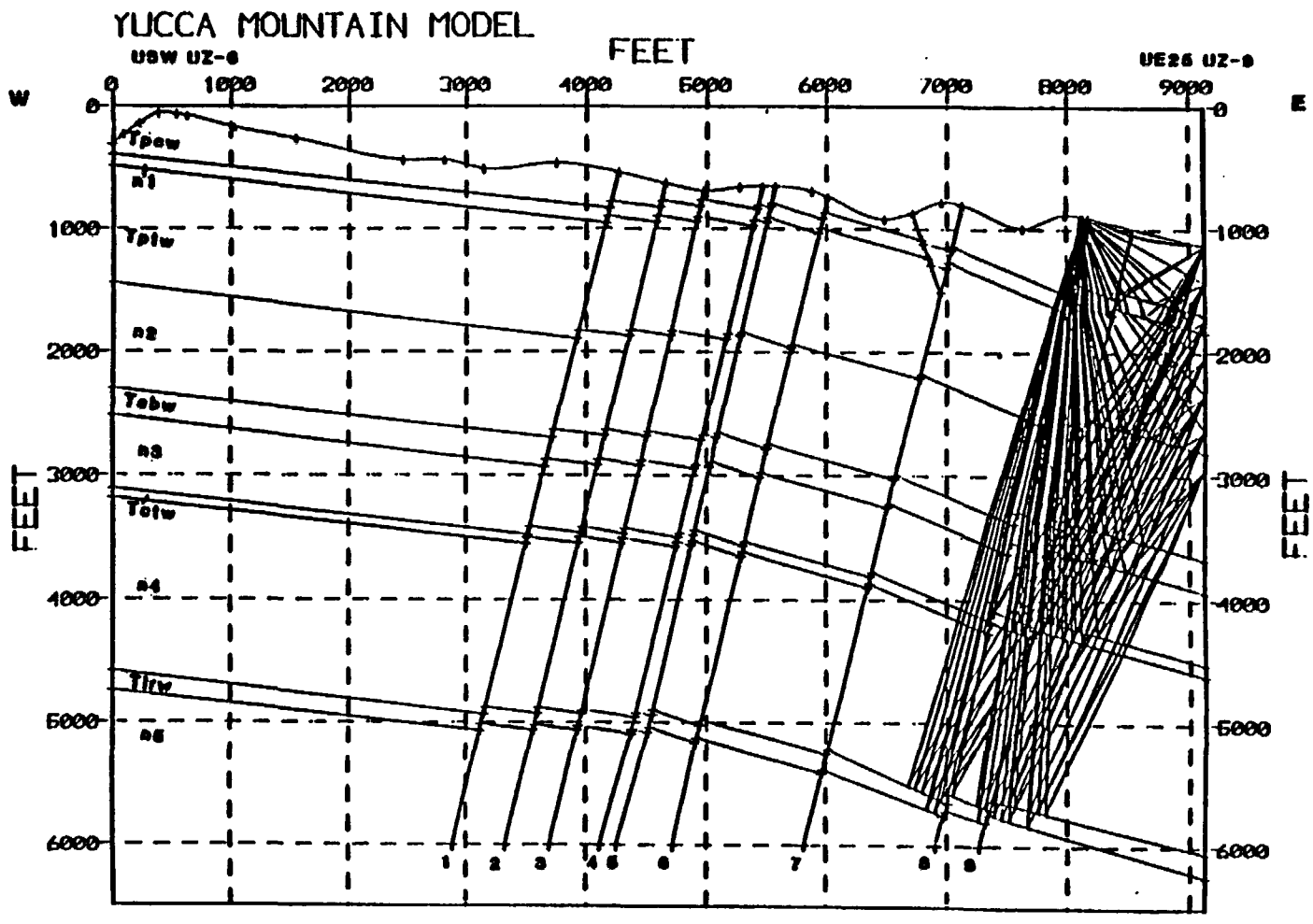

Figure 2.68. Raypath diagram for 1000-foot source offset VSP at borehole UE25 UZ-9.

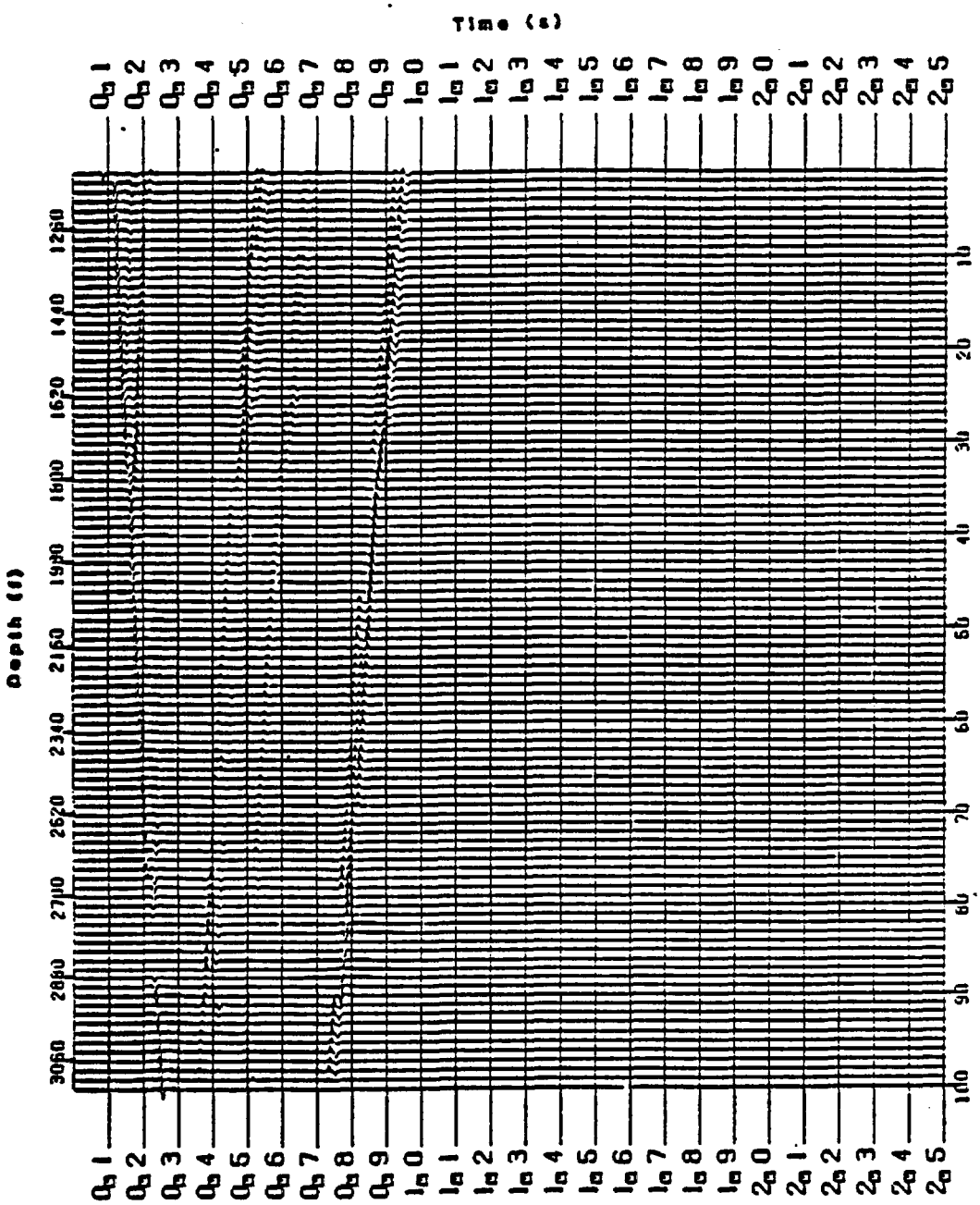

Figure 2.69. Synthetic VSP record generated by the ray tracing in Figure 2.68, after applying AGC. The direct arrival troughs can be seen on traces 1 through 70 and again on traces 88 through 100.

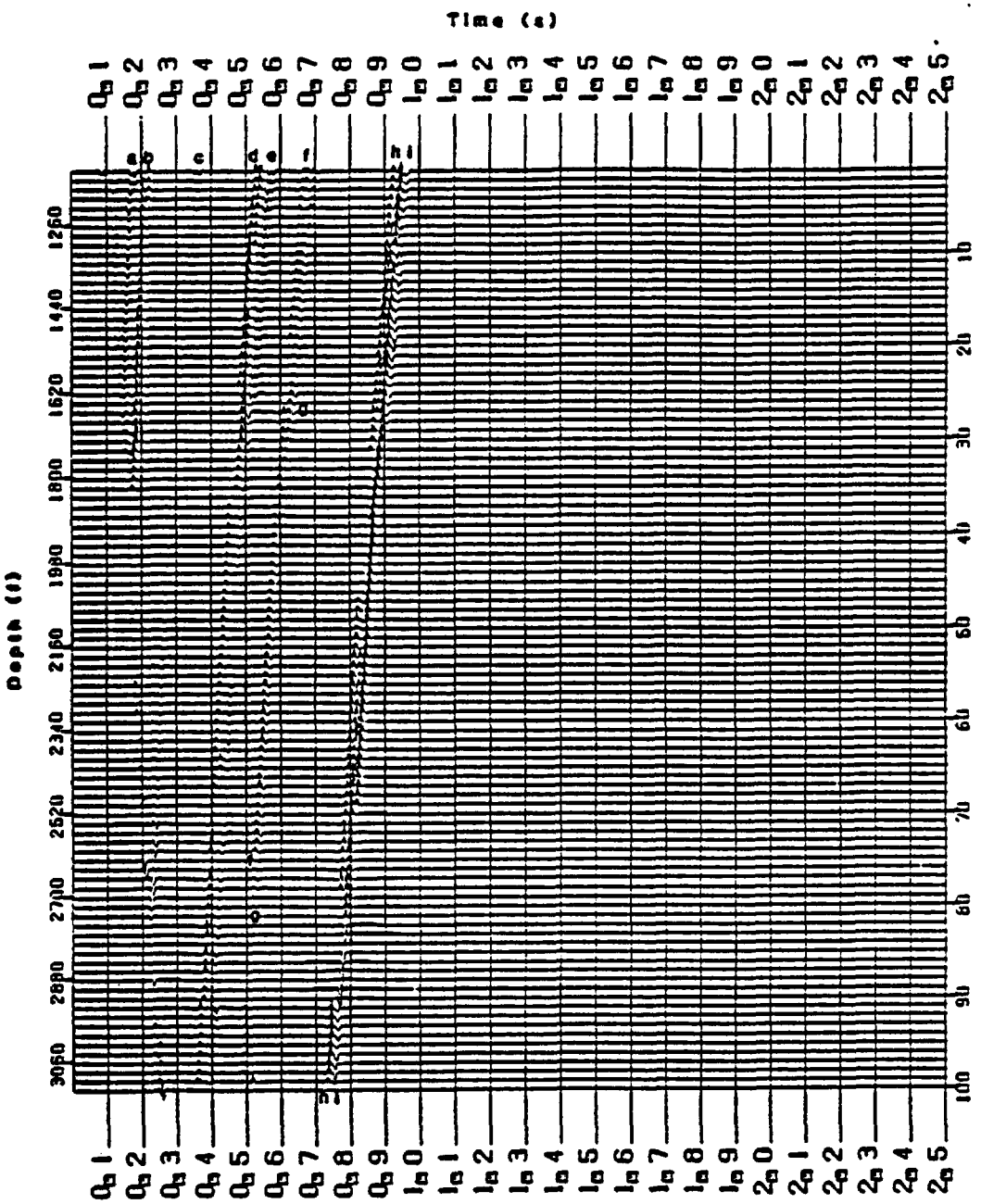

Figure 2.70. Synthetic VSP record for 1000-foot source offset after removing the direct arrivals. Reflections can be identified from n1(a), Tptw(b), n2(c), Tcbw(d), n3(e), Tctw(f), n4(g), Tlrw(h), and n5(i).

2.70. The n1 trough (a) is seen at 0.18 second on traces 1 through 24. The underlying Tptw peak (b) is seen on traces 1 through 35.

The n2 trough is denoted by (c) and appears on traces 1 through 81. On the shallow traces, the event is seen to be a double trough. The reason is apparent from Figure 2.68. Reflections are coming from both the fault block east of fault plane 9 and the fault block between fault planes 8 and 9. The orientation of the fault blocks produces this doubling of reflected events.

The reflections from Tcbw (d) also show this effect on the shallower traces. Lower in the hole, only reflections from the fault block east of fault plane 9 appear on the traces. The same is true for the n3 reflections (e). On the shallow traces, a double trough is seen due to reflections coming from both fault blocks. The deeper traces show only one trough coming from the fault block east of fault plane 9.

Reflections from Tctw (f) and n4 (g) exhibit the same character, other than that high in the borehole three peaks are seen for Tctw. These peaks come from three separate fault blocks. On the deeper traces, only one Tctw peak (f) and one n4 (g) trough appear, and the events are easily identified as reflections from the fault block east of fault plane 9.

Finally, the reflections from Tlrw (h) are seen as multiple peaks on most of the traces. Reflections are coming from three fault blocks, and many arrive at the same receiver locations at slightly different times. Likewise, the double troughs representing n5 (i) on traces 1 through 12 are created as reflections from two different fault blocks arrive at the shallow receivers. The n5 troughs (i) on traces 82 through 99 are reflections from the fault block east of fault plane 9.

2.13 UE25 UZ-9: 2000-foot source offset VSP

The source was positioned 2000 feet west of UZ-9 for the next modeling experiment. The raypath diagram for this model is shown in Figure 2.71. As seen in the model with 1000 foot offset (Figure 2.68), a direct arrival can be seen ignoring the topography and traveling a straight line path between the source and the shallowest receiver. Once again, this flaw does not interfere with the reflected arrivals, and no harm is done to the experiment.

Reflections can be seen from every horizon on the fault block between fault planes 7 and 8. Most of the horizons on the fault block between fault planes 8 and 9 also produce reflections, as do a few of the horizons on the fault block east of fault plane 9.

The synthetic data set created from the preceding ray

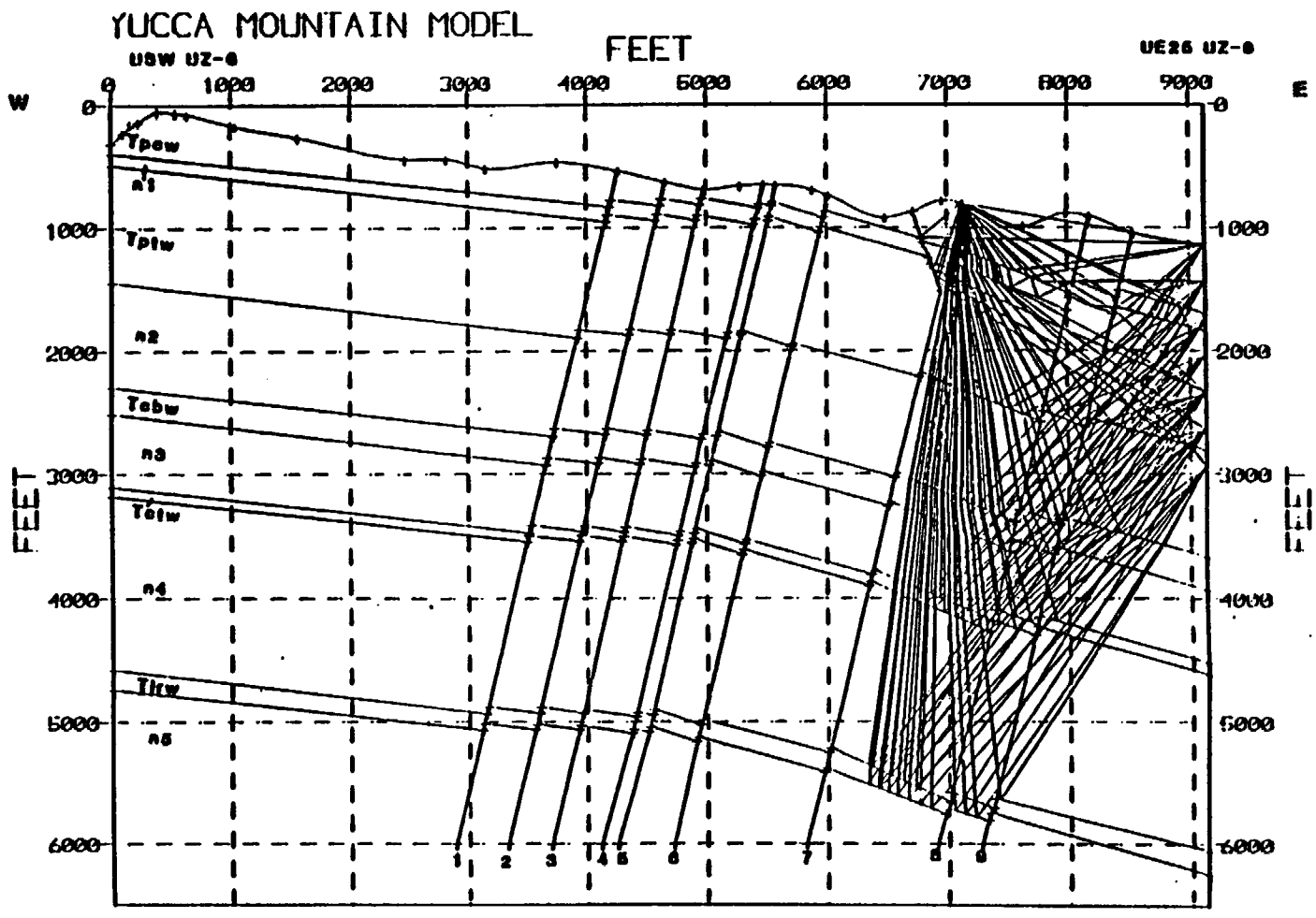

Figure 2.71. Raypath diagram for 2000-foot source offset VSP at borehole UE25 UZ-9.

tracing (after applying AGC) is shown in Figure 2.72. The first arrival trough is visible intermittently on traces 1 through 36 between 0.2 and 0.3 second. The trough is seen more consistently on traces 51 through 100. The gap in the first arrivals is due to a downward refraction of rays as they cross fault plane 9 and enter Tptw. The first arrivals were removed by median filtering.

The resulting upgoing wavefield is seen in Figure 2.73. The troughs on traces 1 through 15 at 0.270 second are reflections from n1 (a) on the fault block between fault planes 7 and 8. The peaks that occur intermittently on traces 1 through 36 at 0.3 second (b) are from Tptw. These events were somewhat damaged by the 11-fold median filtering used to remove the first arrivals.

The reflection from n2 (c) appears as a very small trough on traces 1 through 50. The troughs on traces 1 through 39 are from the fault block between fault planes 7 and 8 and from the fault block between fault planes 8 and 9. The double troughs on traces 40 through 44 and on trace 50 were created by n2 reflections coming from the fault block between fault planes 8 and 9 and from the fault block east of fault plane 9.

The reflections from Tcbw (d) appear as peaks on every trace. The events are generated from all three of the easternmost fault blocks. On traces 51 through 57 at 0.475

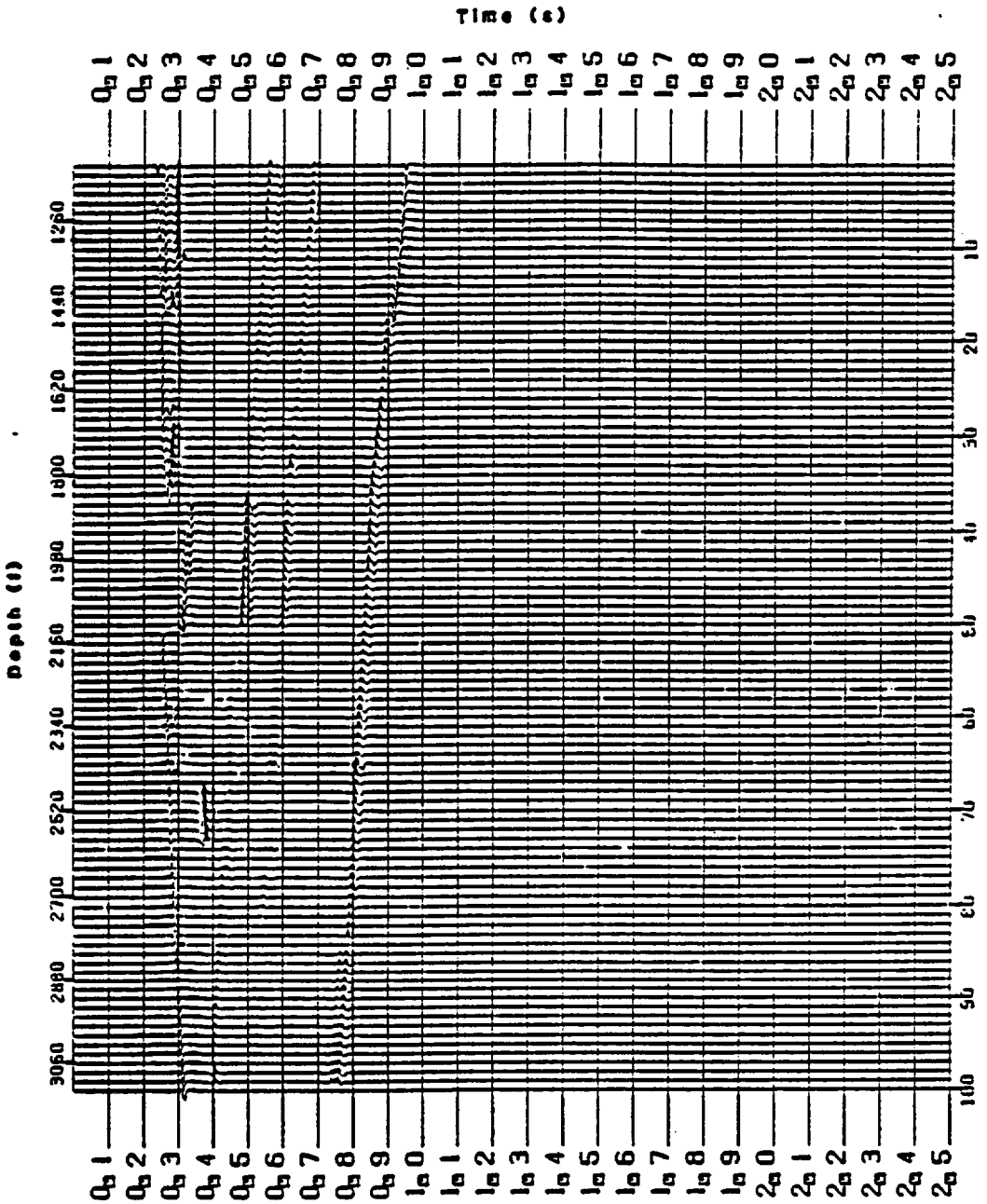

Figure 2.72. Synthetic VSP record generated by the ray tracing in Figure 2.71, after applying AGC. The direct arrival troughs appear intermittently on traces 1 through 36, and more consistently on traces 51 through 100.

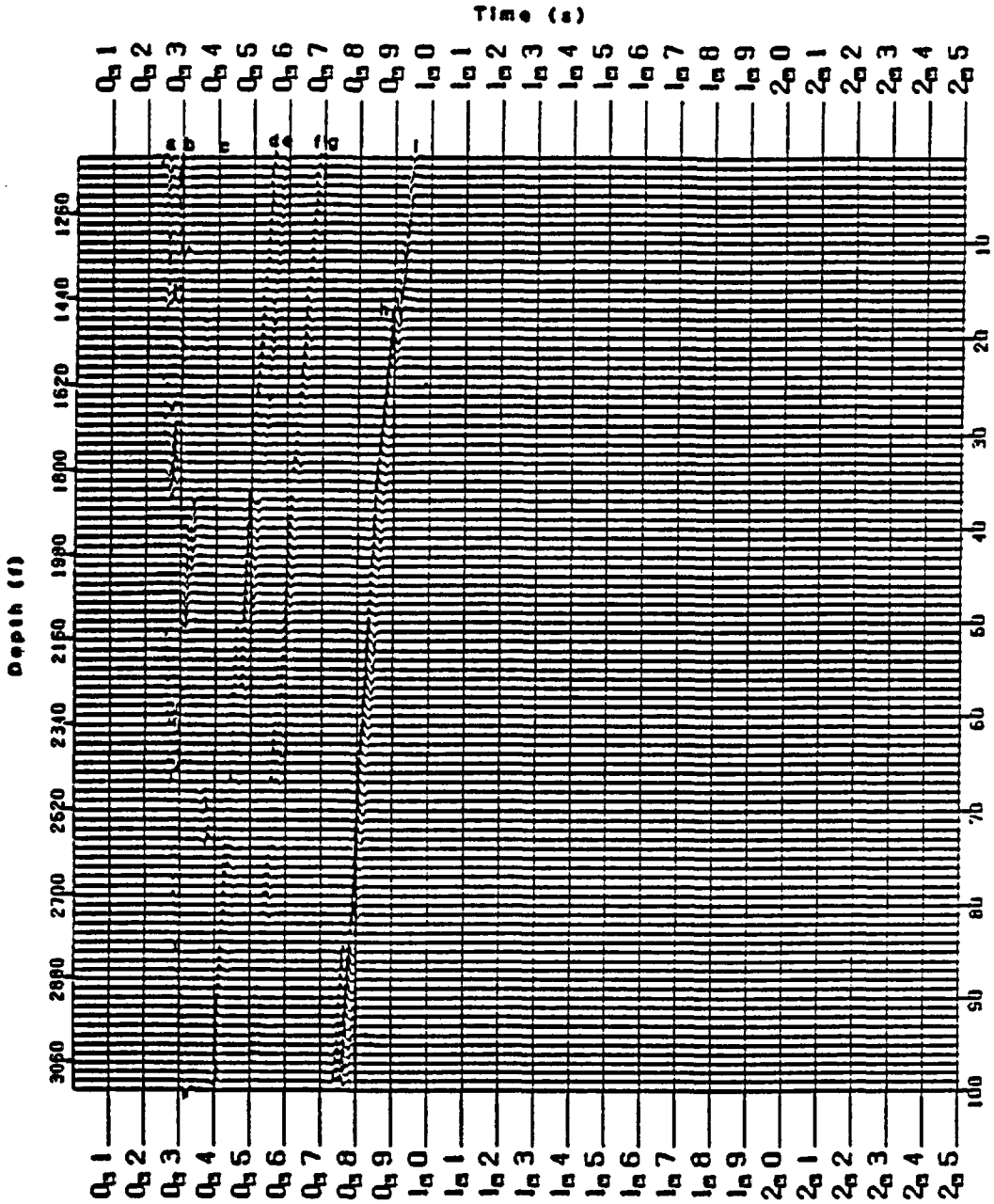

Figure 2.73. Synthetic VSP record for 2000-foot source offset after removing the direct arrivals. Reflections can be identified from n1(a), Tptw(b), n2(c), Tcbw(d), n3(e), Tctw(f), n4(g), Tlrw(h), and n5(i).

second, two Tcbw peaks can be seen on each trace. The peaks are coming from both the fault block between fault planes 7 and 8 and the fault block between fault planes 8 and 9. The trough from n3 (e) is seen on most traces high in the borehole, but it is a weak event or non-existent on the deeper traces. From the raypath diagram, it is seen that the easternmost fault block produces very few reflections from n3.

Reflections from Tctw (f) appear as peaks. Once again, the events are produced from three different fault blocks. Peaks on traces 1 through 67 were generated from the fault block between fault planes 7 and 8. The event appears as a double peak on traces 55 through 67, due to additional reflections from the fault block between fault planes 8 and 9. On the deeper traces, the double peaks appear again. This is caused by Tctw reflections from both the fault block between fault planes 8 and 9 and from the fault block east of fault plane 9. The troughs from n4 (g) are very weak, but can be identified on most of the traces in the data set.

The reflections from Tlrw (h) are generated primarily from the fault block between fault planes 7 and 8. These peaks appear on traces 18 through 99 between 0.750 and 0.900 second. On traces 84 through 99, double and triple peaks appear, signifying that reflections are also coming from the fault block between fault plane 8 and 9 and from the fault block east of fault plane 9. Troughs from n5 (i) show the

same pattern, with most of the reflections coming from the fault block between fault planes 7 and 8. A few double troughs appear on the lower traces.

2.14 UE25 UZ-9: 3000-foot source offset VSP

The final modeling experiment was conducted using a source 3000 feet to the west of borehole UZ-9. A raypath diagram for the model is shown in Figure 2.74. An interesting feature of this diagram is the fact that the direct arrivals are not ignoring topography for this model. No rays are traveling a straight line path from the source to the shallowest receiver due to the aperture angle of the source.

Most of the reflections in this diagram are being generated on the fault block between fault planes 7 and 8. A smaller number of reflections are generated on fault blocks farther to the east. The seven lowest unit boundaries are seen to produce reflections on this diagram, but horizons n1 and Tptw do not appear to generate events.

The synthetic data set created by the preceding ray tracing after applying an AGC appears in Figure 2.75. The first arrival trough can be seen on traces 50 through 100. These events were aligned and removed from the data set by median filtering. The resulting upgoing wavefield is shown in Figure 2.76.

The troughs representing n2 (a) on traces 1 through 57

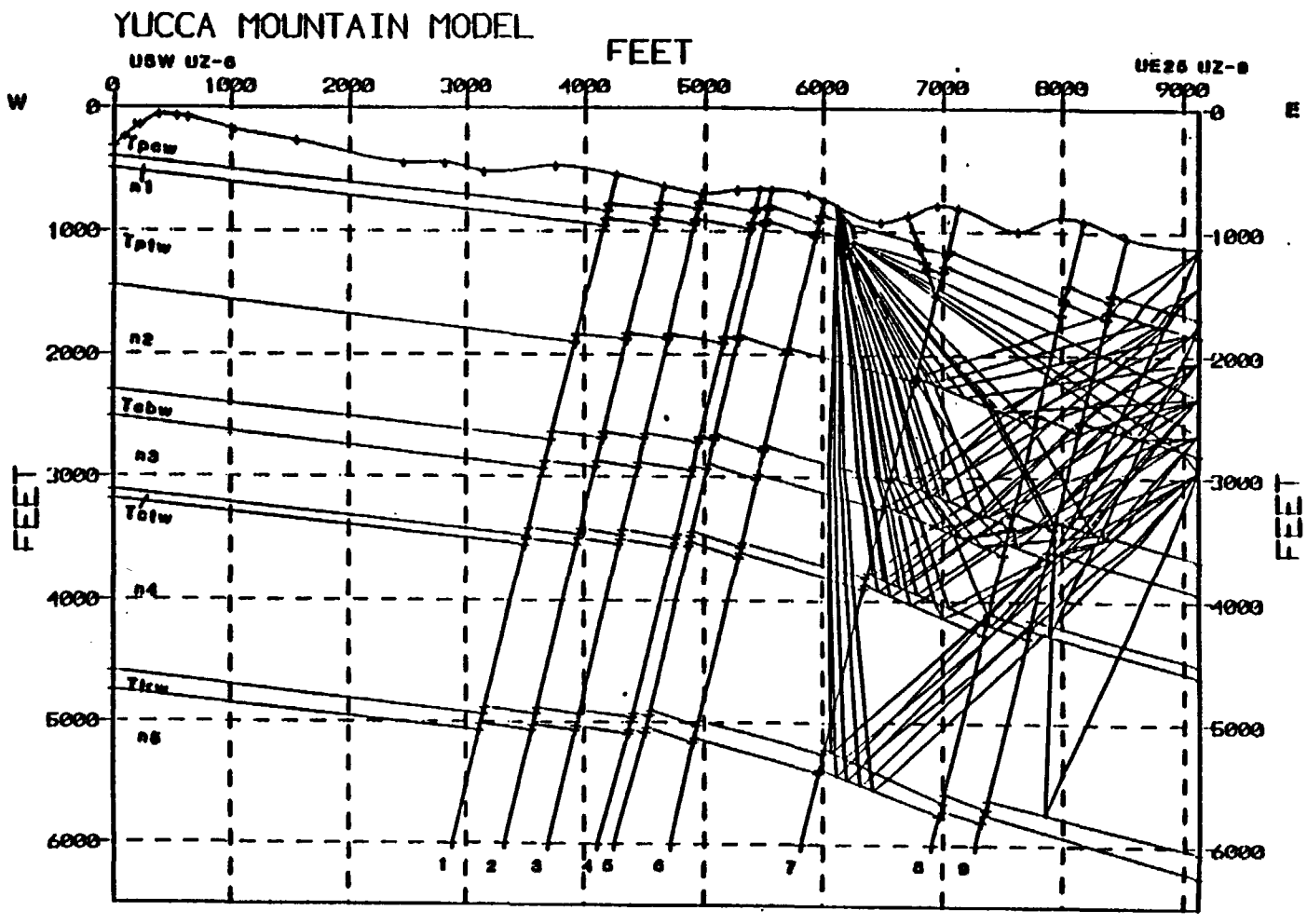

Figure 2.74. Raypath diagram for 3000-foot source offset VSP at borehole UE25 UZ-9. Most of the reflections are coming from horizons on the fault block between fault planes 7 and 8.

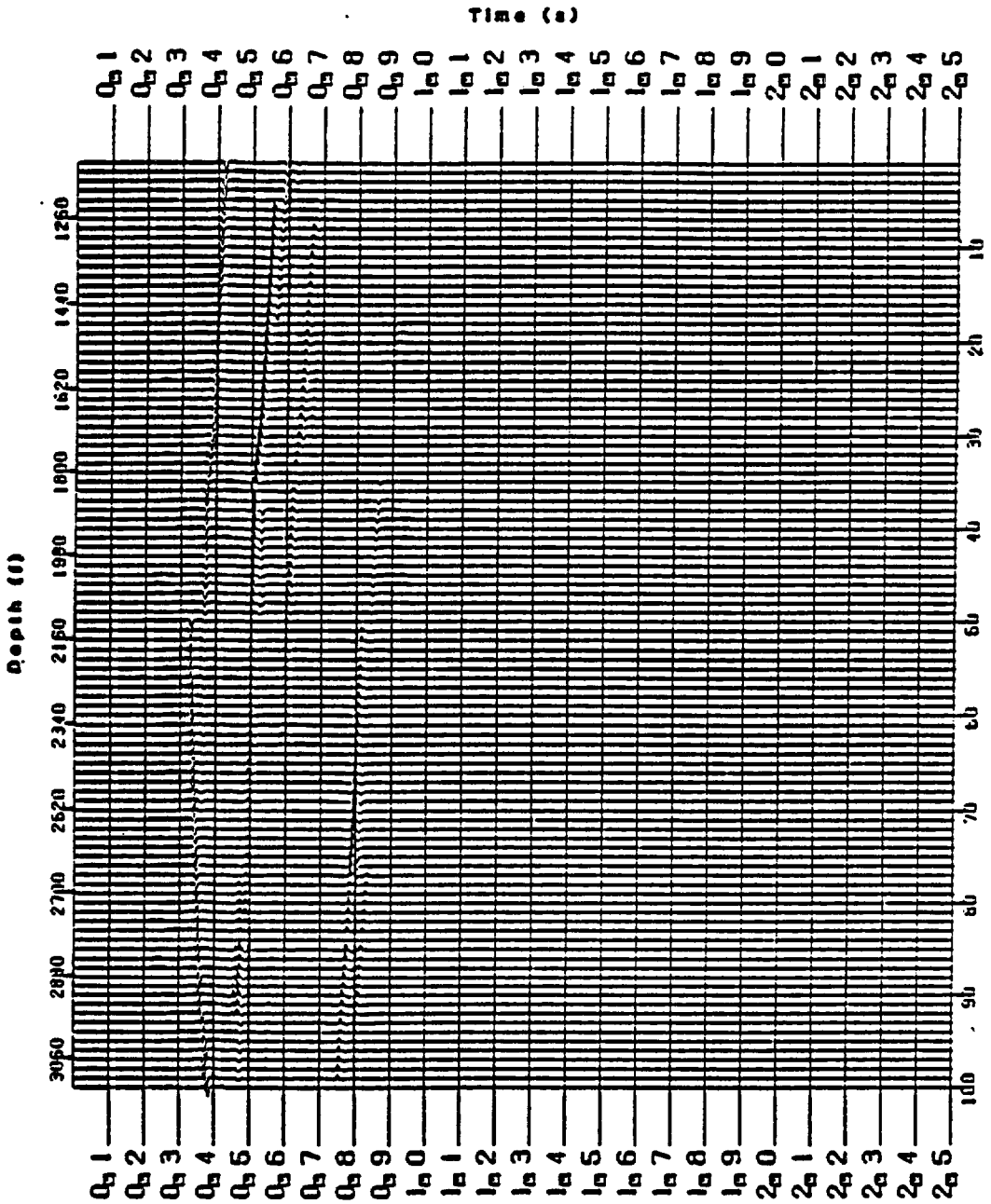

Figure 2.75. Synthetic VSP record generated by the ray tracing in Figure 2.74, after applying AGC. The first arrival trough appears on traces 50 through 100.

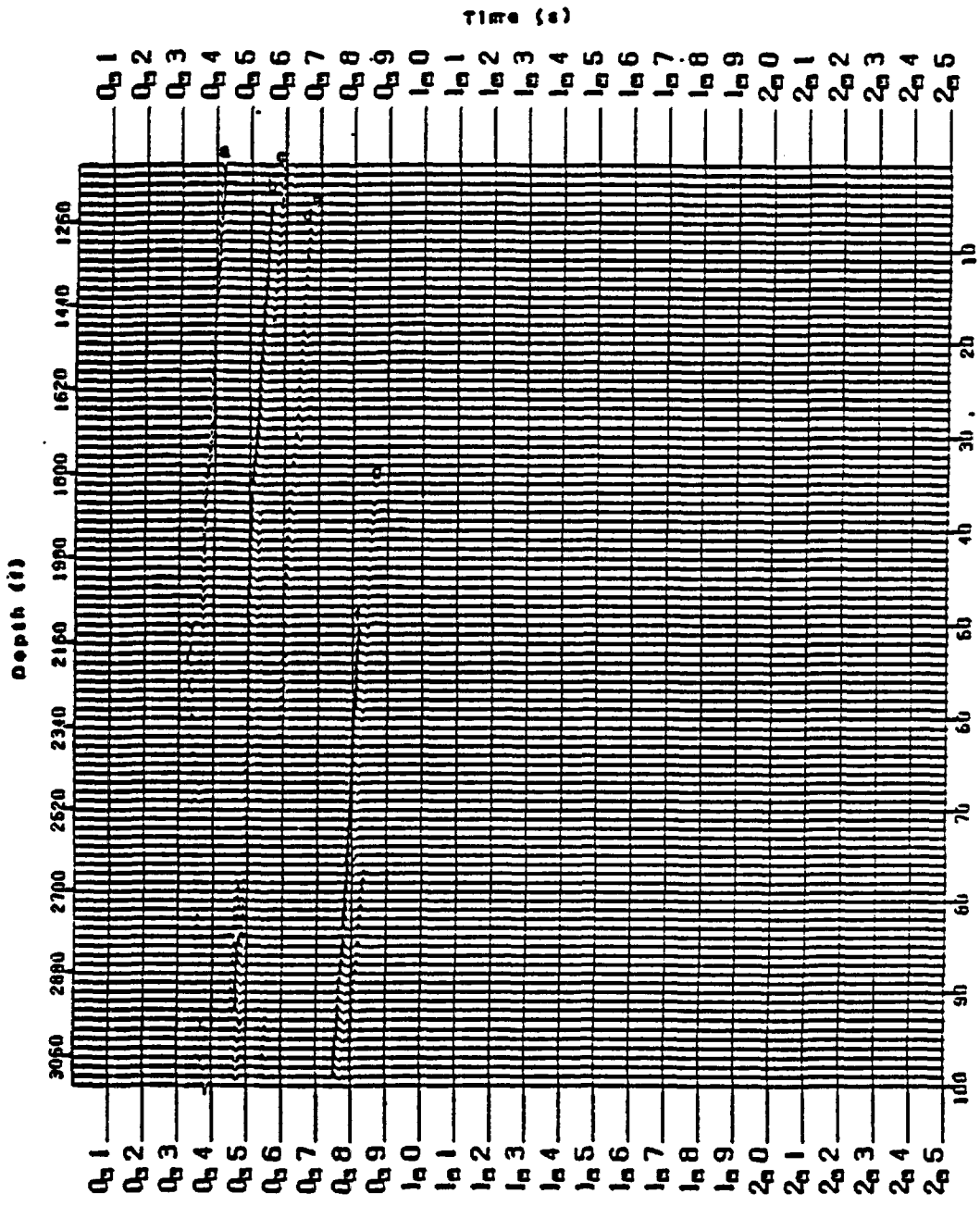

Figure 2.76. Synthetic VSP record for 3000-foot source offset after removing the direct arrivals. Reflections can be identified from n2(a), Tcbw(b), n3(c), Tctw(d), n4(e), Tlrw(f), and n5(g).

are easy to identify. The change in slope of the event at trace 35 corresponds to the n1/Tptw boundary in the borehole. Above trace 35, velocity is lower causing the change in slope on the data. This change can be seen on the other reflections in this data set as well.

Reflections from Tcbw (b) appear as peaks on traces 6 through 92 between 0.50 and 0.55 second. The events are coming primarily from the fault block between fault planes 7 and 8. However, double and triple peaks can be seen on traces 78 through 92, indicating reflections coming from the two fault blocks farther to the east. Reflections from the underlying n3 (c) can be seen best on traces 1 through 18, and on traces 38 through 48.

Reflections from Tctw (d) are relatively weak peaks which do not appear on all traces. Most of the reflections were generated from the fault block between fault planes 8 and 9. The same is true for the troughs (e) representing n4. Interference with the Tctw peaks causes both events to have low amplitudes.

The fault block between fault planes 7 and 8 produces most of the reflections from Tlrw (f) and n5 (g). The Tlrw peaks appear on traces 51 through 99. The troughs from n5 are seen on traces 35 through 99. A second set of peaks appears on traces 77 through 95 between 0.80 and 0.82 second. The reflections are from Tlrw on the easternmost fault block

in the model, and arrive later than the reflections from the fault block between fault planes 7 and 8.

2.15 Conclusions

The computer modeling experiments provided many insights about the quality of data that can be recorded at different offsets at Yucca Mountain. Identifying the reflections from unit boundaries and from fault planes are major objectives of the VSP surveys.

The key horizons to be imaged at Yucca Mountain are n1, Tptw, and n2. These horizons are above the static water table, and Tptw is the potential repository unit. The ability to positively identify the top and bottom of this unit is a primary objective, so that additional interpretation of faults, fractures, and permeability zones within the unit can be made.

The computer modeling experiments show that strong, clearly identifiable reflections from n1, Tptw, and n2 can be seen on data sets with a source offset up to 2000 feet from borehole USW UZ-6. The n1 and Tptw reflections did not appear on the zero-offset data sets, but this was due to limitations of the modeling program. These events would certainly appear on a field record. Beyond 2000 feet, the elevation of the source decreases to the point that reflections from n1 and Tptw are difficult to identify or are

simply absent from the data sets.

The reflection from n2 could be identified on every record out to a source offset of 8000 feet, but the interpretation becomes more difficult as source offset increases. The spacing between the n2 reflection and the deeper events decreases with each offset. On a positive note, the n2 reflection is the easiest event to identify on most of the data sets in the experiment.

Reflections from deeper horizons are confusing on data sets beyond a source offset of 4000 feet. When the polarity of events is honored, reflections from the tops and bottoms of the thin welded units interfere. The interference can be constructive, such as event (b) on Figure 2.53. The interference can also be destructive, such as event (c) on the same data set.

A second objective of the modeling was to test the imaging of the fault planes by the VSP. Reflections from segments of the fault planes within Tptw are clearly identifiable on data sets with source offsets out to 3000 feet. The events are characterized by their near-vertical slopes, in most instances. At a source offset of 4000 feet, the fault plane reflections become more difficult to identify. Reflections from fault planes 3 through 7 interfere with reflections from the unit boundaries. This occurs to a lesser degree on data sets with smaller source offsets, but the

reflections are easy to identify. The four fault planes farthest from UZ-6 were easily identifiable on the 5000-foot source offset record, but overall the modeling experiments suggest that it is unrealistic to expect that fault plane reflections will be clearly identifiable on records with source offsets greater than 4000 feet. Delineation of the Ghost Dance Fault (fault planes 2 and 3) will be of primary importance during the field surveying, and the modeling experiments suggest that this pair of faults can be clearly interpreted on records with source offsets up to 3000 feet. This, of course, assumes that the fault planes at Yucca Mountain will generate reflections.

The computer modeling experiments show that the reflections from fault planes do not always appear with the same slopes. The near-vertical slopes of the fault plane reflections are consistent on most records, but Figure 2.32 shows that a fault plane reflection can also have a slope very similar to the slopes of the unit boundary reflections. Reflections from fault planes 8 and 9 are clearly seen with slopes comparable to the reflections (a) through (g). Another important observation was made on Figure 2.37. Reflections from fault planes 3 and 4 are seen with downgoing slopes, similar to the slope of the direct arrivals. The downgoing slope presents problems when using a median filter to remove the direct arrivals. Aligning the direct arrivals

along a line of equal time will also tend to align these fault plane reflections along a line of equal time. Applying a median filter will remove both events from the data set. It is proposed here that a muting step be added to the median filtering process. The output from the median filter will be a data set consisting of the aligned direct arrival and the aligned fault plane reflections. This data set should be completely muted after the aligned direct arrival. Subtracting the muted data set from the original data set will remove the direct arrival from the record without harming the fault plane reflections with downgoing slopes.

The computer modeling experiments using borehole UE25 UZ-9 also provided useful results. As with the data sets recorded at UZ-6, the key horizons to be imaged are n1, Tptw, and n2. These horizons could be identified on each data set out to a source offset of 2000 feet west of UZ-9. The reflections from n1 and Tptw were not generated on the data set with a source offset of 3000 feet due to the limitations of the source aperture angle in AIMS. The remaining horizons in the section were visible on each data set out to a source offset of 3000 feet, with the exception of two horizons which did not appear on the zero-offset data set due to the source aperture problem.

AIMS was not capable of providing fault plane reflections in these models due to the orientation of the fault

planes and how they must be defined to be read in by AIMS. Evidence of reflections from different fault blocks was apparent on these data sets, however. Several of the reflections on data sets recorded in UZ-9 had double troughs or double peaks caused by the interference of reflections from the same horizon on different fault blocks. If this phenomenon exists at Yucca Mountain, the resulting data sets may be confusing. The problem was greatest on the data set with a source offset of 1000 feet, and became slightly less severe with increasing offset.

Chapter 3

PHYSICAL VSP MODELING PART I

3.1 Introduction

The second segment of the VSP modeling experiments consisted of generating synthetic vertical seismic profiles from a physical model. A laboratory was created in room B70 of the Green Center at the Colorado School of Mines for this purpose, and the lab is the permanent home of the models used in this section.

Figure 3.1 is a schematic of the laboratory set-up used in the generation of the synthetic data. The experiment revolves around the physical model itself. As shown in the diagram, the first model was 8.4 feet long by 4.1 feet high. It is a 1:1000 scale model of the cross-section between boreholes UZ-6 and UZ-9.

The model was created from two 8.4 feet by 4.2 feet sheets of 1/4 inch thick PLEXIGLAS G acrylic. The model cross section was transferred to the masking on one of the sheets, and the welded volcanic units were cut from the sheet as continuous strips. Since none of the high-angle faults has more than 100 feet of offset, the strips could be cut as single pieces. Faults are manifested as the "stair-steps" in a given strip. The proper position of the strips was lightly scribed onto the remaining PLEXIGLAS sheet.

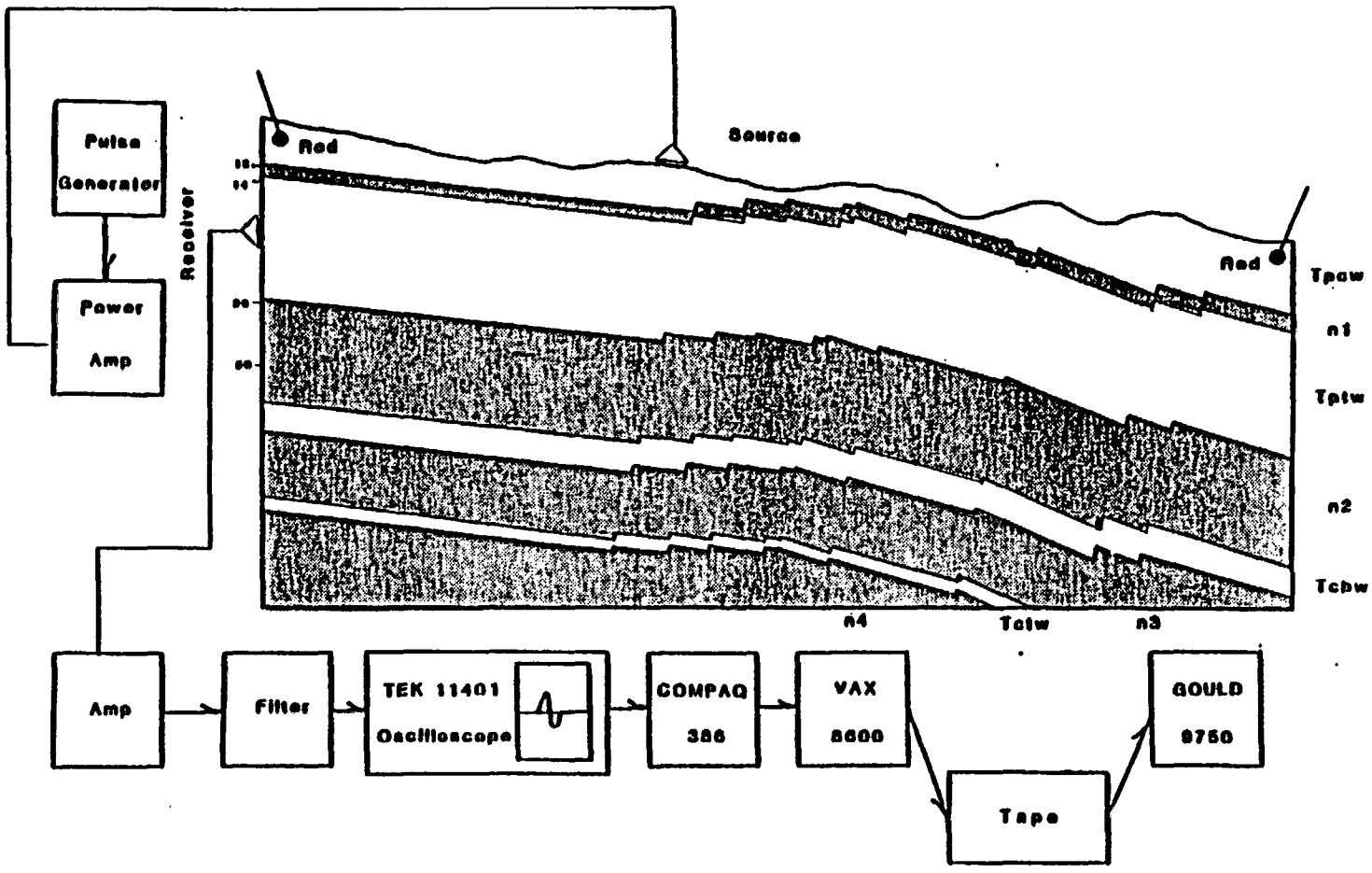

Figure 3.1. Schematic diagram of the laboratory equipment used to generate the synthetic VSP data sets from a physical model. The shaded areas of the model are 1/4 inch thick regions of the model. The white areas are 1/2 inch thick. A source transducer was placed along the surface of the model. A receiver transducer was placed along the left edge, which served as borehole USW UZ-6.

Using an industrial acrylic cement (IPS WELD-ON 3), the continuous strips were attached to the large sheet, taking great care to limit the air bubbles trapped between the two layers. Overall, the seal was very good, with only minor areas of trapped bubbles.

Once dry, the model consisted of 1/2 inch thick PLEXIGLAS for the welded units in the cross section, and 1/4 inch thick PLEXIGLAS for the non-welded units. The shaded areas in Figure 3.1 identify the 1/4 inch thick areas of this model. The model was designed so that changes in thickness would produce seismic reflections on a VSP record. Earlier experiments on a rectangular sheet of PLEXIGLAS showed that reflections from the bottom of the sheet would produce reflected events. This model is a uniform velocity model, since PLEXIGLAS is the only material present. Although the horizons have identical positions to the horizons in the computer models, the density and velocity values of the physical model are constants and do not correlate with the actual density and velocity values at Yucca Mountain. While the computer model values were determined from log information, the density for this physical model was 1.17 gm/cc for each of the layers. The p-wave velocity of the PLEXIGLAS was determined experimentally to be approximately 7600 feet per second.

Two holes were drilled through the model one inch from

the surface topography and one inch in from the left and right edges. Four inch long segments of threaded rod were inserted through the holes and bolted on each side so that 1.5 inches of rod protruded from each side of the model. A silicone rubber sealant was injected around the rods in order to suppress the magnitude of reflections generated by the metal rod where it passed through the model.

Using the threaded rods as hanging posts, the model was suspended two feet above the floor from a 10 feet long by 7 feet high redwood frame. Cotton rope was passed through eye-bolts anchored into the top beam of the frame, and looped around the ends of the threaded rods. Cotton rope was used to suspend the model instead of braided wire in hope that the rope would help dampen vibrations from the room.

A scale representing horizontal distance away from the left edge of the model (used as borehole UZ-6) was painted along the surface topography. Another scale was painted along the left edge of the model to represent 40 foot depth levels in borehole UZ-6 down to 2000 feet below the surface. Since the scale of the model is 1:1000, the depth levels were actually 0.04 feet apart.

On Figure 3.1, it is seen that the process of generating a synthetic VSP trace begins with a pulse generator. A GENERAL RADIO 1340 pulse generator was used to provide square

waves in this experiment. The pulse generator sent a sync pulse to the oscilloscope and a negative pulse to a GENERAL RADIO 1233-A power amplifier to increase the voltage of the pulse. This pulse is transferred to the source transducer, which is positioned on the top edge of the model at some offset from the left edge of the model. For the work in this thesis, all transducers used were products of PANAMETRICS of Waltham, Massachusetts. For this physical model, a PANAMETRICS V101 transducer was used as a source. This transducer vibrates longitudinally to the surface it rests upon in response to the output from the power amplifier. This transducer is analogous to a p-wave seismic source. The V101 transducer is 1 inch in diameter, and has a center frequency of 500,000 hertz.

The source transducer is coupled to the surface topography of the model using a processed honey couplant produced by PANAMETRICS. Seismic waves travel through the two dimensional model and are received by another V101 transducer on the the left edge of the model, which represents a borehole geophone at a specific depth level in borehole UZ-6. The receiver transducer is suspended from a string and coupled to the PLEXIGLAS using the honey couplant.

It is seen on Figure 3.1 that the output from the receiver is passed through a HEWLETT PACKARD 450A amplifier, which provides a gain of 40 db. An unfortunate problem

occurred at this point in the acquisition. Output from the receiver has very low amplitude and requires amplification. The HP amplifier, however, was a very old unit which introduced a large amount of 60 hz noise to the waveform. In order to remove the 60 hz noise, it was necessary to pass the signal through a bandpass filter. The only available unit was a KROHN-HITE 330M bandpass filter, which had an upper bandlimit of 20,000 hz. Signal bandwidth was set at 200-20,000 hz to remove the 60 hz noise. Unfortunately, a great deal of useful signal was lost due to the upper bandlimit.

Ouput from the filter was recorded by a TEKTRONIX 11401 Digitizing Oscilloscope. The TEK11401 has the capability of stacking up to 4096 waveforms to improve signal quality. The stacked waveform can be displayed with 14 bits of resolution. The scope is capable of sampling at 10 picoseconds per sample on a 10,240 sample waveform. For this model, a 2 microsecond sampling interval was used.

For each receiver location, 64 waveforms were stacked to produce a waveform on the TEK11401 screen. The waveform was then transferred to a COMPAQ 386 DESKPRO using a software package called GURU II. The software was developed by TEKTRONIX, and it transfers the waveform on the scope to the PC across a GPIB cable connecting the two machines. The waveform was then stored temporarily on a high-density floppy disk.

After an entire set of traces had been recorded from the model (multiple offsets, 50 traces per offset), the waveforms on floppy disks were transferred to the hard drive of the COMPAQ. Using the KERMIT terminal communications software, the waveforms were uploaded to a VAX 8600 mainframe computer. This process can take up to 16 hours to complete the uploading of 50 traces for 8 different source offsets (400 traces). The traces were stored on the scratch disk of the VAX 8600.

The uploaded traces are diskfiles which contain small headers consisting of oscilloscope settings, followed by strings of 5,120 integers. In order to use advanced VSP processing software on the traces, it is necessary to convert each trace into SEGY format. Kurt Ranzinger, a graduate student at CSM, has developed a series of programs which convert the traces into proper format. Parameters defining source and receiver locations are read from files by the programs in order to insert the information into trace headers for each waveform. After converting the files into SEGY format, the data set is written to magnetic tape.

The magnetic tape containing the complete data set is transferred to another mainframe computer, a GOULD 9750, which houses the VSEIS vertical seismic profiling software. The SEGY traces are read in by VSEIS and treated just as if the data had come from a field survey.

Eight synthetic vertical seismic profiles were recorded using the uniform velocity, variable thickness model. For each of the eight source offsets (a zero-offset data set was not recorded), 50 traces were recorded at 0.04 foot intervals. When scaled by 1000, this meant recording at 40 foot intervals down to 2000 feet. The parameters in Table 3.1 were used to record all traces for this model.

Table 3.1 Recording Parameters

SAMPLE INTERVAL	:	2 microseconds
SAMPLES/TRACE	:	5120
STACKING FOLD	:	64
PULSE FREQUENCY	:	30 milliseconds
PULSE DURATION	:	20 microseconds

3.2 1000-foot source offset VSP

Figure 3.2 shows the data set recorded with the source transducer 1 foot (1000 feet) from the receiver borehole. Depth increases down the page, and is annotated in feet below the top of the borehole (left edge of the model). Just as the distances have been scaled by 1000 fold, so have the times. Time is shown increasing to the right, and is

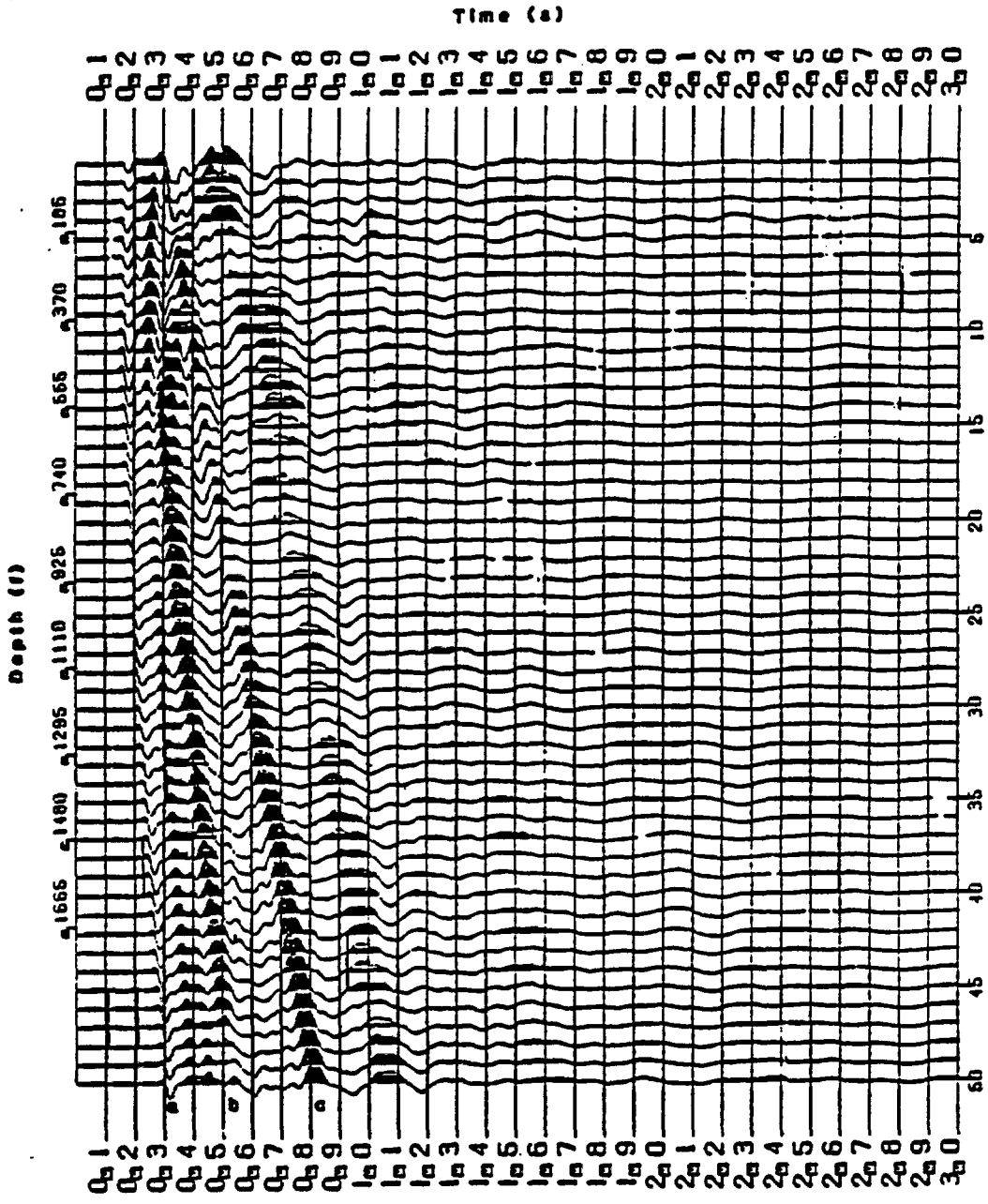

Figure 3.2. VSP data set recorded from the physical model with a source transducer offset of 1000 feet (1 foot). Three distinct events can be identified on the record. The direct p-wave (a) can be seen on every trace. The direct s-wave (b) and the surface wave (c) are clearly visible. The noise spikes are caused by the plotter.

annotated in seconds. The traces are 3.0 milliseconds long, but appear as 3.0 seconds long due to the 1:1000 scale of the model. The traces were chopped from 5120 samples down to 1500 samples without the loss of any valuable signal.

Three events are seen on the figure. The initial trough (a) is the direct p-wave. This event can be positively identified on every trace. The event labeled (b) is a direct s-wave. Since the V101 transducers respond to motion longitudinal to the surface, it should be expected that an s-wave arriving obliquely to the borehole will produce an event on the trace. This also indicates that the V101 source transducer is producing some s-wave energy in addition to the p-wave energy.

The slope of this event is the key to its identification. Its slope is less than that of the direct p-wave, indicating a lower velocity. Also, the event is not seen on the shallow traces. On the shallower traces, a direct arrival strikes the receiver at an angle approaching 90 degrees. Only p-waves would be recorded, not s-waves. The s-waves require an oblique emergence angle to be recorded by a longitudinal transducer.

The third event (c) arrives considerably later in time than the direct arrivals. This event is thought to be a surface wave which travels along the surface topography and down the borehole edge of the model. The event can be

picked due to its constant apparent velocity on every data set. Since the apparent velocity (approximately 3700 feet/second) is the same for any source/receiver configuration, the event must be traveling down the edge of the model. The apparent velocities of events traveling through the model change depending on the source offset. Also, although the slope of the event is constant, the event arrives later in time as the source offset increases. This is consistent with the belief that the wave is traveling along the topography and then down the side of the model.

The three events identified on this data set are all downgoing events which provide information about the velocity structure of the subsurface, but the events also mask the appearance of the upgoing reflections. The events must be removed from the data by median filtering. The first arrival times were picked interactively using VSEIS, and the traces were shifted to align the first arrivals at 0.1 second. Figure 3.3 shows the direct arrivals (a) aligned.

An 11-fold median filter was used to remove the direct arrivals from the data set. Figure 3.4 shows the data set shifted back to its original time position after the first arrivals had been removed. It also appears that the direct s-wave was largely removed during the median filtering, which was an unexpected but welcome result. The surface

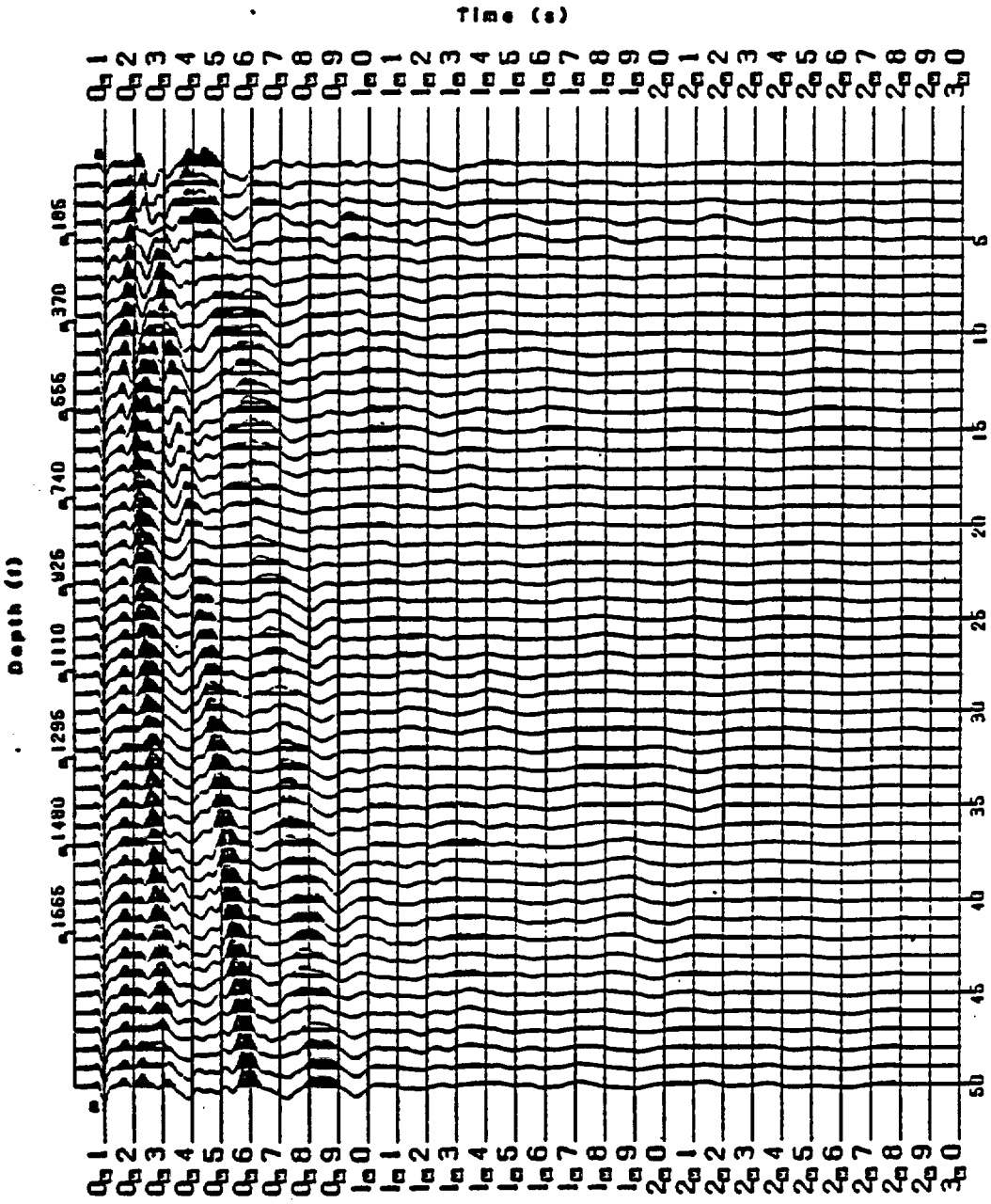

Figure 3.3. VSP data set for 1000-foot source offset with the direct p-wave arrivals aligned at 0.1 second. The events are aligned and scaled in preparation for spatial median filtering.

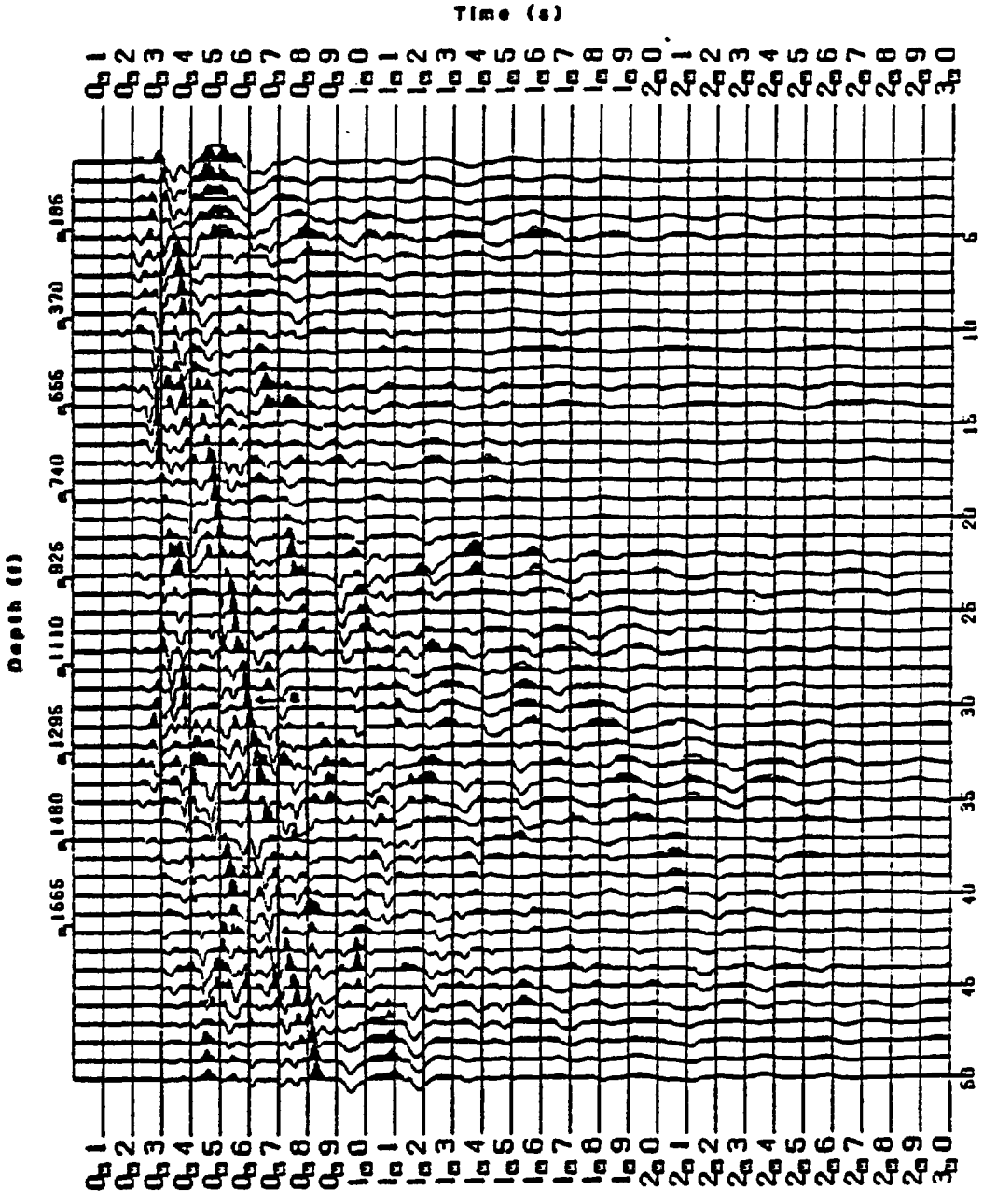

Figure 3.4. VSP data set for 1000-foot source offset after removing the direct p-wave arrivals. A large portion of the direct s-wave was also removed during the filtering.

wave (a) is still quite prominent, however. It is possible to remove this event by median filtering as well. The arrival times for the surface waves were picked and the events were aligned along a line of equal time.

Figure 3.5 shows the surface wave (a) aligned along the 1.0 second time line. If the events were aligned at 0.1 second, as is done for direct arrivals, all information on the traces before the surface wave arrivals would be shifted off of the traces and lost. Aligning the events at 1.0 second circumvents this problem. An 11-fold median filter was used to remove the surface wave from the data set.

Figure 3.6 shows the data shifted back to its original time position after the first arrivals and surface wave had been removed from the data. A few hints of upgoing reflections can be seen in this figure, but it is difficult to make a sound interpretation. In order to enhance the upgoing energy, an FK filter was applied to the data. Figure 3.7 shows the FK spectrum of the data set before filtering. Coherent downgoing energy appears in the left-hand plane. Coherent upgoing energy appears in the right-hand plane. Figure 3.8 shows the FK spectrum of the data set after a filter had been applied to remove energy in the left-hand plane.

Figure 3.9 shows the data set tranformed back into the time domain after the FK filter had been applied. Several

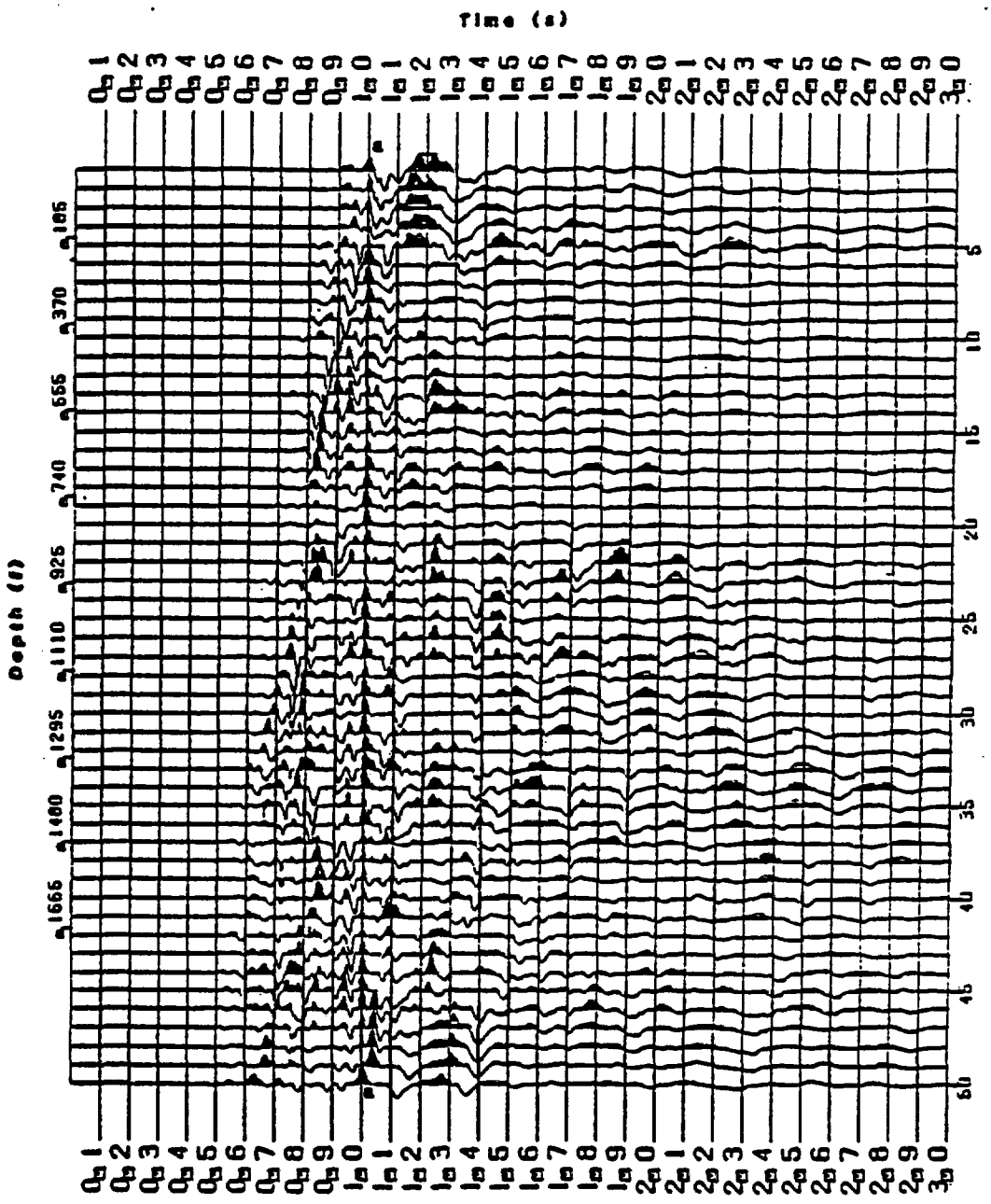

Figure 3.5. VSP data set for 1000-foot source offset after aligning the surface wave (a) along the 1.0 second time line. The events are aligned and scaled in preparation for spatial median filtering.

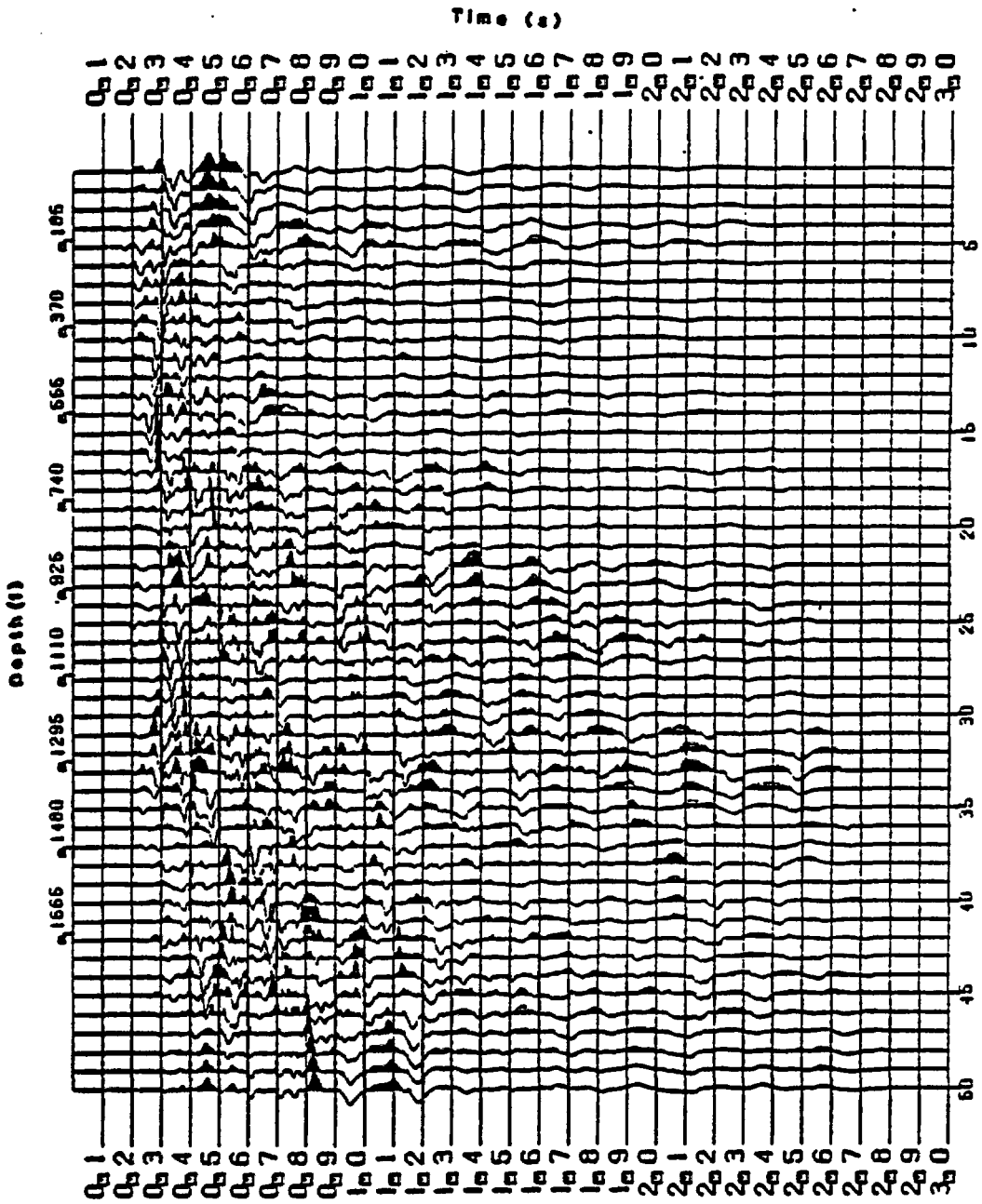

Figure 3.6. VSP data set for 1000-foot source offset after removing the direct p-wave and the surface wave. A few hints of upgoing reflections can be identified in this diagram.

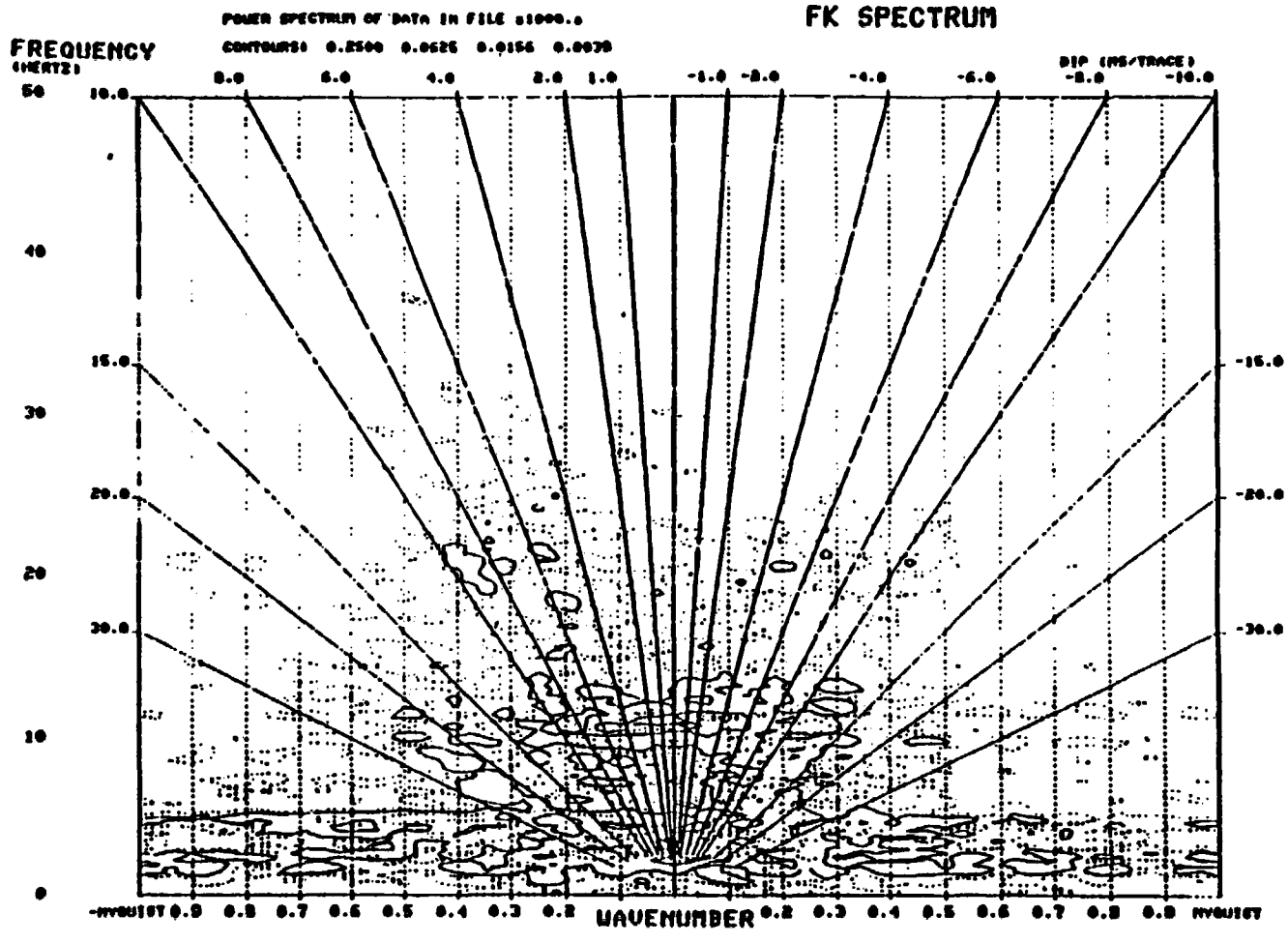

Figure 3.7. FK spectrum of the data set in Figure 3.6. Coherent downgoing energy (noise) appears in the left-hand plane of the diagram. Coherent upgoing energy (reflections) appears in the right-hand plane of the diagram.

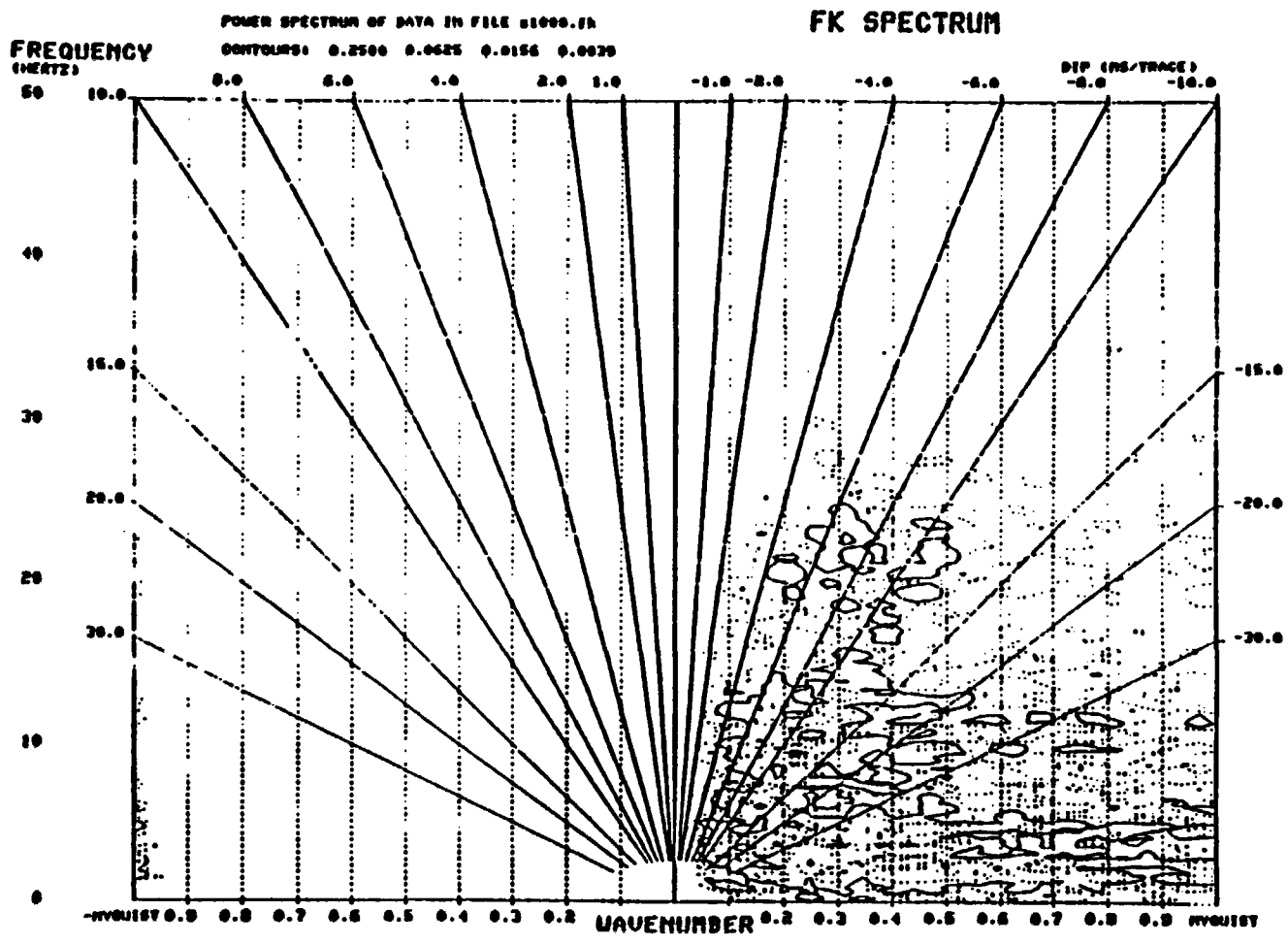

Figure 3.8. FK spectrum of the data set in Figure 3.6 after applying an FK filter to remove downgoing energy. Nearly all of the energy present after filtering is in the right-hand plane.

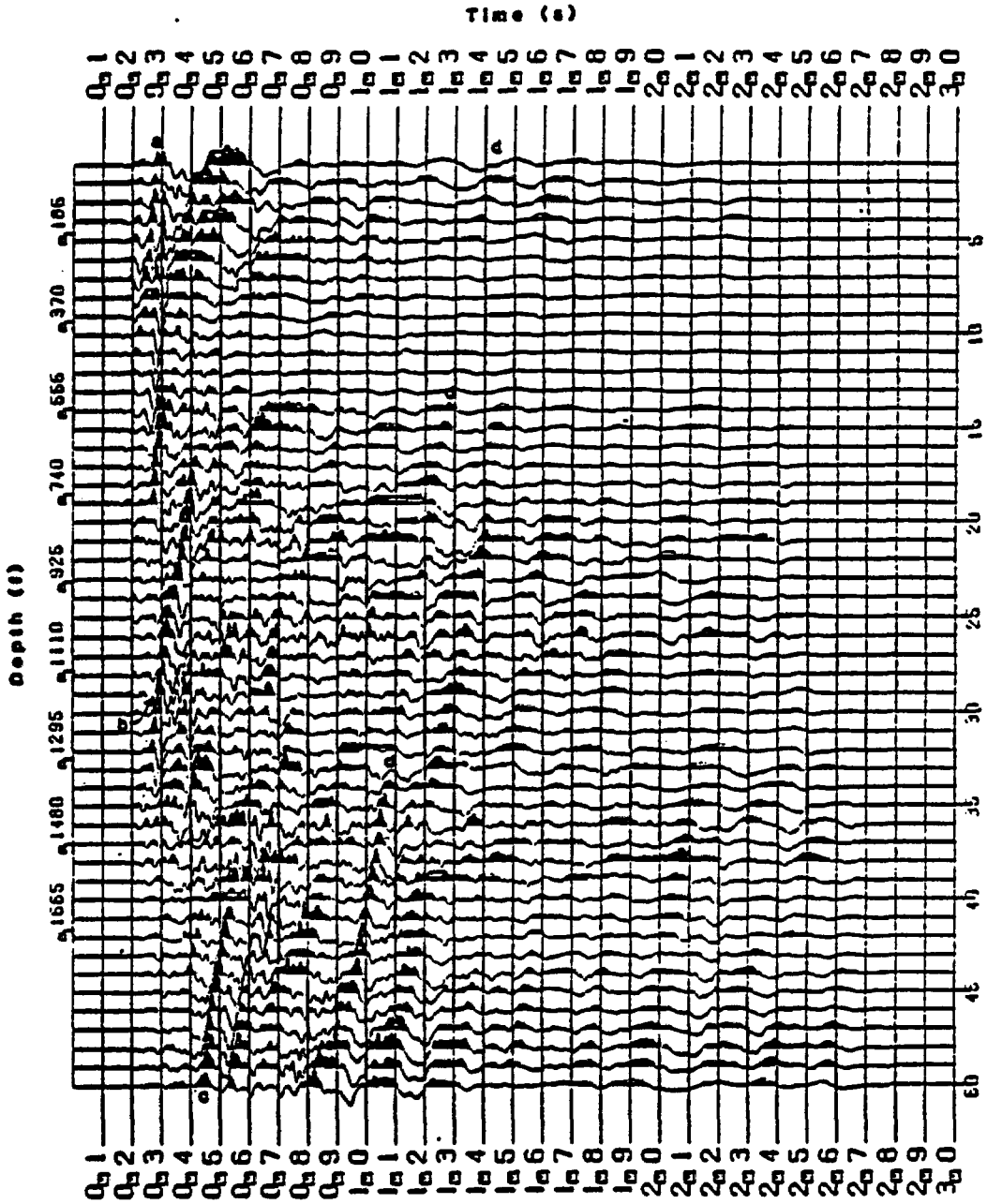

Figure 3.9. VSP data set from Figure 3.6 after applying an FK filter to remove residual downgoing energy. Several upgoing reflections can now be identified. Event (a) is a reflection from the shallowest thin region of the model, n1. Event (b) is a reflection from n2, the next thin region of the model. Event (c) is a reflection from n3, and event (d) is a reflection from the bottom of the model.

coherent reflections are now visible on the data set. The event labeled (a) between 0.2 and 0.3 second on traces 1 through 12 is a reflection from the first thickness change in the physical model. Traces 12 and 13 are levels within the n1 unit of the model, and this reflection is not seen on traces below trace 12.

The model is 1/2 inch thick between depth levels 14 and 35. At trace 36, the thickness changes to 1/4 inch thick to represent the top of the n2 horizon. The event labeled (b) is a reflection from this horizon, and can be seen on traces 17 through 35. It may be seen on traces 10 through 16 as well, but it is a much weaker event. As noted earlier, reflections merge with direct arrival at the depth level of the reflecting horizon.

The thickness of the model increases to 1/2 inch at a level 0.29 feet below the level of trace 50. This corresponds to the top of Tcbw. Tcbw is 0.21 feet thick from top to bottom on the model. The model thins to 1/4 inch thick again at the base of Tcbw to represent the top of n3.

The event labeled (c) is a reflection from either Tcbw or n3. The slope of the event suggests that this reflection would merge with the direct arrival at the depth level of n3. If this were indeed a reflection from Tcbw, it would indicate that reflections can be generated from areas of increasing model thickness (the tops of welded units) as

well as from areas of decreasing model thickness (the tops of non-welded units). It is also possible that this event could be a composite reflection from Tcbw and n3, since the seismic resolution of this profile was limited. The reflection can be seen easily on traces 39 through 50. It is also identifiable on traces 25 through 30 between 0.6 and 0.7 second.

The next change in thickness occurs 1.08 feet below the bottom of the borehole (trace 50). At the top of horizon Tctw thickness increases to 1/2 inch. Tctw is a thin welded unit and is only one inch thick from top to bottom. Although coherent upgoing events appear to the right of event (c) on Figure 3.9, a definitive identification of a reflection from Tctw or n4 can not be made.

A final reflection should be expected from the bottom edge of the model, which is 2.08 feet below the depth level of trace 50. The event labeled (d) is interpreted as this reflection. It is best seen on traces 34 through 46 between 0.9 and 1.1 seconds. The event is weaker but visible on traces 14 through 32 between 1.1 and 1.3 seconds, as well as on traces 2 through 5 near 1.4 seconds. The event was identified by projecting the slope downward to where an intersection with the projected slope of the direct arrival would occur. The result, though inexact, was consistent with an event reflecting from the bottom of the model.

A problem exists in the interpretation of the data set. Figure 3.9 almost certainly contains both p-wave and p to s converted wave reflections. Although the slopes of the events are different, it makes postive identification of every event very difficult. Events which do not have a clear identity have been left uninterpreted. Future modeling work with two-component receivers may aid in the interpretation of s-wave events in data sets in this thesis.

In order to test the interpretation of the data set in Figure 3.9, an AIMS model was created to simulate the data set recorded from the physical model. A velocity of 7600 feet/sec was inserted for every horizon in the computer model used in Chapter 2, and a synthetic data set was created for a source offset of 3000 feet. The data set appears in Figure 3.10.

Event (a) is the reflection from n1 and Tptw. The event arrives roughly 100 milliseconds earlier than the event interpreted as the n1 reflection on Figure 3.9. This time delay suggests that event (a) on Figure 3.9 is actually a reflected s-wave from horizon n1. The event does originate at the proper location for a reflection from n1, and the 100 millisecond delay would be consistent with the velocity for an s-wave reflection instead of a p-wave reflection.

Event (b) is the reflection from n2, and this event corresponds quite well with the event on Figure 3.9. Event (c)

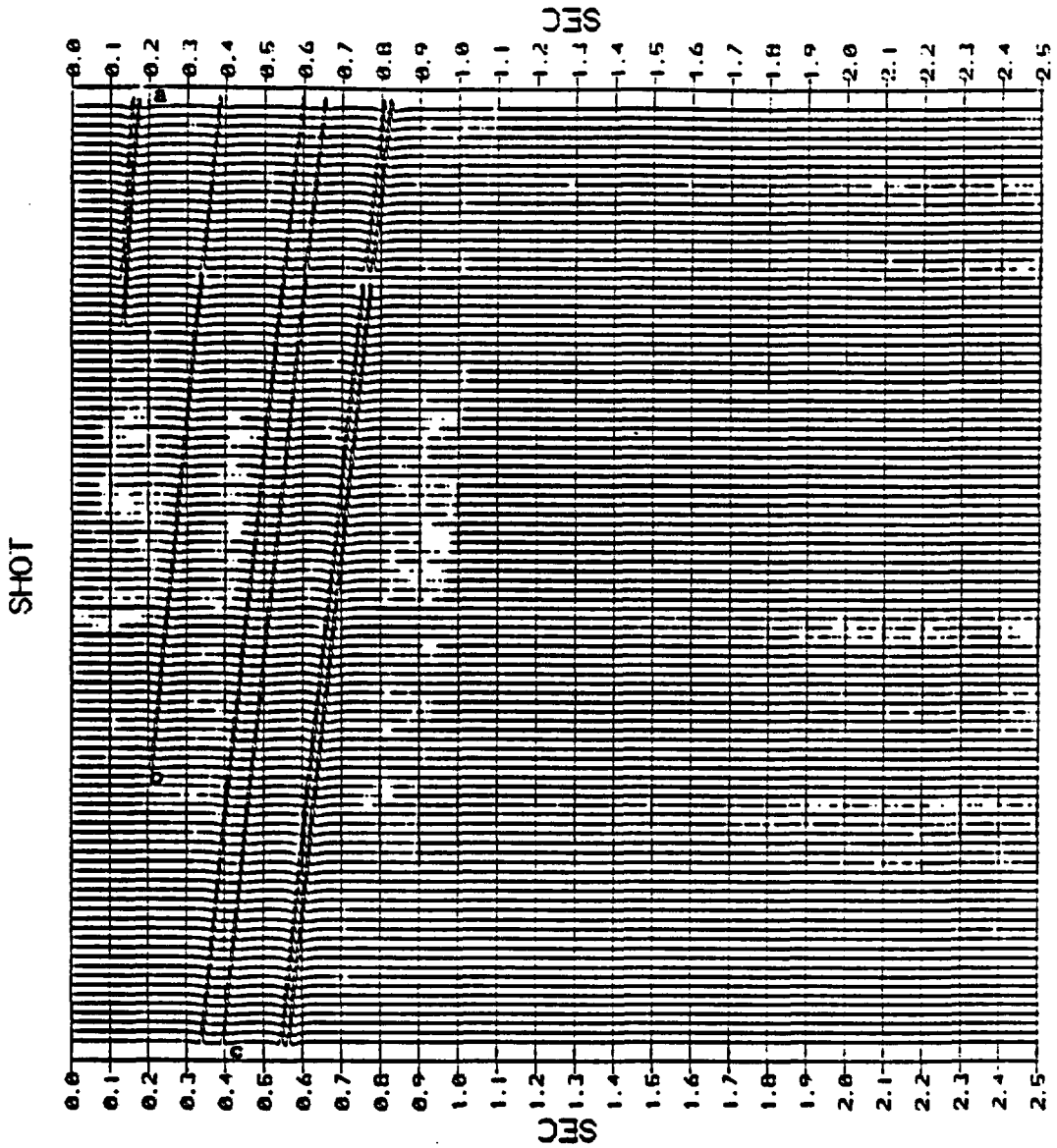

Figure 3.10. Synthetic AIMS data set simulating the 1000-foot source offset data set using the uniform velocity model. Event (a) is the reflection from n1/Tptw. The event arrives 100 milliseconds before the n1 reflection on Figure 3.9, suggesting that the n1 reflection on Figure 3.9 is an s-wave reflection. Reflections from n2(b) and n3(c) correspond quite well (within 20 milliseconds) to their counterparts on Figure 3.9.

is the reflection from n3 and this event corresponds (within 20 milliseconds) of event (c) on Figure 3.9, which was interpreted as a reflection from Tcbw or n3. The reasonably close match between the computer model data and the physical model data suggests that the interpretation of the physical model data set is sound.

The data set in Figure 3.9 was a very encouraging result. It showed that the laboratory set-up was capable of generating and recording synthetic vertical seismic profiles of interpretable quality from a complex model. The model showed that thickness changes in a one-medium model can generate a significant amount of reflected energy.

3.3 2000-foot source offset VSP

The source transducer was moved to 2000 feet from the borehole edge of the model and 50 traces were recorded. The resulting data set is shown in Figure 3.11. Again, three distinct downgoing events can be identified on the record. The event labeled (a) is obviously the direct p-wave arrival. The consistent trough can be seen on every trace between 0.3 and 0.4 second. The character of the event changes with depth due to attenuation.

The direct s-wave (b) is easy to identify on traces 22 through 50. As seen on the data set in Figure 3.2, the event is not apparent on the shallow traces. This is again

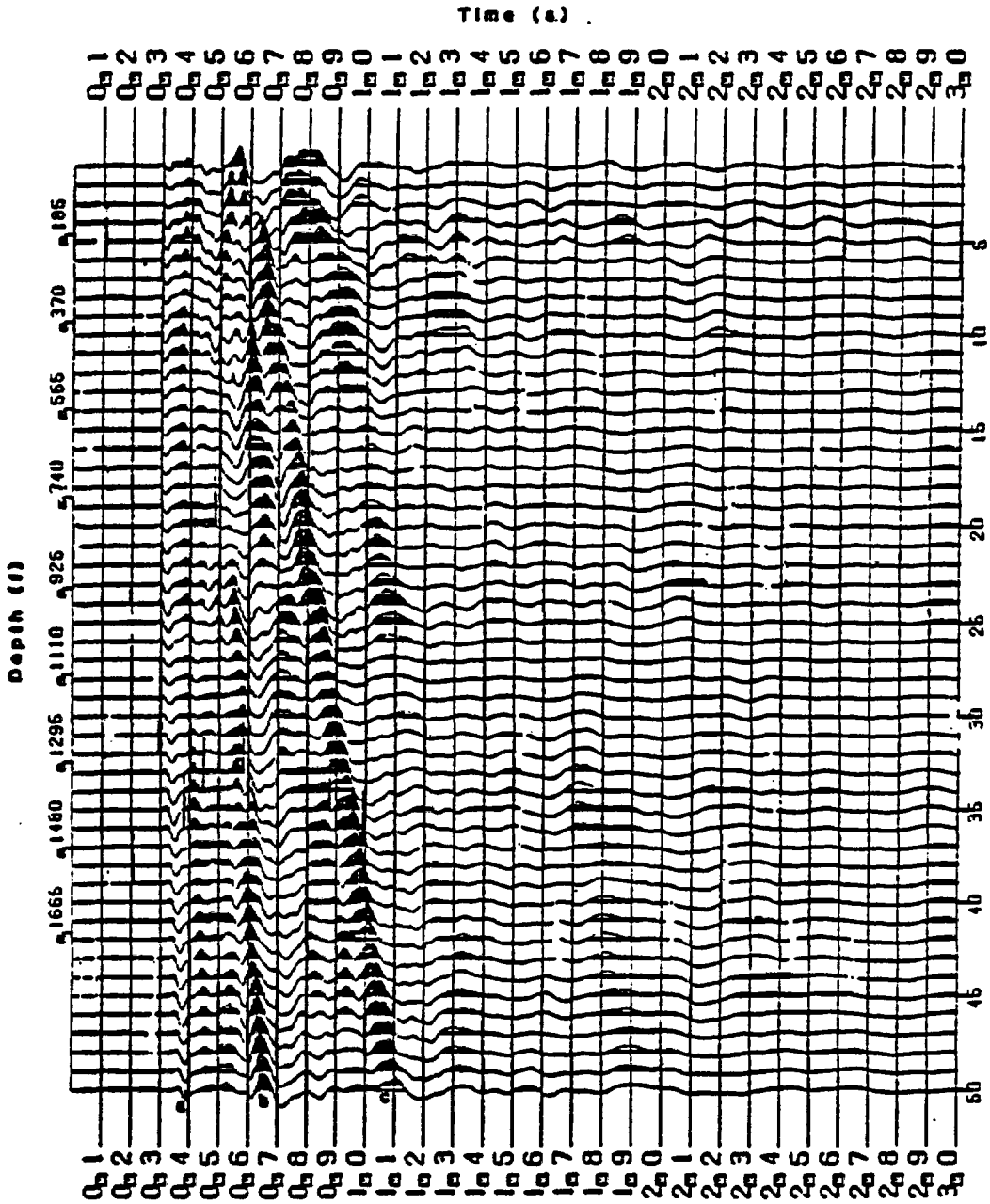

Figure 3.11. VSP data set recorded for a source transducer offset of 2000 feet. Three major downgoing events can be identified on this record. Event (a) is the direct p-wave, event (b) is the direct s-wave, and event (c) is the surface wave. The surface wave is identified by its characteristic constant slope from data set to data set.

due to the fact that direct arrivals emerge at the borehole at an angle approaching 90 degrees on the shallow traces. A shear wave must strike the borehole at an oblique angle to be recorded by the V101 transducer.

The third downgoing event is the surface wave (c). This event has the same slope as the surface wave in Figure 3.2, but it arrives later in time. On trace 50 in Figure 3.2, the surface wave arrives 275 milliseconds after the direct s-wave. On trace 50 in Figure 3.11, the surface wave arrives 450 milliseconds after the direct s-wave. The surface wave can be loosely compared to tube wave noise on a field VSP record. Both events are unwanted noise, and both travel along the borehole wall.

The downgoing events were removed by median filtering. Both the direct p-wave and the surface wave were aligned along lines of equal time and filtered. The direct s-wave was largely removed while filtering out the other two downgoing events. The resulting upgoing wavefield is shown in Figure 3.12.

As seen with the upgoing wavefield for the 1000-foot source offset, a few hints of upgoing reflections can be seen but it is difficult to interpret the individual events. This data set was FK filtered in the same manner as was done to the 1000-foot offset data set. Energy in the left-hand plane of the FK plot was removed and the data set was

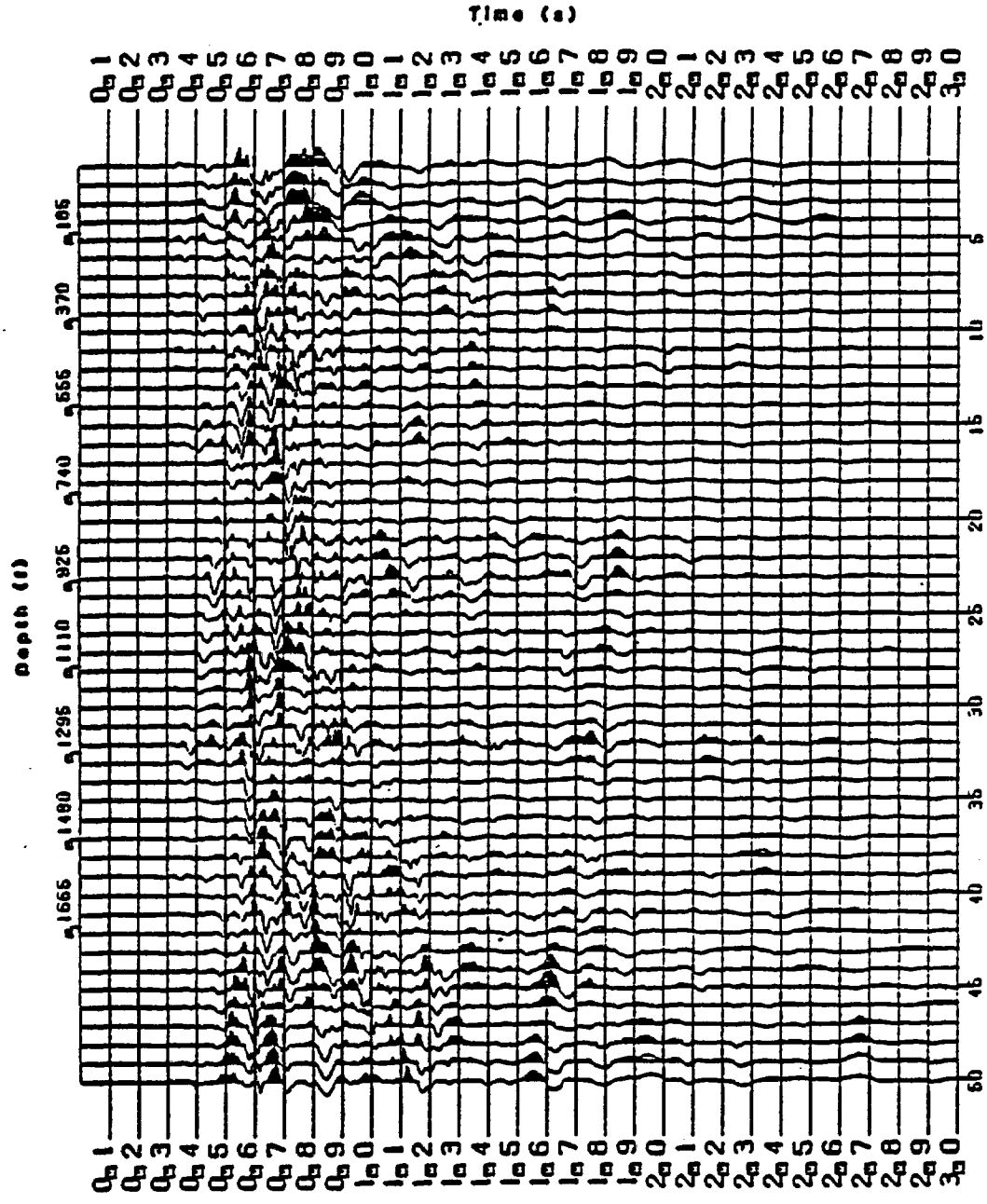

Figure 3.12. VSP data set for 2000-foot source offset with the direct p-wave and the surface wave removed. Upgoing reflections are difficult to identify.

transformed back to the time domain. The resulting data set is shown in Figure 3.13.

The reflection from the first thickness change in the model, the n1 horizon, is labeled (a) on this figure. The small peak appears on traces 1 through 12 between 0.3 and 0.4 second. The early arrival time of this event makes it difficult to separate the event from the direct arrival.

The model thins to 1/4 inch at the boundary between Tptw and n2. As noted earlier, this occurs at depth level 36 on the left edge of the model. The reflection from this horizon is labeled (b) on the data set. The event can be identified on traces 1 through 34, although it is strongest on traces 8 through 25.

The event labeled (c) is the reflection from Tcbw (and/or n3). It is best seen on traces 35 through 50. Although identification is difficult, the peaks on traces 37 through 50 that arrive 150 milliseconds after the Tcbw peaks may be reflected events from Tctw. This event is labeled (d). Since the horizon is so thin, this reflection would be a composite reflection from Tctw and n4.

A reflection from the bottom of the model is not readily apparent. The event labeled (e) is the strongest candidate, but it arrives very late for it to be the bottom reflection. The event can be seen on most of the traces between trace 20 and trace 50.

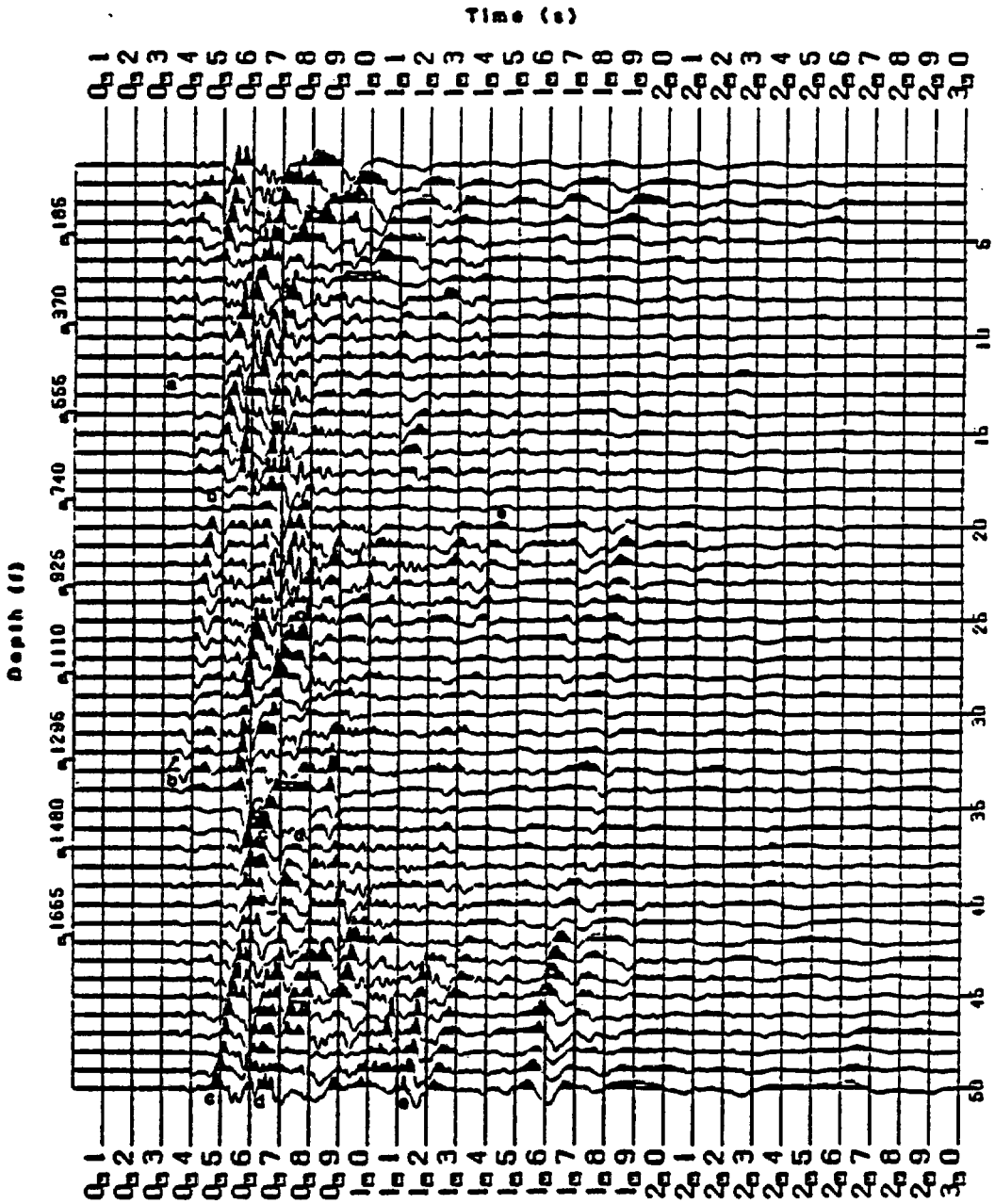

Figure 3.13. Data set in Figure 3.12 after applying an FK filter to remove residual downgoing energy. Reflections can be seen from n1(a), n2(b), Tcbw/n3(c), Tctw/n4(d), and from the bottom of the model (e). The bottom of the model reflection is arriving quite late in time and may be a p-s converted reflection.

As with the 1000-foot source offset data set, an AIMS model was created in order to test the interpretation of Figure 3.13. The synthetic data set appears in Figure 3.14. Event (a) is the reflection from n1, which corresponds within 20 milliseconds of the n1 reflection on Figure 3.13. Reflections from n2(b), n3(c), and Tctw/n4(d) all correspond with their counterparts on Figure 3.13 within 20 milliseconds, suggesting that the interpretation of the physical model data set is sound. Due to the cost of computer model tests, no further computer models were run to test interpretations in Chapter 3. Knowledge gained from the modeling on the 1000-foot and 2000-foot source offset data sets was applied to the interpretation of the remaining data sets.

3.4 3000-foot source offset VSP

Figure 3.15 is the data set recorded for a source offset of 3000 feet. The direct p-wave trough (a) shows a near-vertical slope. As source offset increases and source elevation decreases, this result can be expected on later data sets as well.

The direct s-wave (b) can be seen intermittently on traces 14 through 50. As source offset increases, this event should disappear almost completely. The direct arrivals will emerge almost perpendicular to the borehole at every depth level. The surface wave (c) is seen with its

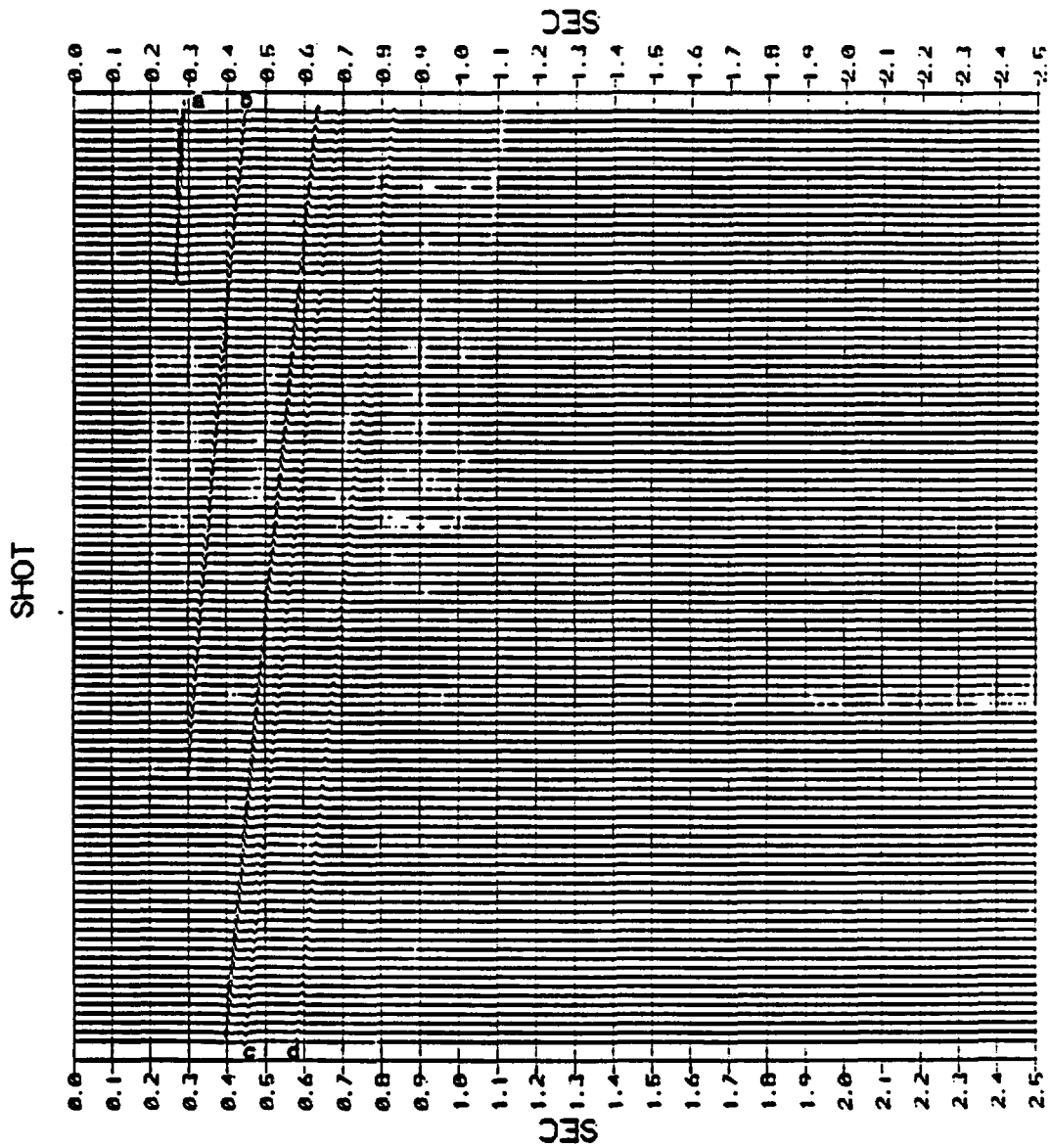

Figure 3.14. Synthetic AIMS data set simulating a 2000-foot source offset record using the uniform velocity model. Event (a) is a reflection from n1 and corresponds well with the n1 reflection on Figure 3.13 (within 20 milliseconds. Reflections from n2(b), n3(c), and Tctw/n4 (d) all correspond with their counterparts on Figure 3.13 within 20 milliseconds.

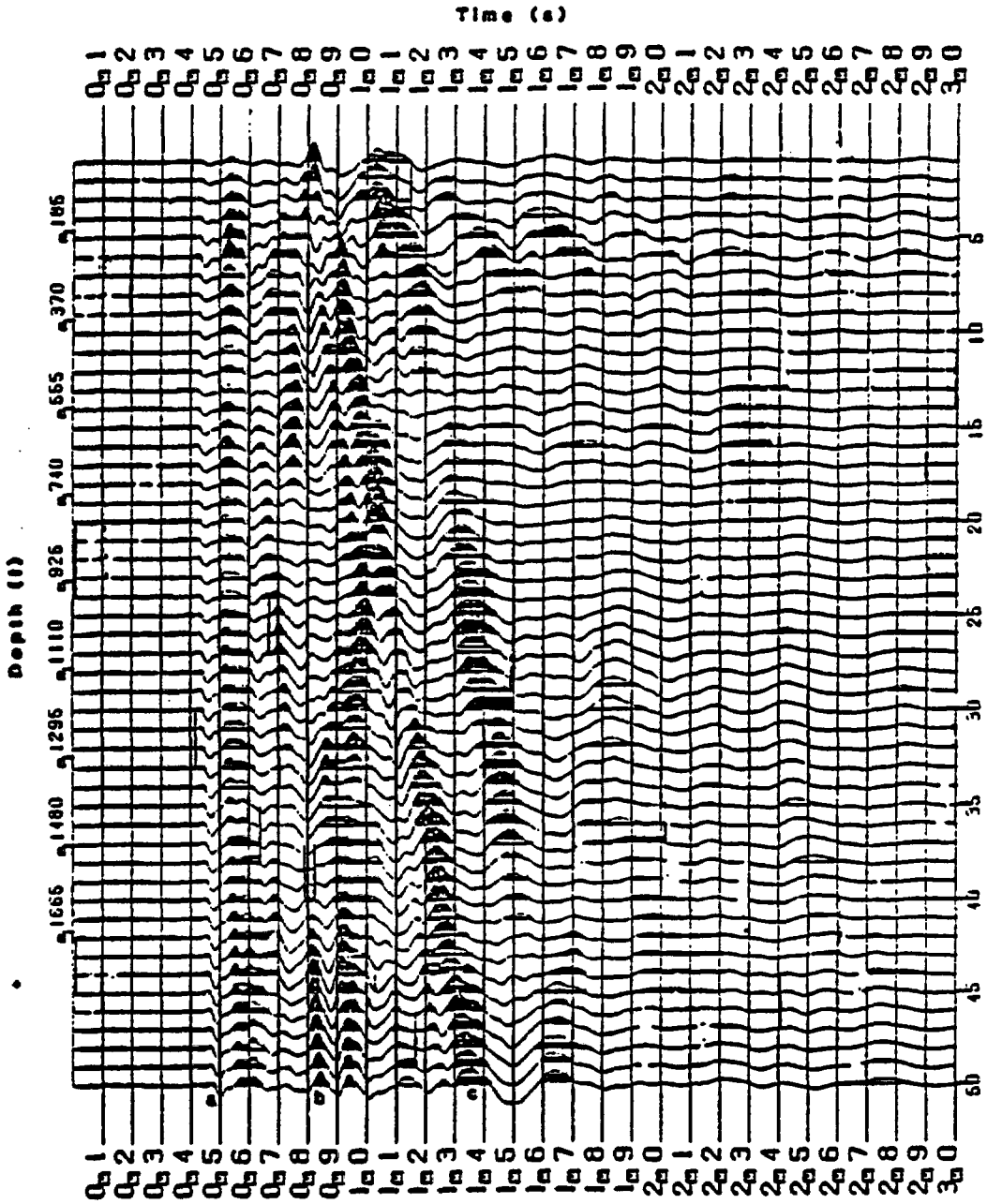

Figure 3.15. VSP data set recorded for 3000-foot source offset. Three downgoing events can be identified. Event (a) is the direct p-wave. Event (b) is the direct s-wave, which is best seen on the deeper traces. Event (c) is the surface wave, which has the same slope on every data set but continues to arrive later in time.

characteristic slope on traces 5 through 50. It continues to arrive later in time as source offset increases.

Times were picked to align the direct arrivals and surface wave along lines of equal time. Both events were removed by median filtering. The direct s-wave largely disappeared during the median filtering. The resulting upgoing wavefield is shown in Figure 3.16.

Once again, a few upgoing reflections can be seen. The FK filter was used to enhance the upgoing events and to eliminate any remaining coherent downgoing energy. The data set after FK filtering is shown in Figure 3.17.

A faint hint of the reflection from n1 (a) can be seen on traces 4 through 11 between 0.45 and 0.55 second. The peaks are very weak and difficult to identify.

The n2 horizon (depth level 36) provides both an identifiable p-wave reflection (b) and what appears to be a p to s converted reflection (c). Both events appear to originate at trace 35, which identifies them as n2 reflections. The reflections have decidedly different slopes, however, indicating different velocities.

The n3 reflection is labeled (d), and is best seen on traces 35 through 50. The slope of this event suggests that it is a p to s converted reflection, although this can not be proved. The best candidate for a reflection from the bottom of the model is event (e). It is difficult to

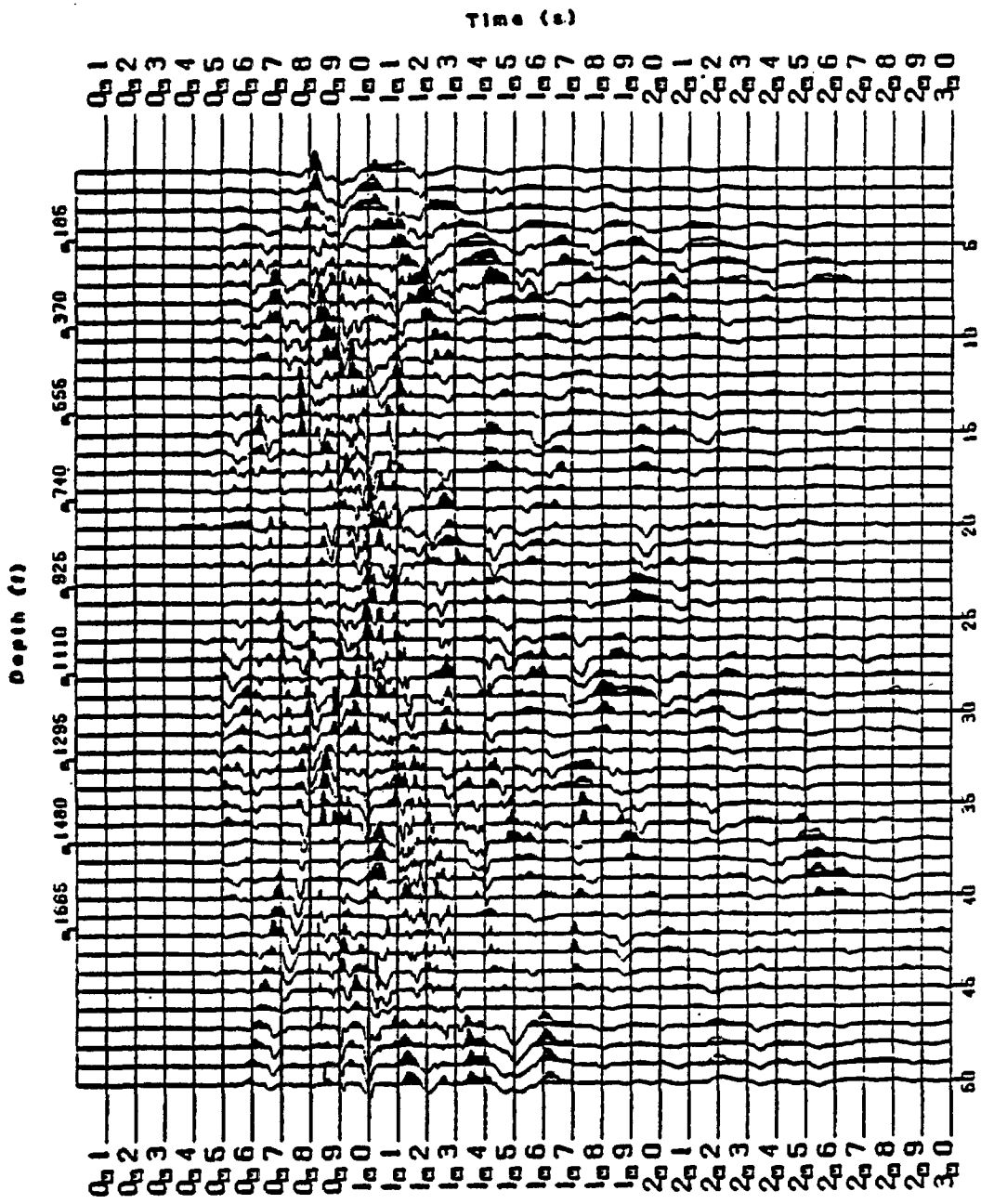

Figure 3.16. VSP data set for 3000-foot source offset after removing the direct p-wave and the surface wave. Upgoing reflections can be seen, but are difficult to identify.

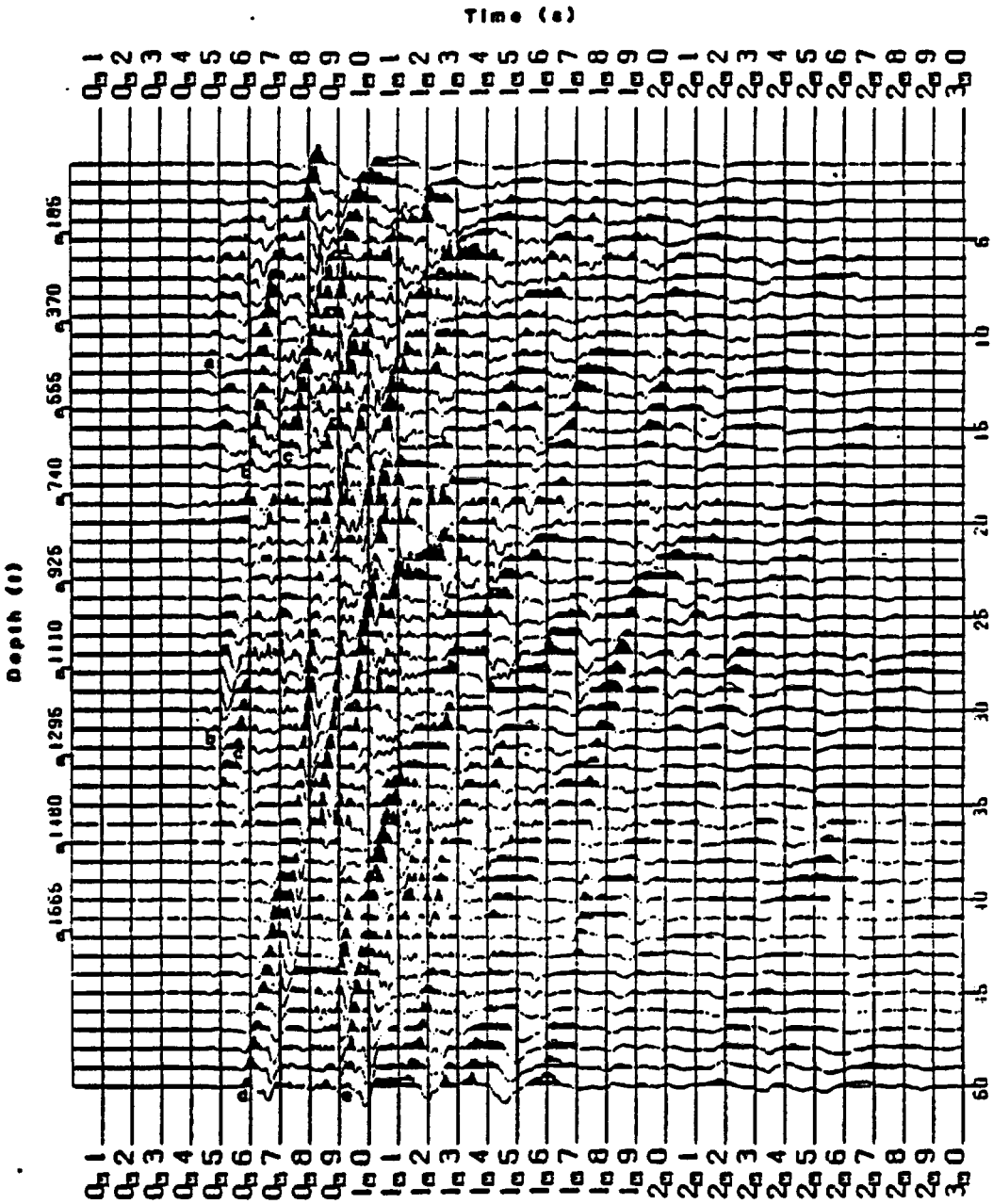

Figure 3.17. VSP data set from Figure 3.16 after applying an FK filter to remove residual downgoing energy. A faint hint of the n1(a) reflection can be seen on the shallow traces. Event (b) is a p-wave reflection from n2, while event (c) is most likely a p to s converted reflection from n2. Event (d) is a reflection from n3, and event (e) may be a reflection from the bottom of the model.

positively identify reflections which do not merge with the direct arrival, however.

This data set appears to contain a wide mixture of p-wave and s-wave reflections. Several coherent events appear in this data set that have not been identified.

3.5 4000-foot source offset VSP

Fifty traces were recorded with the source transducer 4000 feet from the borehole. The resulting data set is shown in Figure 3.18. The direct p-wave arrival (a) is seen on every trace. This event now has a nearly vertical slope. There are only 15 milliseconds of time difference between its arrival time on trace 1 and its arrival time on trace 50. The direct s-wave (b) is best seen on traces 40 through 50. As noted earlier, the s-wave must emerge at an oblique angle to be recorded. A sufficiently oblique emergence angle exists only on the deeper traces. The characteristic slope of the surface wave (c) makes this event easy to identify on this data set.

The direct p-wave was removed with an 11-fold median filter, as was the surface wave. The resulting upgoing wavefield is shown in Figure 3.19. The n3 reflection (a) is the only upgoing reflection which can be positively identified on this record. As with previous data sets, an FK filter was applied to suppress remaining downgoing energy

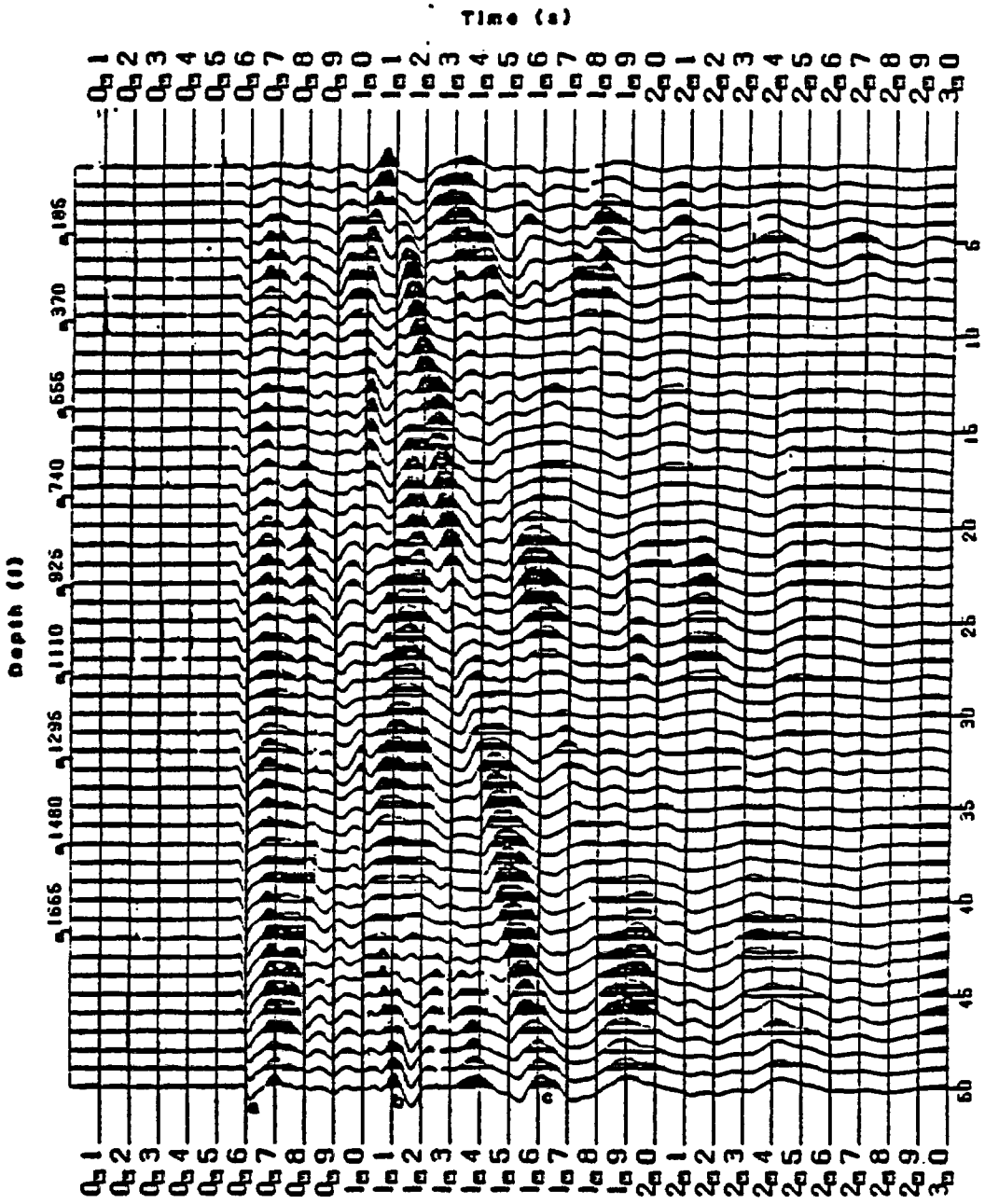

Figure 3.18. VSP data set recorded for 4000-foot source offset. The three major downgoing events can be identified. Event (a) is the direct p-wave. Event (b) is the direct s-wave. This event is best seen on the deeper traces, due to a shallower angle of emergence. Event (c) is the surface wave.

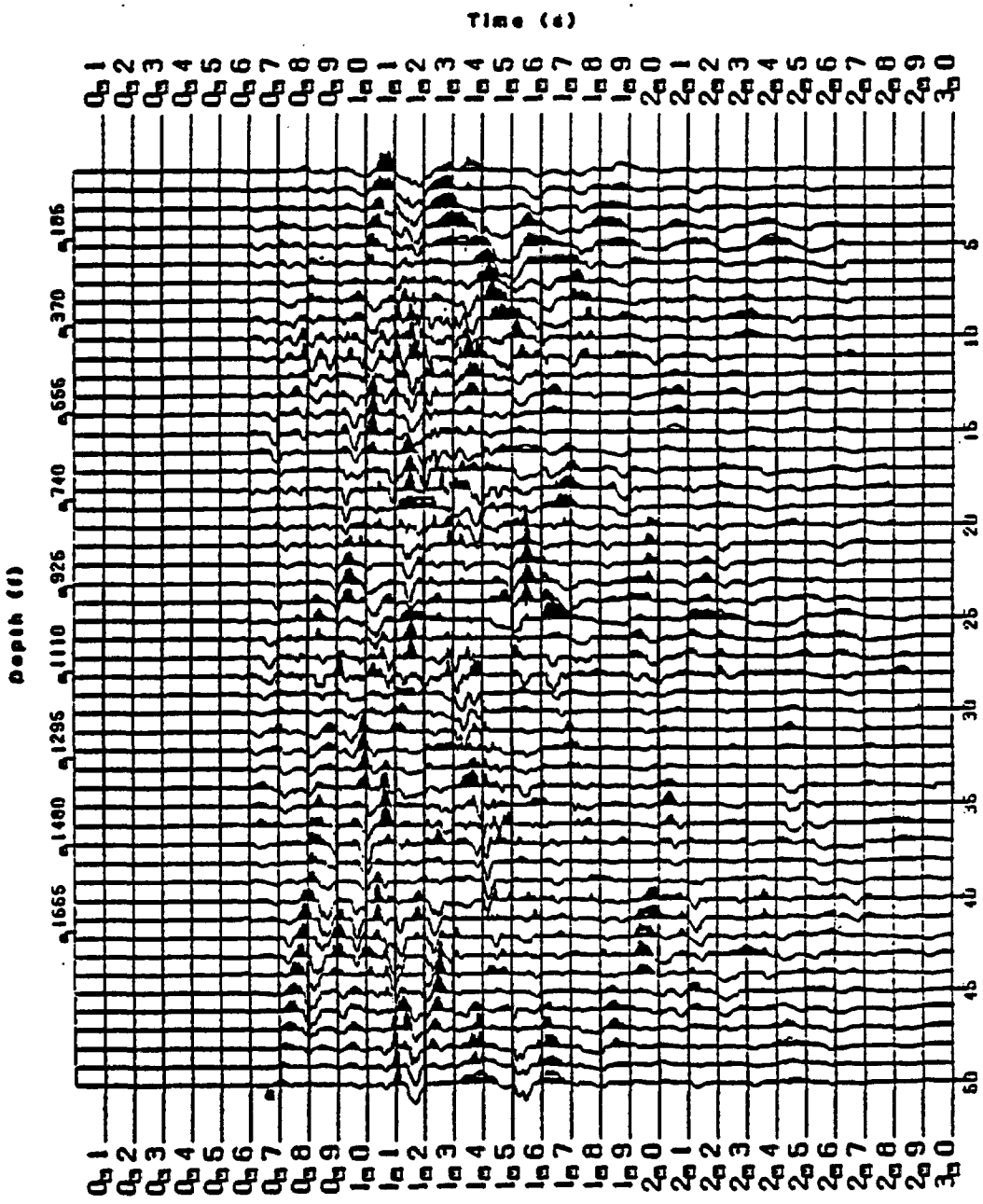

Figure 3.19. VSP data set for 4000-foot source offset after removing the direct p-wave and the surface wave. Event (a) is interpreted to be a reflection from n3.

in the data set. Figure 3.20 shows the data set after an FK filter was applied.

The reflection from n1 (a) is still visible on this data set. The peaks occur on traces 3 through 10 between 0.6 and 0.75 second. This event would be impossible to identify without prior knowledge of its position from the previous data sets.

The 3000 foot offset data set showed both a p-wave and a p to s converted reflection from horizon n2. This occurs again on this data set. Event (b) is a p-wave reflection from n2. The event is strongest on traces 6 through 14, but it appears to originate at trace 35, where an n2 reflection would merge with the direct arrival. The p to s converted reflection (c) also originates at trace 35. This event has a lesser slope than event (b), indicating its lower velocity.

The n3 reflection (d) is a strong event on the deeper traces. The event labeled (e) may or may not be a reflection from n4. If it is not an n4 reflection, it could be an s-wave reflection from Tcbw. The event labeled (f) has an arrival time consistent with an event reflecting from the bottom of the model.

On the computer models, the reflections grew closer together as the source offset increased. Interpretation became increasingly difficult. The same effect is beginning

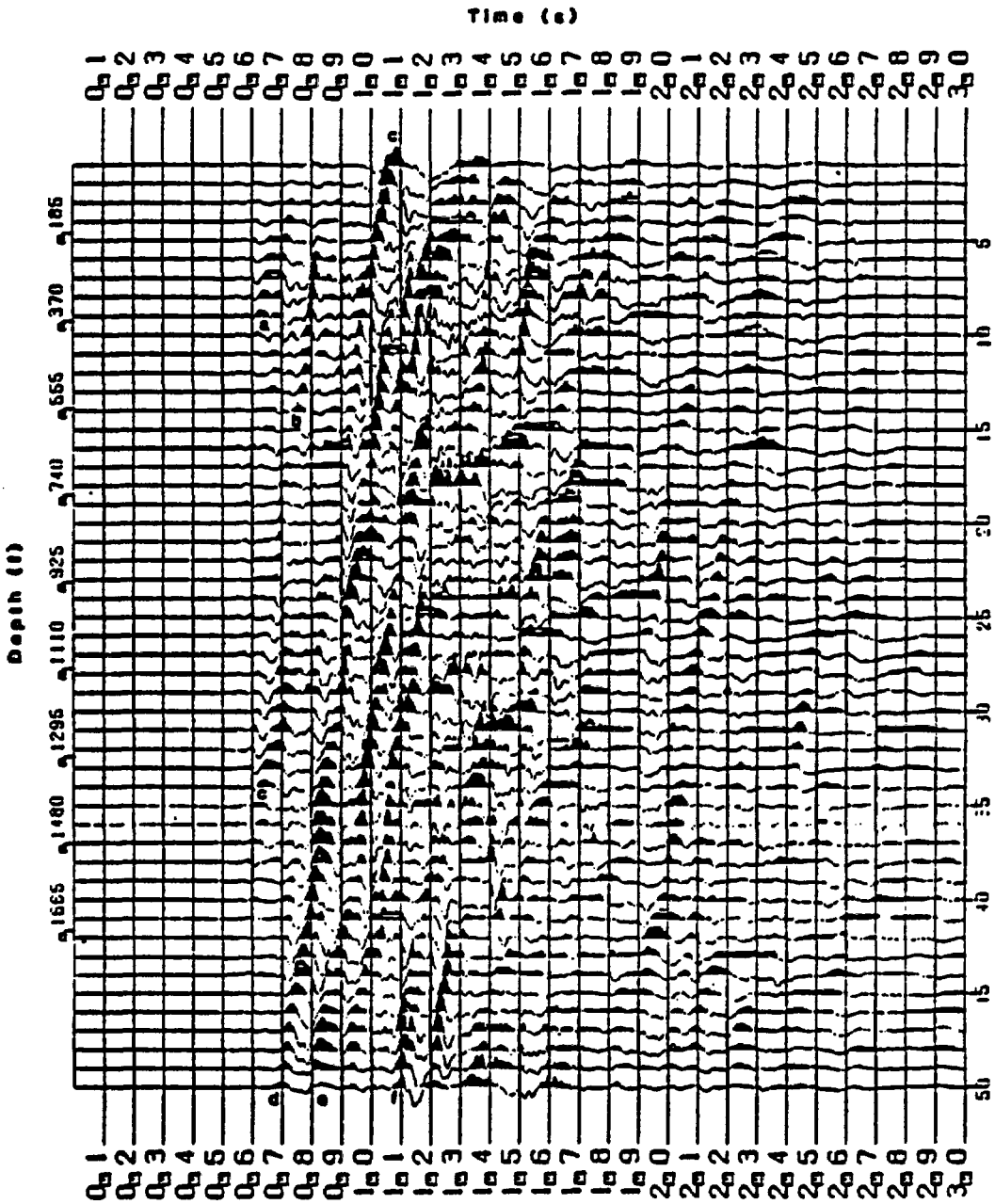

Figure 3.20. VSP data set in Figure 3.19 after applying an FK filter to remove residual downgoing energy. Reflections can be identified from n1(a), n3(d), n4(e), and from the bottom of the model (f). The event labeled (b) is a p-wave reflection from n2, and event (c) is a p-s converted reflection from n2.

to occur on the physical model data sets.

3.6 5000-foot source offset VSP

The source transducer was next positioned 5000 feet from the receiver borehole. Traces were recorded at each of the 50 depth levels. The data set for this profile is shown in Figure 3.21. Two of the three major downgoing events can be identified. The direct p-wave arrival (a) is seen nearly aligned at 0.74 second on each trace. The surface wave (b) can also be identified later on the traces. The direct s-wave is not obvious on the data. It is possible that the direct s-wave is now arriving so nearly perpendicular to the borehole that the V101 transducer can not pick up the motion.

The direct p-wave and the surface wave were removed with an 11-fold median filter. The resulting data set is shown in Figure 3.22. The data were passed through an FK filter in order to enhance the faint upgoing reflections. The data set after applying the FK filter is shown in Figure 3.23.

The event labeled (a) appears to be a reflection from n2. It is difficult to positively identify, but it is certainly possible that this event is a p to s converted reflection from n2. The slope of the event suggests an s-wave, not a p-wave.

The n3 reflection (b) is a strong event on the deeper

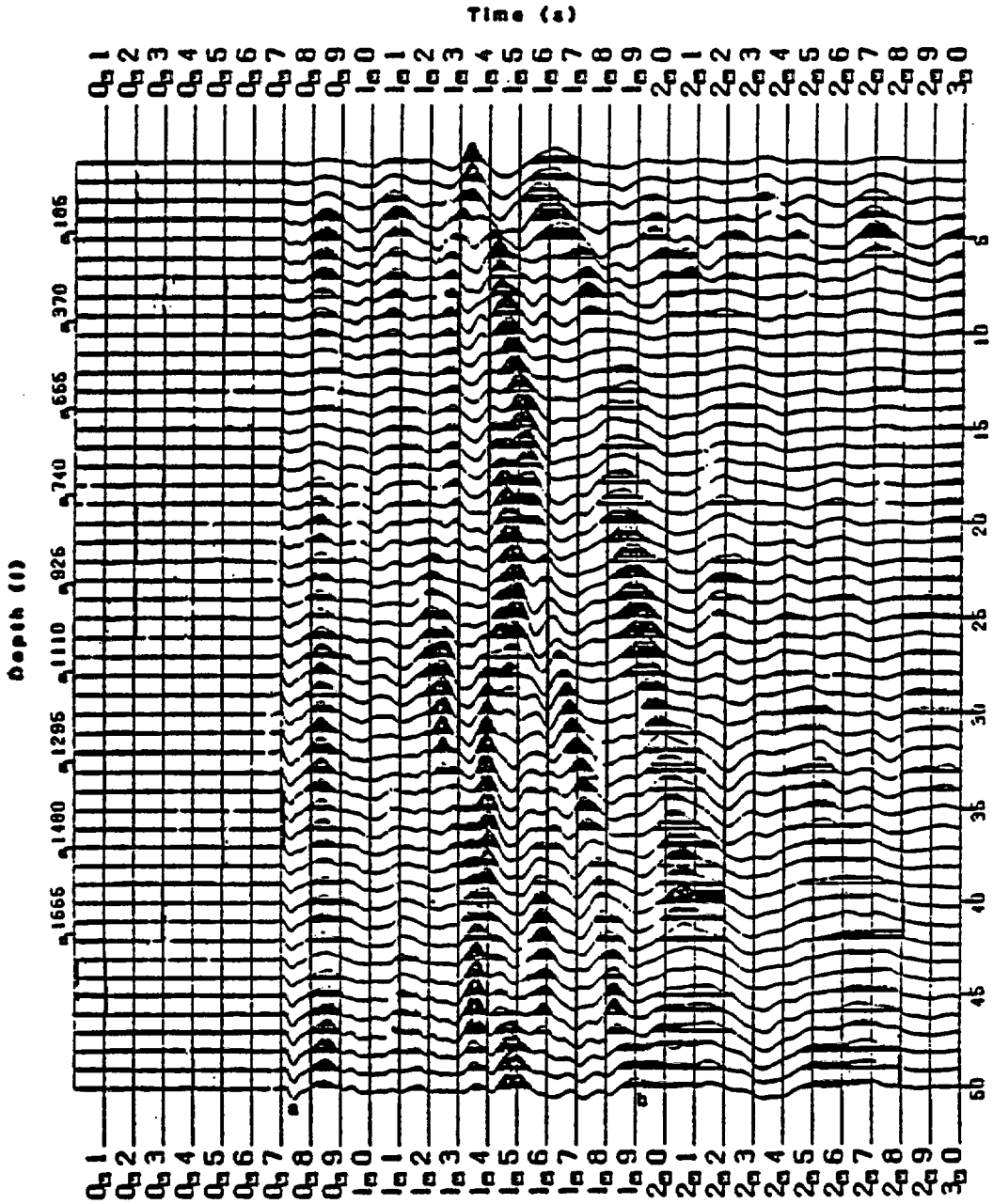

Figure 3.21. VSP data set recorded for 5000-foot source offset. The direct p-wave (a) and the surface wave (b) are clearly seen. The direct s-wave is not obvious on the data set.

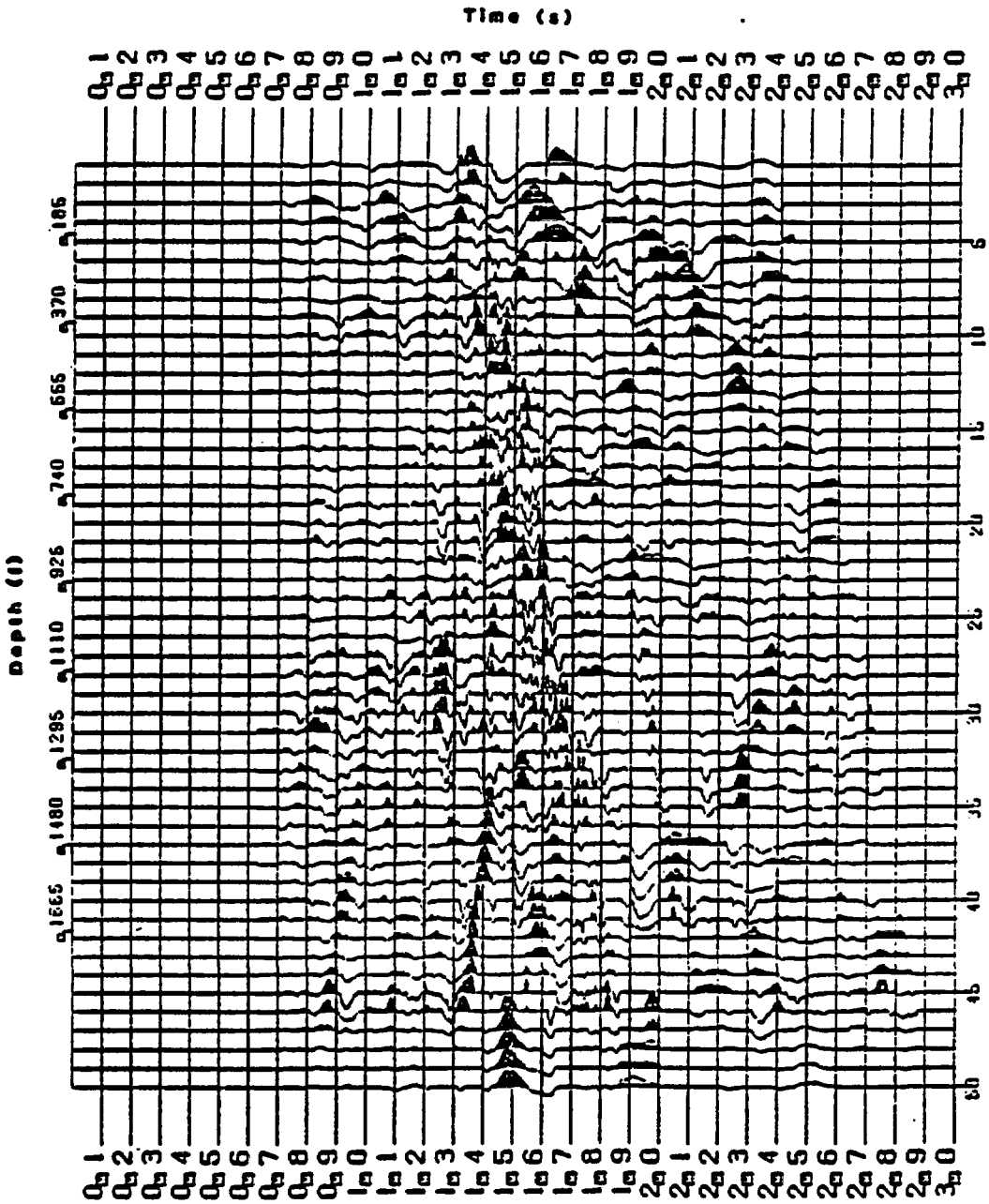

Figure 3.22. VSP data set for 5000-foot source offset after removing the direct p-wave and the surface wave. A few faint upgoing reflections can be seen.

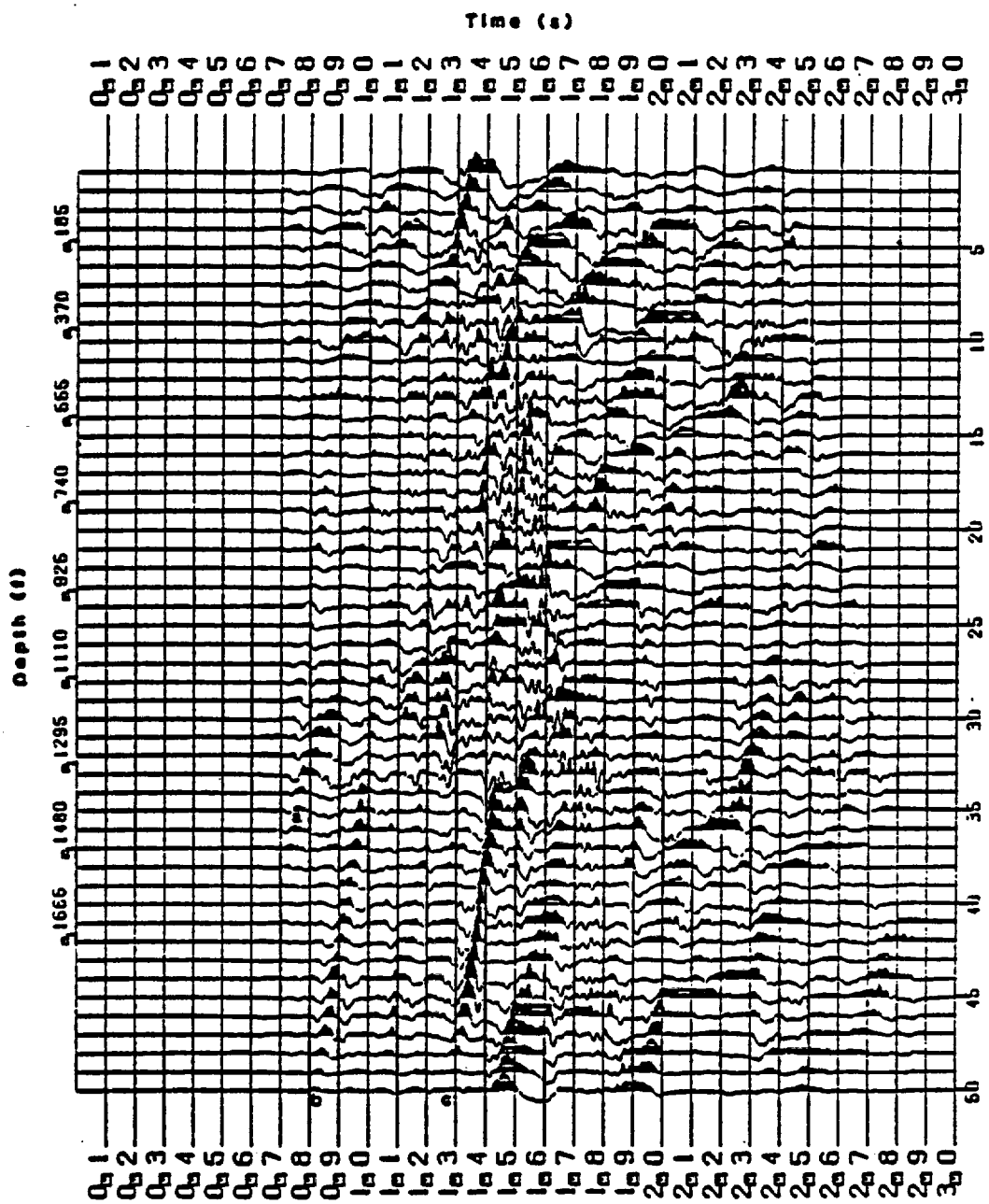

Figure 3.23. VSP data set from Figure 3.22 after applying an FK filter to remove residual downgoing energy. The faint reflection labeled (a) is a reflection from n2, possibly a p-s converted reflection. The n3 reflection (b) is a strong event on the deeper traces. The event labeled (c) is probably a reflection from the bottom of the model.

traces. It is clearly seen on traces 25 through 50. The slope of the event suggests that this is a reflected p-wave. The final event that may be identified with reasonable confidence is the event labeled (c). This event is in the proper position to be a p-wave reflection from the bottom of the model. It is best seen on traces 34 through 48.

3.7 6000-foot source offset VSP

In order to keep the source spacing consistent with the computer models, the V101 source transducer was placed 6000 feet away from the borehole edge of the model. Referring to Figure 2.48, it is seen that a source 6000 feet from the borehole rests on the east side of a dry stream valley. On the physical model, a source transducer positioned at this offset points away from the receiver edge of the model. This caused a substantial decrease in the amplitude of the recorded signal. Fifty traces were recorded for the 6000 foot source offset. The resulting data set is shown in Figure 3.24.

The first arrival trough (a) is difficult to see on the shallow traces. This was completely expected, when the source orientation is taken into account. The event is more prominent on the deeper traces, such as on traces 24 through 50 at 0.875 second. The surface wave (b) can be identified on the record, but it is not as clear as it had been on

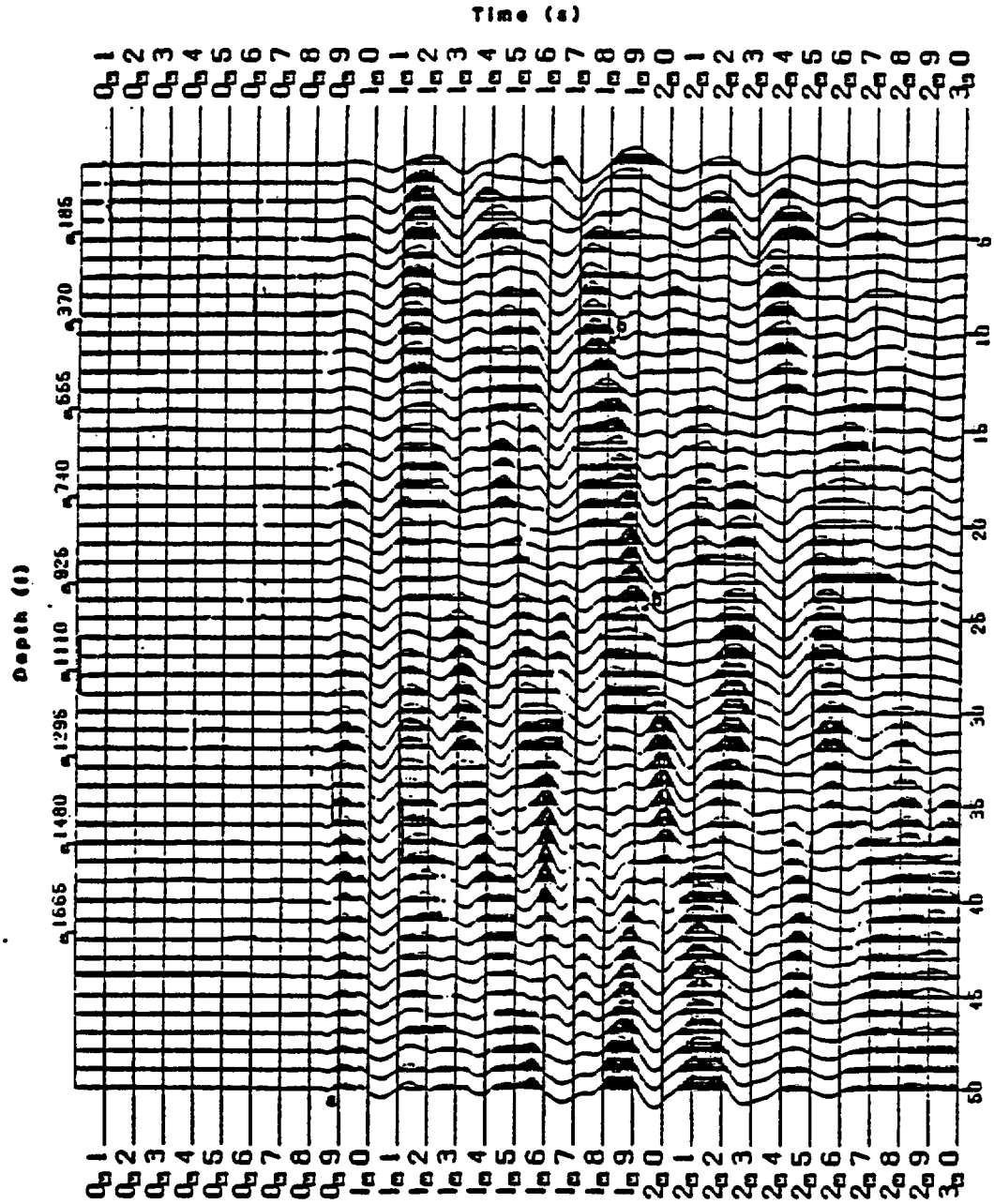

Figure 3.24. VSP data set recorded for 6000-foot source offset. The direct p-wave (a) is difficult to see on the shallow traces, due to the orientation of the source transducer. The surface wave (b) is also difficult to see on certain traces in this record.

previous data sets.

The direct p-wave and surface wave were removed by median filtering. The resulting data set is shown in Figure 3.25. No upgoing events are obvious on this record. An FK filter was applied to the data in order to bring out any coherent upgoing energy that existed on the record. The data set after filtering is shown in Figure 3.26.

Only one event on this data set is identifiable. Event (a) is quite possibly a reflection from the bottom of the model. The arrival time and slope of the event suggest that this is a p to s converted reflection.

The orientation and offset of the source transducer were obviously detrimental to the quality of the traces in this data set. No useful information about the subsurface could be obtained from this record.

3.8 7000-foot source offset VSP

Fifty traces were recorded with the source 6850 feet from the borehole. A stream valley appears 7000 feet from the borehole, and the one inch wide V101 source transducer would not properly rest on the model at this point. Therefore, the source had to be positioned on the west bank of the small valley.

The data set recorded for this source offset appears in Figure 3.27. The first arrival (a) appears aligned along

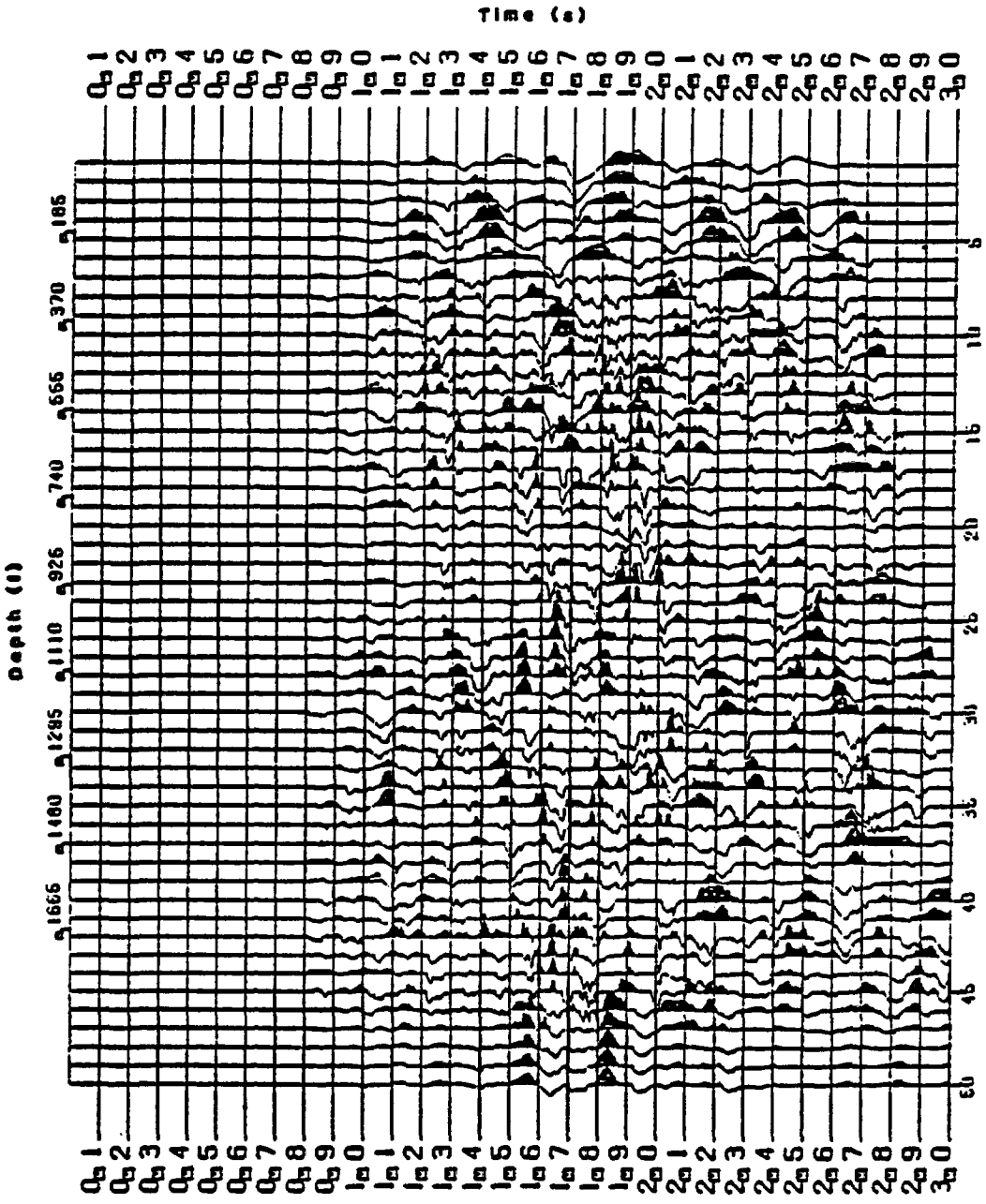

Figure 3.25. VSP data set for 6000-foot source offset after removing the direct p-wave and the surface wave. No up-going events are obvious on this record.

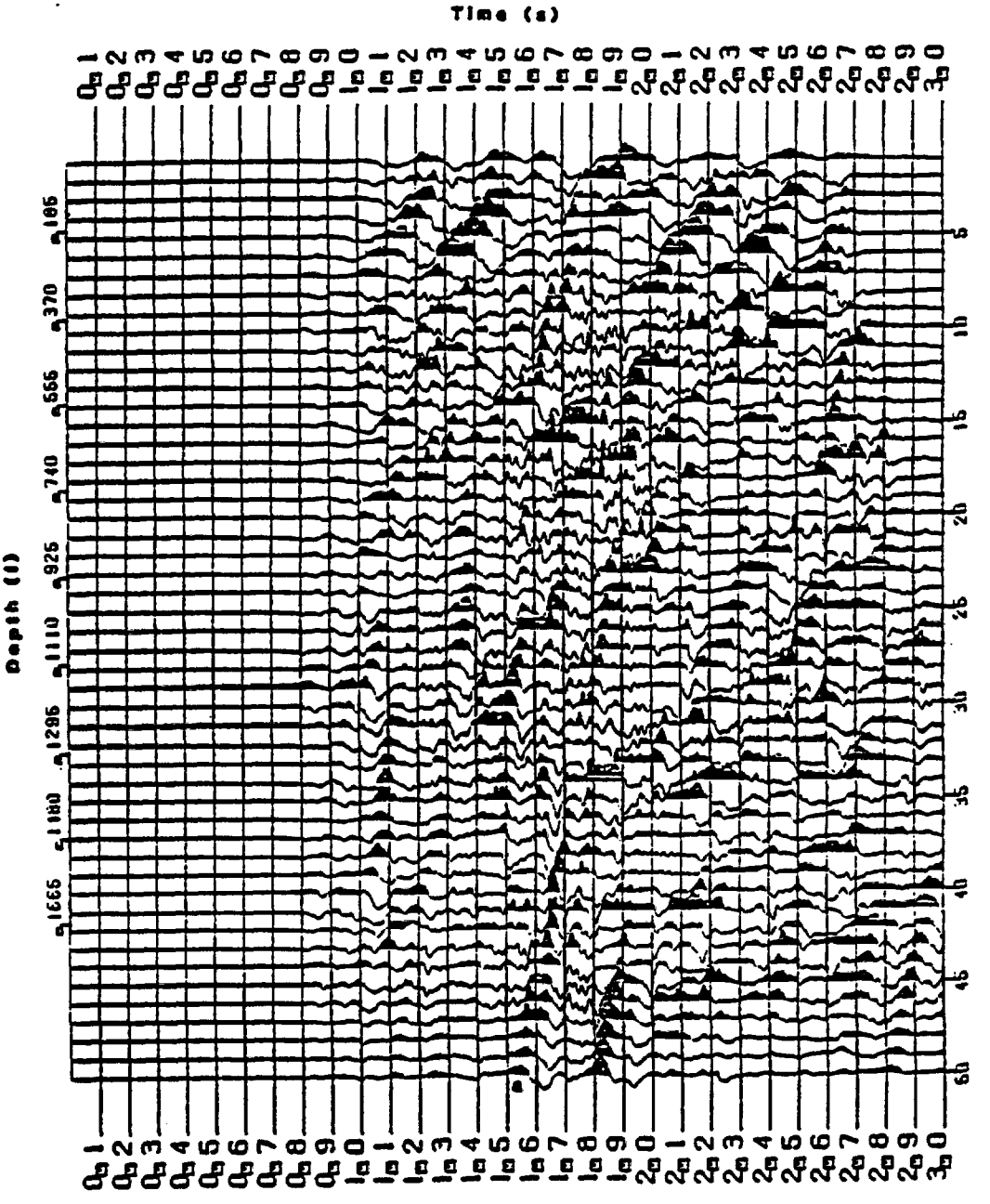

Figure 3.26. VSP data set from Figure 3.25 after applying an FK filter to remove residual downgoing energy. Event (a) may be a reflection from the bottom of the model, possibly a p to s converted reflection. The orientation and offset of the source transducer were very detrimental to the quality of this data set.

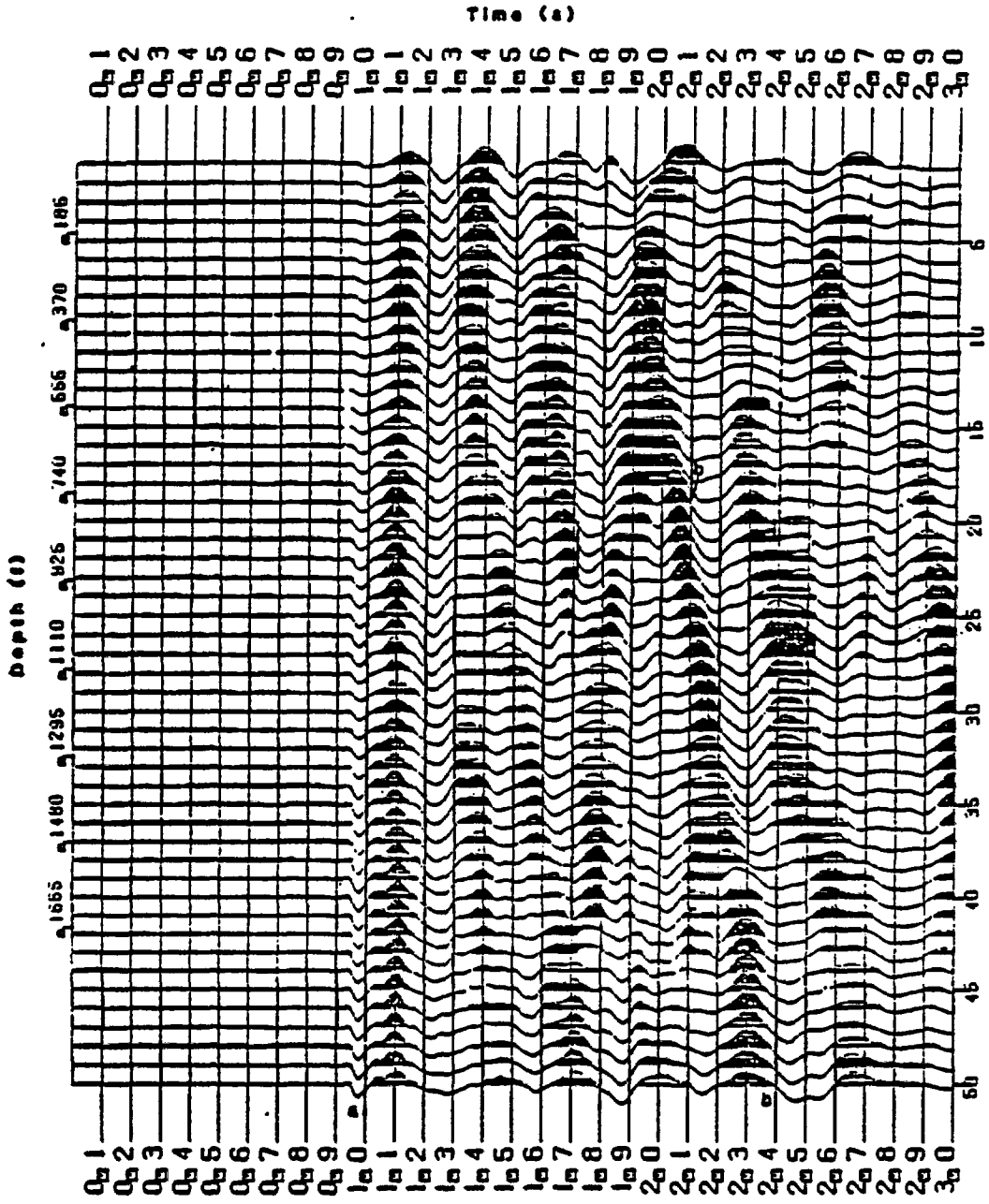

Figure 3.27. VSP data set recorded for 7000-foot source offset. The direct p-wave (a) and the surface wave (b) can both be identified on this record.

the 1.0 second time line. At this offset, the first arrivals actually appear earlier on the deeper traces than on the shallower traces. The surface wave (b) is slightly more difficult to identify on this data set than on previous data sets.

At this offset, any upgoing reflections would have very steep slopes. This suggests that using a higher fold median filter to separate wavefields would be in order. Figure 3.28 shows the data after applying an 11-fold median filter to remove the direct p-wave. The event labeled (a) is an upgoing reflection which is fairly coherent. A 15-fold median filter was then applied to the original data set to remove the direct p-wave. The resulting data set is shown in Figure 3.29. The upgoing event (a) is slightly more coherent on traces 35 through 50 than on the same traces in Figure 3.28. Since the reflection quality was better with the higher fold filter, the 15-fold filter was used for both the 7000-foot and 8000-foot source offset data sets.

The surface wave was removed with a 15-fold median filter as well, and the resulting data set is shown in Figure 3.30. It is very difficult to identify the reflected events. An FK filter was applied to the data to enhance the upgoing energy. The resulting data set is shown in Figure 3.31.

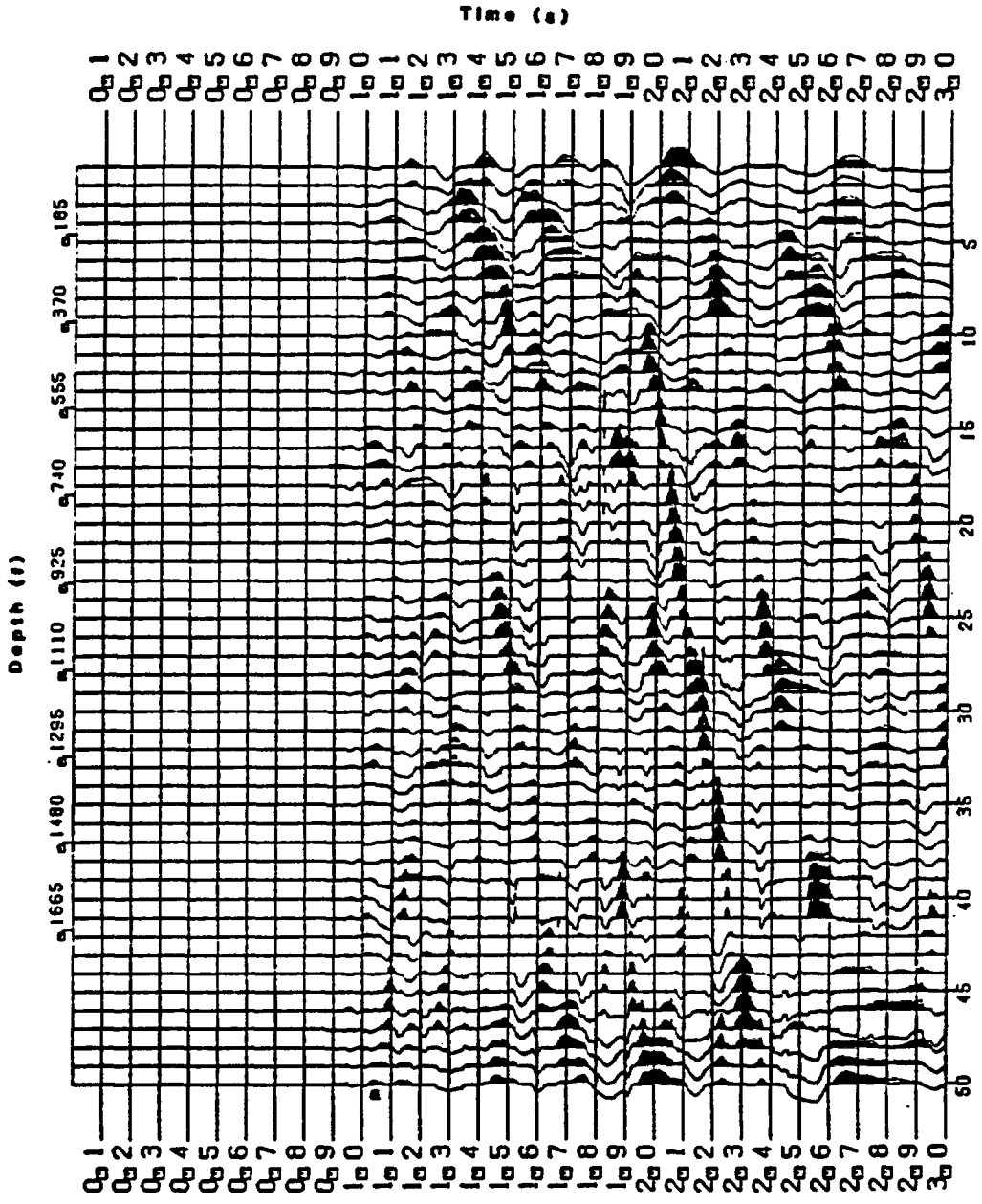

Figure 3.28. VSP data set for 7000-foot source offset after using an 11-fold median filter to remove the direct p-wave. An event labeled (a) can be seen on traces 36 through 50.

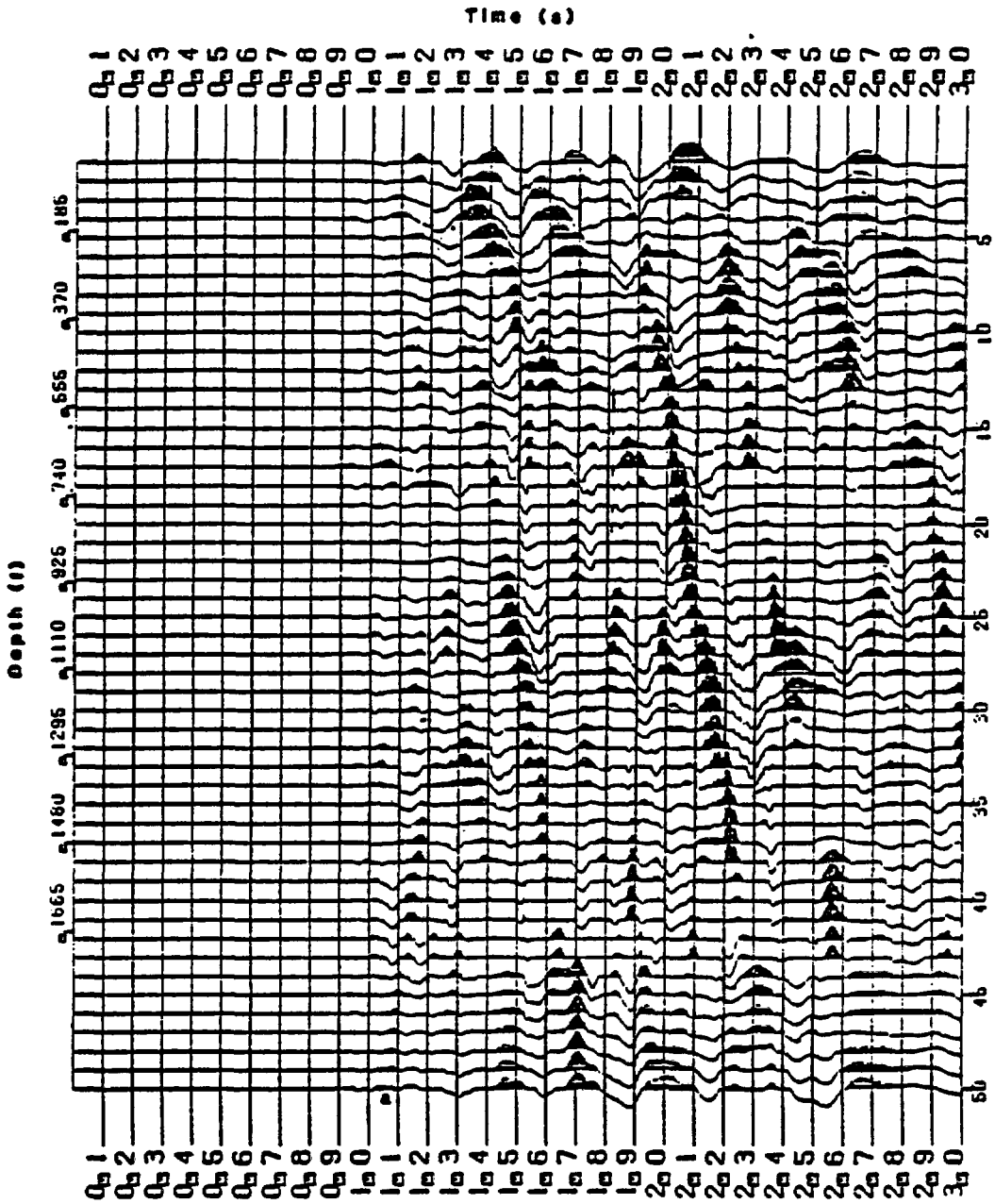

Figure 3.29. VSP data set for 7000-foot source offset after using a 15-fold median filter to remove the direct p-wave. The event labeled (a) is slightly more coherent and visible on traces 35 through 50 than it was in Figure 3.28. Since reflection quality was improved by using the higher fold filter, a 15-fold filter was used for the 7000-foot and 8000-foot source offset data sets.

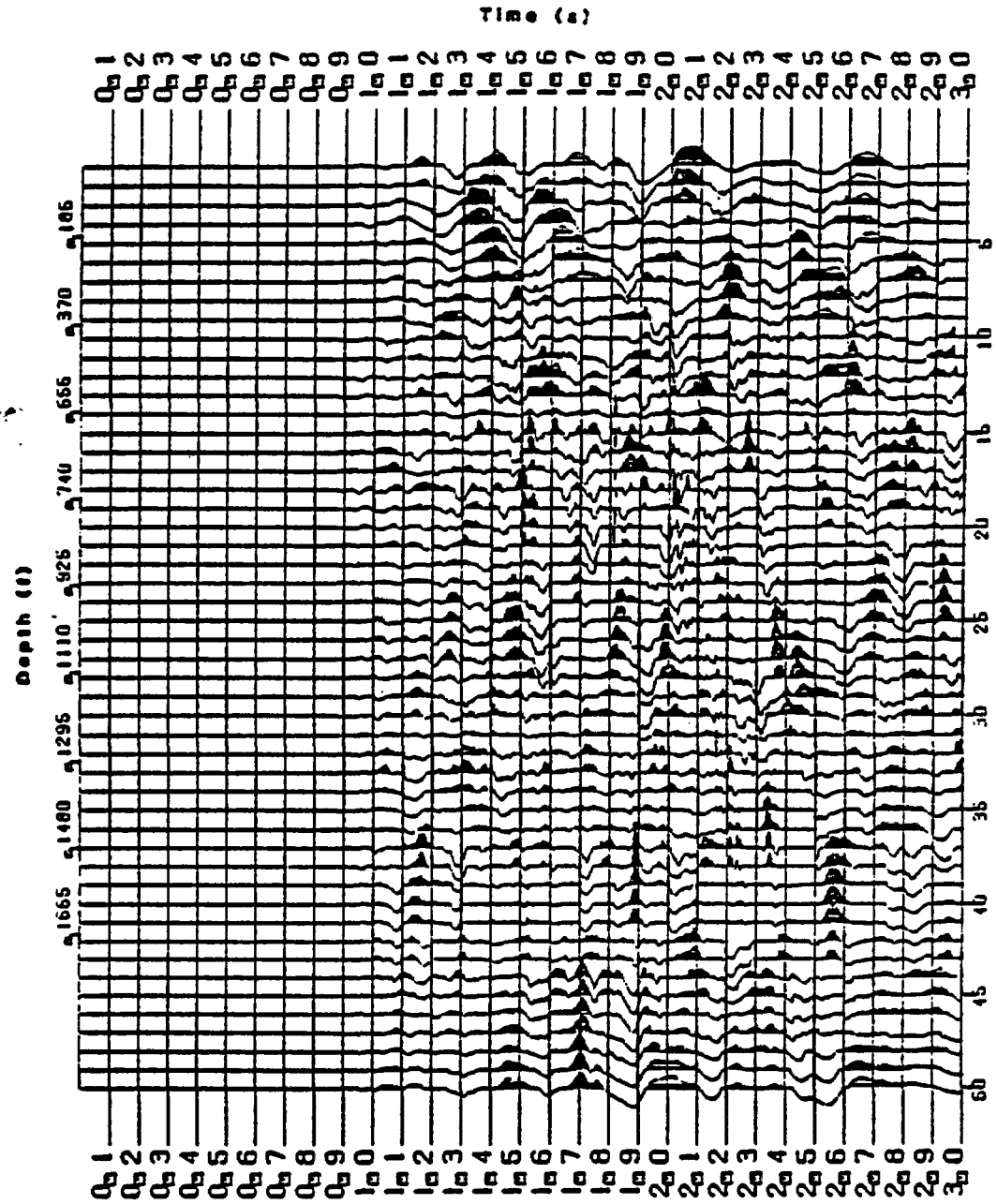

Figure 3.30. VSP data set for 7000-foot source offset after removing the direct p-wave and the surface wave with 15-fold median filters. Upgoing reflections are very difficult to identify.

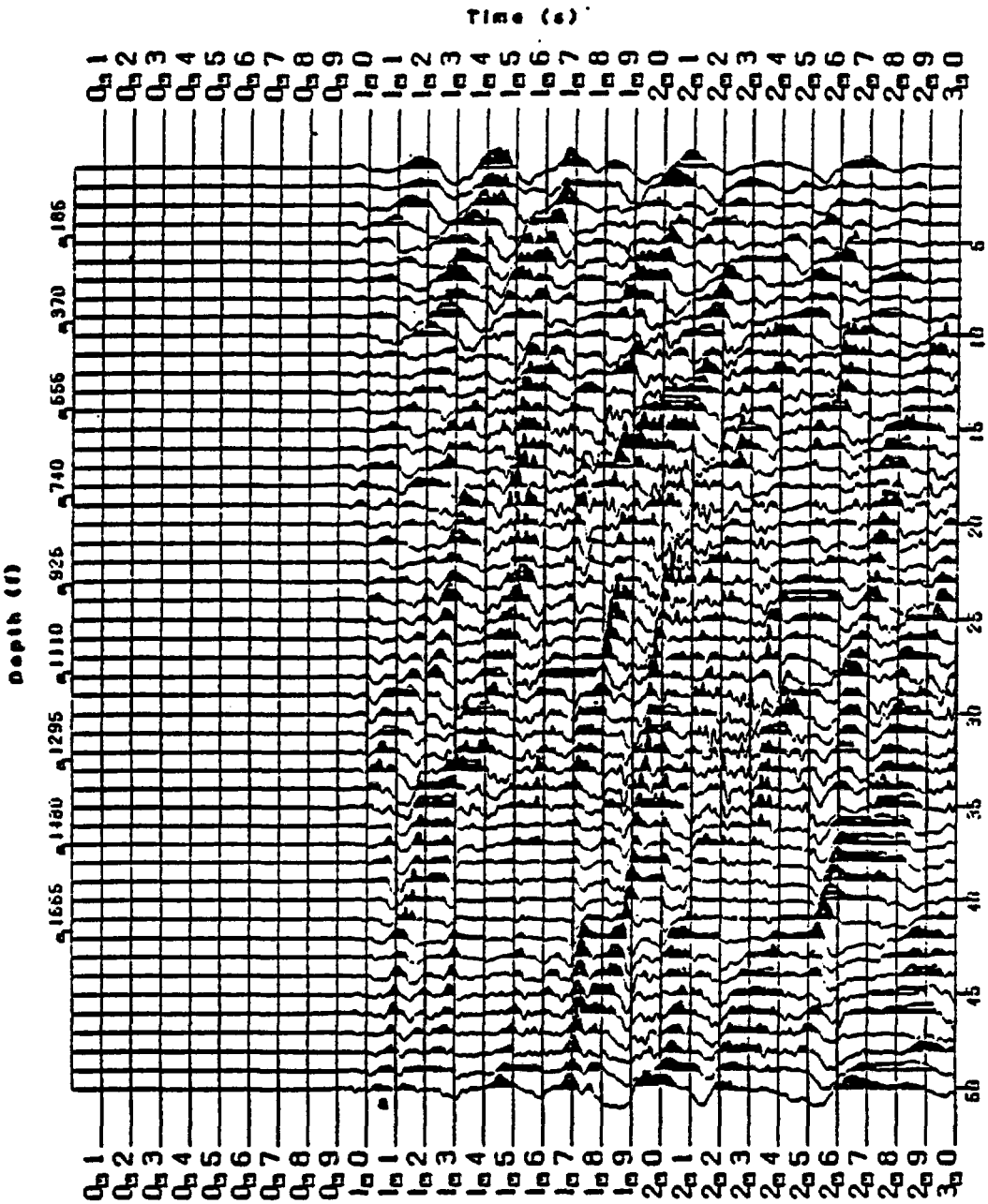

Figure 3.31. VSP data set from Figure 3.30 after applying an FK filter to remove residual downgoing energy. The event labeled (a) may be a reflection from n3, or possibly a reflection from the bottom of the model. It is difficult to make a positive identification at this offset.

The reflected event (a) may be a reflection from the n3 horizon. At this offset, positive identification is difficult. Event (a) can be seen on traces 19 through 29 and again on traces 34 through 50. It is also possible that this event is a p-wave reflection from the bottom of the model, although its arrival time is slightly early for a bottom reflection.

3.9 8000-foot source offset VSP

The final data set recorded for the uniform velocity, variable thickness model was taken with a source offset of 8000 feet. The fifty traces are shown in Figure 3.32. The direct arrival (a) can be identified on every trace at 1.15 seconds. The only other identifiable event is the surface wave (b).

The direct p-wave and the surface wave were removed from the data set using a 15-fold median filter. The resulting data set is shown in Figure 3.33. Very little upgoing energy can be seen in this diagram. An FK filter was applied to the record to try to enhance the reflected events. The data set after filtering is shown in Figure 3.34.

At this great offset, interpretation is difficult, even on the computer generated data sets in the preceding chapter. Only one upgoing reflection is strong enough to warrant an attempted interpretation. Reflection (a) may be a

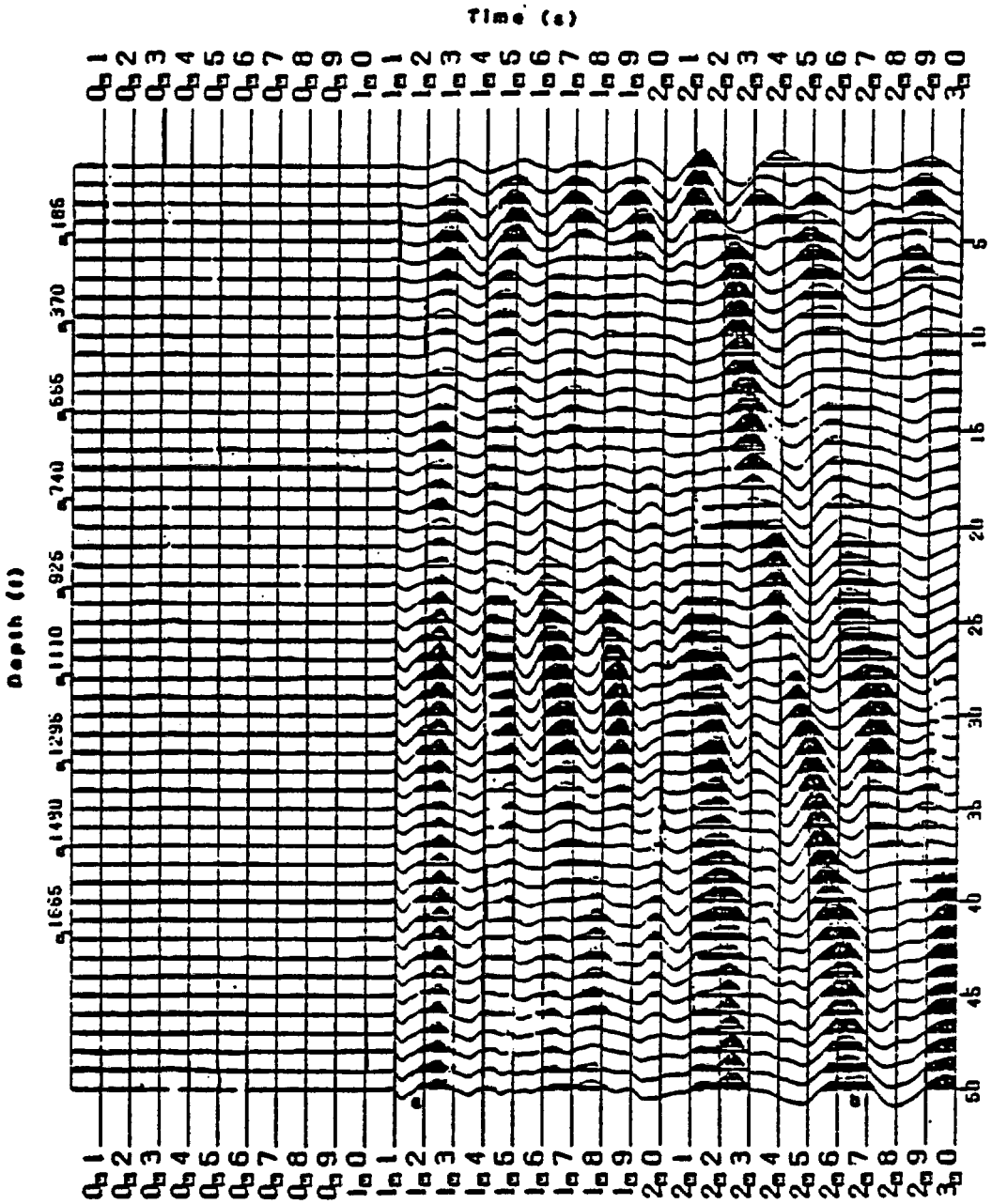

Figure 3.32. VSP data set recorded for 8000-foot source offset. The direct p-wave (a) and the surface wave (b) are clearly seen.

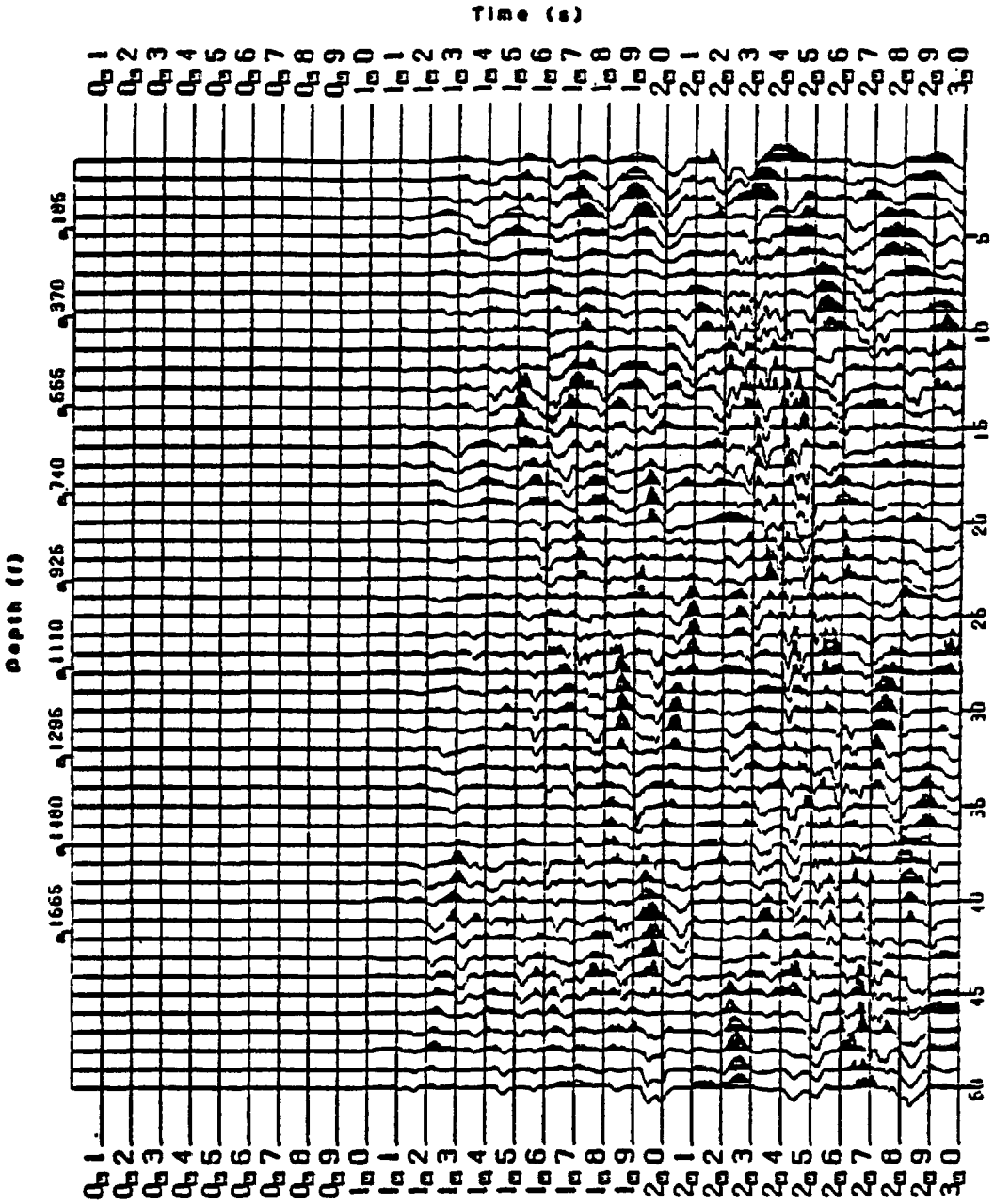

Figure 3.33. VSP data set for 8000-foot source offset after removing the direct p-wave and the surface wave. Very little upgoing energy can be seen on the record.

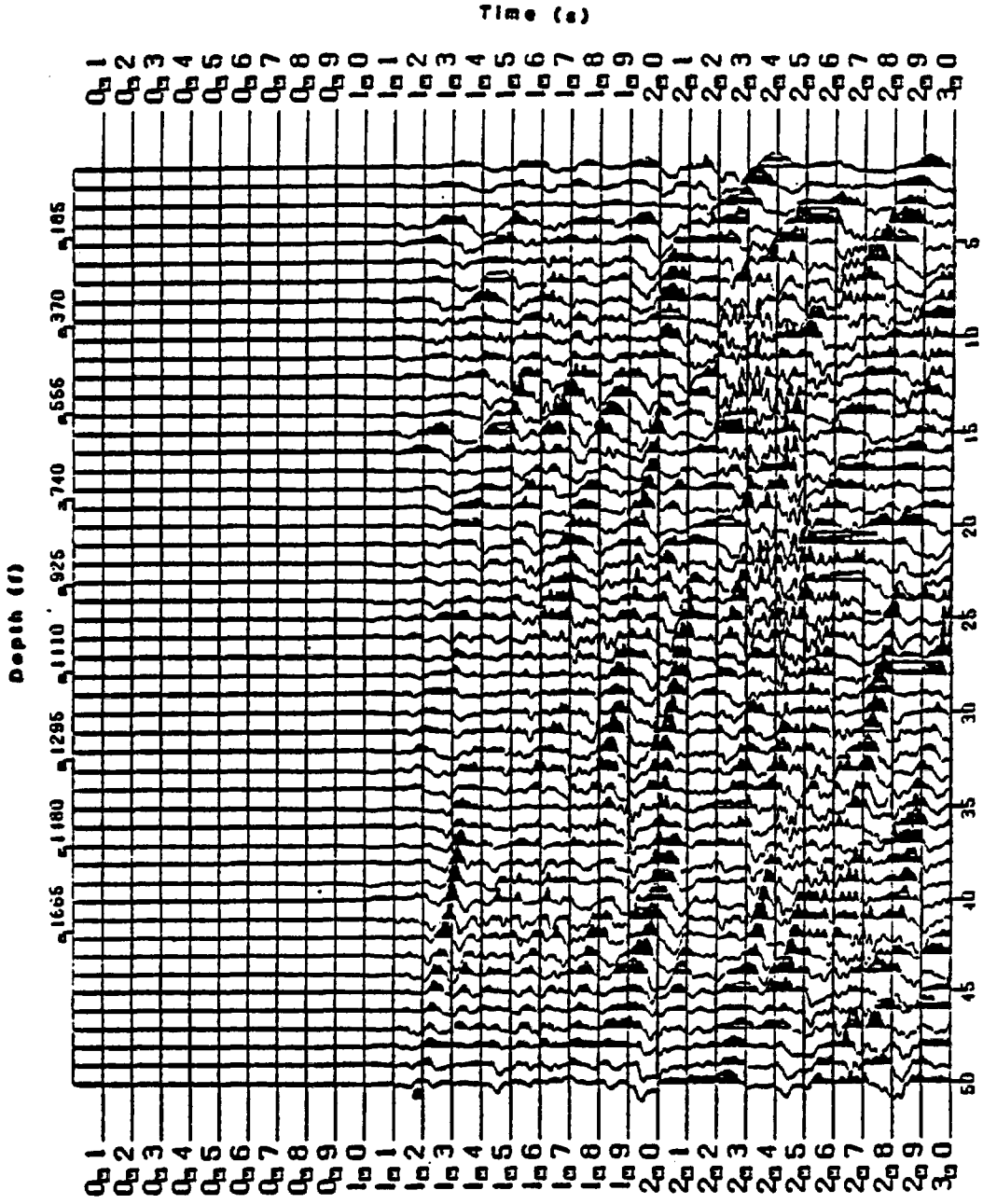

Figure 3.34. VSP data set from Figure 3.33 after applying an FK filter to remove residual downgoing energy. The event labeled (a) may be a reflection from n3 or a reflection from the bottom of the model. Positive identification is difficult.

p-wave reflection from n3. It can be seen on traces 32 through 50. It is also possible that this is a reflection from the bottom of the model. Positive identification is impossible on this record.

3.10 Conclusions

The results in Chapter 3 indicate that the system used to generate and record synthetic VSP records functioned very well and that it is possible to model VSP surveys at Yucca Mountain with a physical model.

A major objective at Yucca Mountain is to delineate the repository unit. The reflections from n1, Tptw, and n2 are the most important events on the records, since these horizons are in the unsaturated zone. A reflection which is identified as an n1 reflection is seen on data sets with source offsets as great as 4000 feet. Beyond 4000 feet, the effect of topography keeps the n1 horizon from being imaged.

The reflection from n2 can be identified on data sets with source offsets as great as 5000 feet. Beyond 5000 feet, the event can not be identified.

The most consistent event from record to record is the reflection from n3. It can be identified on data sets with source offsets as great as 5000 feet, and may even be visible on the 7000-foot and 8000-foot source offset data sets. Although the delineation of this horizon is not as critical

as the delineation of horizons in the unsaturated zone, it is encouraging that some of the deeper horizons are identifiable on the VSP records.

The uniform velocity physical model did not contain any fault planes which could be imaged, other than the small stair-steps in the welded units. No indication of a reflection from these small segments was seen on any of the data sets.

The quality of the data sets in Chapter 3 was very encouraging, since the 200-20,000 hz bandpass filter was in the recording system. Even though a large amount of high frequency signal was lost during the recording process, the resolution of the reflections was still quite good. Many events could clearly be identified, and the close correspondence with the computer models confirmed that the interpretations were sound.

The data sets contained a large amount of upgoing shear wave energy. These events can also provide a great deal of information about the subsurface and will be discussed again in Chapter 5.

Chapter 4

PHYSICAL VSP MODELING PART II

4.1 Introduction

The physical VSP modeling in Chapter 3 was conducted using a model composed of PLEXIGLAS. Although the thickness of the model varied, seismic velocity was uniform throughout. A second model of the Yucca Mountain cross section between boreholes UZ-6 and UZ-9 was created using two materials with different seismic velocities.

The first material was once again 1/4 inch thick PLEXIGLAS G acrylic sheet. The p-wave velocity was stated earlier to be 7600 feet/second. The second material used was 1/4 inch thick LEXAN sheet, a polycarbonate which has many applications in the bullet-proofing industry. Several factors made LEXAN the material chosen for the model. First, the LEXAN has a p-wave velocity of 5250 feet/second (determined experimentally). This provided a velocity contrast with the PLEXIGLAS, but not an extreme contrast. Second, the material was relatively inexpensive ($150 for a 4 feet by 8 feet sheet). Third, creating a model from two plastics was easier than creating a model from a plastic and a metal, for example. Aluminum sheet was considered as a possibility for the model, but many factors ruled against it. Cost, weight, and the high p-wave velocity (approximately 20,000

feet/second) all made aluminum a poor choice.

Figure 4.1 shows the model created from the two materials. White areas of the model were made from the higher velocity PLEXIGLAS and represent the welded units in the section. Shaded areas of the model were made from the lower velocity LEXAN and represent the non-welded units. While the first model had uniform velocity and variable thickness, this model had variable velocity and uniform thickness.

Creation of the model began by cutting 4 feet long strips of the materials to represent the volcanic units. For example, the n1 unit is 80 feet thick. Since the model has a scale of 1:1000, a sheet of LEXAN was cut into a rectangle 4 feet long and 15/16 inch wide. The PLEXIGLAS strip representing Tptw (870 feet thick) was cut into a rectangle 4 feet long and 10 7/16 inches wide.

The seven 4 feet long strips were cemented together side by side in sequence to form a rectangular cross section of Yucca Mountain. An industrial acrylic cement, IPS WELD-ON 40, was used to hold the pieces together. Three of these 4 feet long cross sections were completed before moving ahead in the creation of the model.

After the cement had hardened sufficiently (24 hours), faults were cut across the rectangular sheets that represented the nine high-angle faults in the cross section. The proper offset along each fault was calculated and the

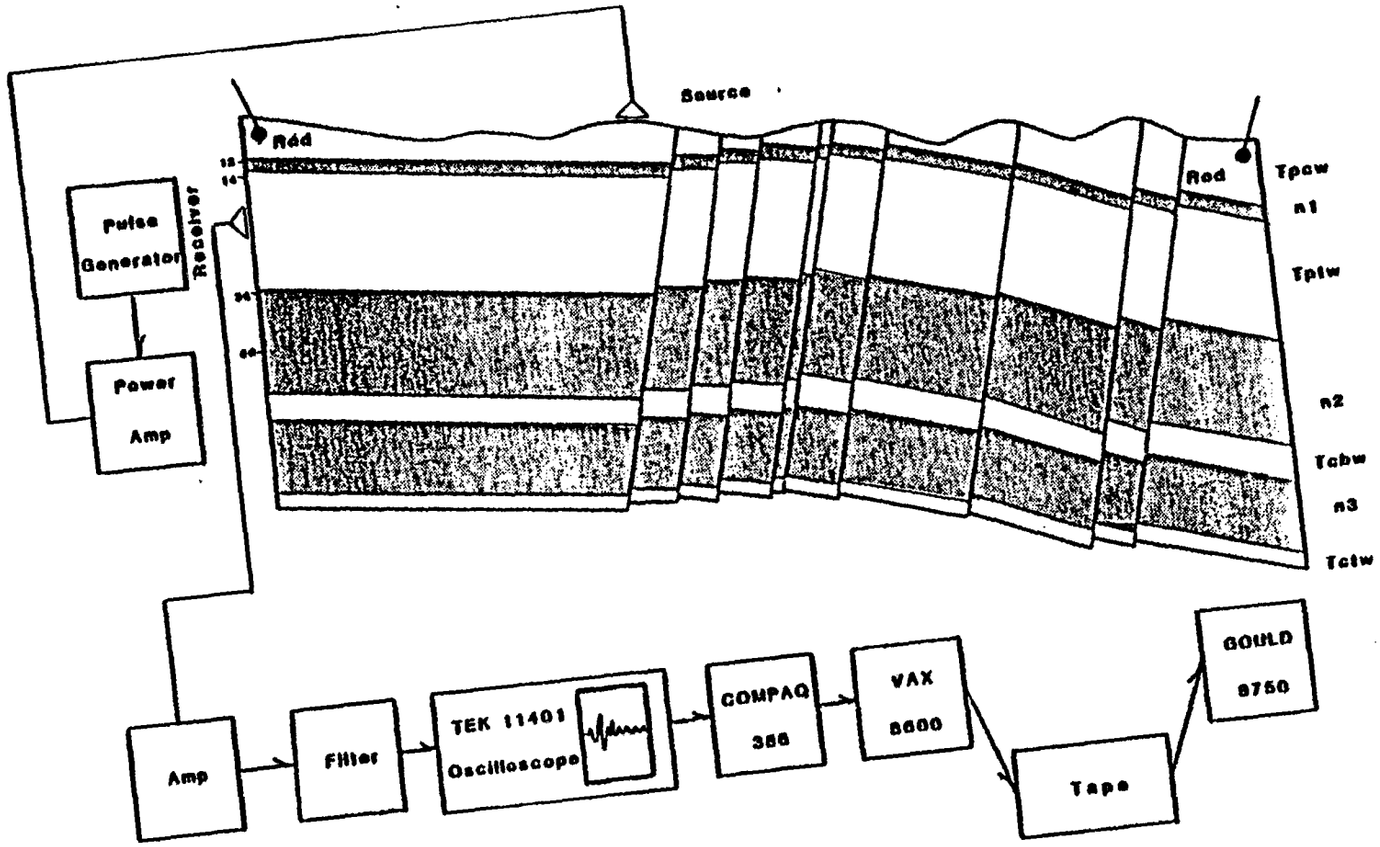

Figure 4.1. Schematic diagram showing the recording system and the physical model used for the variable velocity VSP experiments. White areas of the model are made from PLEXIGLAS and represent welded units. Shaded areas of the model are made from LEXAN and represent non-welded units.

pieces were cemented back together using the industrial cement. Since several of the fault blocks in the cross section had been rotated, it was necessary to maintain proper dip on each fault block in the model. Instead of cutting the fault on the rectangular sheet and cementing the two pieces back together again with a small offset, it was often necessary to cut a pie-shaped section off one of the pieces. When the two pieces were cemented back together again, horizons on each fault block had the proper dip. Since the faults in this modeling experiment all have an identical dip of 75 degrees but several of the fault blocks have different dips, it was necessary to solve the obvious space problem by shaving off small sections of some of the fault blocks.

Once the entire model had hardened, the surface topography was cut along the top of the model with a hand held saw. Threaded rods were later inserted through the top corners of the model to serve as hanging posts. Cotton rope was used to suspend the model from the redwood frame. Distance scales were painted along the surface and down the borehole edge of the model to assist with the placement of the transducers.

This model differs from the uniform velocity model in many ways. The model in Chapter 3 had a flat bottom surface while this model stops at the bottom of the Tctw unit. As previously mentioned, this model consists of two materials

with different seismic velocities. Also, the model actually contains fault planes (cemented together), while the uniform velocity model contained only offset horizons. The faults in this model may be a good representation of the faults at Yucca Mountain. In the model, a thin layer of cement holds the horizons across the fault together. In most cases, the horizons across the faults are the same material. The situation at Yucca Mountain is similar. As noted earlier, it is possible that mineralization has occurred along the fault planes, and the planes may act as reflecting horizons. The faults in the model could provide a system for testing how well fault planes can provide reflections.

Two configurations for the recording system were used for the variable velocity model, the second of which will be discussed in Section 4.10. The first configuration is shown in Figure 4.1 The sequence of components is identical to the recording sequence in Figure 3.1 The signal begins in the pulse generator and is passed to the power amplifier. The power amp drives the V101 source transducer, which is placed at various offsets from the left edge of the model.

Another V101 transducer acts as the borehole geophone and is coupled to the left edge of the model. Output from the transducer is passed through a gain amplifier. At this point, the recording system in Figure 4.1 differs from the system in Figure 3.1. The filter used in Chapter 3 was a

200-20,000 hz bandpass filter which severely limited the quality of the data. The filter in Figure 4.1 is a 50,000-1,600,000 hz bandpass filter designed by Kurt Ranzinger. This filter allowed the signal to be recorded without interference from the 60 hz noise and without cutting out the high freqencies.

Output from the filter is displayed by the TEK11401 oscilloscope. The waveform is transferred to the COMPAQ 386 by the GURU software package. As before, the waveforms are then transferred to the VAX 8600 mainframe. The data are converted to SEGY format shot records and written to magnetic tape. The traces are read from tape by VSEIS on the GOULD 9750, and additional VSP processing on the records is carried out.

The following parameters were used to record the traces for each of the eight source offsets:

Table 4.1 Recording Parameters

SAMPLE INTERVAL	:	400 nanoseconds
SAMPLES/TRACE	:	5120
STACKING FOLD	:	128
PULSE FREQUENCY	:	30 milliseconds
PULSE DURATION	:	20 microseconds

4.2 1000-foot source offset VSP

The first set of fifty traces was recorded for a source offset of 1000 feet. The resulting data set is shown in Figure 4.2 The amplitude of the signal output from the bandpass filter was very low and the vertical resolution of the oscilloscope had to be maximized during the recording of the data. For this reason, the noise level of the data sets will continue to grow as source offset increases. In Figure 4.2, the direct p-wave (a) is seen to dominate the record.

Several features of the direct p-wave are interesting. The p-wave travels through PLEXIGLAS to reach the receiver transducer at depth levels 1 through 11. The character of the direct p-wave is very consistent on these traces. The receiver is coupled to the LEXAN strip representing n1 at depth levels 12 and 13, however. The amplitude of the direct p-wave drops off slightly at these depth levels. This phenomenon is labeled (1) on the data set.

The receiver is coupled to PLEXIGLAS at depth levels 14 through 35, and the character of the direct p-wave is very consistent once again. At depth level 36, the receiver is coupled to LEXAN which represents the n2 horizon. The character of the direct p-wave is consistent on traces 36 through 50, but different from the direct p-wave on traces 14 through 35. More noticeable is the change in slope of the direct p-wave at trace 36, labeled (2). The lower

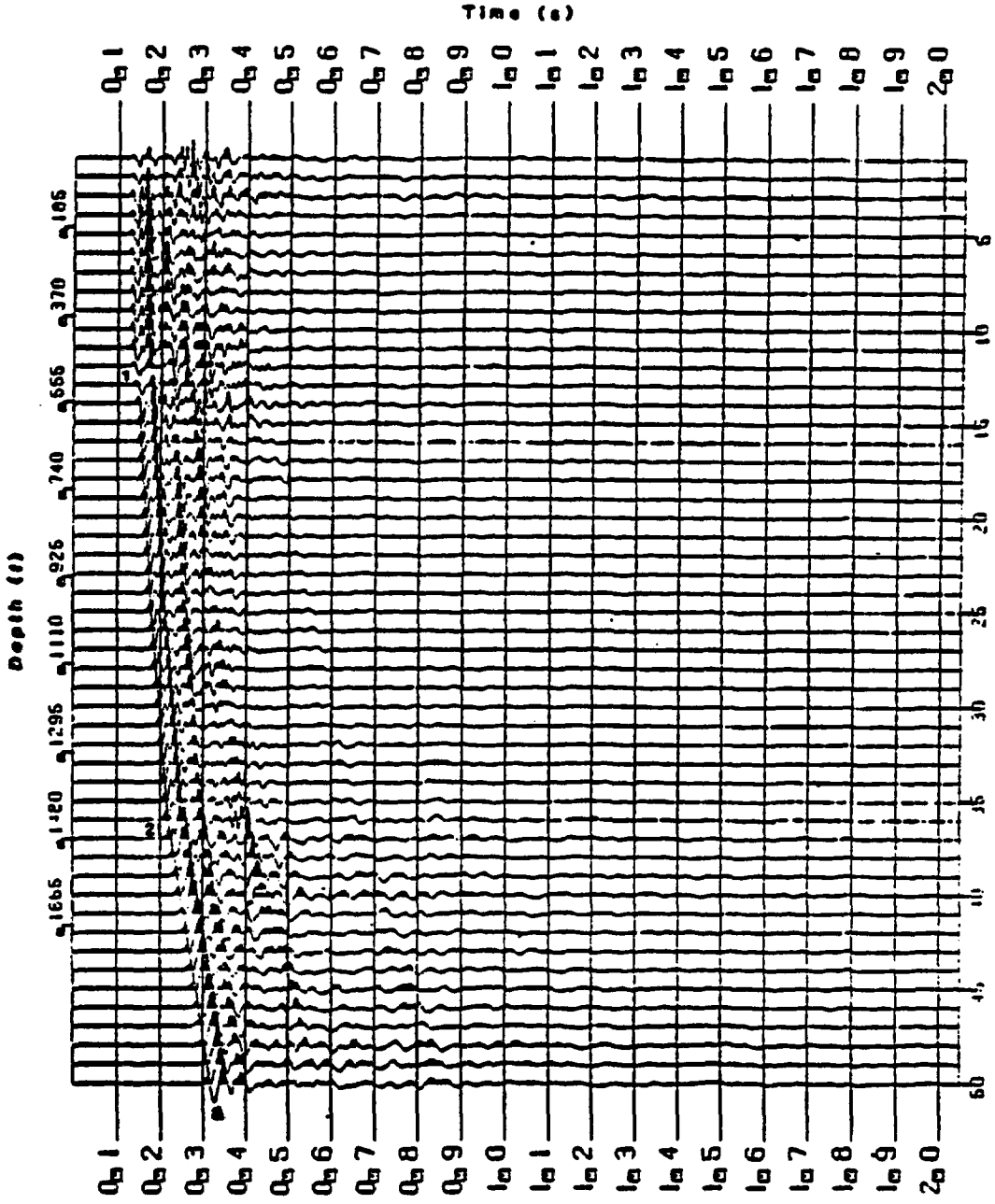

Figure 4.2. Data set recorded for a source offset of 1000 feet. The direct p-wave (a) dominates the data set. At traces 12 and 13, the receiver is coupled to LEXAN and the amplitude of the p-wave decreases noticeably (1). Also, when the p-wave enters the n2 horizon at trace 36 (2), the slope of the event changes dramatically indicating that it has entered a lower velocity medium.

velocity of the LEXAN causes this obvious change in slope of the direct p-wave.

This data set was median filtered to remove both the direct p-wave and the direct s-wave. The median filtering module in VSEIS can only accomodate 4000 samples per trace, which presented a problem on this data since it contains 5120 samples per trace. By carefully aligning unwanted events along early time lines, it was possible to remove the unwanted events and still preserve most of the important reflection energy on the 4000 sample long traces output by the median filtering module. Before shifting the filtered record back to its proper time position, the traces had to be padded with zeros to extend the length of the traces back to 5120 samples. The traces could then be shifted back to their proper time position without losing events off the trailing ends of the traces. The resulting data set is shown in Figure 4.3.

The data appear very noisy in Figure 4.3. Median filtering did not do a thorough job of removing the direct arrivals. In order to improve the appearance of the data, a zero-phase, low pass filter was applied. The high-cut half amplitude point was 100 hz with a roll-off slope of 12 db/octave (100/12). The data set, after application of the filter, is shown in Figure 4.4. It is still very difficult to identify any upgoing reflections. The reflection labeled

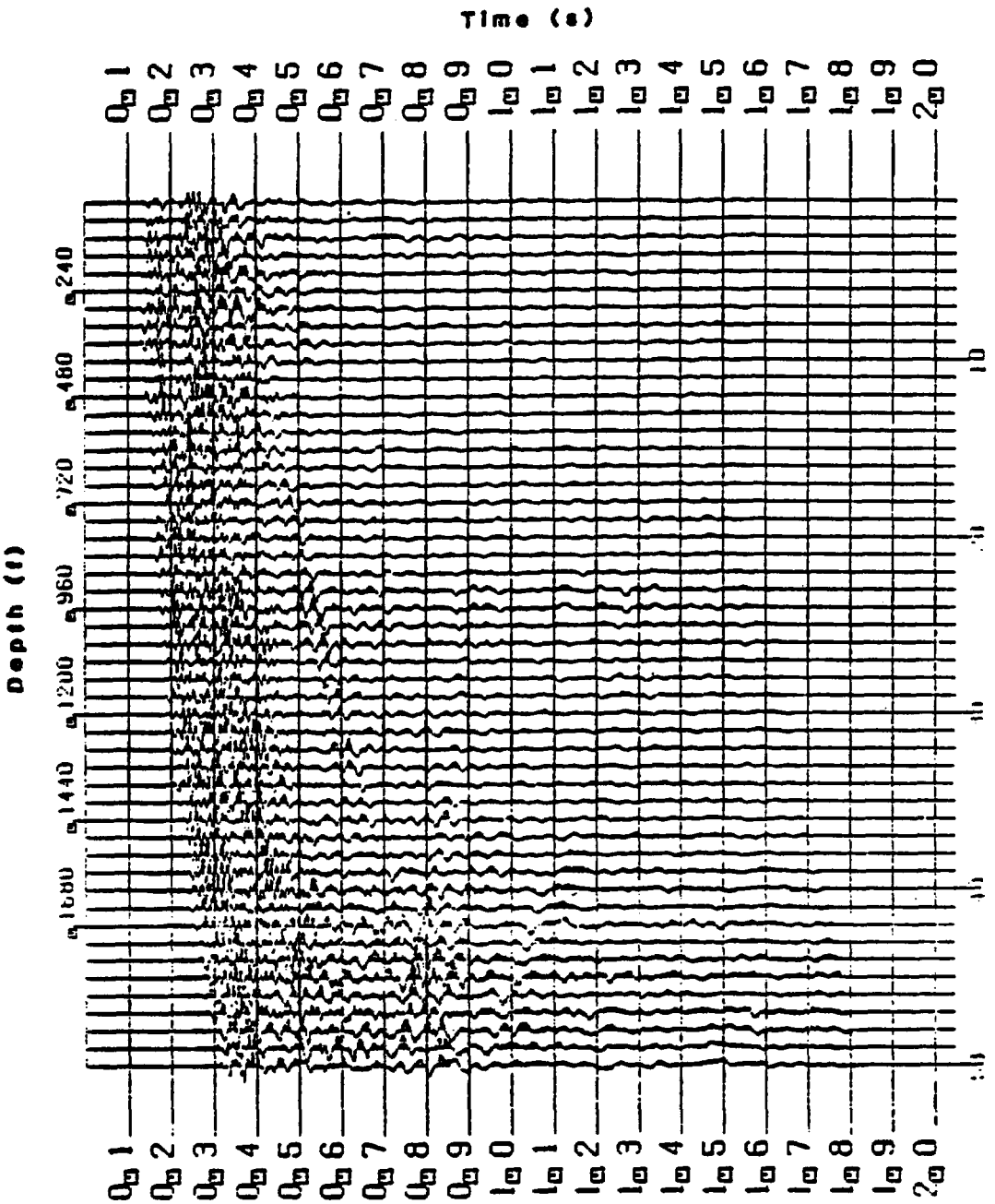

Figure 4.3. Data set in Figure 4.2 after removal of the direct p-wave and the direct s-wave. The data set is very noisy and no upgoing reflections can be identified.

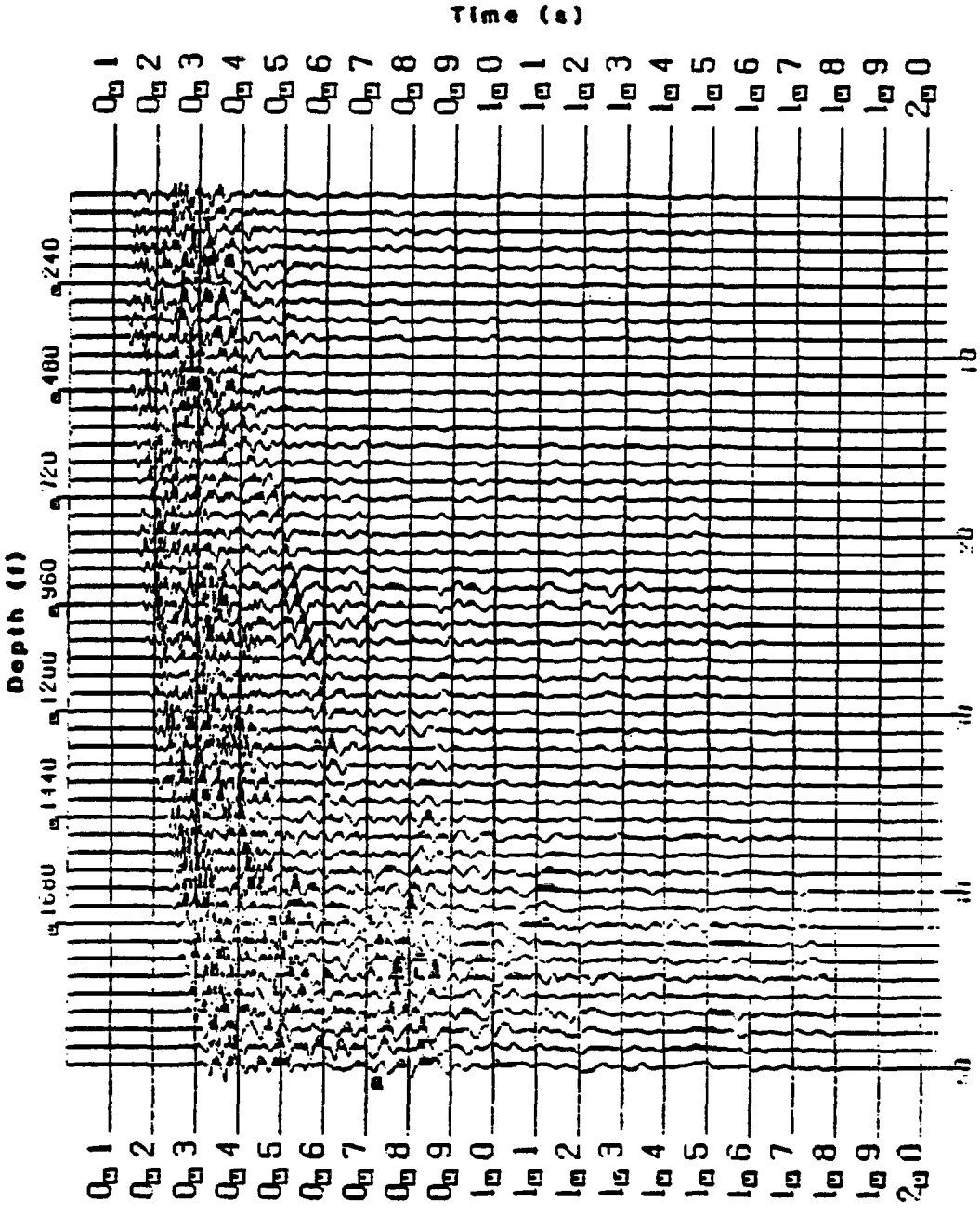

Figure 4.4. Data set in Figure 4.3 after application of a 100/12 low pass filter to remove high frequency noise. The filter did little to improve the quality of the up-going reflections. Only the reflection from the bottom of the model (a) is seen.

(a) appears to be a reflection from the bottom of the model.

In order to enhance the quality of the upgoing events, an FK filter was applied to the data. Unfortunately, the VSEIS module for applying an FK filter outputs a trace that is only 2048 samples in length. Before applying the filter, a bulk shift was applied to the data set to remove the dead portion of the traces before the direct p-wave arrived. In this way, a larger portion of the important data is saved during the filtering.

The FK spectrum of the data set in Figure 4.4 is shown in Figure 4.5. As noted earlier, the coherent upgoing energy is plotted in the right-hand plane. Coherent downgoing energy is plotted in the left-hand plane. Any reflections from a fault plane would be expected to have a near-vertical slope on the data, and would plot along the vertical axis of the FK plot. Reflections from fault planes are an important objective of the experiment, so the FK filter must be designed to preserve the events if they exist. Figure 4.6 shows the FK filter that was applied to the data. The filter was chosen to pass all energy in the right-hand plane as well as energy having a downgoing slope up to 2 milliseconds per trace. Fault plane reflections should be passed by such a filter. Figure 4.7 shows the FK spectrum of the data set after application of the filter.

The data were transformed back into the time domain and

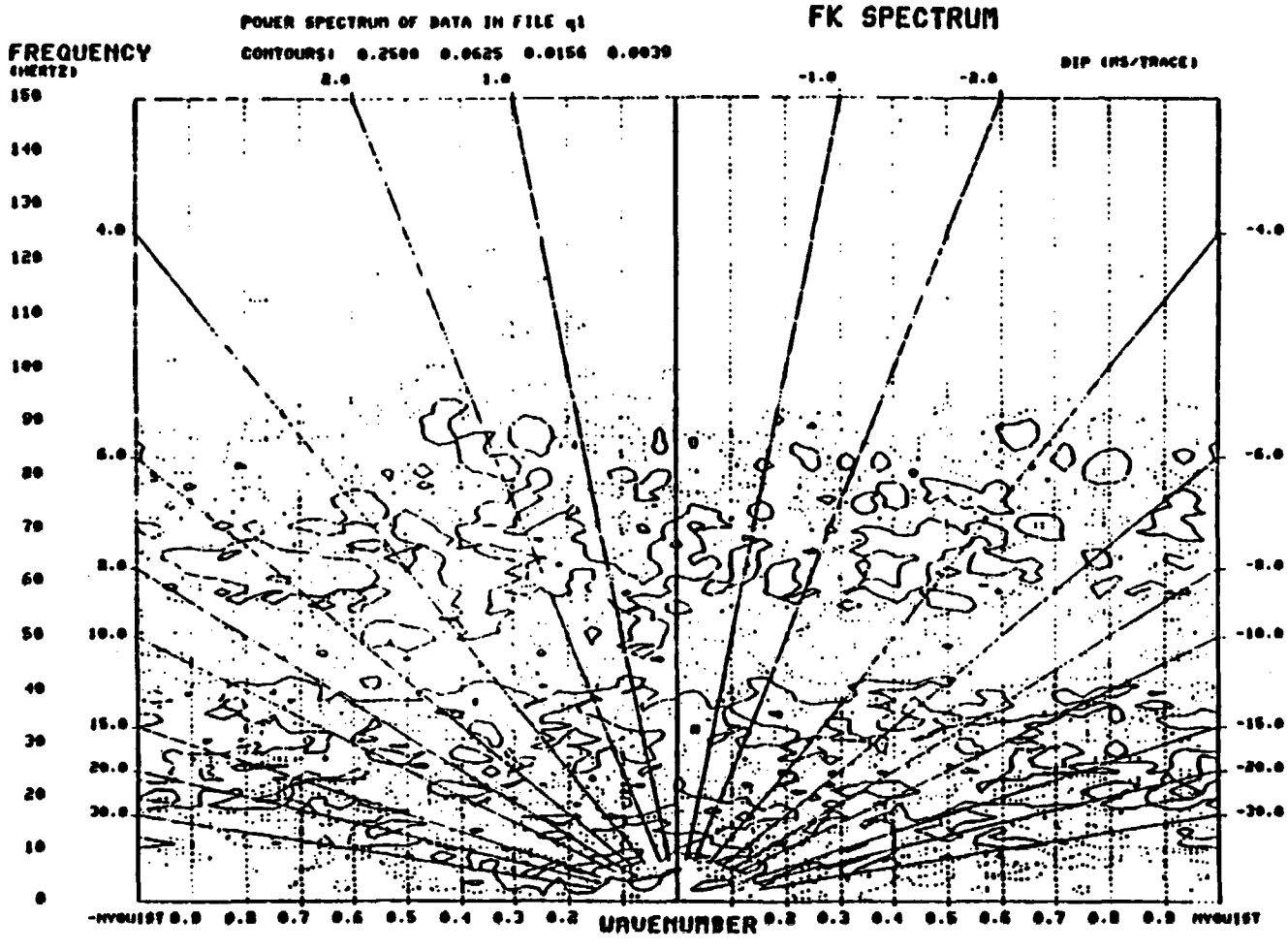

Figure 4.5. FK spectrum of the data set in Figure 4.4. Upgoing energy appears in the right-hand plane. Downgoing energy appears in the left-hand plane.

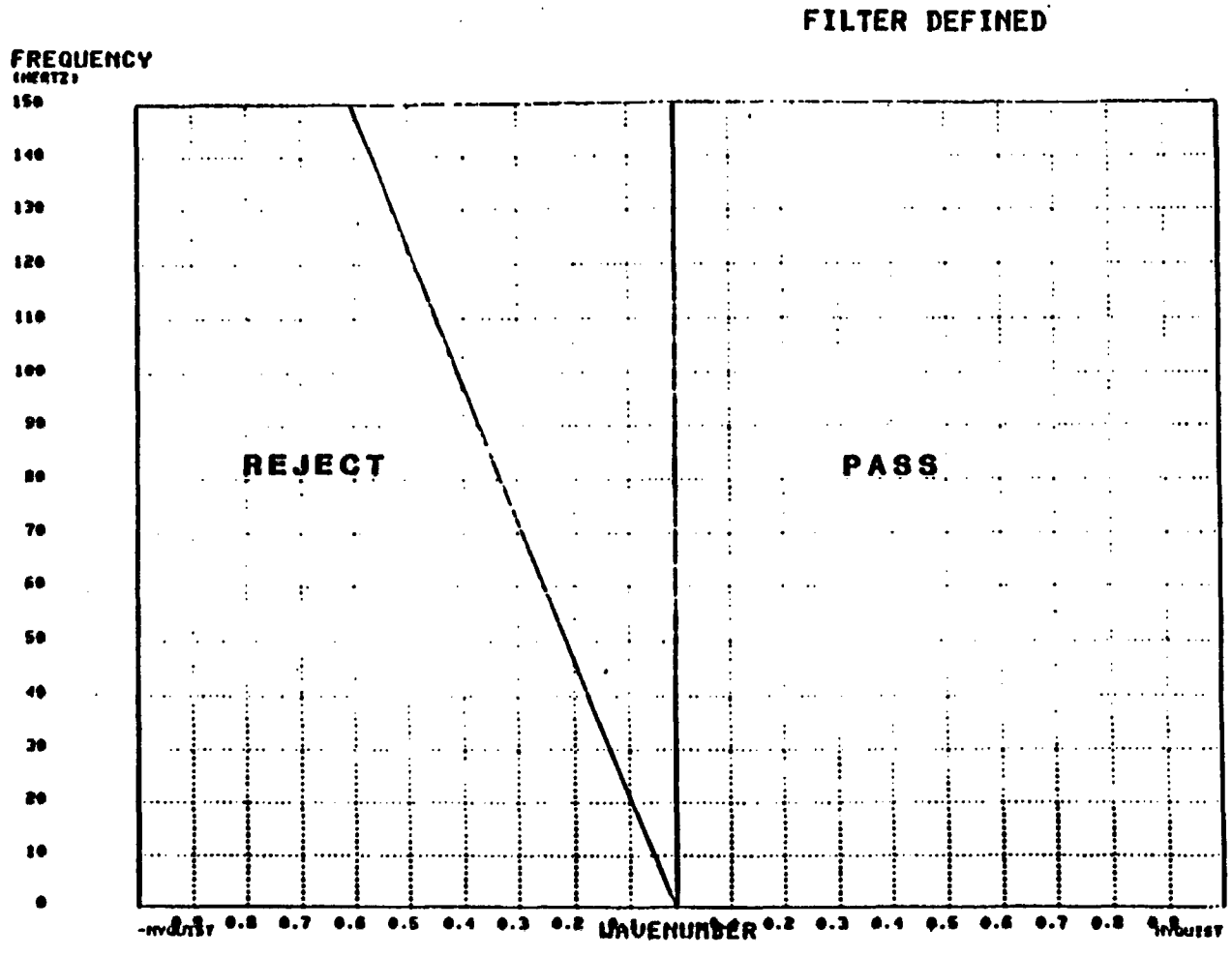

Figure 4.6. FK filter designed to preserve upgoing energy in the right-hand plane as well as downgoing events having a slope up to 2 milliseconds per trace. Since fault plane reflections could have a slight downgoing slope, this filter was designed to preserve these events, if they exist, on the data set.

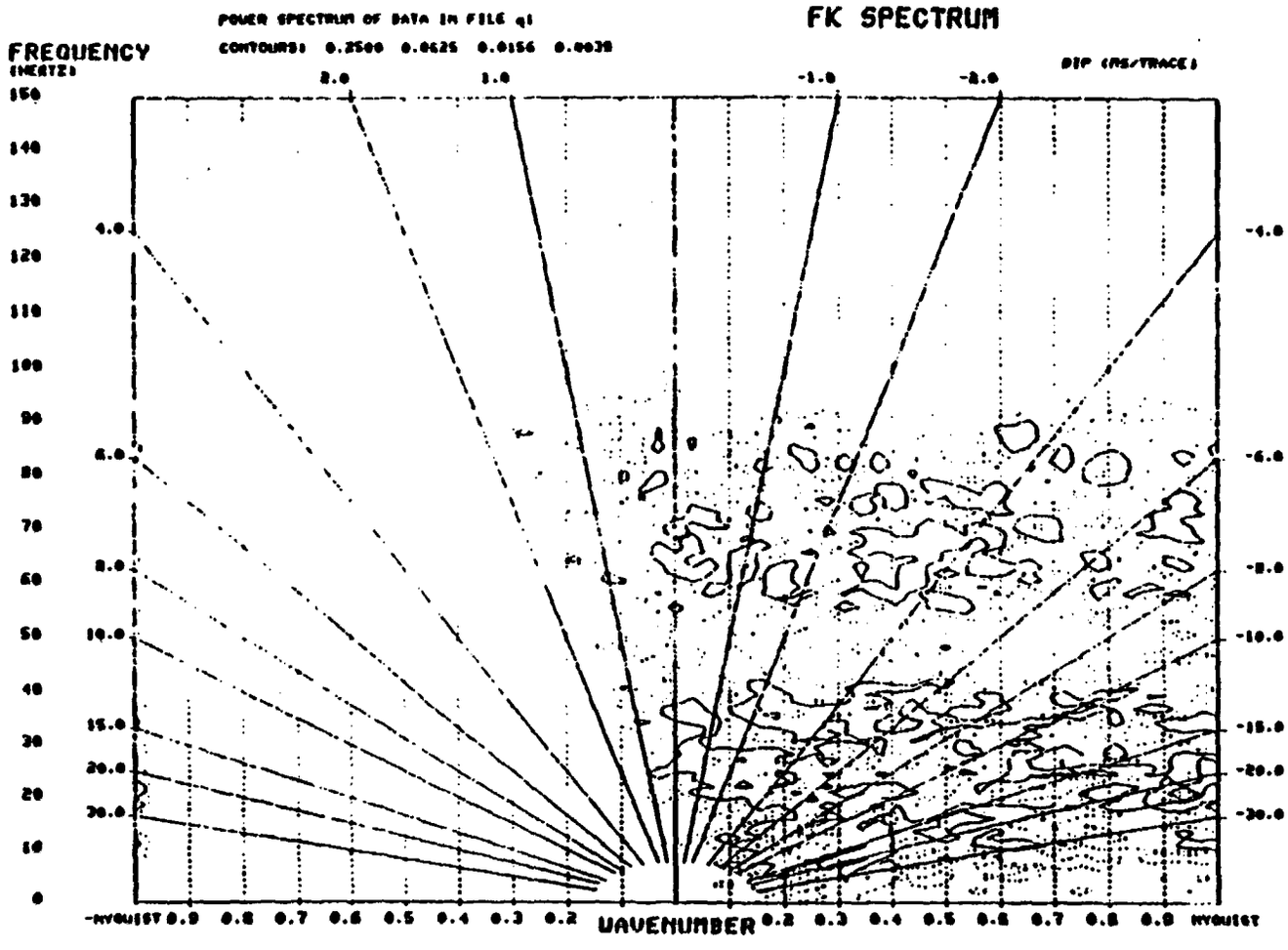

Figure 4.7. FK spectrum of the data set in Figure 4.4 after application of the FK filter in Figure 4.6.

shifted back to the proper time position. The data set appears in Figure 4.8. Several upgoing reflections can be identified. Event (a) is a reflection from Tptw, the LEXAN/PLEXIGLAS contact which occurs at depth level 14. Event (b) is a p-wave reflection from n2, the PLEXIGLAS/LEXAN contact at depth level 36. The event labeled (c) is a p to s converted reflection that reflects from n2. The merging of this event with the direct p-wave at trace 36, and the difference in slope from event (b), are the criteria that were used to identify this event.

The event labeled (d) is a reflection from n3. This event is best seen on traces 36 through 50. The event labeled (e) is interpreted as the reflection from the bottom of the model.

A reflection from a fault plane would have to travel approximately 7000 feet to reach the borehole. At the very earliest, the event would appear as a near-vertical event between 0.9 and 1.0 second. Due to the limitations on trace length in the FK filtering module, it was not possible to save any information after 0.9 second on this data set.

The interpretation of the data set in Figure 4.8 was verified by computer modeling. The AIMS model in Chapter 2 was modified to contain seismic velocities which corresponded to the PLEXIGLAS and LEXAN horizons in the physical model. Figure 4.9 is the synthetic data set created by

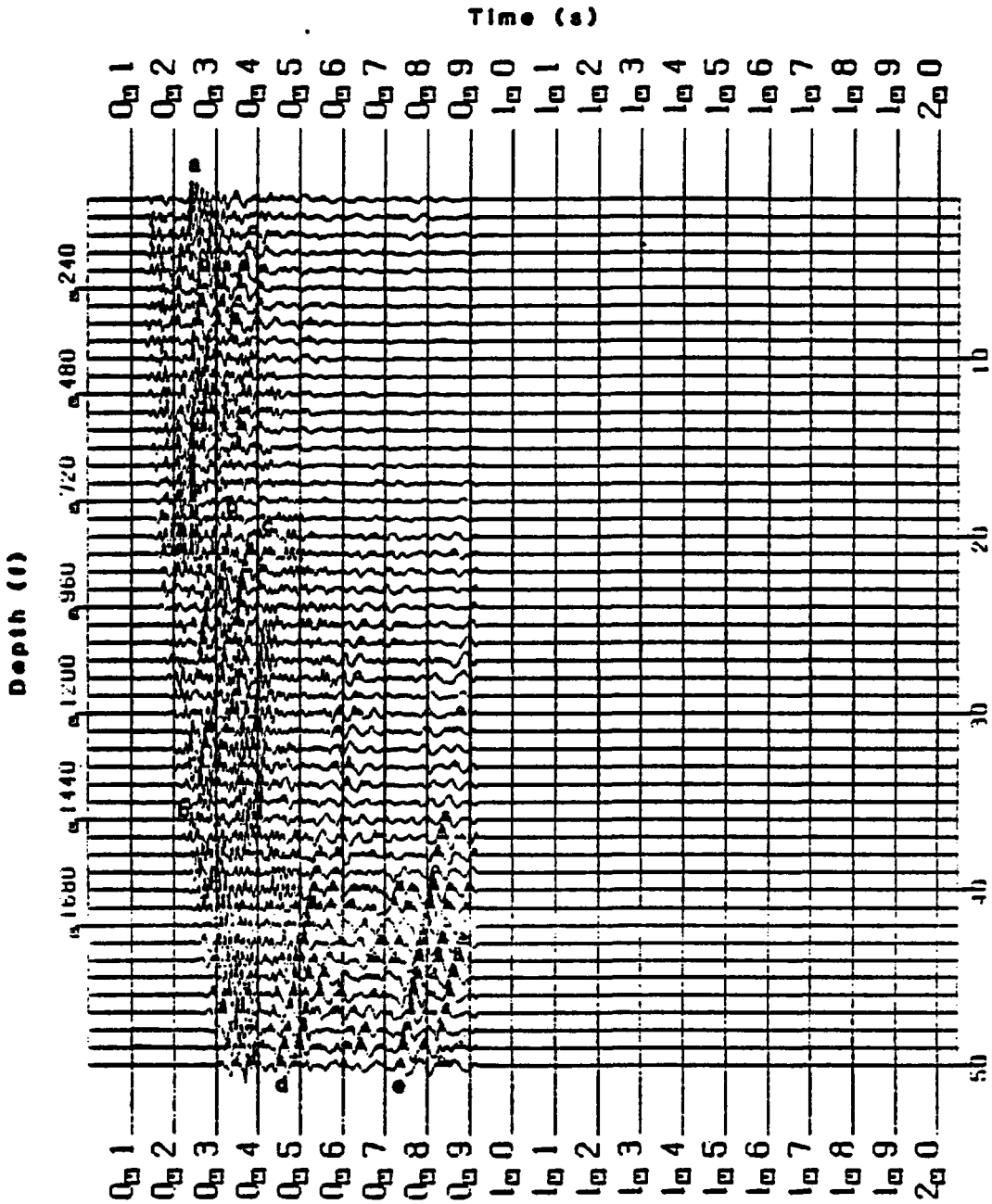

Figure 4.8. Data set for 1000-foot source offset after application of the FK filter in Figure 4.6. Event (a) is a reflection from Tptw. Event (b) is a p-p reflection from n2. Event (c) is a p-s reflection from n2. Event (d) is a reflection from n3. The event labeled (e) is interpreted to be a reflection from the bottom of the model.

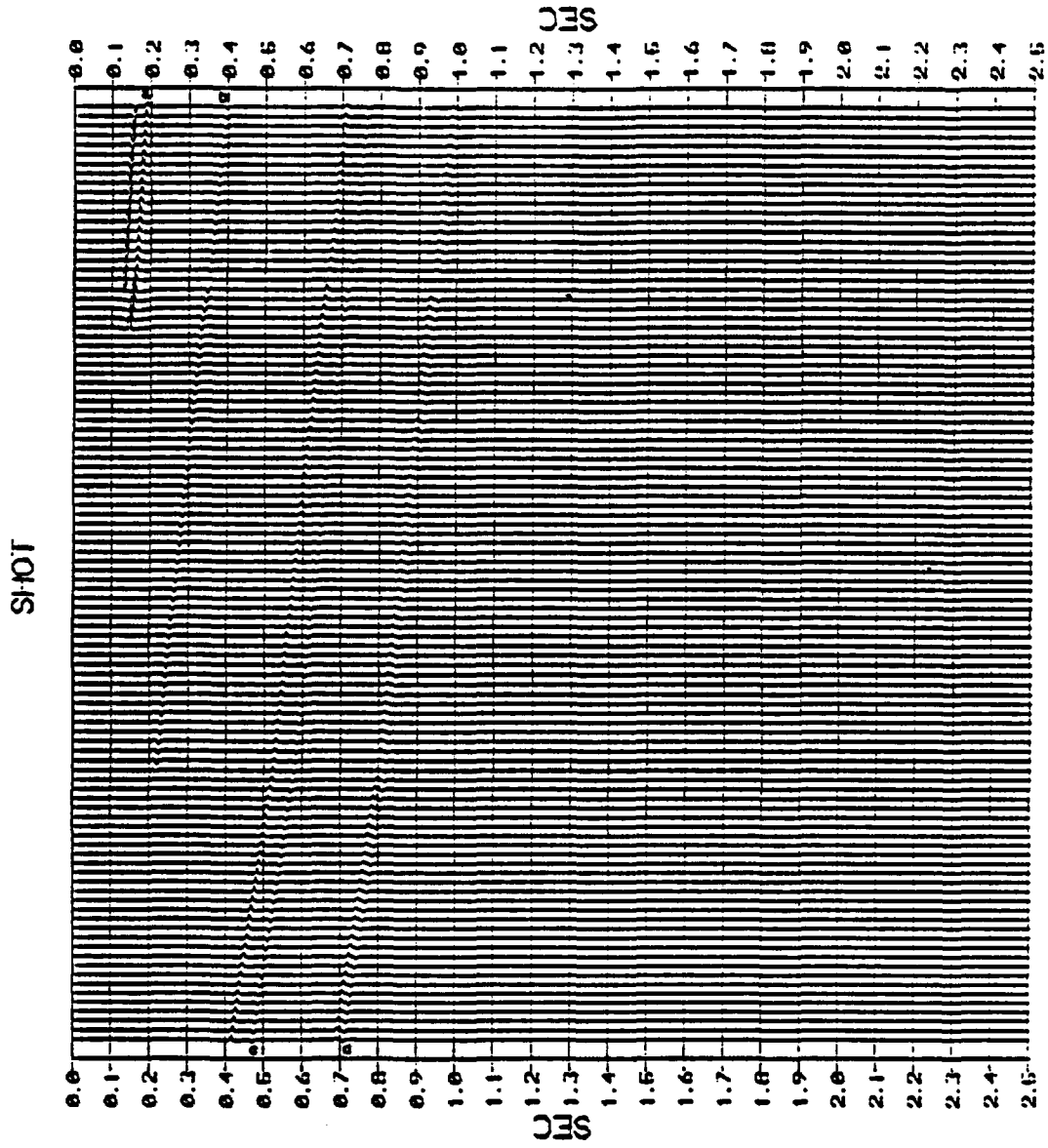

Figure 4.9. Synthetic AIMS data set simulating the 1000-foot source offset data set in Figure 4.8. Event (a) is the reflection from Tptw. The event arrives 40 milliseconds before the Tptw reflection on Figure 4.8. Reflections from n2(b), n3(c), and n4(d) all correspond well with the reflections from these horizons on Figure 4.8.

AIMS. Event (a) is the reflection from Tptw. This event arrives earlier than the Tptw reflection on the physical model data set in Figure 4.8 by about 40 milliseconds. The cause of this delay is not clear, but it is possible that slight differences exist between the computer cross section and the physical cross section. This may be causing the slight difference in arrivals times from this horizon.

Event (b) is the reflection from n2, and corresponds quite well with the n2 reflection on the physical model data set. The arrival time of the p-p reflection on Figure 4.8 is almost identical to the arrival time of event (b) on Figure 4.9

Event (c) is the reflection from n3, and the arrival time of this event is very close to the arrival time of the n3 (d) reflection on Figure 4.8. Event (d) is the reflection from n4 on the computer model. This corresponds to event (e) on Figure 4.8, which is the reflection from the bottom of the model (n4). The difference in arrival times of the two events is very small, on the order of 10 milliseconds.

The close correspondence of the computer model data set to the physical model data set suggests that the interpretation of Figure 4.8 is sound.

4.3 2000-foot source offset VSP

The source was placed 2000 feet from the borehole and fifty traces were recorded. The data set for this offset appears in Figure 4.10. Three major downgoing events can be identified. The direct p-wave is labeled (a). As noted on Figure 4.2, changes can be noted in the direct p-wave. Amplitude of the direct p-wave on traces 12 and 13 (labeled 1) is seen to be much less than on surrounding traces. This corresponds to the depth levels at which the receiver is coupled to LEXAN (n1).

Event (b) is the downgoing direct s-wave, which is best seen on traces 36 through 100. The surface wave (c) is difficult to identify on many of the traces.

An additional event appears on this data set that has not been identified to this point in the thesis. Event (d) can be seen to originate at depth level 36, where it merges with the downgoing direct s-wave. The point of origin and the slope of the event suggest that this is a downgoing s to p converted wave, which is converted at the n2 boundary.

The three major downgoing events were individually aligned and median filtered. The resulting upgoing wavefield is shown in Figure 4.11. A considerable number of upgoing reflections can be seen on traces 25 through 50. The reflections, however, are from deeper horizons and do not merge with the direct p-wave. This makes identification

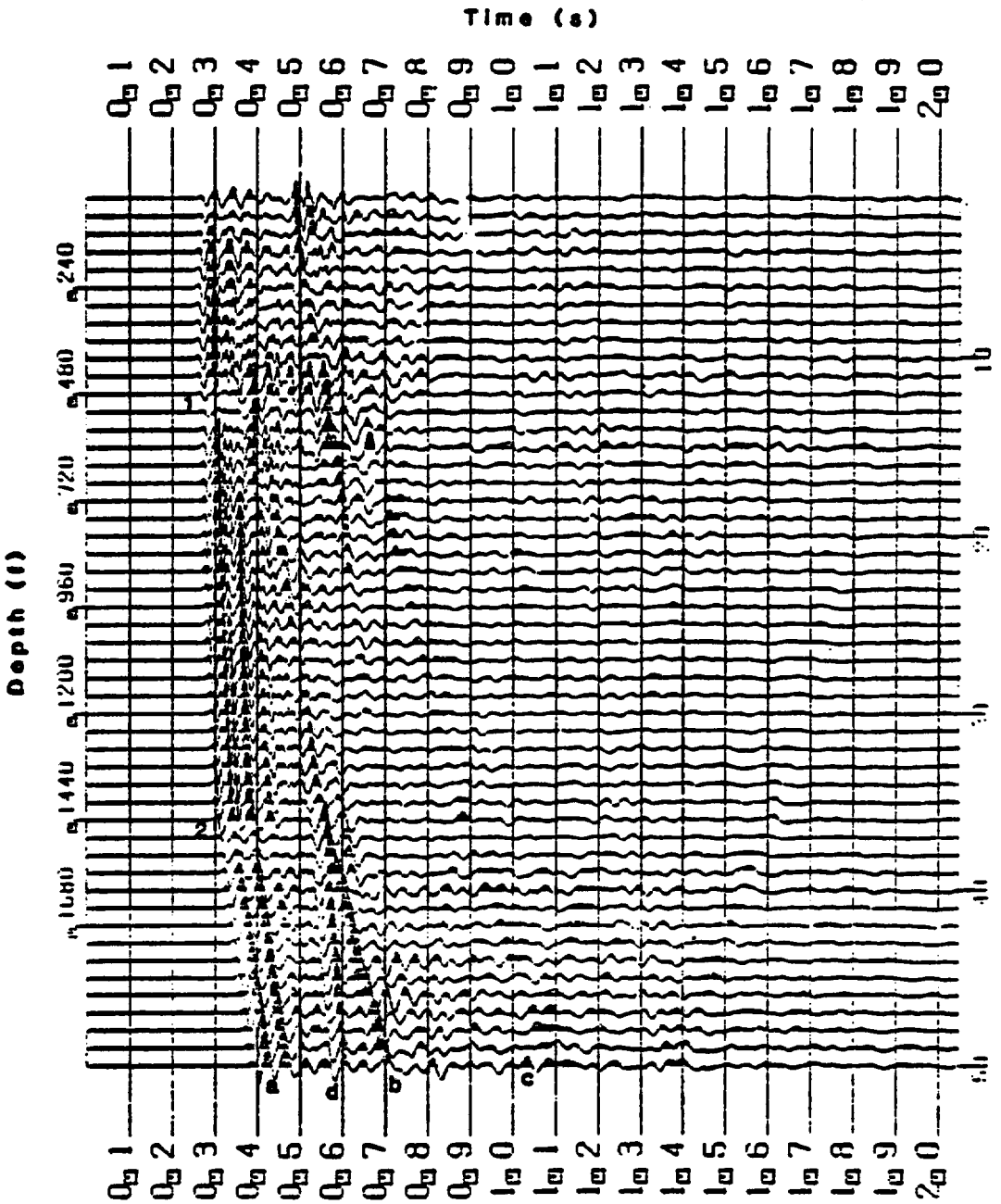

Figure 4.10. Data set recorded for a source offset of 2000 feet. The amplitude of the direct p-wave (a) is seen to decrease on traces 12 and 13 (1). The slope of the event changes at trace 36 (2) as the p-wave enters n2. The s-wave (b) and the surface wave (c) can also be identified on the record. The event labeled (d) originates at trace 36 and appears to be an s to p converted wave.

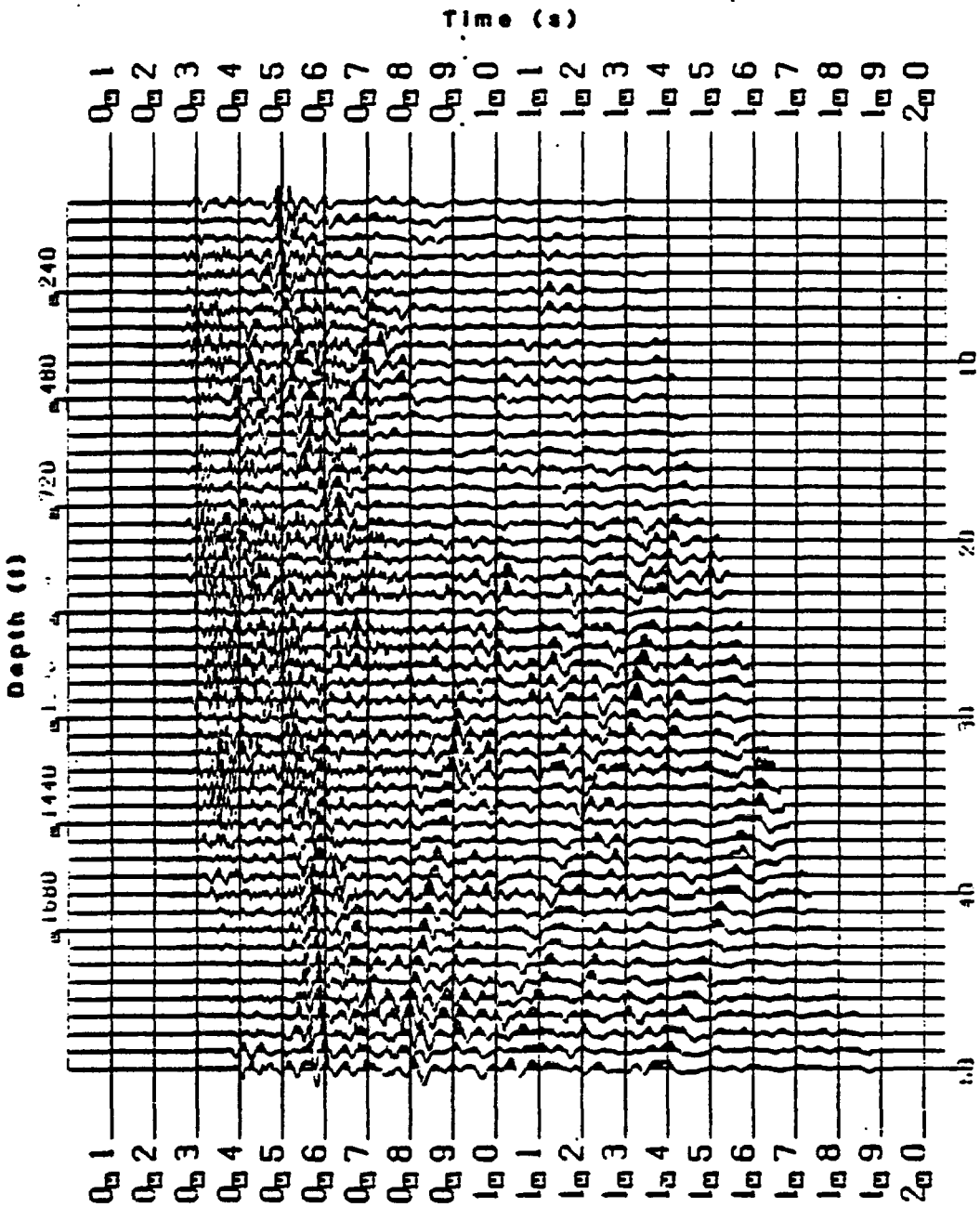

Figure 4.11. Data set in Figure 4.10 after removal of the direct p-wave, the direct s-wave, and the surface wave. A number of upgoing reflections can be seen on the data, but the events can not be positively identified.

difficult. Shallow reflections are obscured by noise. In order to remove the high frequency noise, a 100/12 low pass filter was applied to the data. The resulting data set is shown in Figure 4.12.

Using the low pass filter did little to improve the quality of the shallow reflections. The reflection from the bottom of the model (a) is the only prominent reflection which can be identified. The other prominent event in this data set is not even a reflection. Event (b) is the down-going s to p converted wave, which survived the median filtering.

The traces in Figure 4.12 were shifted 250 milliseconds toward zero time so that an FK filter could be applied to as much of the valuable information as possible. The data were filtered with the FK filter shown in Figure 4.6 in order to preserve both upgoing reflections and any fault plane reflection that might be present in the data. The resulting data set is shown in Figure 4.13.

The FK filter vastly improved the quality of the upgoing wavefield. Event (a) is a reflection from Tptw. It is seen to originate at trace 14, as expected. Reflections from n2 are more difficult to identify on this data set than on Figure 4.8. The event labeled (b) appears to be a p-wave reflection from this horizon, however.

Event (c) is a reflection from n3 and is easy to

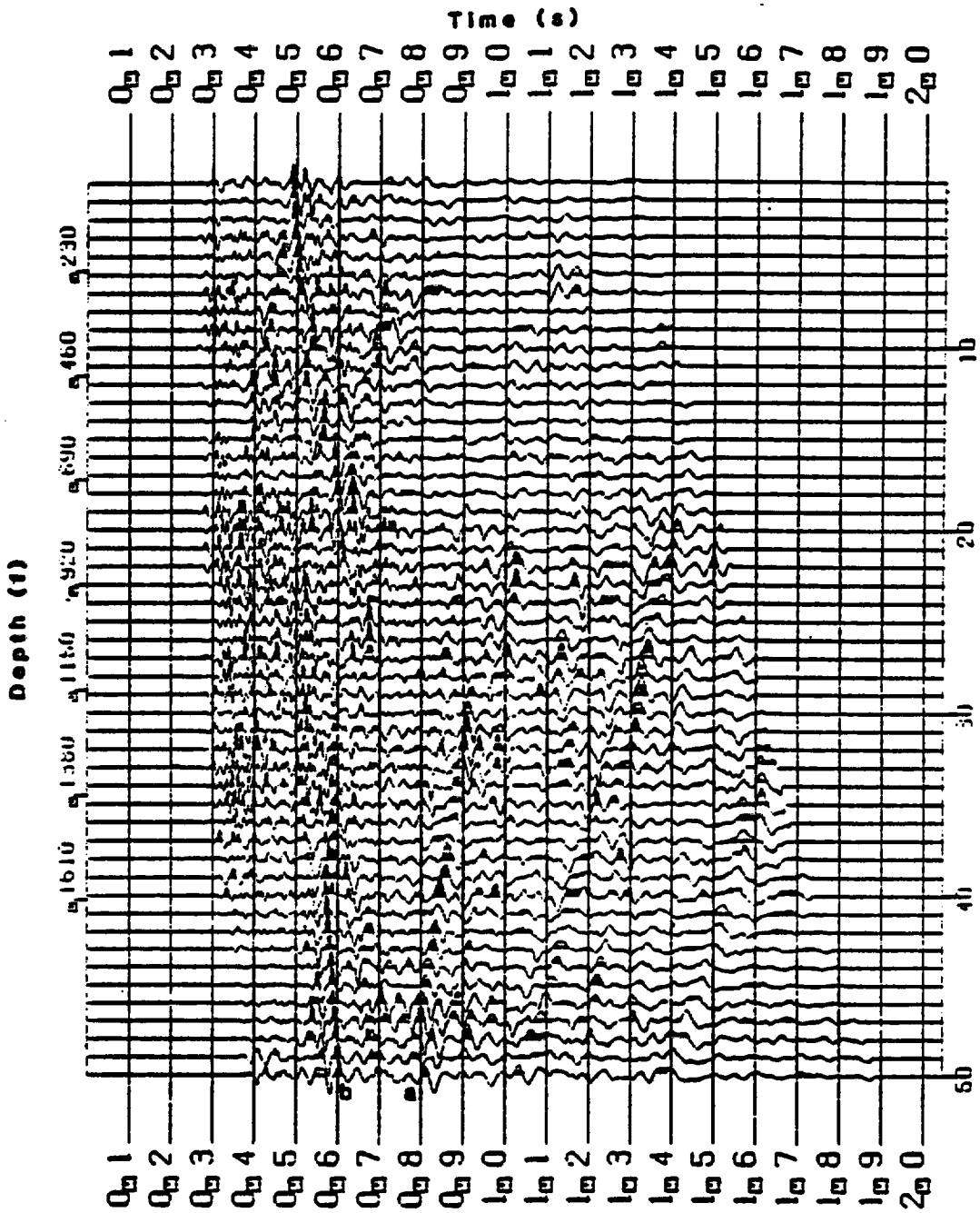

Figure 4.12. Data set in Figure 4.11 after application of a 100/12 low pass filter to remove high frequency noise. The filter did little to improve the quality of the shallow reflections. Event (a) is the reflection from the bottom of the model. Event (b) is the s to p converted wave.

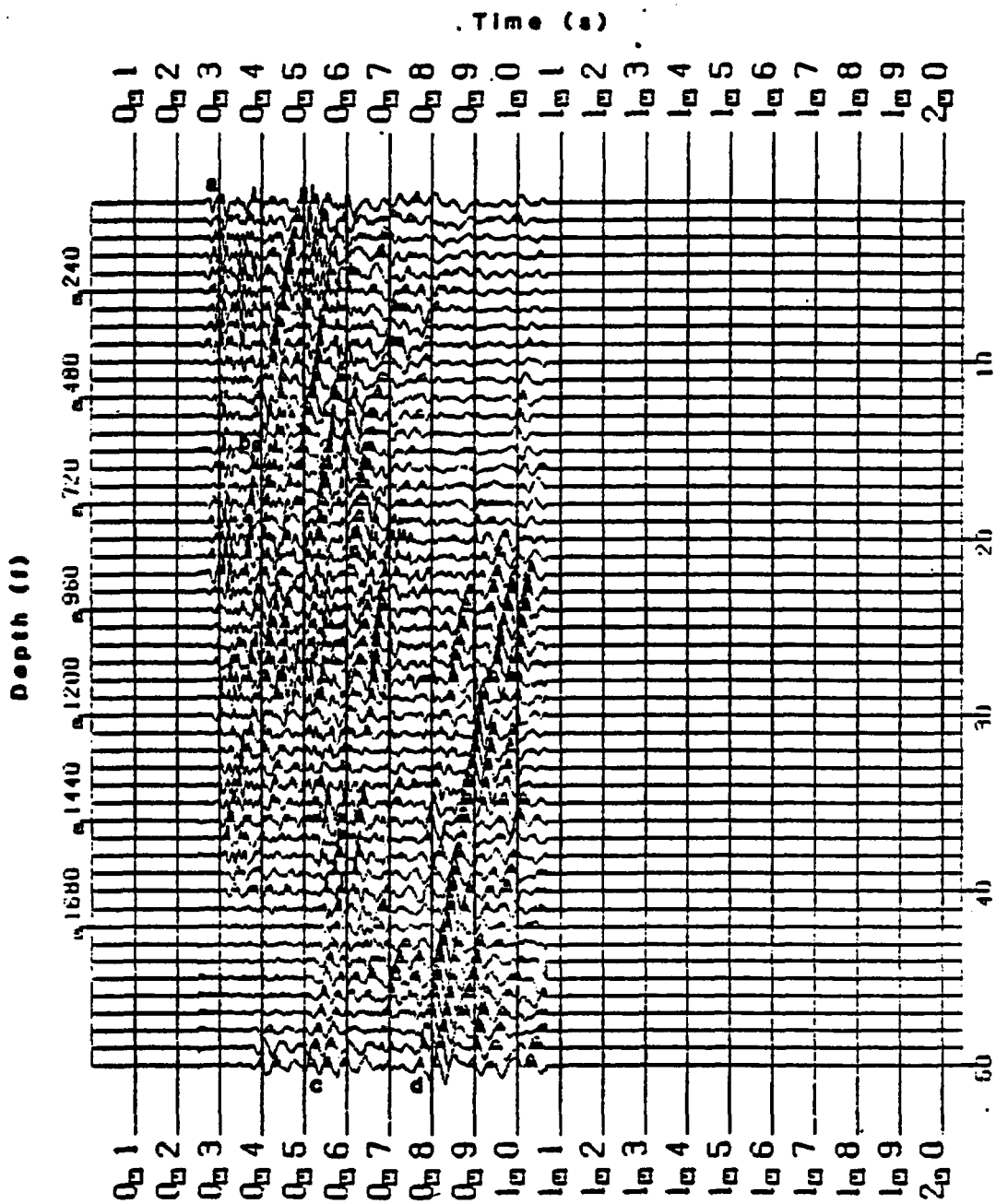

Figure 4.13. Data set for 2000-foot source offset after application of the FK filter in Figure 4.6. Reflections are seen from Tptw(a), n2(b), n3(c), and from the bottom of the model (d).

identify on traces 23 through 50. The event labeled (d) appears to be a reflection from Tctw or from the bottom of the model.

A reflection from a fault plane could not be identified on this data set. Such a reflection should appear as a near-vertical event between 0.8 and 1.0 second, but no event meeting this description is seen.

As for the data with an offset of 1000 feet, an AIMS modeling experiment was conducted to test the interpretation. The synthetic data set is shown in Figure 4.14. Event (a) is the reflection from Tptw, which corresponds almost perfectly with the Tptw reflection on Figure 4.13. Since this event matched on the data sets for this offset, it is not clear why the event did not match perfectly on the data sets for a 1000-foot source offset.

Event (b) is the reflection from n2, which corresponds nicely with the n2 (b) reflection on Figure 4.13. Event (c) is the reflection from n3, which matches the n3 (c) reflection on Figure 4.13. Event (d) is the reflection from n4, and it also matches the physical model data quite well. Event (d) on Figure 4.13 is the reflection from the bottom of the model, which corresponds to the n4 horizon.

The excellent match between the computer and physical model data sets suggests that the interpretation of Figure 4.13 is sound. Due to the cost of the computer modeling

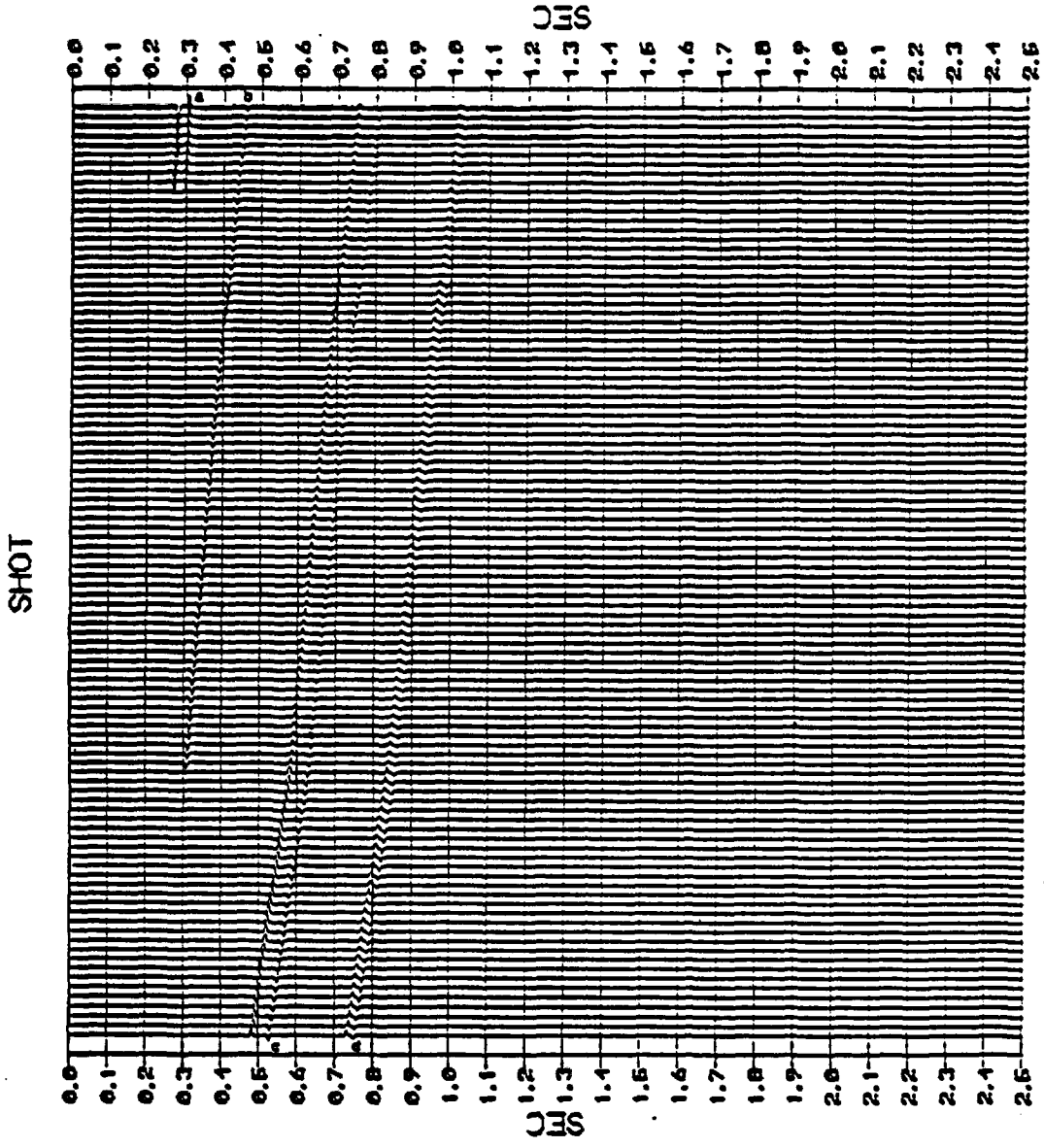

Figure 4.14. Synthetic AIMS data set simulating a 2000-foot source offset data set for the physical model. Reflections from Tptw(a), n2(b), n3(c), and n4(d) all correspond quite well with their counterpart reflections on Figure 4.13.

studies and the success of the experiments for the first two source offsets, computer modeling was not performed on the remaining data sets, except for the 4000-foot offset record.

4.4 3000-foot source offset VSP

Figure 4.15 shows the data set recorded for a source offset of 3000 feet. The direct p-wave (a) dominates the record. As seen on earlier data sets, p-wave amplitude decreases when the receiver is coupled to n1 at depth levels 12 and 13 (1). The change in waveform must be due to the properties of the LEXAN sheet, or due to the bonding between the PLEXIGLAS and the LEXAN strips. The slope of the direct p-wave is seen to change at depth level 36 (2), where the model changes from PLEXIGLAS to LEXAN.

The direct s-wave (b) is best seen on traces 36 through 50. As seen in Chapter 3, the direct s-wave must strike the receiver obliquely to be recorded. For that reason, the direct s-wave will always be most apparent on the deeper traces of these records. The surface wave (c) is difficult to identify until the direct arrivals have been removed from the data set.

Event (d) appears to be the s to p converted wave that was first seen in Figure 4.10. The event originates on trace 36, the level where the direct s-wave enters n2. The event has a higher velocity within n2 than does the direct

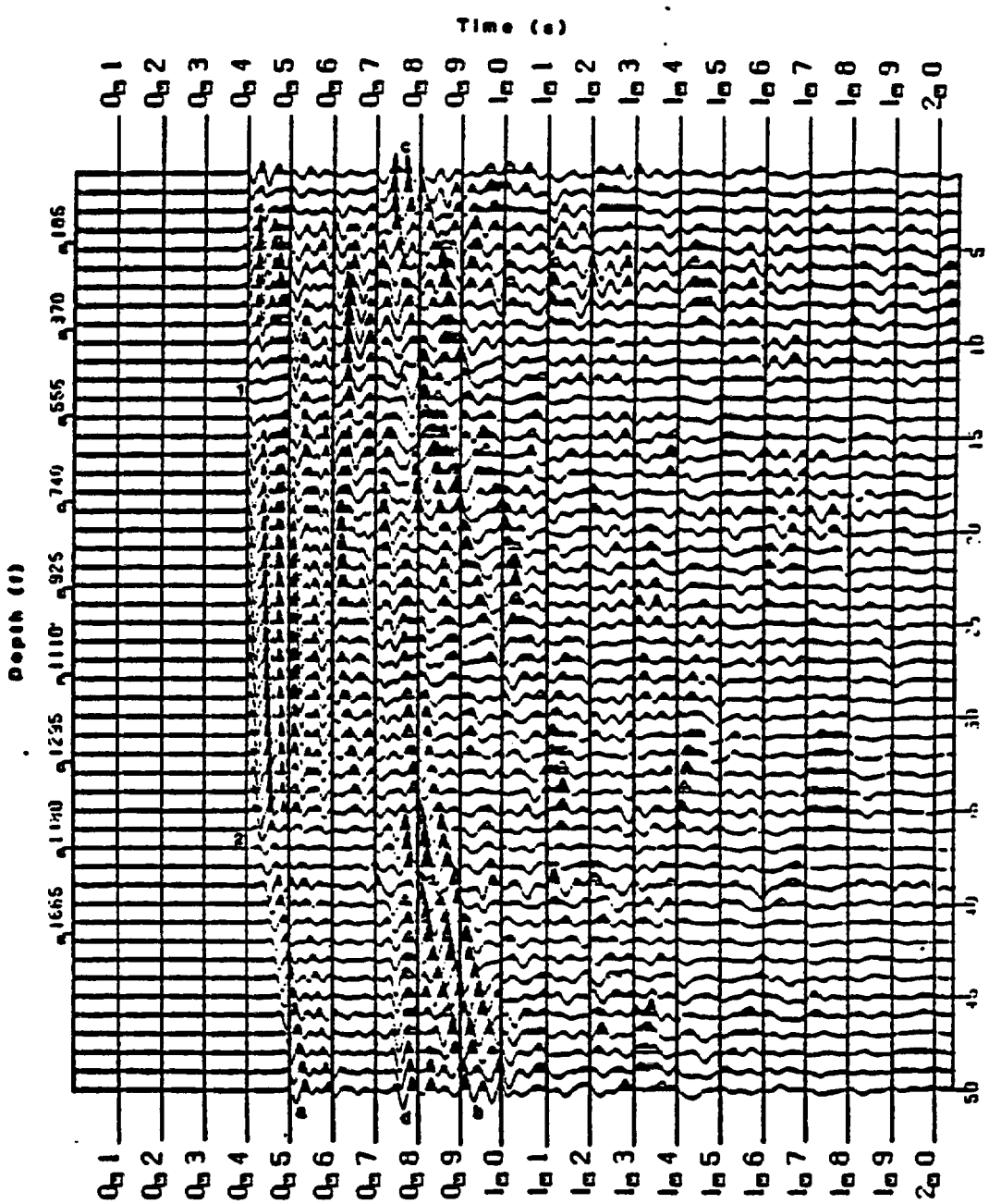

Figure 4.15. Data set recorded for a source offset of 3000 feet. Amplitude of the direct p-wave (a) decreases at traces 12 and 13 (a). The slope of the event changes at trace 36, where the p-wave enters n2. The direct s-wave (b) and the surface wave (c) can be identified. The event labeled (d) is the s to p converted wave which originates trace 36.

s-wave.

The three major downgoing events were individually aligned and removed from the data set by median filtering. The resulting data set is shown in Figure 4.16. This data set does not show many identifiable reflections. At this offset, the amplitude of the signal on the oscilloscope was starting to decrease noticeably. The vertical resolution of the oscilloscope had already been maximized and nothing else could be done to increase the amplitude. The noisy appearance of this data set is due to the very low signal amplitude. This data set was filtered with a 100/12 low pass filter, and the resulting data set is shown in Figure 4.17.

The low pass filter did little to improve the quality of the data. The only event which is clearly identifiable is the s to p converted arrival (a).

The traces were shifted by 300 milliseconds toward zero time, and the FK filter in Figure 4.6 was applied to the data set. The traces were transformed back to the time domain and shifted back to their original time position. The resulting data set is shown in Figure 4.18.

The event labeled (a) is the p-wave reflection from Tptw. The faint peaks can be seen on traces 1 through 6. Event (b) is an interesting set of peaks that also appears to originate at trace 12. The slope of the event suggests

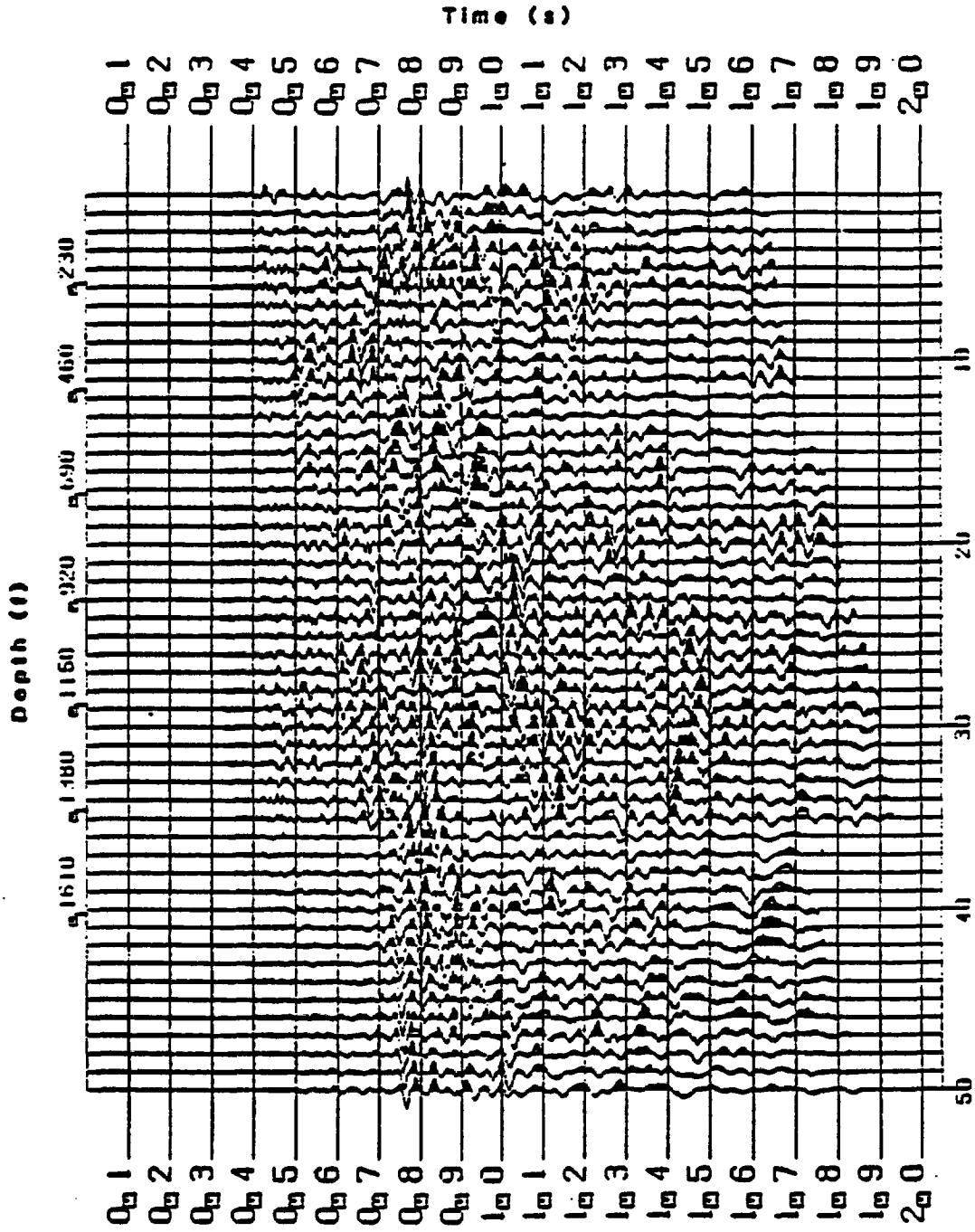

Figure 4.16. Data set for 3000 foot source offset after removing the direct p-wave, the direct s-wave, and the surface wave. Very few upgoing reflections are seen.

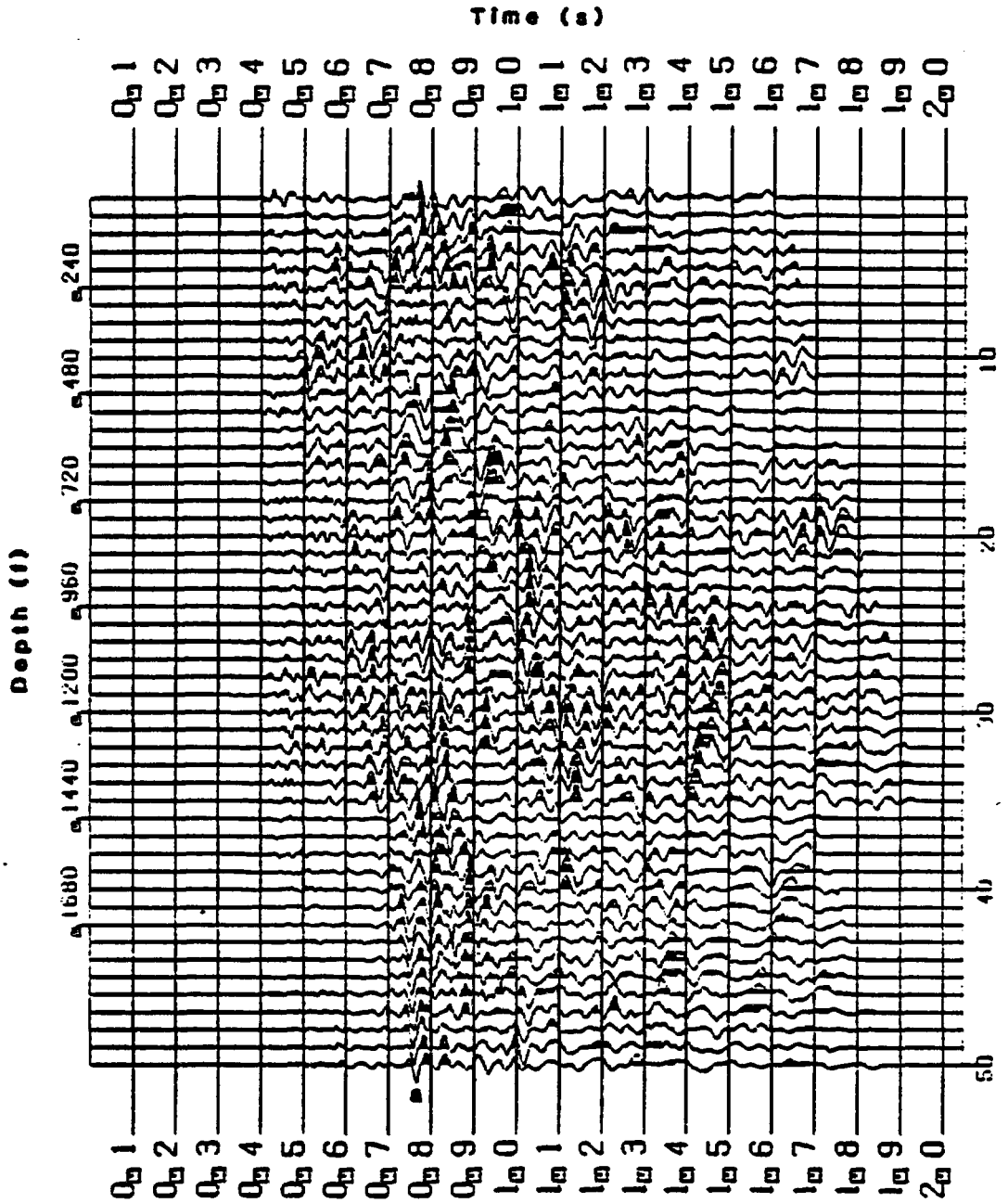

Figure 4.17. Data set in Figure 4.15 after application of a 100/12 low pass filter. The filter improved the quality of the data, but only the s to p converted arrival (a) can be positively identified.

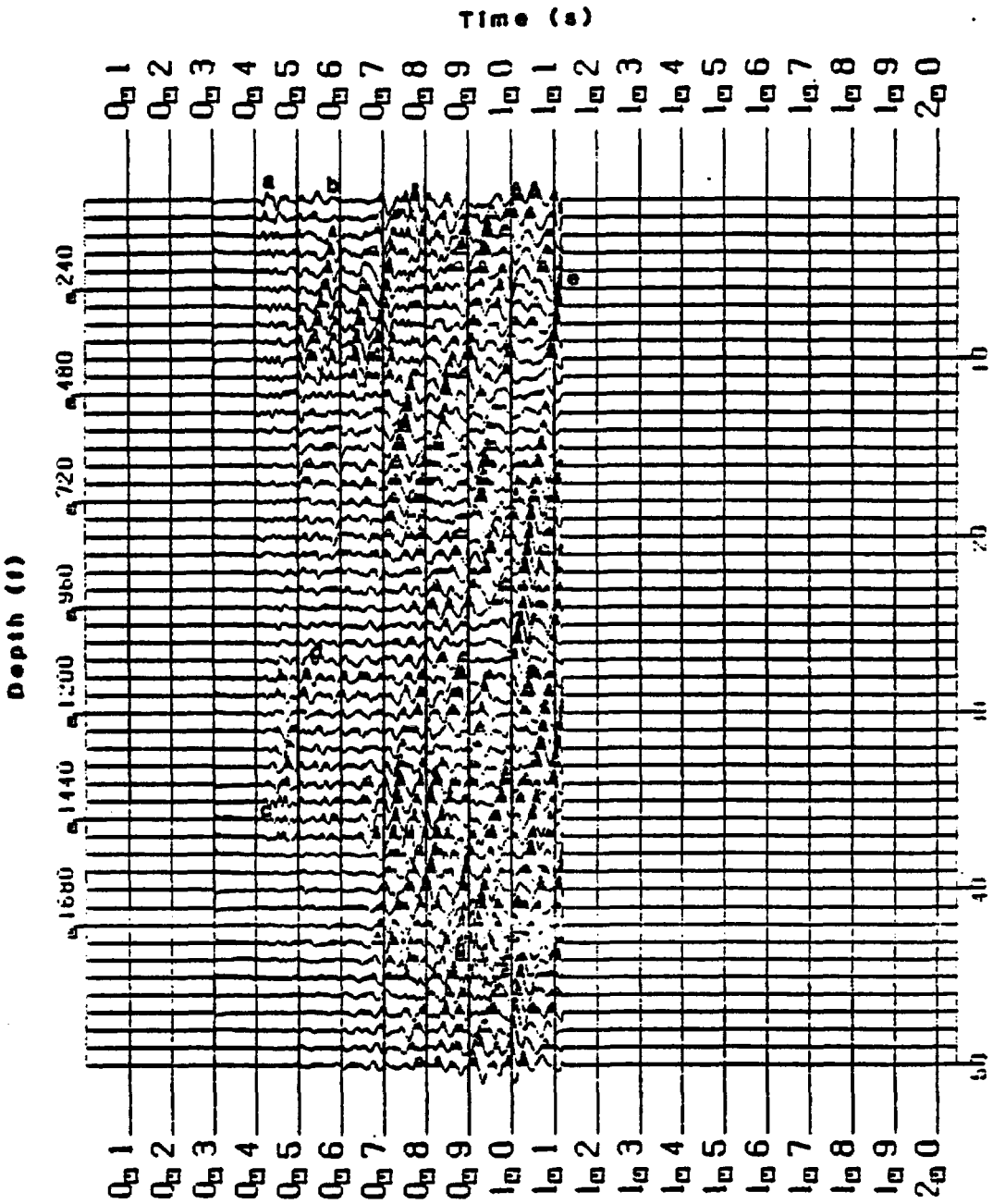

Figure 4.18. Data set for 3000-foot source offset after application of the FK filter in Figure 4.6. Event (a) is the p-p reflection from Tptw. Event (b) appears to be an s-s reflection from Tptw. Event (c) is the p-p reflection from n2. Event (d) is the p-s reflection from n2. The reflection from the bottom of the model is labeled (e).

that it is an s-s reflection from Tptw.

Horizon n2 produces two faint reflections that originate at trace 35. Event (c) is the p-wave reflection from the horizon. Event (d) appears to be the p to s converted reflection from the horizon. Both events are very faint.

Reflections from n3 are not easily identified on this data set and can not be located on the deeper traces as had been the case on previous data sets. Event (e) appears to be the reflection from the bottom of the model, and is best seen on traces 5 through 27. As with the previous data sets, a fault plane reflection can not be identified on this record.

4.5 4000-foot source offset VSP

Figure 4.19 shows the data set recorded for a source offset of 4000 feet. Once again, the direct p-wave (a) dominates the data set. The familiar amplitude loss on traces 12 and 13 (1) is seen again on this data set.

The direct s-wave (b) is seen on traces 33 through 50. The event becomes more prominent after the direct p-wave is removed. The same holds true for the surface wave (c).

All three major downgoing events were individually aligned and median filtered. The resulting data set is shown in Figure 4.20. Once again, a 100/12 low pass filter was applied to remove the high frequency noise from the

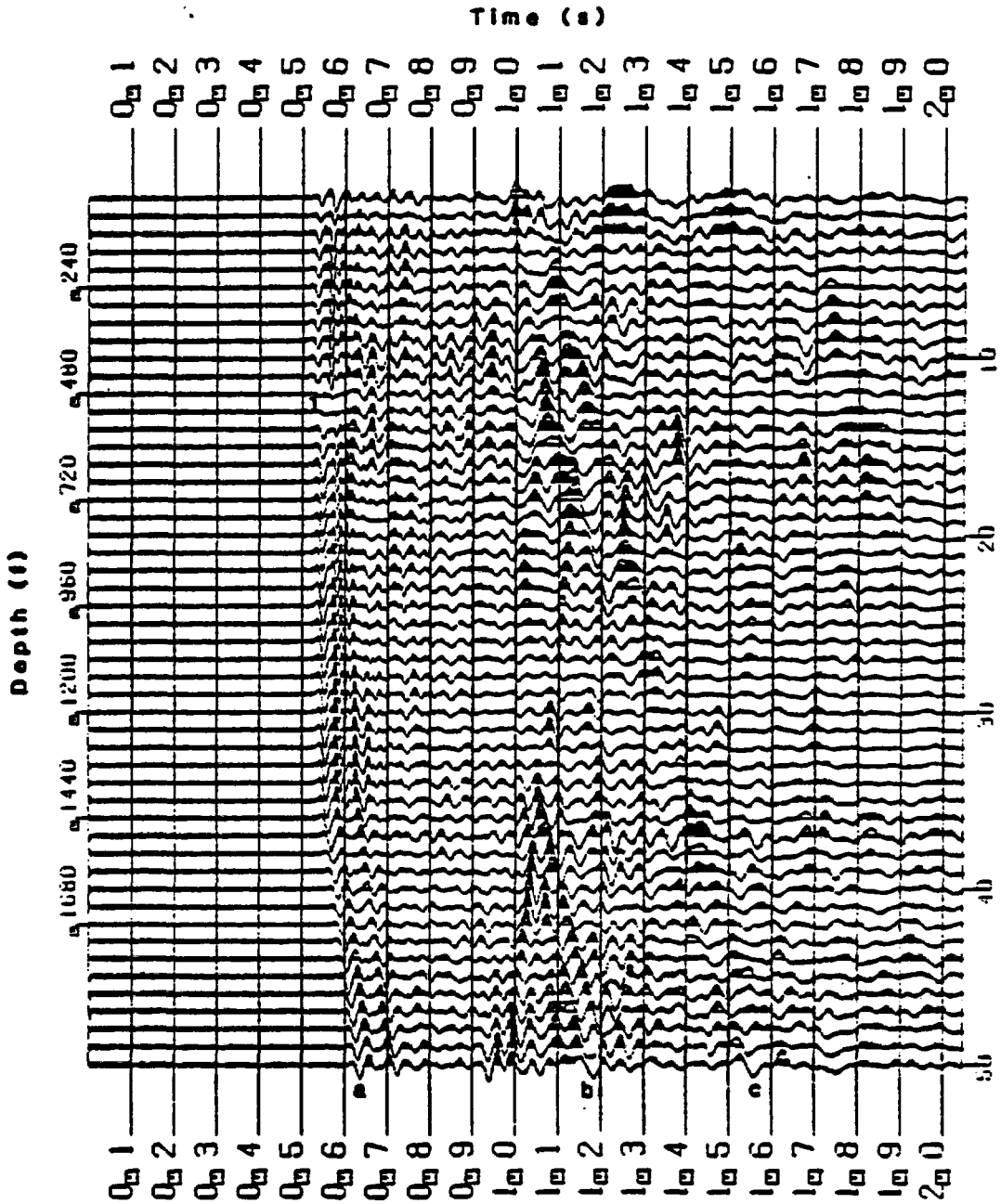

Figure 4.19. Data set recorded for a source offset of 4000 feet. The amplitude of the direct p-wave (a) is seen to decrease at traces 12 and 13 (1). The direct s-wave (b) and the surface wave (c) can also be identified.

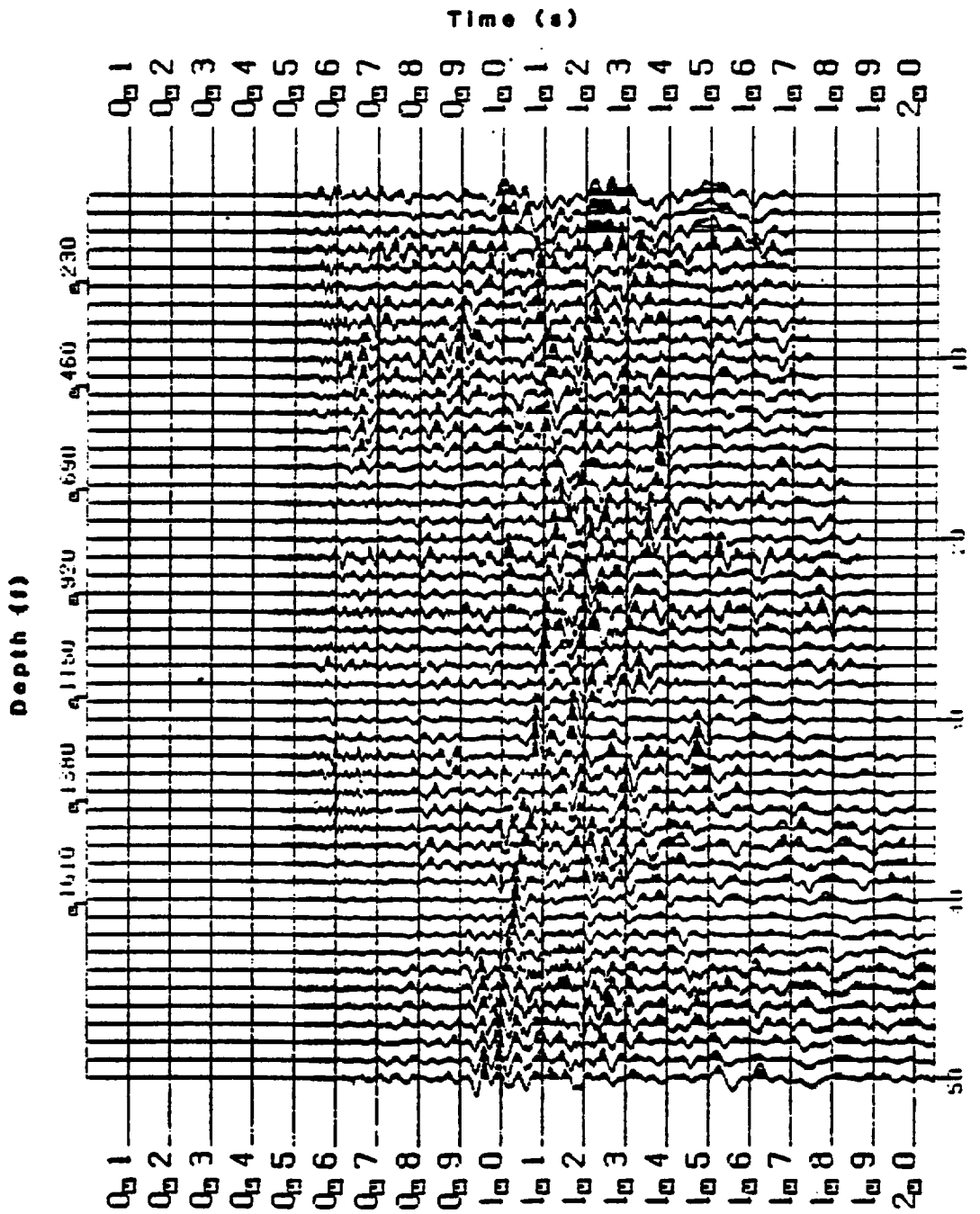

Figure 4.20. Data set in Figure 4.19 after removal of the direct p-wave, the direct s-wave, and sufrace wave. This data set is very noisy.

data. The filtered data set is shown in Figure 4.21.

The only reflection which can be identified on this record is event (a), the reflection from the bottom of the model. This reflection can be seen primarily on traces 18 through 50.

The traces were shifted by 500 milliseconds toward zero time before applying the FK filter in Figure 4.6. The data were transformed back into the time domain and shifted back to proper time position. The resulting data set is shown in Figure 4.22.

The reflections are becoming more difficult to identify as source offset increases. Increasing the stacking fold may increase the signal quality slightly and provide a record with stronger reflections. Event (a) is a faint hint of the reflection from Tptw, although it is extremely weak. The event labeled (b) is a reflection from n2. It originates at trace 35, and has the slope of a p-wave reflection.

Event (c) appears to be a reflection from n3 and is seen as a weak event on the deeper traces. Event (d) is almost certainly a reflection from the bottom of the model.

One event on the data set appears to be a reflection from a fault plane. Event (e) has a very steep slope on traces 20 through 36. The arrival time of the event is consistent with the time expected for a reflection from fault plane 3. An AIMS model was created for this offset, using

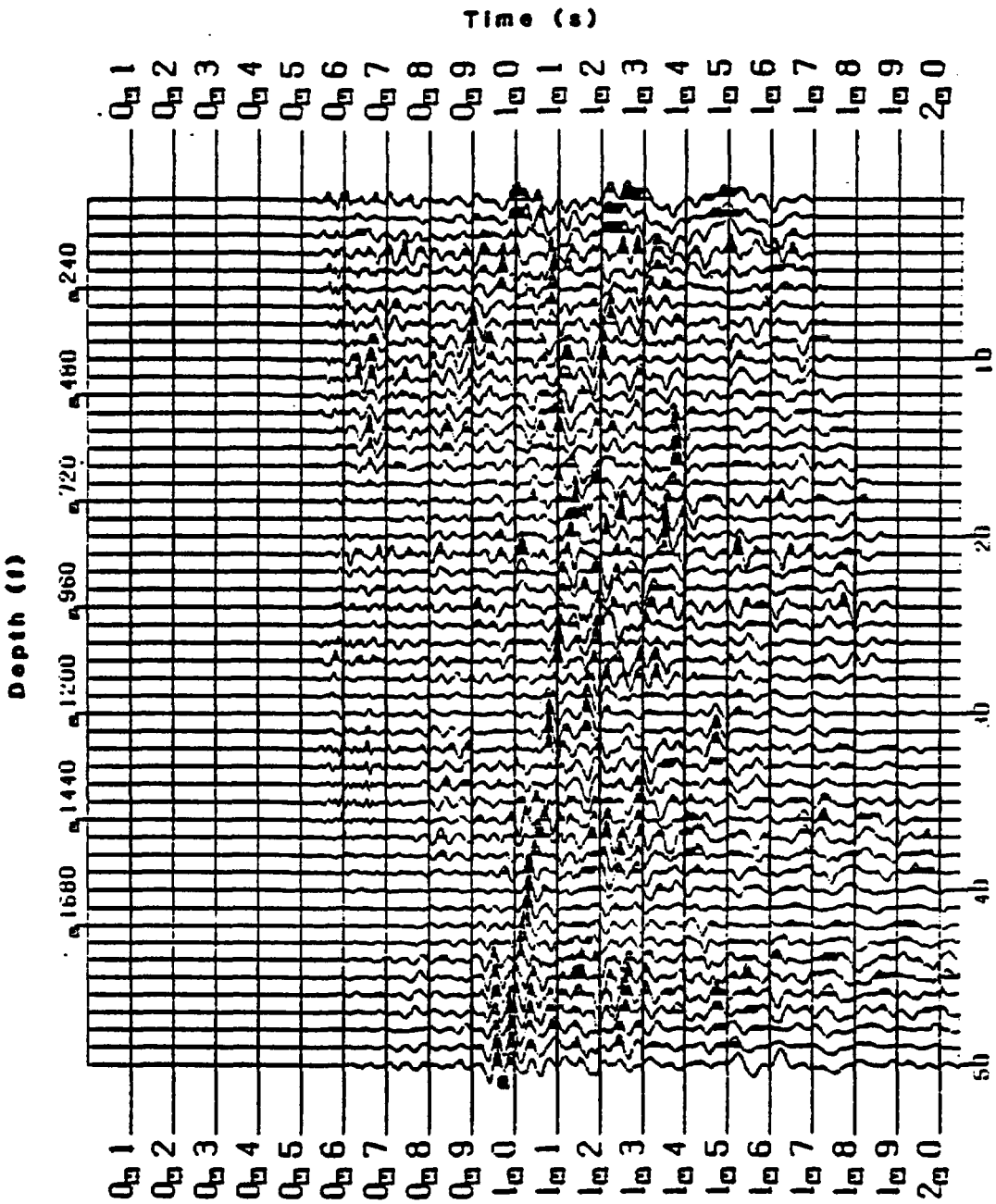

Figure 4.21. Data set in Figure 4.20 after application of a 100/12 low pass filter. The filter improved the quality of the data set but only event (a), the reflection from the bottom of the model, can be identified.

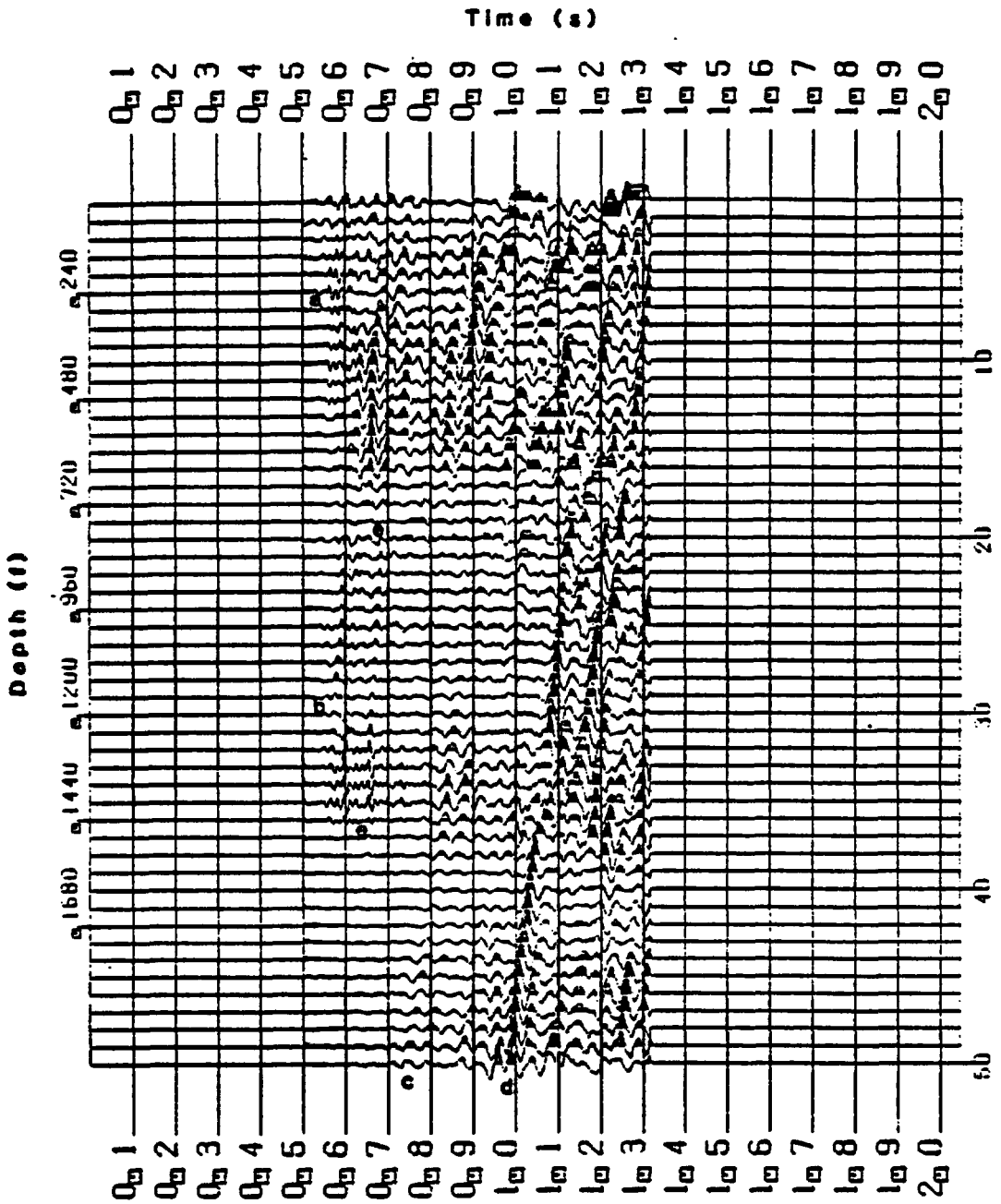

Figure 4.22. Data set for 4000-foot source offset after application of the FK filter in Figure 4.6. Reflections can be identified from Tptw(a), n2(b), n3(c), and from the bottom of the model (d). Event (e) has a very steep slope and is interpreted to be a reflection from fault plane 3.

only fault plane reflections from faults 3, 4, and 5. The data set is shown in Figure 4.23. Event (a) is the reflection from fault plane 3, and corresponds quite well with the arrival time of event (e) in Figure 4.22. The close match between the two events suggests that a fault plane reflection has been recorded from the physical model. Event (b) is the reflection from fault plane 4 and event (c) is the reflection from fault plane 5. These events were included so that their arrival times could be compared with the arrival time for event (a).

4.6 5000-foot source offset VSP

The signal on the oscilloscope was very weak for a source offset of 5000 feet. Figure 4.24 shows the data set recorded for this offset. The data are very noisy, although the three major downgoing events can be identified. The direct p-wave (a) can be seen on every trace, although it becomes very weak on the shallow traces. The direct s-wave (b) can be seen on the deeper traces. The surface wave (c) is visible on traces 1 through 37.

The three downgoing events were removed by median filtering. The resulting noisy data set is shown in Figure 4.25. A few faint upgoing reflections can be seen on the data. To remove the high frequency noise, a 100/12 low pass filter was applied to the data and the result is shown

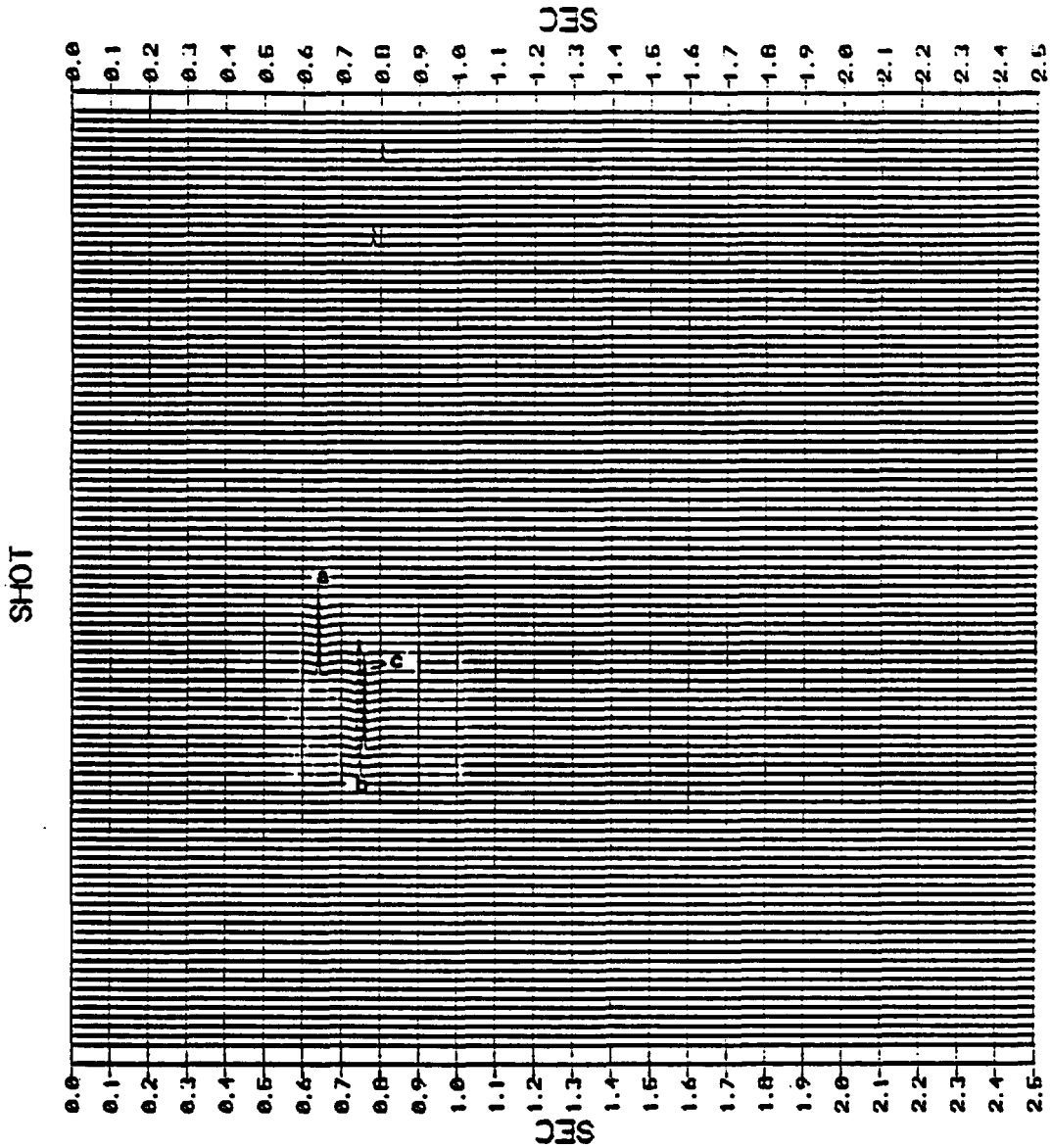

Figure 4.23. Synthetic AIMS data set simulating the fault plane reflections from fault planes 3(a), 4(b), and 5(c) for a source offset of 4000 feet. Event (a) corresponds well with the reflection from fault plane 3 (e) on Figure 4.22, suggesting that a fault plane reflection has been recorded from the physical model.

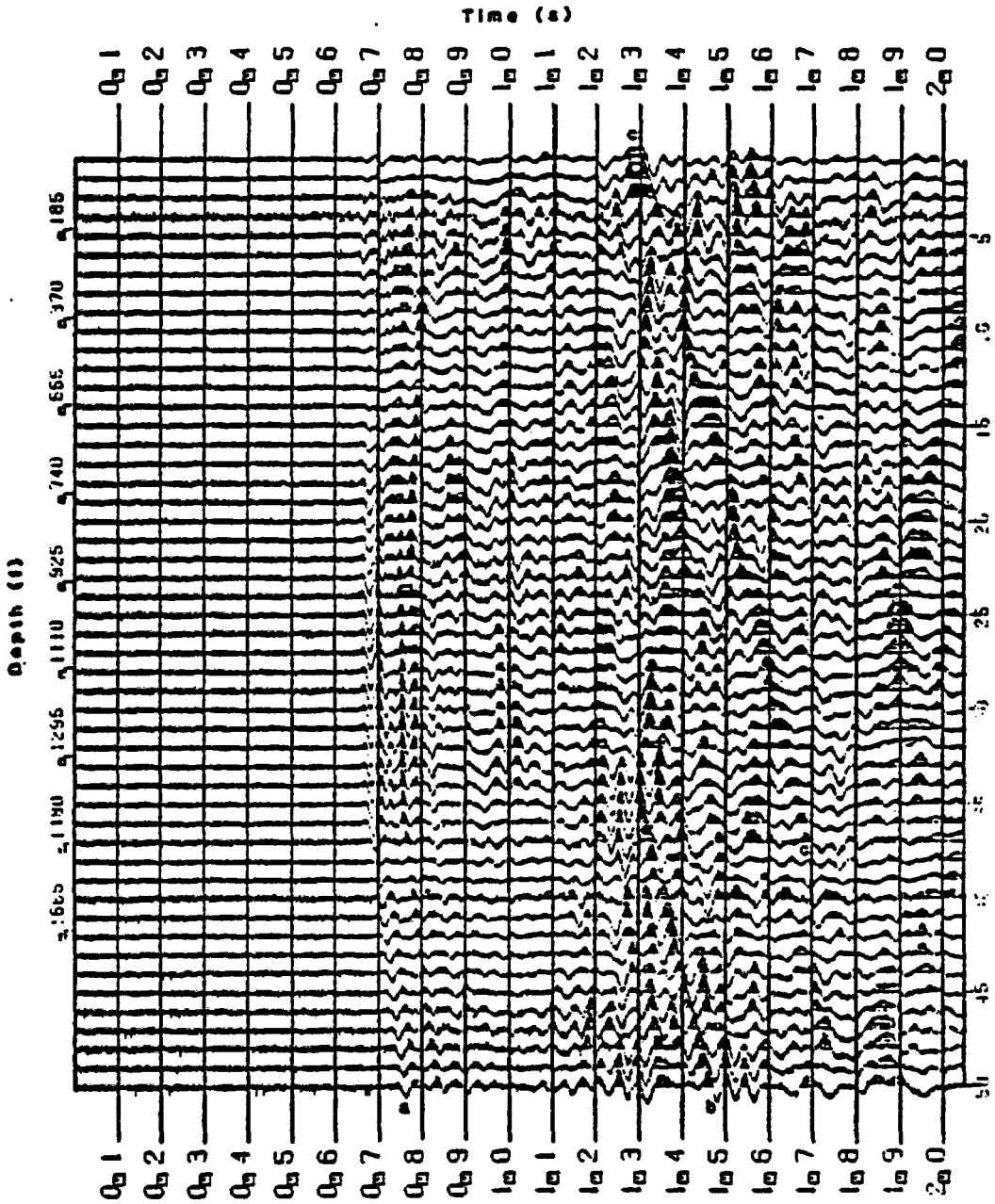

Figure 4.24. Data set recorded for a source offset of 5000 feet. The data are very noisy, but the three major downgoing events can be identified. The direct p-wave is labeled (a), the direct s-wave is labeled (b), and the surface wave is labeled (c).

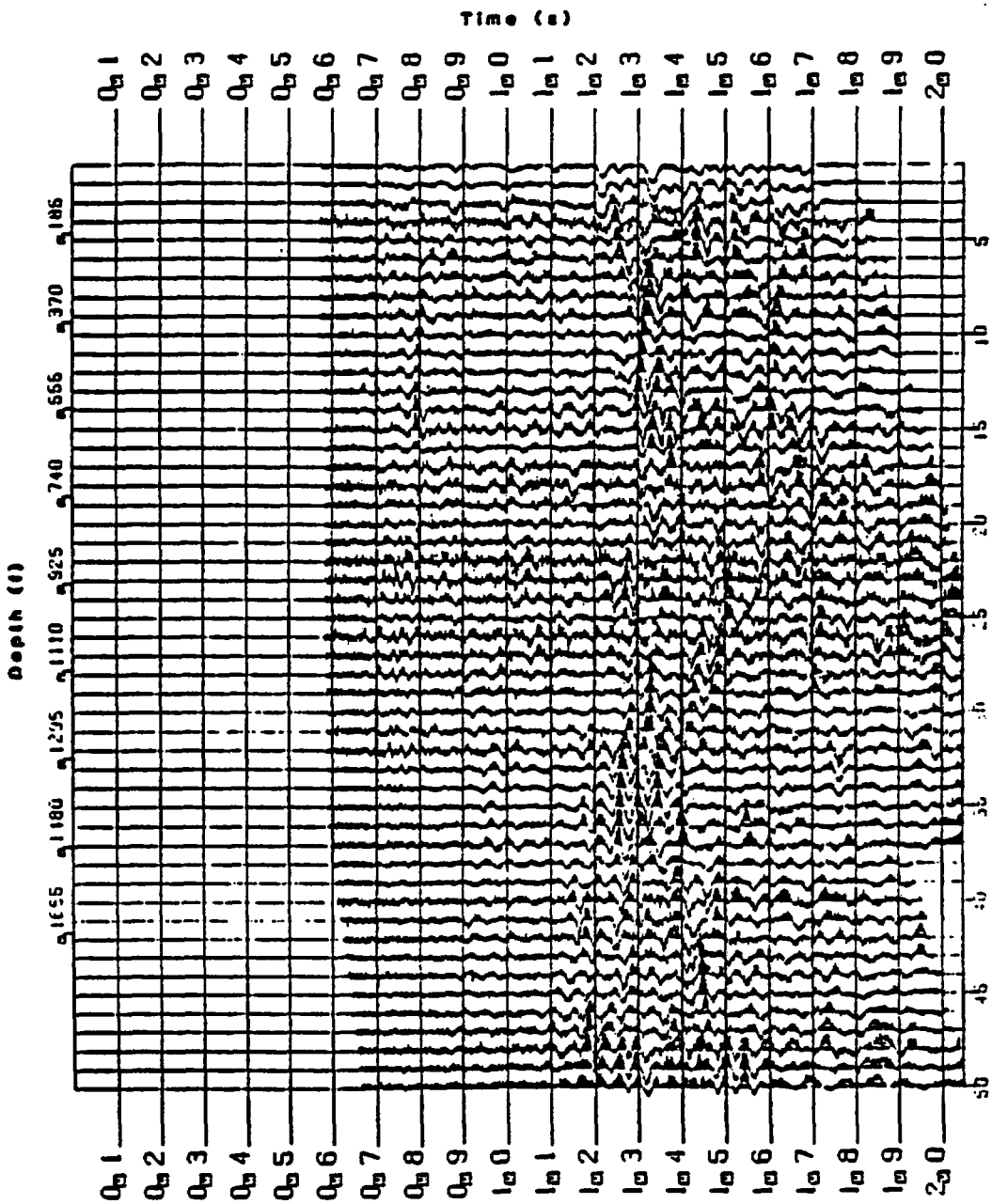

Figure 4.25. Data set in Figure 4.24 after removal of the direct p-wave, the direct s-wave, and the surface wave.

in Figure 4.26.

Very few identifiable upgoing reflections are seen in Figure 4.26. The traces were shifted toward zero time by 650 milliseconds and the FK filter in Figure 4.6 was applied to the data. The traces were transformed back into the time domain and shifted back to their proper time position. The data set is shown in Figure 4.27.

The reflected events are still very weak. Event (a) appears to be a reflection from n2. The event labeled (b) could be a reflection from n3, but it is not possible to positively identify the event. Finally, the event labeled (c) is almost certainly a reflection from the bottom of the model.

No fault plane reflections were identified on this data set.

4.7 6000-foot source offset VSP

In order to record a 5,120 sample trace at a 400 nanosecond sample interval for this offset, it was necessary to shift each trace by 500 milliseconds before recording. The direct p-wave does not arrive until 0.9 second, so no information is lost by shifting the traces.

Signal amplitude was very low at this offset, which made for a very noisy data set. Figure 4.28 shows the fifty traces which comprise this record. The direct p-wave (a) is

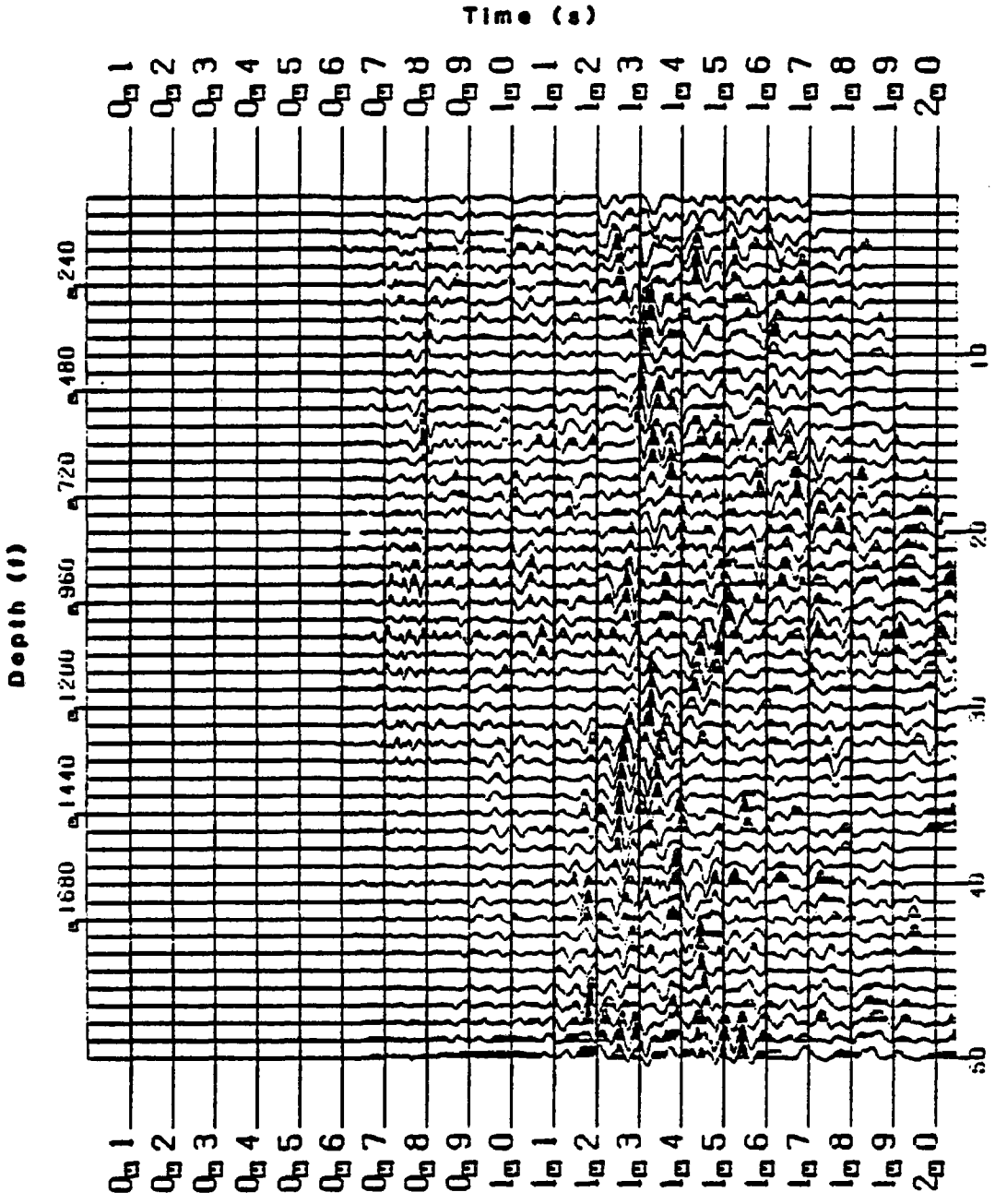

Figure 4.26. Data set in Figure 4.25 after application of a 100/12 low pass filter. The filter improved the quality of the data significantly, but no upgoing reflections can be positively identified.

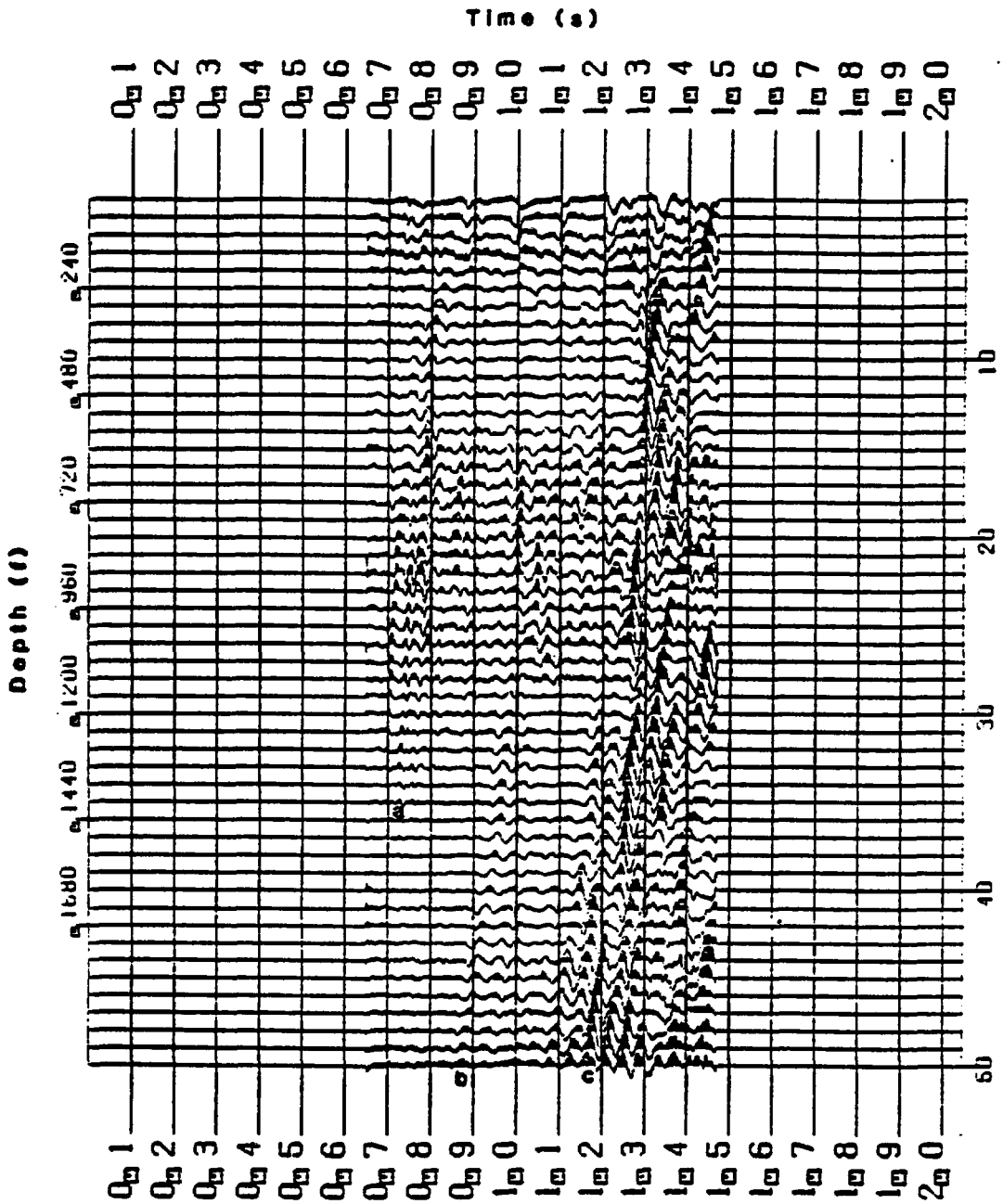

Figure 4.27. Data set for 5000-foot source offset after application of the FK filter in Figure 4.6. Reflections are seen from n2(a), n3(b), and from the bottom of the model (c). No fault plane reflections can be identified.

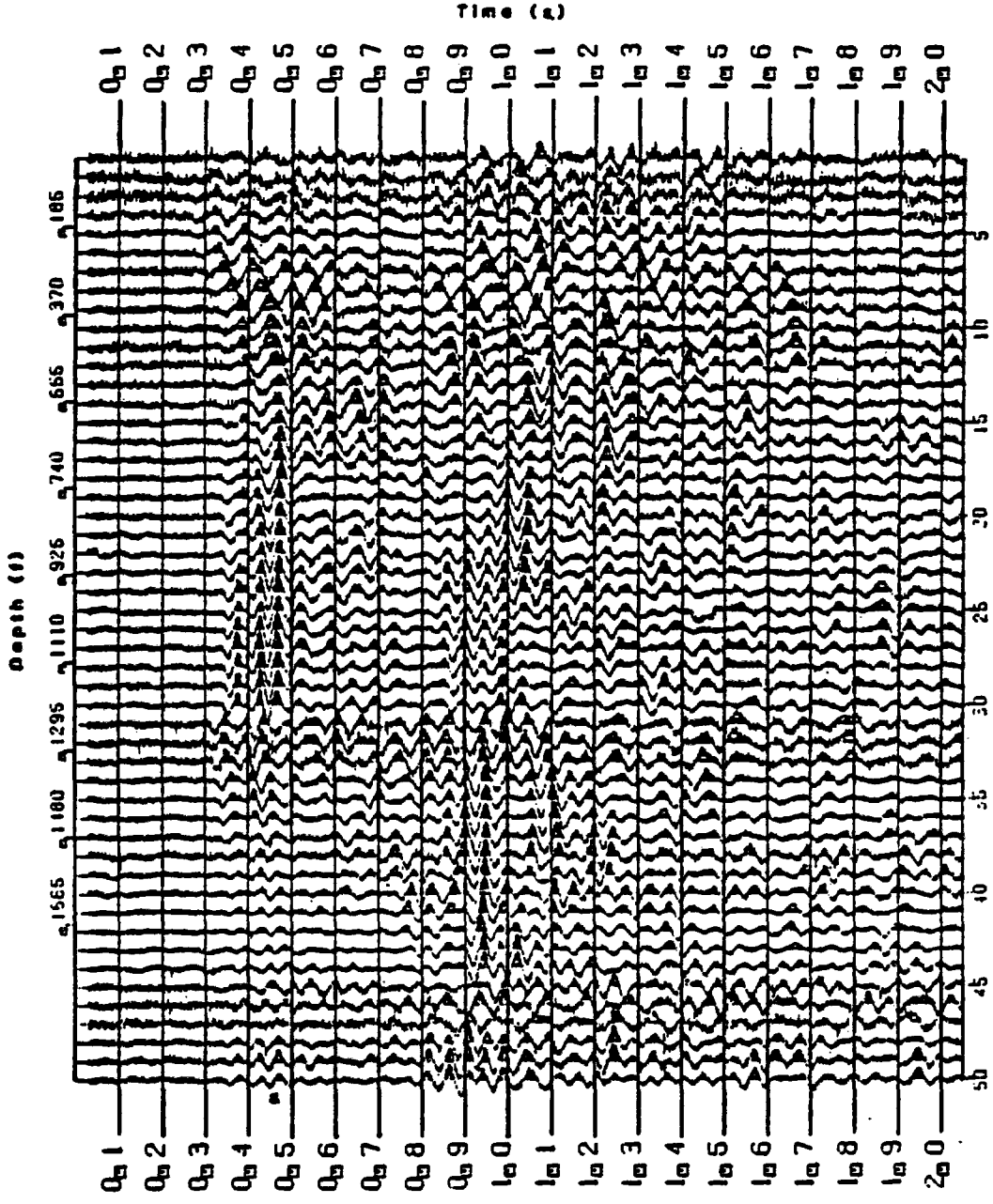

Figure 4.28. Data set recorded for a source offset of 6000 feet. The traces were shifted toward zero time by 500 milliseconds during recording. The direct p-wave (a) is difficult to see on all traces since the data are so noisy.

difficult to identify on every trace, although it is consistent on traces 14 through 30.

Since the direct p-wave is so inconsistent, aligning the event along a line of equal time was not performed. An FK filter was used to separate wavefields for this data set, without first using the median filter. For median filtering to be effective, accurate time picks are crucial. It is not possible to make the accurate time picks on this data set.

The FK filter was applied to the data set after using a 100/12 low pass filter to remove the high frequency noise. Figure 4.29 shows the data after application of the FK filter.

The only events which can be identified are the reflection from n2 (a) and from the bottom of the model (b). Even this interpretation is suspect. It is possible that no upgoing reflections can be identified for this offset.

4.8 7000-foot source offset VSP

Figure 4.30 shows the data set recorded for an offset of 6850 feet. Placing the transducer at 7000 feet was not possible for the reason mentioned in Chapter 3. A small stream valley appears at 7000 feet, and the V101 transducer is too wide to couple properly at this location.

As with the 6000-foot offset data set, these traces have been shifted toward zero time by 500 milliseconds. The

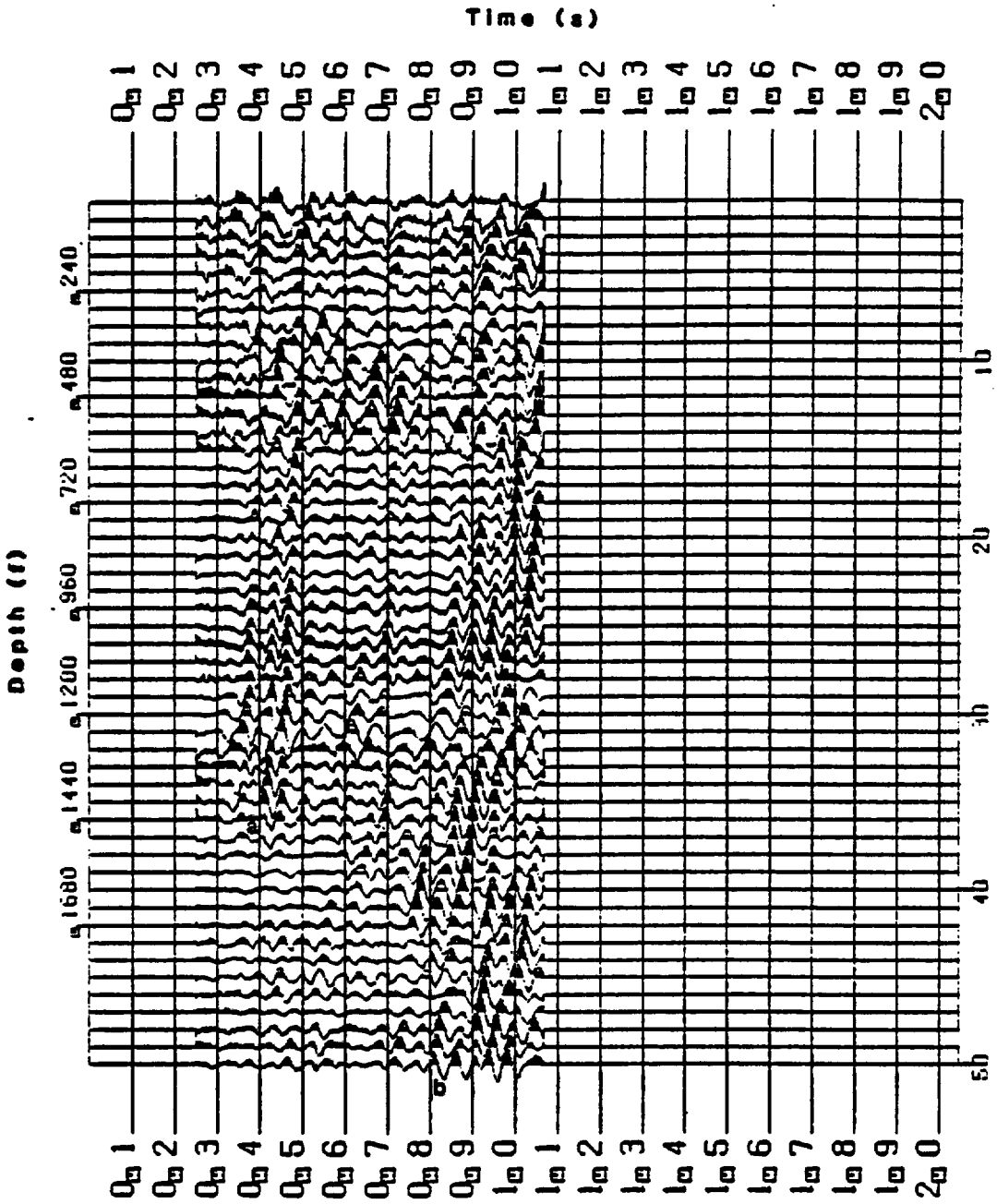

Figure 4.29. Data set for 6000-foot source offset after application of a 100/12 low pass filter and an FK filter to remove the downgoing energy present in the data. Event (a) appears to be a reflection from n2, although this interpretation is suspect. Event (b) is interpreted as the reflection from the bottom of the model.

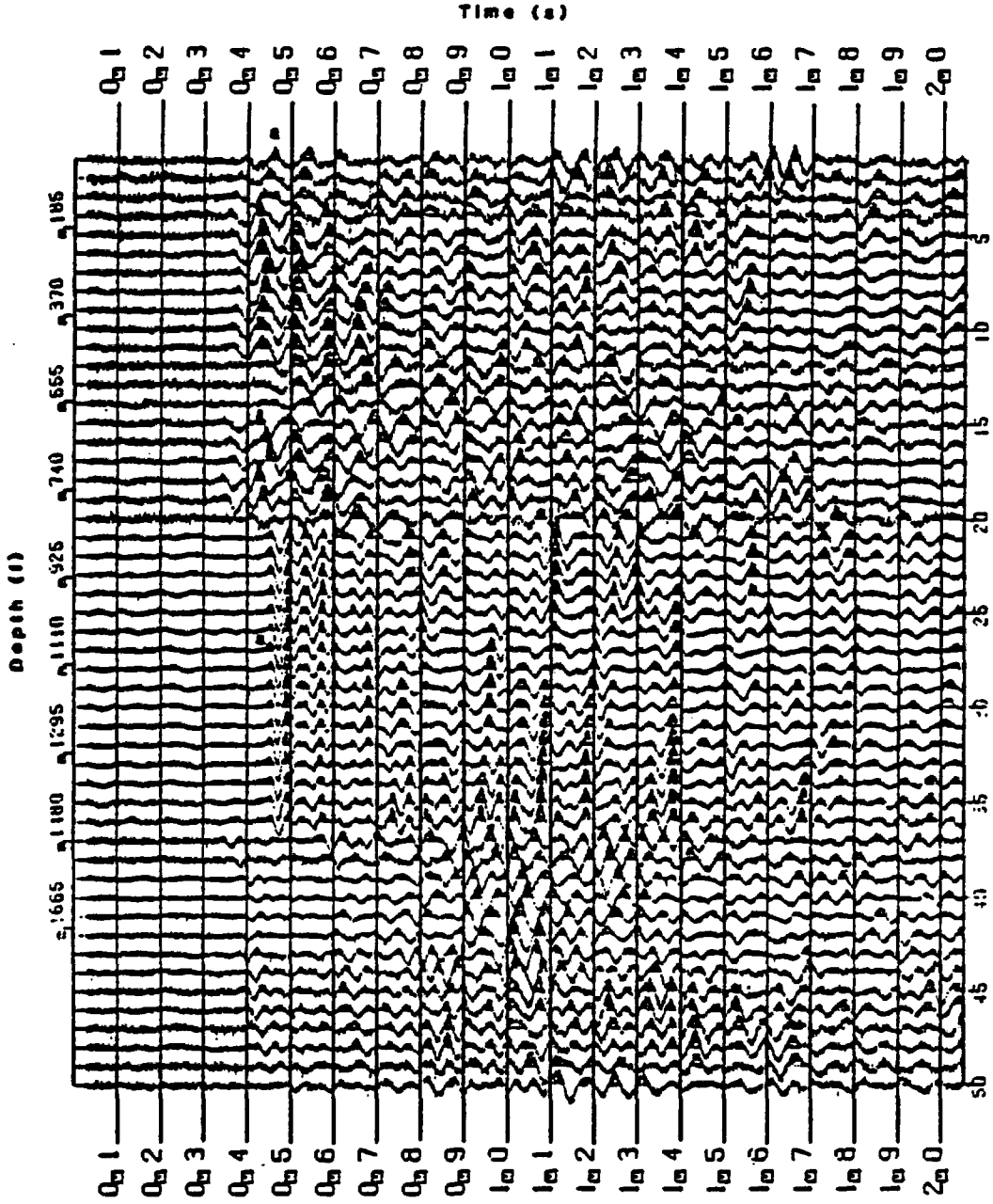

Figure 4.30. Data set recorded for a source offset of 7000 feet. Traces were shifted toward zero time by 500 milliseconds during recording. The direct p-wave (a) can be seen on several of these very noisy traces.

direct p-wave (a) can be clearly seen on traces 21 through 36. The event is not as obvious on the remaining traces. For this reason, median filtering was not used to remove the direct p-wave.

The data set was filtered with a 100/12 low pass filter to remove the high frequency noise. An FK filter was then applied to separate the upgoing and downgoing wavefields. The resulting data set is shown in Figure 4.31.

The upgoing wavefield contains a few coherent events, particularly on traces 20 through 38. The poor data quality on the remaining traces makes identification of the events very difficult, since no reflection can be seen merging with the direct arrival. No events are positively identifiable on this record.

4.9 8000-foot source offset VSP

The final data set recorded with this configuration of the recording system used a source offset of 8000 feet. The extremely noisy data set is shown in Figure 4.32. The data quality is so poor that even the direct p-wave can not be identified on this data set.

The data set was filtered using a 100/12 low pass filter to remove the high frequency noise. An FK filter was then applied to the traces to see if any upgoing energy existed in the data set. The resulting data set is shown in Figure

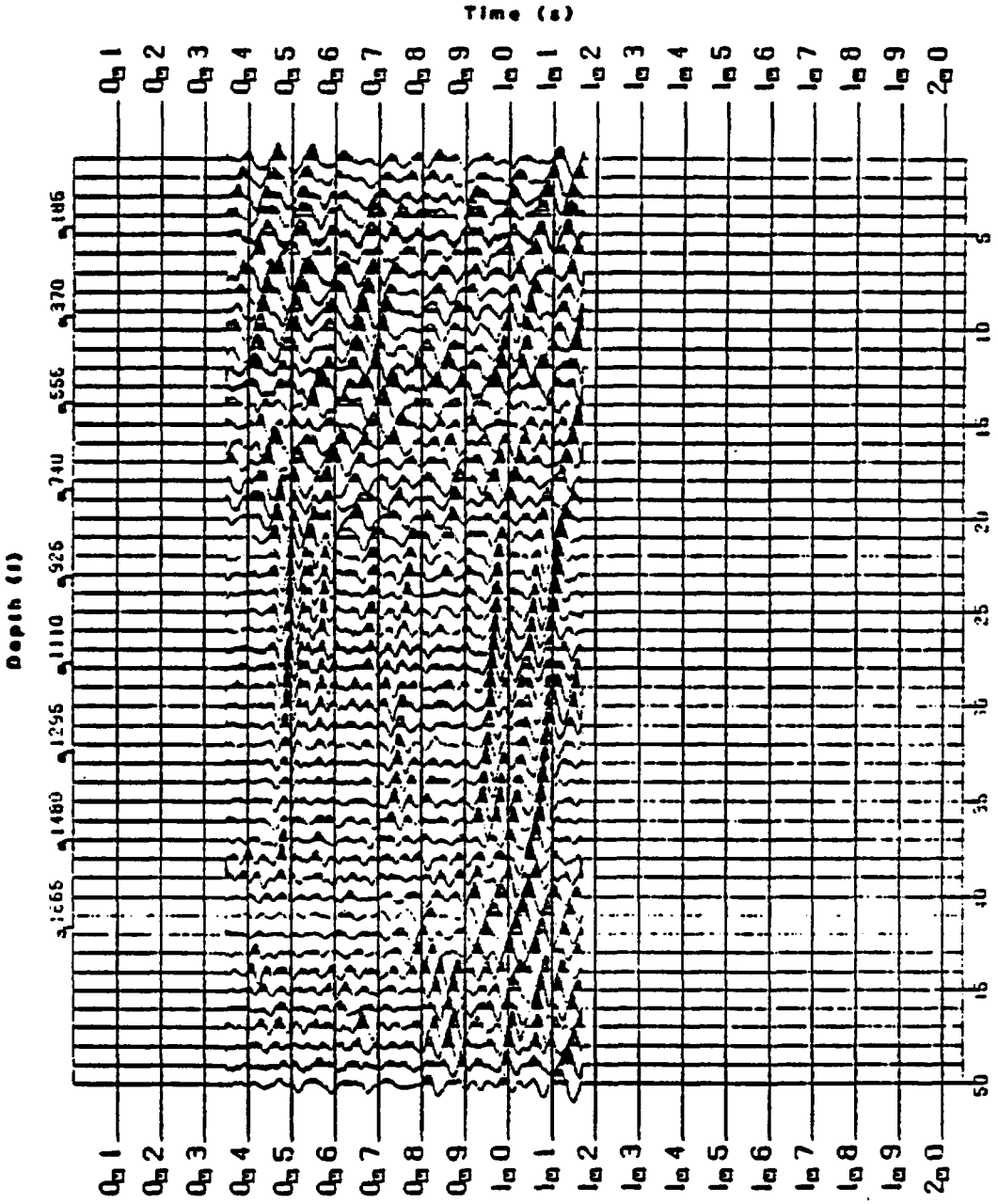

Figure 4.31. Data set for 7000-foot source offset after application of a 100/12 low pass filter and an FK filter to remove downgoing energy from the record. No coherent reflections merge with the direct arrival, and no positive identification of a reflection is attempted.

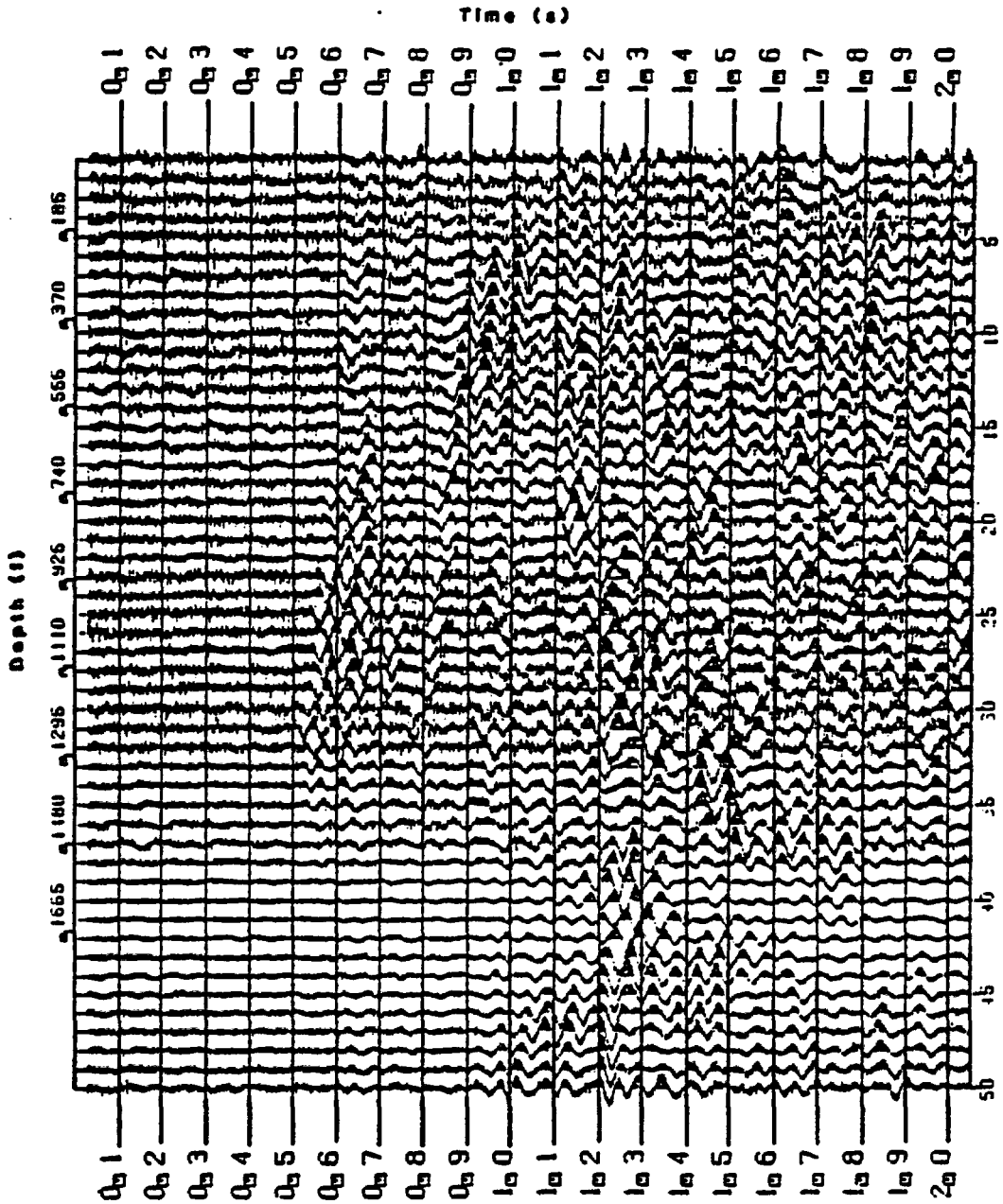

Figure 4.32. Data set recorded for a source offset of 8000 feet. The traces were shifted toward zero time by 500 milliseconds during recording. No coherent downgoing events can be identified on this noisy record.

4.33.

Surprisingly, the data set in Figure 4.33 does contain a few coherent upgoing events. The reflection labeled (a) appears to originate at trace 35, suggesting that it is a reflection from n2. The slope of the event suggests that it is a p to s converted reflection, but that can not be substantiated.

No other events can be positively identified in this data set.

4.10 An additional recording configuration

The acquisition of new electronic equipment during the Summer of 1988 allowed the recording of additional traces from the variable velocity model. A new pair of source and receiver transducers was used to record two additional data sets. PANAMETRICS V133 transducers were used as a source and as a receiver. The transducers are only 1/4 inch in diameter and have a center frequency of 5,000,000 hz. It is possible to send much higher frequency signals into the model using these transducers.

A new device for pulsing the source transducer was acquired from PANAMETRICS, a PANAMETRICS 5055 pulser/receiver. This unit was substituted for the GENERAL RADIO pulse generator and power amplifier in Figure 4.1. The PANAMETRICS unit was able to supply a higher voltage to the transducer

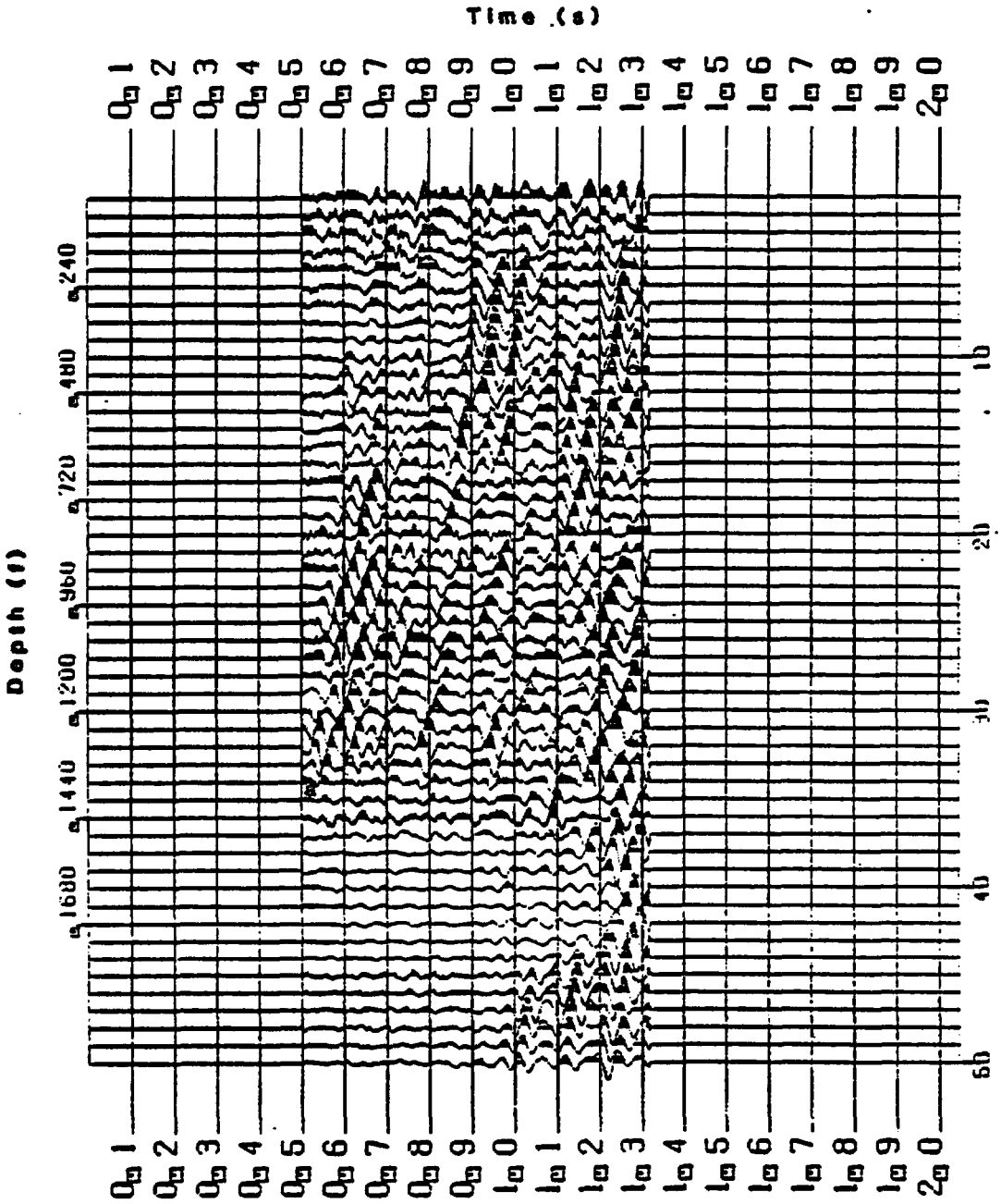

Figure 4.33 Data set for 8000-foot source offset after application of a 100/12 low pass filter and an FK filter to remove downgoing energy from the data set. The event labeled (a) is interpreted to be a p-s reflection from n2.

than was the power amplifier.

The PANAMETRICS unit also served as a 40 db gain amplifier for the receiver transducer. Since the HP gain amplifier could now be removed from the acquisition system, the primary source of 60 hz noise was gone. The 50,000-1,600,000 hz bandpass filter was also removed from the acquisition system since the 60 hz problem had been eliminated. In effect, the PANAMETRICS pulser/receiver replaced four of the boxes in Figure 4.1. Output from the PANAMETRICS amplifier was fed directly to the digitizing oscilloscope and the waveforms were recorded.

4.11 1000-foot source offset VSP

Fifty traces were recorded using the small V133 transducers for a source offset of 1000 feet. Figure 4.34 shows the recorded data set. For all of the advantages provided by the PANAMETRICS pulser/receiver, there was also a major disadvantage. Cross-feed into the amplifier output caused a noise burst to appear on the output channel that was synchronized with the triggering pulse. The noise burst can be seen on Figure 4.34, aligned at zero time. The burst has a tail (a) which lasts for 300 milliseconds (scaled down to real time, the tail is only 300 microseconds in length).

This data set contains dozens of spikes that are distributed randomly on the traces. Actually, the spikes do

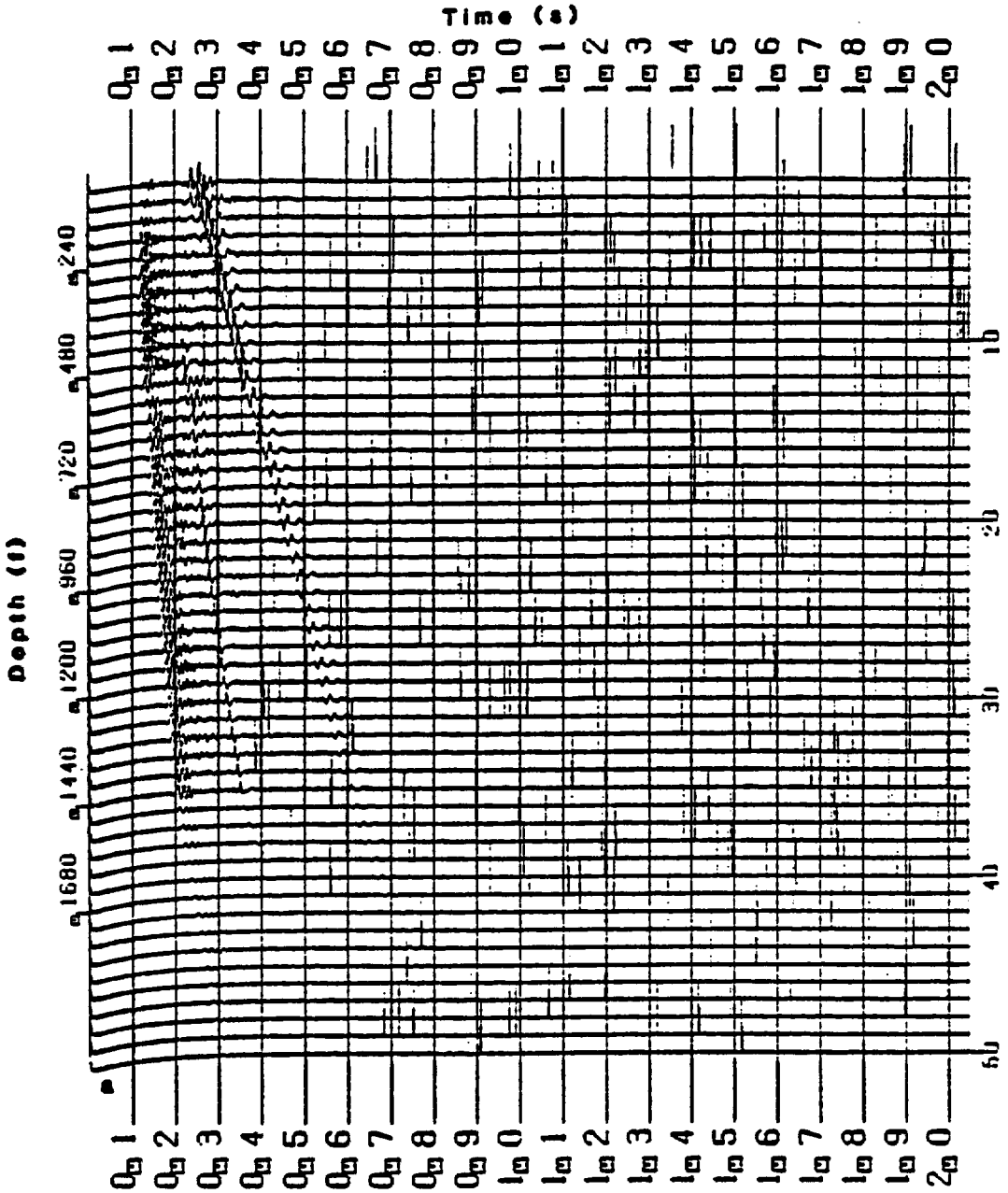

Figure 4.34. Data set recorded for a source offset of 1000 feet using the PANAMETRICS 5055PR pulser/receiver. The noise burst is seen as the spike aligned along the zero time line. The noise burst has a tail (a) which lasts out to 0.3 second on this scaled data set. The dozens of randomly appearing spikes on the traces are caused by the electrostatic plotter and are not actually in the data set.

not appear in the data. Interactive processing on graphics terminals did not show the spikes, which appear only on plots from the electrostatic plotter. In fact, the spikes only appeared when plotting the initial data set that was transferred to the GOULD from the VAX. The spikes disappear after additional processing is done on the data set. There may be a minor flaw in the programs which send the traces from one mainframe to the other that causes these spikes on the paper plots. Since the spikes do not actually exist on the traces the problem is harmless.

Since the noise bursts were perfectly aligned on the zero second time line, it was possible to apply a median filter to the data to remove the events. A 17-fold spatial median filter was used for the separation. The filtered data set appears in Figure 4.35. Traces recorded at depth levels 35 through 50 are very noisy compared to the remainder of the record. These traces were recorded with the receiver coupled to LEXAN instead of PLEXIGLAS.

Figure 4.35 shows that the noise burst was largely removed by the median filtering. However, since the amplitude of the signal was very low to begin with, removing the high amplitude noise spike made the data appear much noisier. A 100/12 low pass filter was applied to the data set. The resulting traces are shown in Figure 4.36.

The three major downgoing events are now clearly seen.

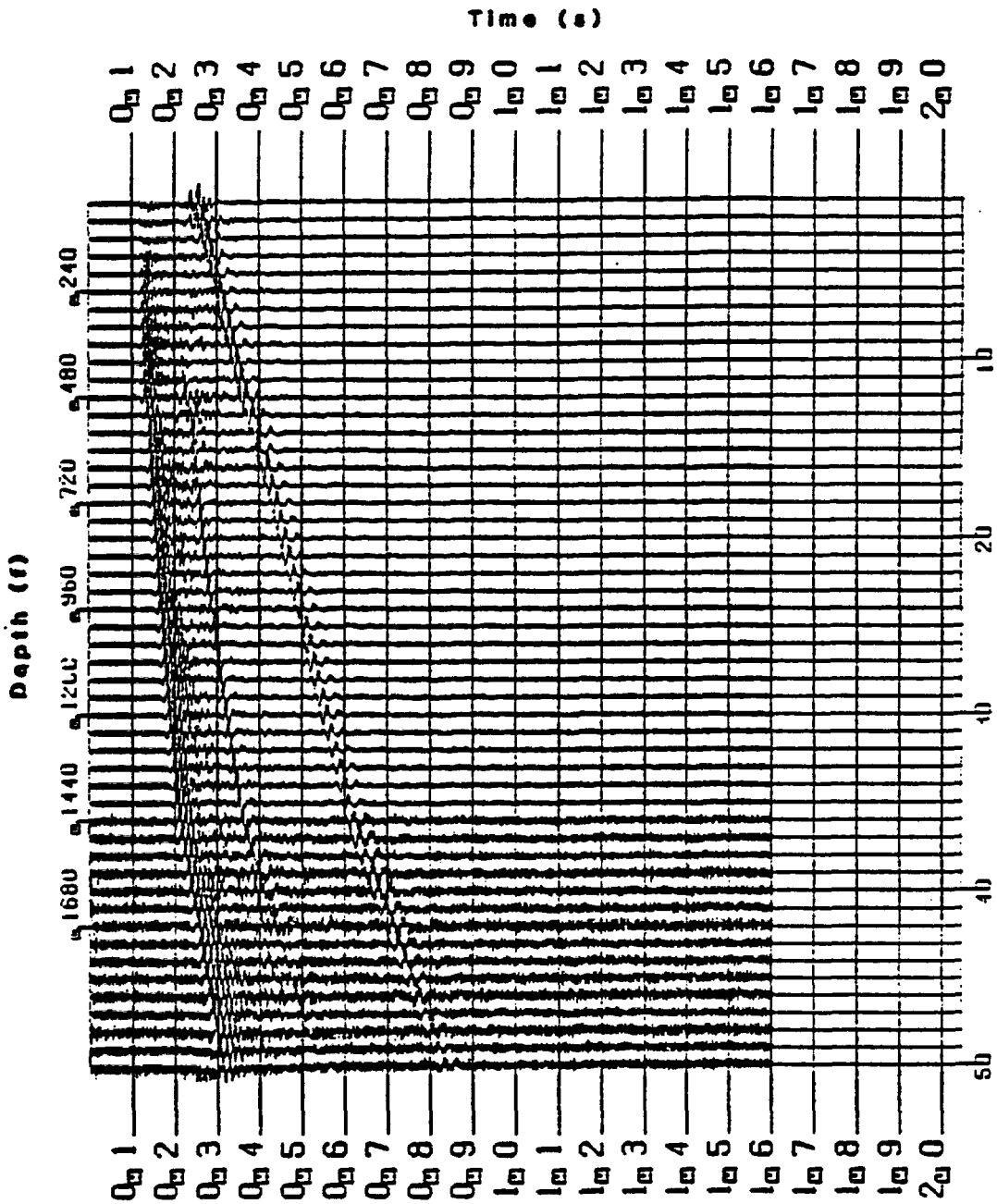

Figure 4.35. Data set in Figure 4.34 after application of a 17-fold median filter to remove the noise burst.

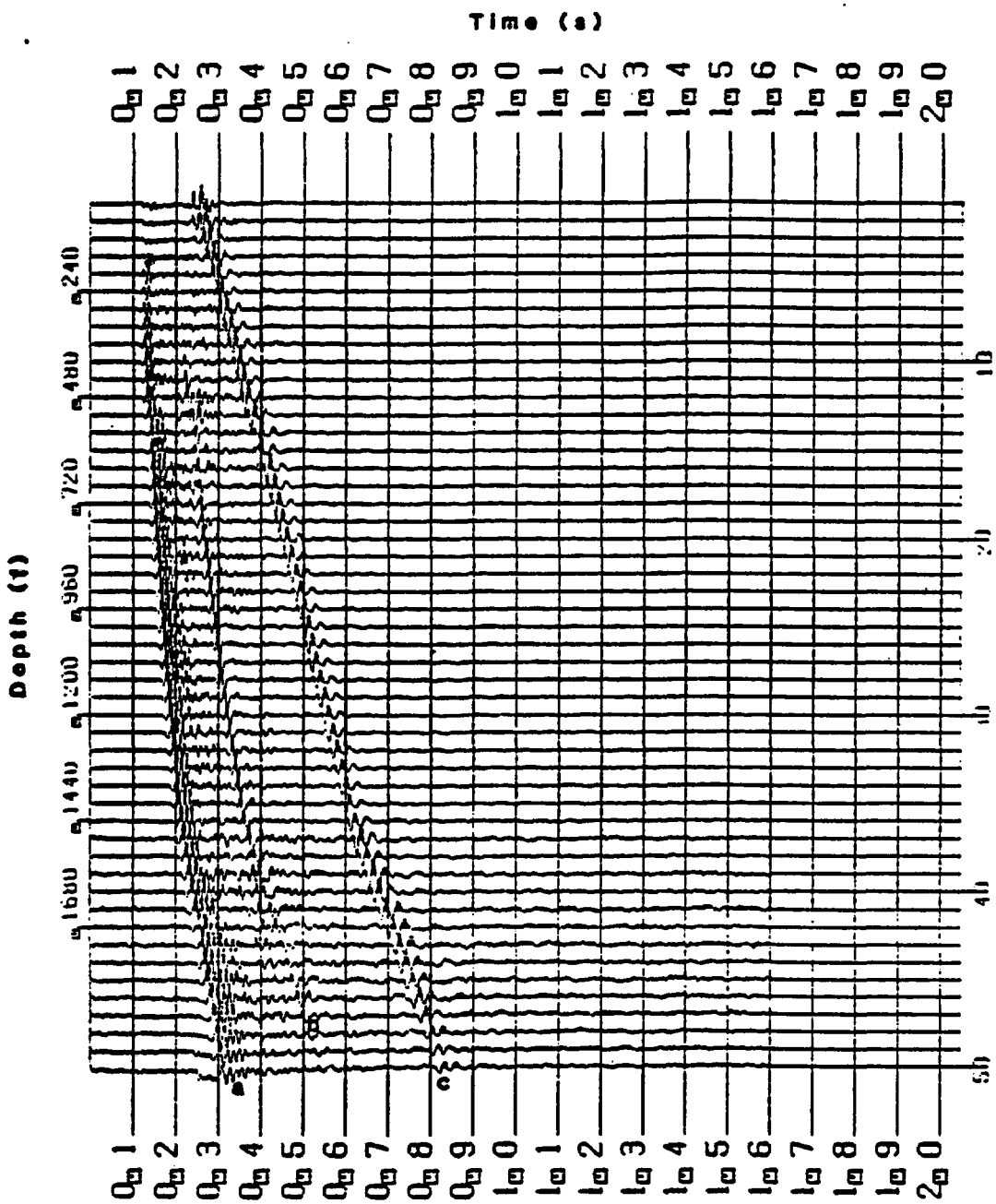

Figure 4.36. Data set in Figure 4.35 after application of a 100/12 low pass filter to remove the high frequency noise. The three major downgoing events are now clearly seen. The direct p-wave (a), the direct s-wave (b), and the surface wave (c) can be identified.

The direct p-wave (a) is a very ringy event, which is somewhat discouraging. The direct s-wave (b) is seen as a much sharper pulse on traces 9 through 46. The surface wave (c) is very consistent on every trace. The slopes of all three events change at trace 36 as the events enter the lower velocity LEXAN.

The downgoing events were aligned along lines of equal time and removed by median filtering. Figure 4.37 shows the data set after removing the direct p-wave. The direct s-wave (a) and the surface wave (b) dominate the data set. The median filter was not completely effective in removing the direct p-wave, particularly on traces 36 through 50.

Figure 4.38 shows the data set after the removal of the surface wave. The median filter was considerably more effective in removing this event. Only the direct s-wave (a) remains on the record.

The direct s-wave was also removed by median filtering. The data set is shown in Figure 4.39. Unfortunately, the data are still so noisy that no upgoing reflections can be identified. The FK spectrum of the record is shown in Figure 4.40. A filter was designed to remove all energy in the left-hand plane. The resulting spectrum is shown in Figure 4.41.

Figure 4.42 shows the record after application of the FK filter. The data set is strangely devoid of identifiable

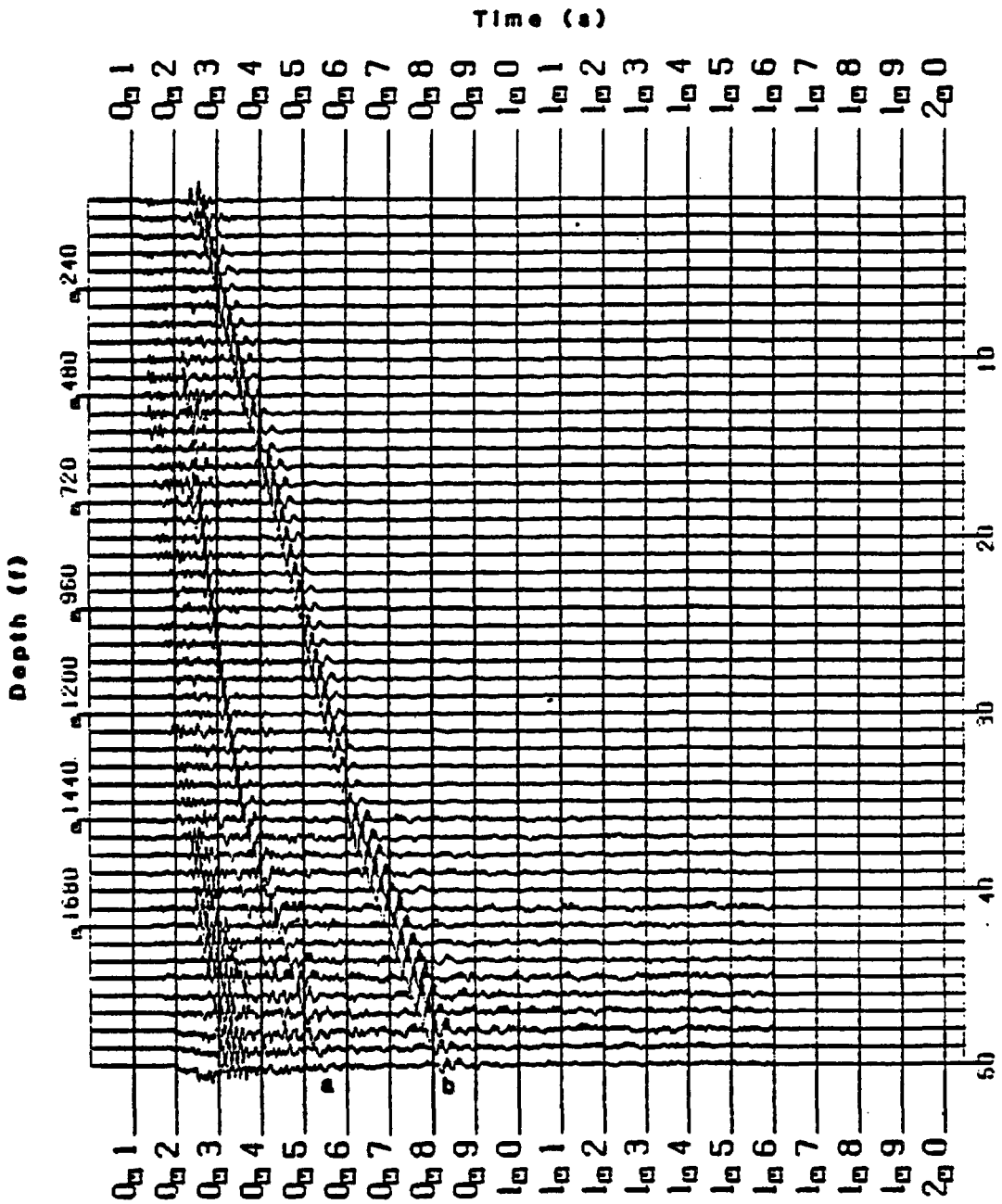

Figure 4.37. Data set in Figure 4.36 after removal of the direct p-wave by median filtering. The filter did a poor job of removing the ringy arrival on the deeper traces. Event (a) is the direct s-wave and event (b) is the surface wave.

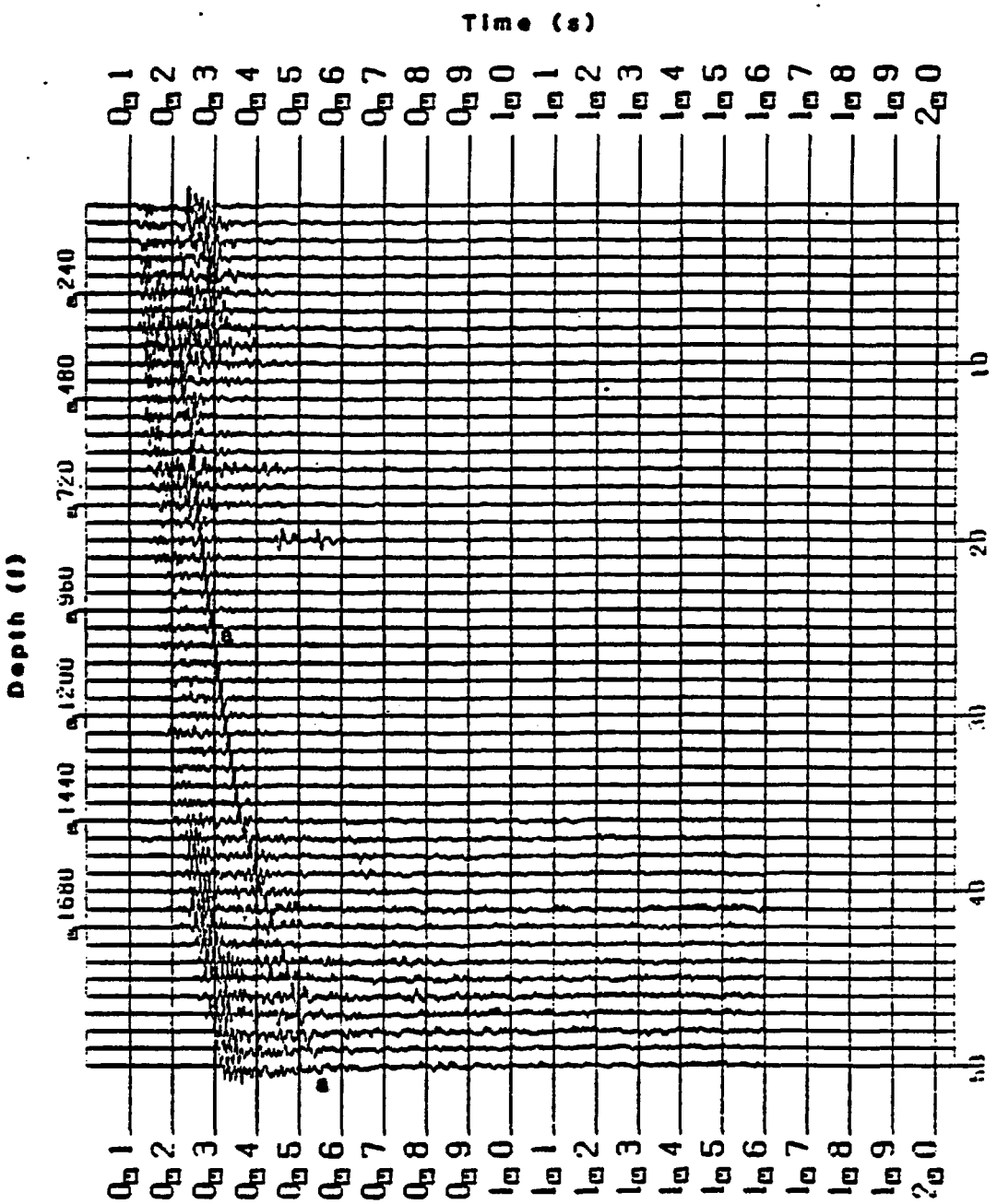

Figure 4.38. Data set in Figure 4.37 after removal of the surface wave by median filtering. The median filter was much more effective in removing the surface wave than it was in removing the direct p-wave. Event (a) is the direct s-wave.

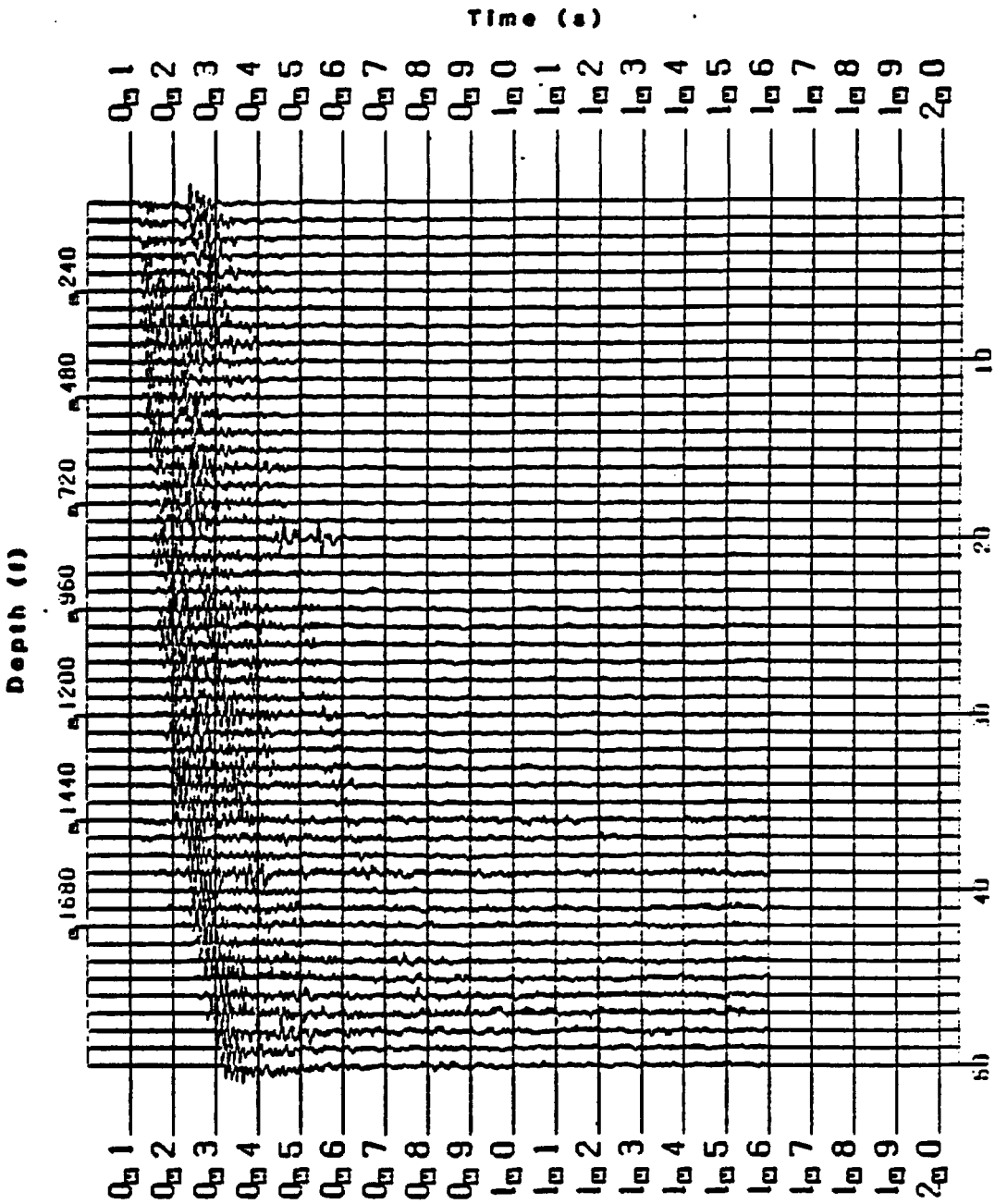

Figure 4.39. Data set in Figure 4.38 after removing the direct s-wave by median filtering. The resulting upgoing wavefield is still extremely noisy and no upgoing reflections can be identified.

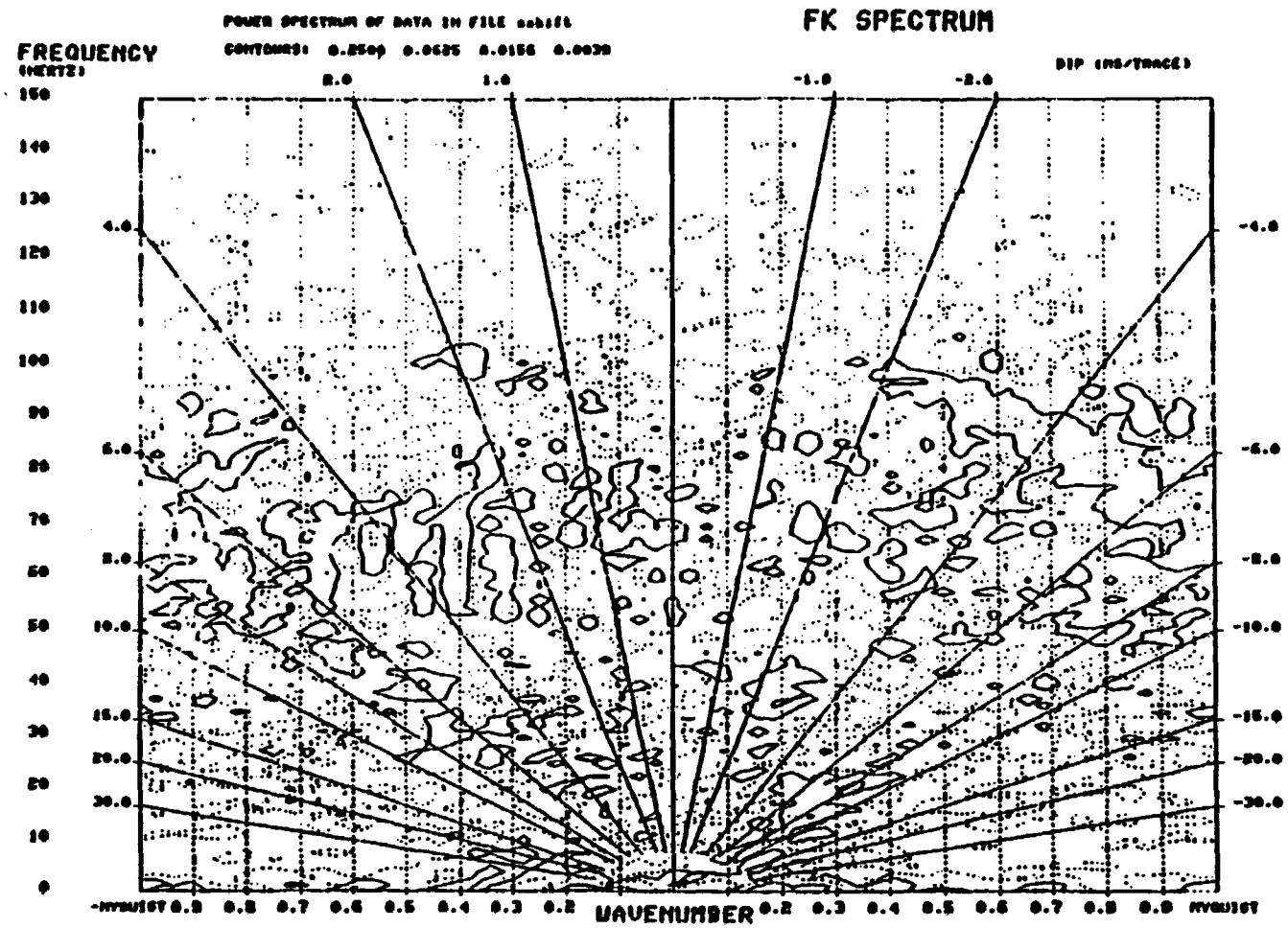

Figure 4.40. FK spectrum of the data set in Figure 4.39. Upgoing energy appears in the right-hand plane. Downgoing energy appears in the left-hand plane.

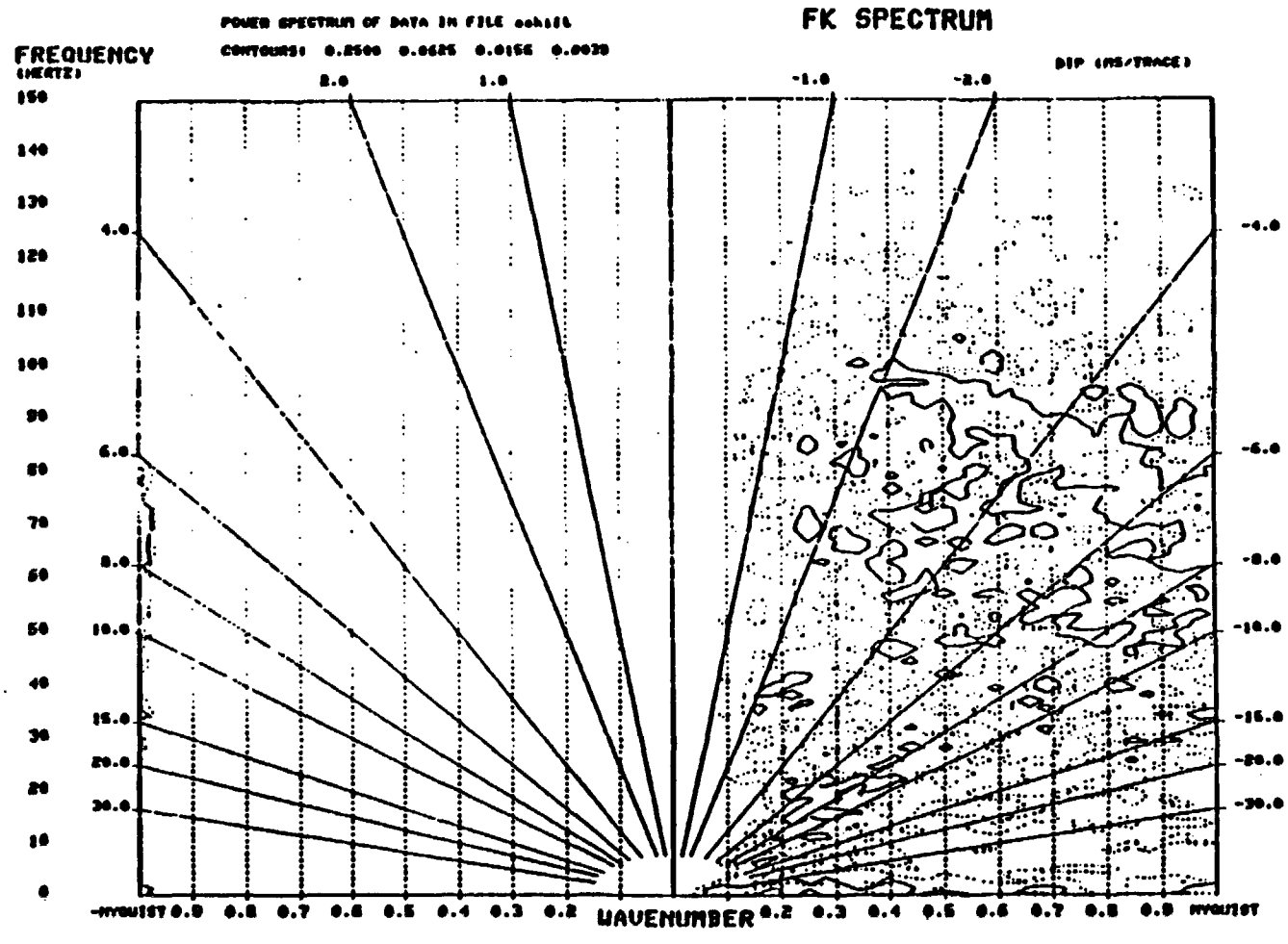

Figure 4.41. FK spectrum of the data set in Figure 4.39 after application of an FK filter to remove energy in the left-hand plane of the diagram.

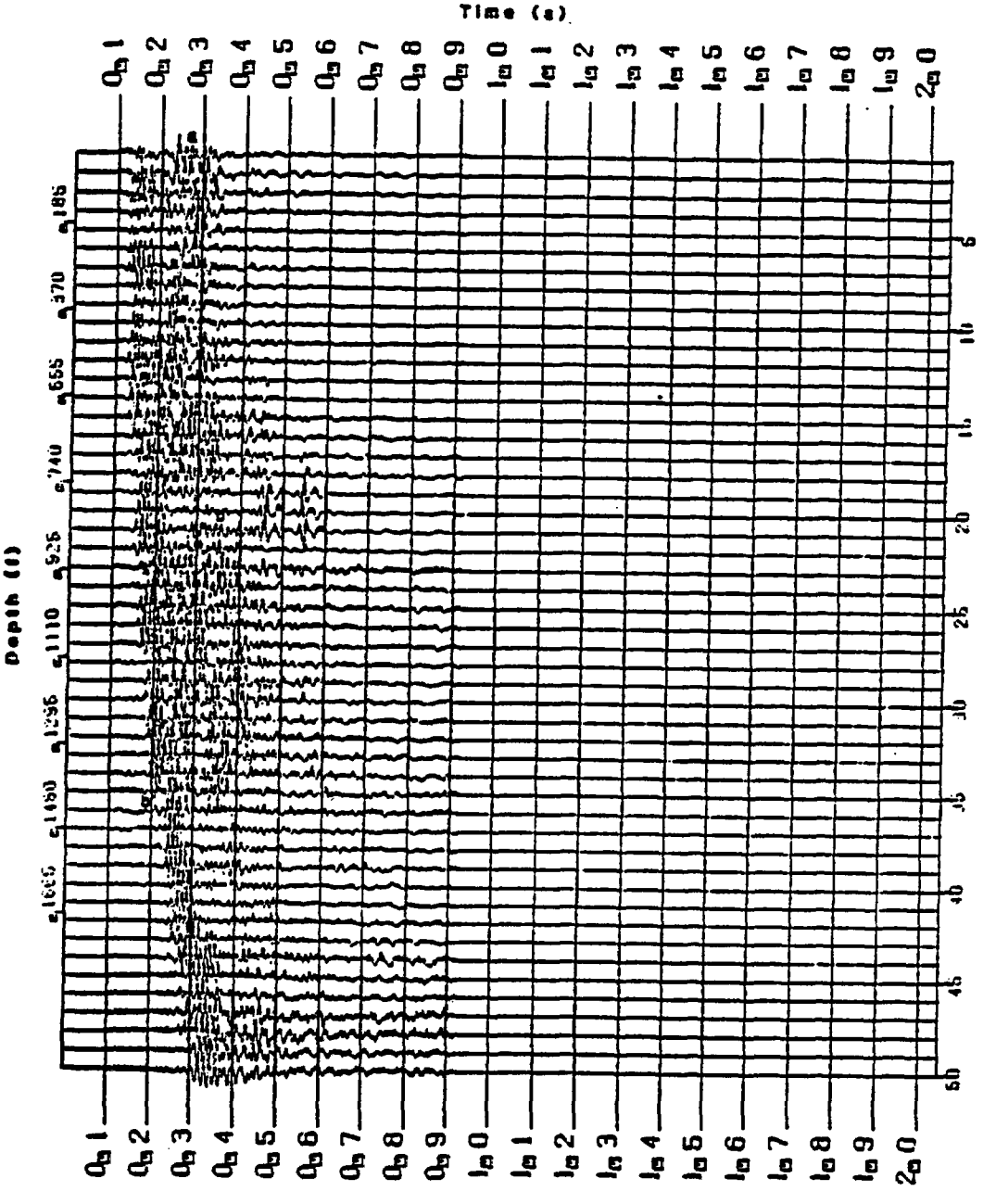

Figure 4.42. Data set for a source offset of 1000 feet after application of the FK filter. The event labeled (a) appears to be an s-s reflection from n1. Event (b) originates at trace 35 and is interpreted as a p-s converted reflection from n2.

upgoing reflections. The event labeled (a) appears to be an s-s reflection from n1. The p-wave reflection can not be identified.

Only one other upgoing reflection is seen on this data set. Event (b) is a reflection which originates at trace 35. It appears to be a p to s converted reflection from horizon n2.

The major obstacle to seeing more upgoing reflections is the high amplitude of the direct p-wave residue left after median filtering. The poor job of removing the event is possibly due to the removal of the noise burst at the beginning of the processing. If a portion of the direct p-wave arrivals was lost during the median filtering of the noise burst, it is possible that the shape of the arrivals changed enough to effect the median filtering of the direct p-wave. If the arrivals are not sufficiently consistent from trace to trace, median filtering is not very effective.

4.12 2000-foot source offset VSP

The final VSP data set collected from the physical model was recorded using the small transducers and a source offset of 2000 feet. The data set appears in Figure 4.43. As seen in the previous data set, the noise burst appears aligned along the zero second time line. The tail on the noise burst (a) is seen to last 300 milliseconds on the record.

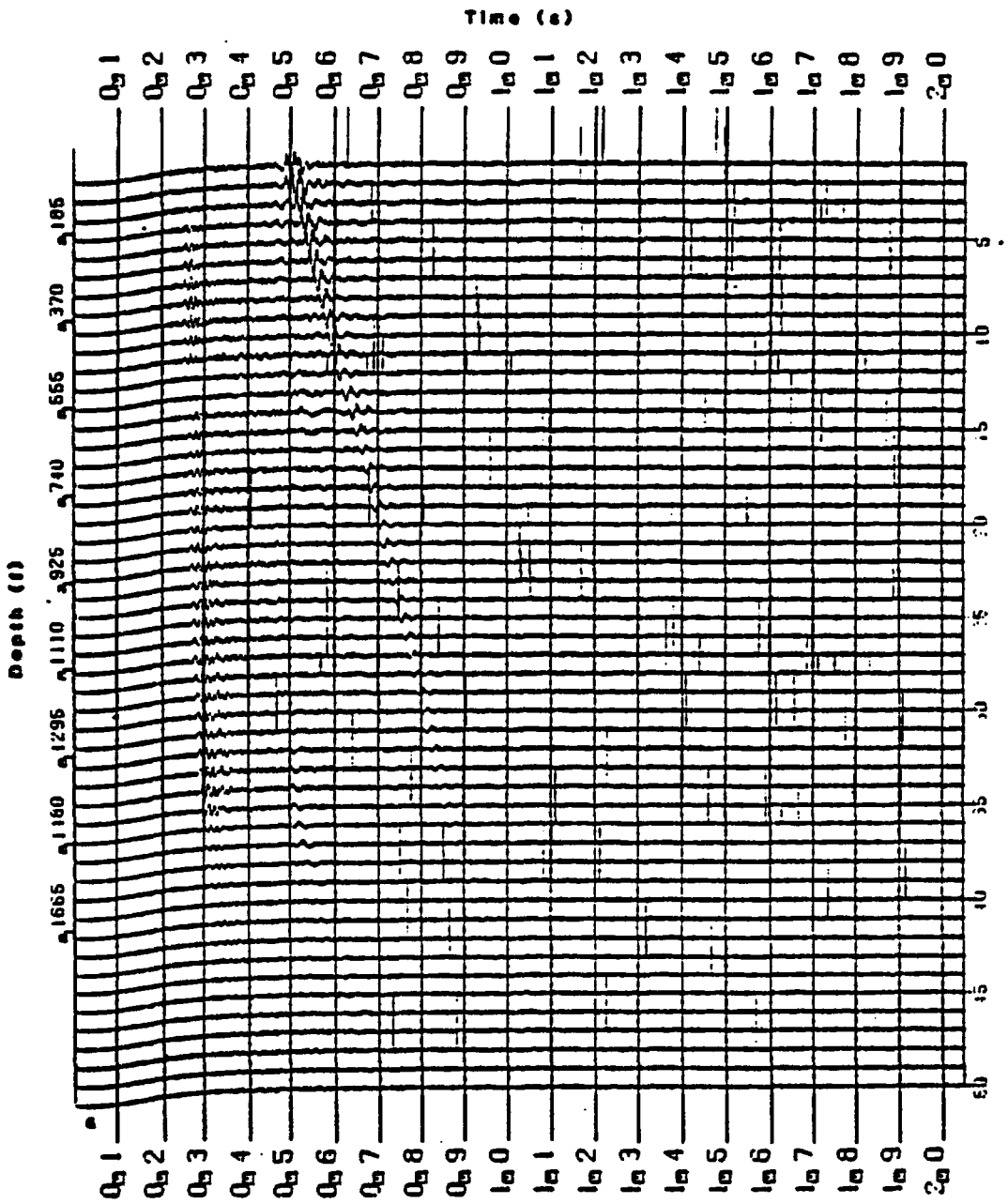

Figure 4.43. Data set recorded for a source offset of 2000 feet using the PANAMETRICS 5055PR pulser/receiver. The noise burst is aligned at zero time and the tail (a) is seen to extend out to 0.3 second. Once again, the numerous random spikes on the traces are due to the electrostatic plotter and do not actually appear in the data set.

Also, the phantom spikes that appeared on Figure 4.34 are seen on this diagram. The spikes are a function of the plotter, and do not actually exist on the traces.

A 17-fold median filter was used to remove the noise burst from the data set. The result is shown in Figure 4.44. The noise burst was largely removed from what is now an extremely noisy data set. A slight bow appears on the deepest traces between 0.0 and 0.3 second, suggesting that the median filtering was not quite as effective on the last traces of the data set.

A 100/12 low pass filter was applied to this data set to remove the high frequency noise. The resulting data set is shown in Figure 4.45. The major downgoing events are now clearly visible. The direct p-wave (a) is best seen on traces 10 through 50, although it appears on every trace. The direct s-wave appears to split into two waves at trace 36, as was seen earlier in the chapter. Event (b) is an s to p converted wave, while event (c) is the direct s-wave. The difference in slope of the two events supports this interpretation. The surface wave (d) is the most consistent event on the entire data set and is seen on every trace except trace 50.

The major downgoing events were aligned and removed from the data by median filtering. The resulting upgoing wavefield is shown in Figure 4.46. Several coherent reflections

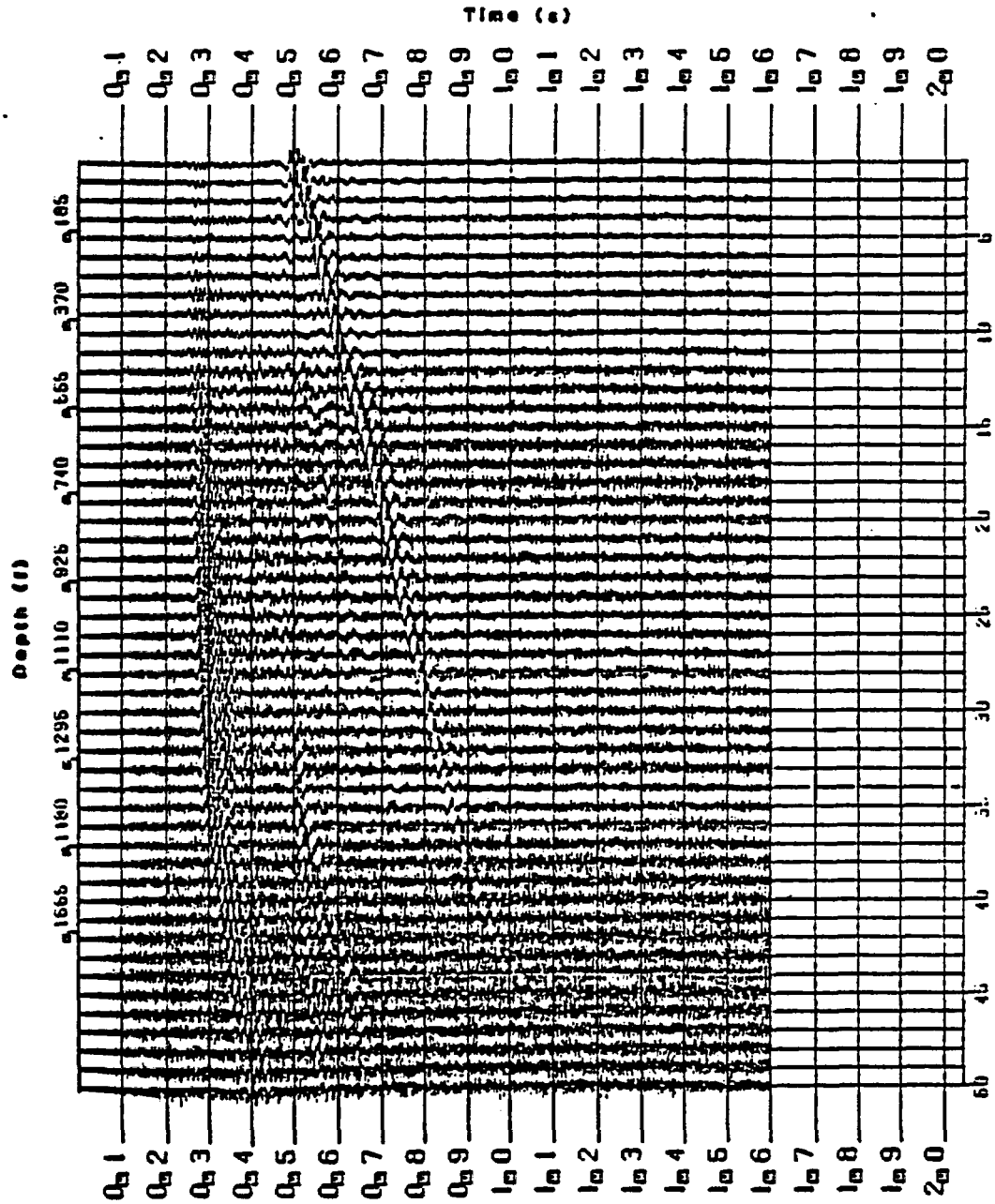

Figure 4.44. Data set in Figure 4.43 after application of a 17-fold median filter to remove the noise burst.

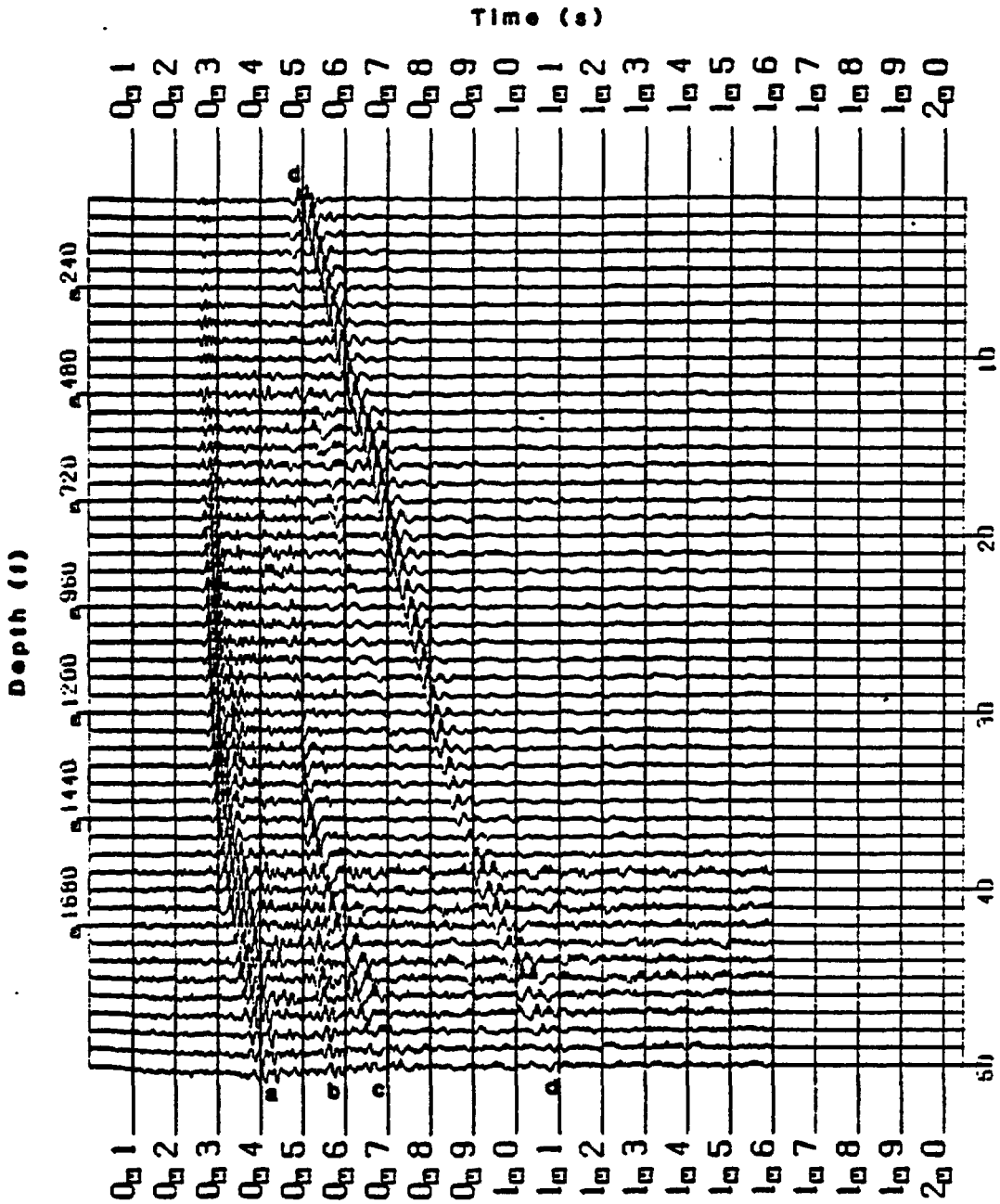

Figure 4.45. Data set in Figure 4.44 after application of a 100/12 low pass filter to remove the high frequency noise. The major downgoing events can be identified. Event (a) is the direct p-wave. Event (b) is the s to p converted wave, which is seen to originate at trace 36. Event (c) is the direct s-wave. Event (d) is the surface wave.

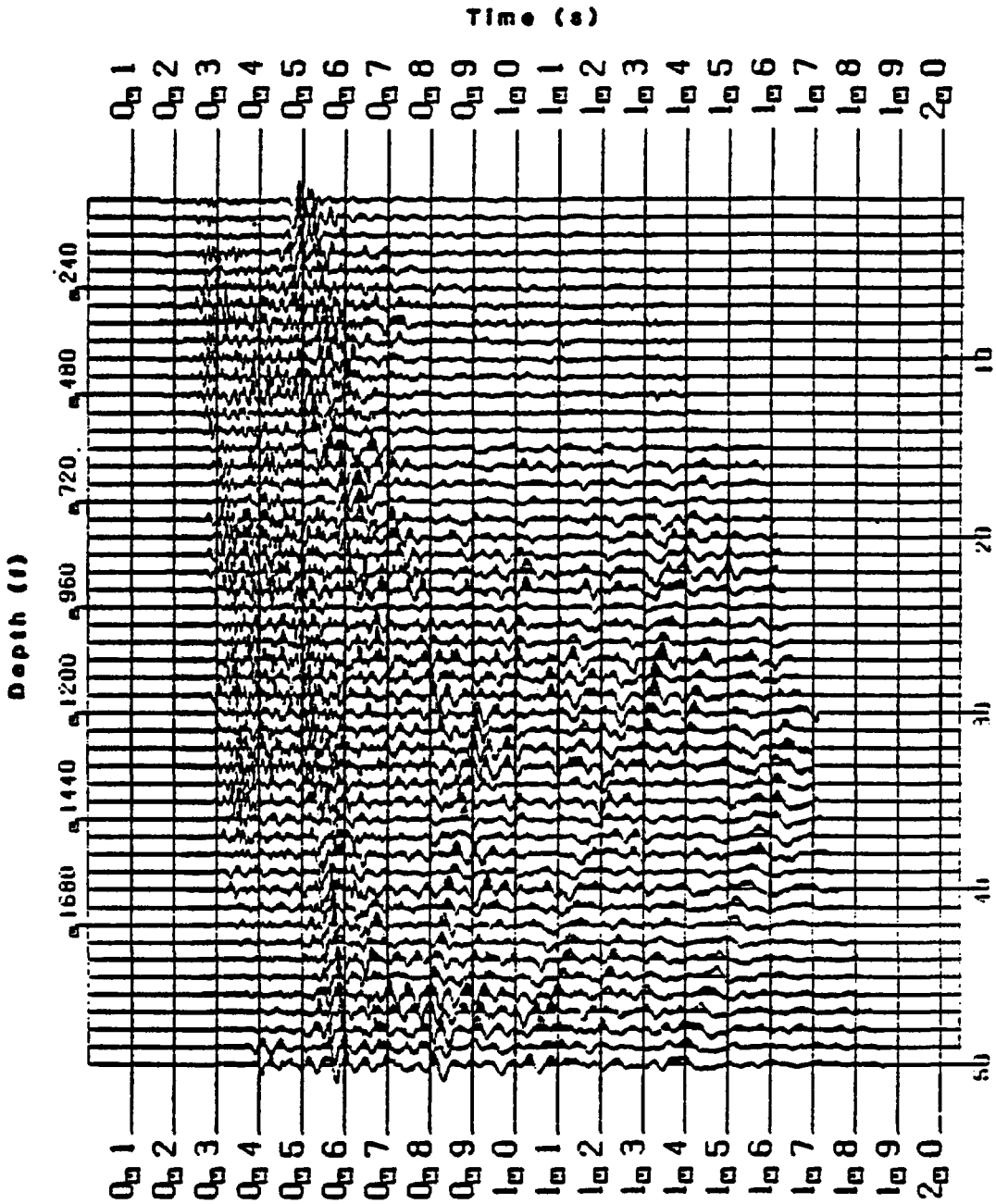

Figure 4.46. Data set in Figure 4.45 after removal of the direct p-wave, the direct s-wave, and the surface wave. Several coherent reflections are seen, but they are difficult to identify.

can be seen on this data set, although the events are difficult to identify. An FK filter was applied to the data to remove any remaining downgoing energy in the record. The resulting data set is shown in Figure 4.47.

Several upgoing reflections can now be identified. Event (a) is the p-wave reflection from horizon n1. The event is difficult to see through the noise, but the event certainly exists. Event (b) is the reflection from n2, and is seen to originate at trace 35. The slope of the event suggests that it is an upgoing p-wave.

The event labeled (c) is very distinct on traces 40 through 50. The event is interpreted to be a reflection from n3. The event labeled (d) is interpreted to be the reflection from the bottom of the model. Due to the limitations on trace length in the FK filtering module of VSEIS, the two strong reflections appearing later than 1.0 second on Figure 4.46 were removed from the record.

The quality of this data set is extremely good compared to the data set using a 1000-foot source offset. On that data set, the reflected events generally arrived so soon on the record that they were obliterated by the ringy direct p-wave. That was not a problem on this data set and the data provided many interpretable events.

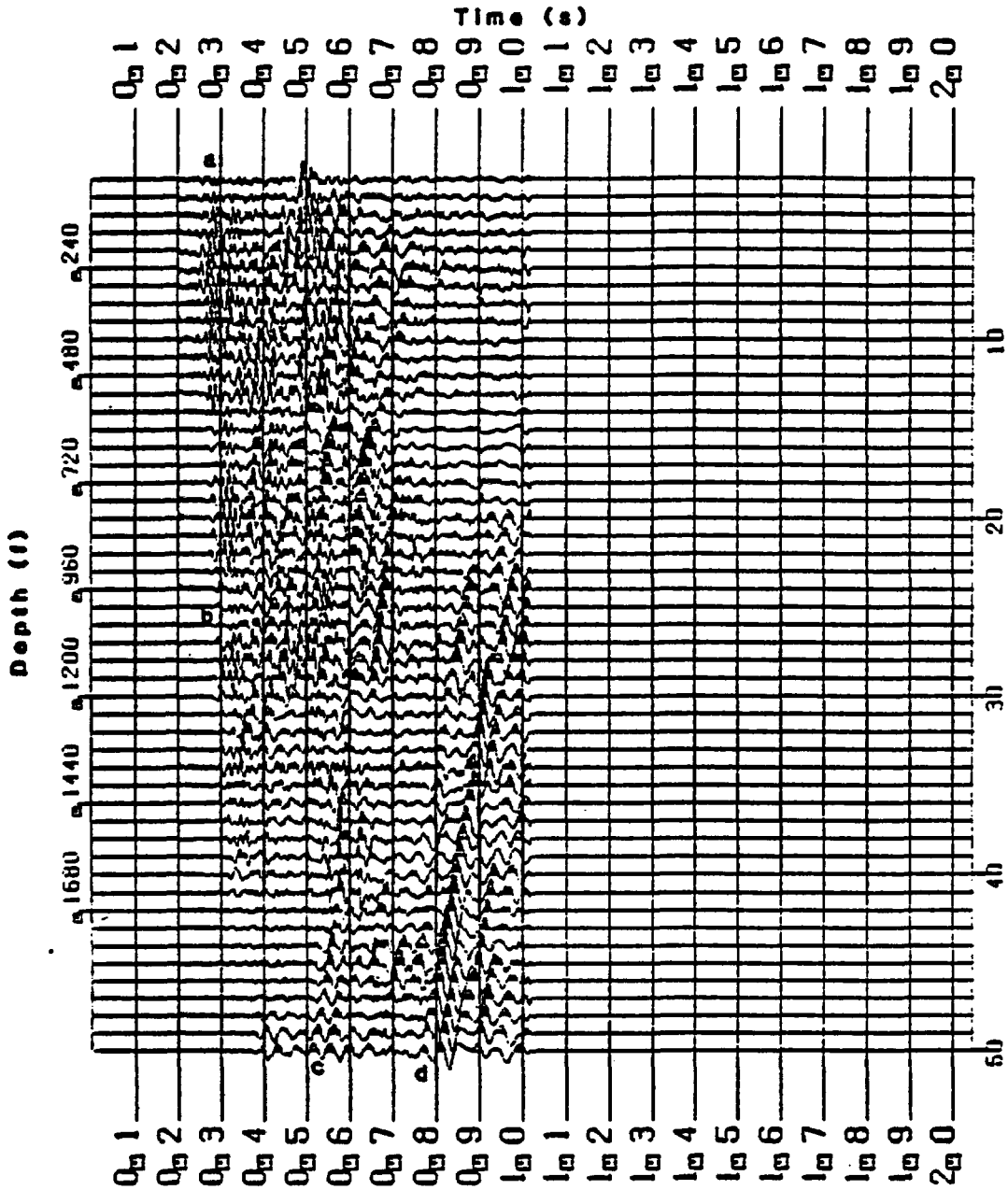

Figure 4.47. Data set for 2000-foot source offset after application of an FK filter to remove downgoing energy. Event (a) is the p-p reflection from n1. Event (b) originates at trace 35 and appears to be a reflection from n2. Event (c) is interpreted to be a reflection from n3. Event (d) is a reflection from the bottom of the model. No fault plane reflections can be identified.

4.13 Conclusions

The variable velocity model represented the highest degree of realism of the physical modeling experiments in this investigation. The effects of the velocity contrasts were apparent. The slopes of the major downgoing events clearly changed at trace 36 on most of the recorded data sets. The change in slope was due to the events exiting the higher-velocity PLEXIGLAS and entering the lower-velocity LEXAN.

On the data sets using the large (V101) transducers, the key subsurface horizons were delineated using several source offsets. The Tptw horizon could be identified on data sets with source offsets as great as 4000 feet. On the 3000-foot source offset data set (Figure 4.18), an s-wave reflection from this horizon was also observed.

The reflection from the n2 horizon was the most consistently appearing event on the data sets. It was identified on each data set, with the exception of the 7000-foot offset data set. It is encouraging that the reflections from the top and bottom of the potential repository unit (Tptw and n2) are identifiable on so many of the data sets. Delineating the repository unit remains a major goal of the VSP experiments at Yucca Mountain.

Reflections from n3 were visible on data sets with source offsets out to 5000 feet (the reflection was not identifiable on the 3000-foot source offset data set).

Since the reflection from the bottom of the model was so strong, it could be seen on all data sets with source offsets out to 6000 feet. On this physical model, the bottom of the model corresponded to the n4 horizon.

A fault plane reflection from fault plane 3 was identified on the 4000-foot source offset data set (Figure 4.22). The identification of fault planes is a major goal of the investigations, and Figure 4.22 shows the only indication of fault plane reflections on any of the physical model data sets. Not seeing fault plane reflections on more of the data sets was a disappointing aspect of the physical modeling.

Another disappointment was the quality of the data recorded with the small (V133) transducers. The 1000-foot offset data set recorded with the V133 transducers (Figure 4.42) was of lower quality than the 1000-foot source offset data set recorded with the V101 transducers. The quality of the 2000-foot source offset data sets using both sets of transducers was virtually identical, although the data set recorded using the V133 transducers required more processing. It had been hoped that the higher frequency transducers would improve the resolution of the reflections, but the noise problems associated with the PANAMETRICS pulser/receiver were very harmful to the data sets. The acquisition of another pulser/receiver unit that does not introduce

noise into the output channel would increase the usefulness of the high frequency transducers.

The data sets in Chapter 4 show once again that the quality of VSP data at Yucca Mountain will be much higher on data sets with source offsets within 4000 feet of borehole UZ-6. The key reflections can be identified, and the chance of identifying a fault plane reflection is much greater on data sets with these source offsets.

Chapter 5
CONCLUSIONS

5.1 Introduction

In order to maximize the success of the VSP surveys at Yucca Mountain, modeling experiments were conducted to provide insight into how key subsurface horizons can best be delineated. Computer and physical modeling experiments were conducted along a cross section of Yucca Mountain between boreholes at the USW UZ-6 and UE25 UZ-9 sites. This cross section corresponds to the proposed initial line of VSP activity at Yucca Mountain.

The computer modeling experiments were conducted using the AIMS modeling package, developed by GEOQUEST. The modeling involved the use of a 269 horizon model of the subsurface and multiple-offset surveys at both the USW UZ-6 and UE25 UZ-9 borehole sites. These experiments incorporated realistic seismic velocities and unit densities into the modeling study.

The physical modeling experiments were conducted using two models of Yucca Mountain created from plastics. The first model was made solely from PLEXIGLAS G acrylic sheet. The model was designed such that the thickness of the model changed to represent the various welded and non-welded units in the cross section. This model had a uniform velocity

throughout, and reflections were generated from the boundaries where model thickness changed.

The second physical model was created from PLEXIGLAS G sheet and LEXAN polycarbonate sheet. This model was of uniform thickness, but the two materials possessed different acoustic velocities. Reflections were generated from the velocity and density contrasts between the two materials.

Analysis of the data sets generated by the computer and physical modeling experiments showed that several recommendations can be made regarding the placement of the seismic sources for the delineation of certain subsurface horizons. The modeling study also provided data that can be used to test processing software that is being developed for the field VSP data from Yucca Mountain.

5.2 Yucca Mountain Recommendations

The majority of the modeling in this thesis was performed using USW UZ-6 as the receiver borehole. The results of the computer and physical modeling experiments allow several recommendations to be made concerning how field VSP data can be acquired along the line between UZ-6 and UZ-9 to maximize the chances of successfully delineating the key subsurface horizons.

The modeling showed that the quality of the VSP records will be highest when the seismic source is within 4000 feet

of borehole USW UZ-6. Quality is defined here by how well the key horizons in the subsurface can be identified on the VSP record. The key horizons are the unit boundaries in the unsaturated zone, namely the Shardy Base (n1), the Topopah Spring Member (Tptw), and the Calico Hills Tuff (n2). The modeling experiments showed that identification of n1 and Tptw becomes difficult when the source offset exceeds 2000 feet from UZ-6. A reflection from n1 or Tptw was seen out to a source offset of 4000 feet on physical model data sets, but the events were very weak.

The effect of Yucca Mountain's topography is very damaging to the imaging of n1 and Tptw. The elevation of the source decreases significantly as source offset increases to the east of UZ-6. As a result, a raypath reflecting from these horizons reflects at a very shallow angle. If the ray even makes it to the borehole, the travel path of the ray would be virtually identical to the travel path of the direct arrival. Separating the direct arrival from the reflection would be extremely difficult, if not impossible. The topography at Yucca Mountain does not significantly damage the imaging of the horizons below Tptw, however.

The third key horizon is n2, which represents the base of the potential repository unit. The reflection from this horizon was readily identifiable on records with source offsets as great as 4000 feet. In fact, the modeling studies

suggested that this horizon can be identified on records with source offsets as great as 7000 or 8000 feet, although interpretation of the event becomes more difficult beyond a source offset of 4000 feet.

Reflections from horizons below the static water table (roughly 2200 feet below the crest of Yucca Mountain) can be identified on records with large source offsets. The reflection from n3, the non-welded unit between the Bullfrog Member and the Tram Member of the Crater Flat Tuff, is identifiable on records with source offsets as great as 7000 feet, although interpretation of the event generally becomes more difficult when the source offset reaches 5000 feet. An interesting feature of the events from the deeper horizons was seen in Figure 2.59 (page 116). For an offset of 7000 feet, the reflection from Tcbw (the Bullfrog Member of the Crater Flat Tuff) arrived later than the reflection from the underlying n3 horizon. Due to the large source offset and the high velocity of Tcbw, a reflection from the bottom of Tcbw reached the receiver borehole sooner than a reflection from the top of Tcbw. If the velocity structure at Yucca Mountain has been accurately represented by the computer model, this phenomenon could be seen on the field records.

Although the imaging of the horizons in the saturated zone is not as critical to the project as the imaging of the horizons in the unsaturated zone, the modeling experiments

suggest that it will be possible to interpret the deeper reflections. Reflections from the deeper horizons could be identified in many of the data sets in this thesis.

The second major goal of the field VSP surveys will be to delineate the high-angle faults, such as the Ghost Dance Fault. If the fault planes at Yucca Mountain do generate reflected raypaths, the computer modeling experiments have provided valuable insight into how the fault planes can best be delineated.

From the computer generated data sets, it is seen that reflections from fault planes can best be identified on data sets with source offsets no greater than 4000 feet to the east of UZ-6. On data sets with offsets greater than 4000 feet, the reflections from the fault planes become very difficult to interpret. The fault plane reflections interfere with reflections from the unit boundaries on the data sets with large offsets. The data set with a source offset of 4000 feet (Figure 2.38 on page 84) shows how much interference can take place between the fault plane reflections and the unit boundary reflections.

The computer modeling experiments showed that it should be possible to delineate the Ghost Dance Fault (fault planes 2 and 3) out to a source offset of 3000 feet. The physical model data set in Figure 4.22 on page 252 indicated that a reflection from fault plane 3 could be recorded and

identified at a source offset of 4000 feet. The reflections are somewhat difficult to identify due to interference with reflections from the unit boundaries.

If the fault planes at Yucca Mountain do provide seismic reflections, the modeling experiments showed that it will be the segments of the fault planes within Tptw that will provide the most interpretable events on the records. The events will be characterized by their near-vertical slopes on the VSP records.

An interesting feature of the computer modeling experiments was the observation that although the slope of a fault plane reflection was usually near-vertical, several fault plane reflections had slopes that were not near-vertical. On Figure 2.32 (page 74), reflections from fault planes 8 and 9 have slopes similar to the upgoing slopes of the unit boundary reflections. On Figure 2.37 (page 82), reflections from fault planes 3 and 4 have slopes similar to the downgoing slopes of the direct arrivals.

Since delineating the high-angle fault planes is a major goal of the experiments, special care must be taken to preserve these events while processing the VSP record. The modeling experiments showed that the following processing recommendations can be made:

First, since the slopes of the fault plane reflections are usually near-vertical, a higher fold median filter is

needed to remove the direct arrivals from a data set. Figures 2.9 through 2.12 on pages 37 through 42 show that if the fold of the median filter is not sufficiently large, fault plane energy will be lost during the filtering. The modeling experiments suggest a median filter fold of at least 11 for the small offset records. A median filter fold of 15 or more may be necessary to separate the upgoing and downgoing wavefields on data sets with very large source offsets (7000+ feet).

Second, since the slope of a fault plane reflection may be similar to that of a downgoing direct arrival, a muting step should be added to the median filtering process. After applying a median filter to a data set with aligned direct arrivals, the processor will have a data set containing only direct arrivals and the fault plane reflections which have similar slopes. This data set should be muted after the direct arrivals to remove the fault plane energy. Subtracting the muted data set from the original data set will remove the direct arrivals without damaging the fault plane reflections with downgoing slopes. This muting process, used in conjunction with the high fold median filter, should be sufficient to efficiently remove the direct arrivals from the field records.

Third, when an FK filter is applied to the data to enhance the upgoing reflections, it is necessary to remember

the slope of the fault plane reflections. Figure 4.6 on page 227 shows a typical FK filter which will help preserve fault plane reflections. The filter passes all energy to the right of the sloping line. This preserves all upgoing energy in the right-hand plane, as well as all downgoing energy with a slope no greater than 2 milliseconds/trace. The existence of a fault plane reflection on the data set from the variable velocity physical model with a source offset of 4000 feet (Figure 4.22 on page 252) shows that this filter was effective in enhancing the event.

The computer modeling experiments also showed that very interpretable VSP records can be obtained using UE25 UZ-9 as a receiver borehole. The key subsurface horizons could all be imaged with a source offset as great as 2000 feet to the west of the borehole. Horizons deeper than Tptw were all clearly identifiable out to a source offset of 3000 feet, and the experiments suggested that high quality records could be recorded at even larger offsets.

Evidence of reflections from different fault blocks was very apparent on these data sets. Quite often, an event on the record would appear as a double peak or a double trough. This indicated that reflections from identical horizons on different fault blocks were reaching the receiver almost simultaneously. Several events were repeated on the records for this reason, and had the appearance of "ghosts."

AIMS was not capable of generating fault plane reflections at this borehole due to limitations on how subsurface horizons must be defined. However, recording fault plane reflections at UE25 UZ-9 must be considered a possibility at Yucca Mountain.

5.3 Future Modeling Work

The AIMS batch file used to create the complex computer model of Yucca Mountain is included in the Appendix. When submitted to AIMS, this file produces a file named "projectname.SUB" which can be used for modeling experiments. This batch file and a model file named "YUCCA.SUB" have been stored on magnetic tape, as were all synthetic data sets shown in this thesis. The magnetic tapes are stored in the acoustics lab at the Colorado School of Mines, under the supervision of Dr. A. H. Balch.

The AIMS model can be easily modified to conduct additional modeling experiments. If additional data from Yucca Mountain suggest that the velocity or density structure of the model needs updating, only a few lines of the file need to be altered. As shown in Chapter 4, the model can be modified to simulate the physical models simply by supplying the proper velocities. This can be a useful tool for confirming interpretations of physical model data sets.

Another important function of the computer model data

sets (as well as the physical model data sets) will be the testing of a reverse-time migration program being developed for this project. The program will migrate the reflections from the VSP data sets acquired at Yucca Mountain into their proper spatial positions to provide data sets that can be interpreted in the same manner as data from a reflection seismic survey. The complex data sets generated by the computer modeling will provide a very good test for the final version of the program.

In the more distant future, the model can be used to study converted waves in the subsurface at Yucca Mountain. The most current version of the AIMS package allows the modeler to trace p-wave to s-wave conversions on synthetic VSP data sets. This version of AIMS did not exist at CSM at the time this thesis was written.

Future work in the physical model laboratory is almost unlimited. As better methods of pulsing the source transducer become available, the quality of the VSP data sets will improve dramatically. The same is true once a better gain amplifier is found for the receiver transducer. The acquisition system is fundamentally sound, however, as was shown by the quality of the physical model data sets presented in this thesis.

Additional modeling experiments can be performed on both of the existing physical models. First, data sets can be

recorded using the opposite (right) edge of the models, which represents borehole UE25 UZ-9. This would enhance the knowledge gained from the computer modeling done using this borehole. Second, VSP records could be recorded using deeper receiver boreholes. The boreholes used in this thesis were 2000 feet deep, but perhaps data quality would increase significantly if the borehole were 3000 or 4000 feet deep. However, drilling a borehole which penetrated the saturated zone at Yucca Mountain could result in the contamination of the unsaturated zone. The modeling experiments could show whether or not deeper receiver boreholes would increase the data quality substantially. If a significant increase in data quality were obtained from deeper receiver boreholes on the model data, any decision to actually drill deeper holes would have to weigh the benefits of better VSP data versus the problems caused by the contamination of the unsaturated zone.

The work at Yucca Mountain will rely heavily on recorded s-wave data. The surveys will be conducted with three-component sources and receivers. Additional modeling can be done on the physical models using PANAMETRICS V156 shear wave transducers as sources and receivers. Since the models are only two-dimensional, a two-component data set could be simulated by recording both a p-wave trace and an s-wave trace at each borehole geophone location. Studying data

sets with different sources and receivers is the next logical step in the physical modeling experiments.

5.4 Closing Remarks

The data presented in this thesis will help improve the quality of the VSP experiments at Yucca Mountain and in the long run contribute significantly to the decision concerning the permanent emplacement of nuclear waste at Yucca Mountain. The work was performed in order to provide insight into how key subsurface horizons, such as the Shardy Base, the Topopah Spring Member of the Paintbrush Tuff, and the Calico Hills Tuff can best be imaged using vertical seismic profiles at Yucca Mountain. The effects of topography and source offset on the delineation of the various subsurface horizons have been presented in this thesis.

The thesis is designed to be a guidebook for the initial interpretation of the hundreds of field VSP records that will be recorded at Yucca Mountain. Before the interpretation of fractures and permeability zones on the field records can begin, it is crucial to first positively identify the horizons that are being studied. This thesis will be useful for that purpose.

REFERENCES CITED

Anderson, Lennart A. 1984. Rock property measurements on large-volume core samples from Yucca Mountain USW GU-3/G-3 and USW G-4 boreholes, Nevada Test Site, Nevada: U. S. Geological Survey Open-File Report 84-552.

Carr, W. J., F. M. Byers, Jr., and P. P. Orkild. 1984. Stratigraphic and volcano-tectonic relations of Crater Flat Tuff and some older volcanic units, Nye County, Nevada: U. S. Geological Survey Open-File Report 84-114.

Monastersky, Richard. 1988. The 10,000 year test. Science News. 27 Feb., 139-141.

Muller, D. C. and J. E. Kibler. 1985. Preliminary analysis of geophysical logs from the WT series of drill holes, Yucca Mountain, Nye County, Nevada: U. S. Geological Survey Open-File Report 86-46.

Scott, Robert B. and Jerry Bonk. 1984. Preliminary geologic map of Yucca Mountain, Nye County, Nevada with geologic sections: U. S. Geological Survey Open-File Report 84-494.

Spengler, R. W. and M. P. Chornack. 1984. Stratigraphic and structural characteristics of volcanic rocks in core hole USW G-4, Yucca Mountain, Nye County, Nevada: U. S. Geological Survey Open-File Report 84-789.

SELECTED READINGS

Barry, Charles T. 1980. A study of the vertical vibrator source for seismic profiling in the Yucca Mountain area of the Nevada Test Site. Master's thesis, Colorado School of Mines, Golden, Colo.

Rousseau, J. P., et al. 1986. Characterization of percolation in the unsaturated zone: Surface-based borehole investigations. NNWSI Project USGS Scientific Investigation Plan. USGS-SIP-3343G-01, RO.

APPENDIX

BATCH FILE USED TO GENERATE THE YUCCA MOUNTAIN COMPUTER MODEL IN AIMS

```
!!!!!!!!!!!!!!!!!!!!!!!!!!!!!!!!!!!!!!!!!!!!!!!!!!!!
! CUNNINGHAM AIMS MODEL OF YUCCA MOUNTAIN NEVADA   !
! THIS CROSS SECTION RUNS BETWEEN BOREHOLES         !
! UZ-6 AND UZ-9 IN AN EAST-WEST DIRECTION          !
!!!!!!!!!!!!!!!!!!!!!!!!!!!!!!!!!!!!!!!!!!!!!!!!!!!!

XAXIS/FEET 1200,1000,1000
ZAXIS/FEET 1200,1000,1000

!DEFINE THE SUBSURFACE MODEL

SUBSRF
INPUT/BRIEF
TITLE 'YUCCA MOUNTAIN MODEL'
MODEL 600,0,9125,0,6500

! DEFINE SURFACE TOPOGRAPHY

H1 V8700 D2.37
X0 Z316 X90 Z229 X222 Z137 X384 Z54
X535 Z63 X626 Z75 X1028 Z173 X1545 Z264
X2460 Z441 X2809 Z442 X3413 Z515 X3747 Z465
X4262 Z542 X4652 Z631 X4970 Z691 X5269 Z659
X5462 Z651 X5567 Z655 X5873 Z693 X6010 Z741
X6480 Z919 X6711 Z865 X6951 Z781 X7125 Z804
X7624 Z988 X7982 Z879 X8172 Z904 X8529 Z1043
X9125 Z1123

! FIRST SET OF FAULTS

H10 V8700 D2.37 X4202 Z780 X4262 Z542
H11 V8700 D2.37 X4618 Z769 X4652 Z631
H12 V8700 D2.37 X4954 Z765 X4970 Z691
H13 V8700 D2.37 X5427 Z807 X5462 Z651
H14 V8700 D2.37 X5538 Z791 X5567 Z655
H15 V8700 D2.37 X5980 Z864 X6010 Z741
H16 V8700 D2.37 X6711 Z865 X6790 Z1091
H17 V8700 D2.37 X7041 Z1148 X7125 Z804
H18 V8700 D2.37 X8045 Z1434 X8172 Z904
H19 V8700 D2.37 X8411 Z1508 X8529 Z1043

! TOP OF SHARDY BASE (n1)
```

```
H30 V6400 D1.66 X0 Z396 X4186 Z832
H31 V6400 D1.66 X4186 Z832 * X4202 Z780 *
H32 V6400 D1.66 X4202 Z780 X4604 Z821
H33 V6400 D1.66 X4604 Z821 * X4618 Z769 *
H34 V6400 D1.66 X4618 Z769 X4940 Z815
H35 V6400 D1.66 X4940 Z815 * X4954 Z765 *
H36 V6400 D1.66 X4954 Z765 X5420 Z839
H37 V6400 D1.66 X5420 Z839 * X5427 Z807 *
H38 V6400 D1.66 X5427 Z807 X5529 Z820
H39 V6400 D1.66 X5529 Z820 * X5538 Z791 *
H40 V6400 D1.66 X5538 Z791 X5965 Z918
H41 V6400 D1.66 X5965 Z918 * X5980 Z864 *
H42 V6400 D1.66 X5980 Z864 X6790 Z1091
H43 V6400 D1.66 X6790 Z1091 * X6804 Z1126 *
H44 V6400 D1.66 X6804 Z1126 X7032 Z1174
H45 V6400 D1.66 X7032 Z1174 * X7042 Z1148 *
H46 V6400 D1.66 X7042 Z1148 X8018 Z1541
H47 V6400 D1.66 X8018 Z1541 * X8045 Z1434 *
H48 V6400 D1.66 X8045 Z1434 X8396 Z1563
H49 V6400 D1.66 X8396 Z1563 * X8411 Z1508 *
H50 V6400 D1.66 X8411 Z1508 X9125 Z1701

! SECOND SET OF FAULTS

H60 V6400 D1.66 X4174 Z899 X4186 Z832
H61 V6400 D1.66 X4586 Z894 X4604 Z821
H62 V6400 D1.66 X4921 Z902 X4940 Z815
H63 V6400 D1.66 X5395 Z931 X5420 Z839
H64 V6400 D1.66 X5508 Z910 X5529 Z820
H65 V6400 D1.66 X5947 Z993 X5965 Z918
H66 V6400 D1.66 X6804 Z1126 X6849 Z1243
H67 V6400 D1.66 X7010 Z1275 X7032 Z1174
H68 V6400 D1.66 X8011 Z1570 X8018 Z1541
H69 V6400 D1.66 X8379 Z1640 X8396 Z1563

! TOP OF TOPOPAH SPRING MEMBER (Tptw)

H80 V10800 D2.30 X0 Z490 X4157 Z953
H81 V10800 D2.30 X4157 Z953 * X4174 Z899 *
H82 V10800 D2.30 X4174 Z899 X4573 Z943
H83 V10800 D2.30 X4573 Z943 * X4586 Z894 *
H84 V10800 D2.30 X4586 Z894 X4908 Z940
H85 V10800 D2.30 X4908 Z940 * X4921 Z902 *
H86 V10800 D2.30 X4921 Z902 X5383 Z976
H87 V10800 D2.30 X5383 Z976 * X5395 Z931 *
H88 V10800 D2.30 X5395 Z931 X5500 Z946
H89 V10800 D2.30 X5500 Z946 * X5508 Z910 *
H90 V10800 D2.30 X5508 Z910 X5933 Z1039
```

```
H91 V10800 D2.30 X5933 Z1039 * X5947 Z993 *
H92 V10800 D2.30 X5947 Z993 X6849 Z1243
H93 V10800 D2.30 X6849 Z1243 * X6868 Z1296 *
H94 V10800 D2.30 X6868 Z1296 X6997 Z1325
H95 V10800 D2.30 X6997 Z1325 * X7010 Z1275 *
H96 V10800 D2.30 X7010 Z1275 X7986 Z1669
H97 V10800 D2.30 X7986 Z1669 * X8011 Z1570 *
H98 V10800 D2.30 X8011 Z1570 X8365 Z1698
H99 V10800 D2.30 X8365 Z1698 * X8379 Z1640 *
H100 V10800 D2.30 X8379 Z1640 X9125 Z1844

! THIRD SET OF FAULTS

H110 V10800 D2.30 X3935 Z1829 X4157 Z953
H111 V10800 D2.30 X4357 Z1822 X4573 Z943
H112 V10800 D2.30 X4700 Z1828 X4908 Z940
H113 V10800 D2.30 X5168 Z1850 X5383 Z976
H114 V10800 D2.30 X5284 Z1838 X5500 Z946
H115 V10800 D2.30 X5710 Z1940 X5933 Z1039
H116 V10800 D2.30 X6779 Z2179 X6946 Z1516 X6997 Z1325
H117 V10800 D2.30 X7782 Z2489 X7986 Z1669
H118 V10800 D2.30 X8151 Z2544 X8365 Z1698
H119 V10800 D2.30 X6868 Z1296 X6946 Z1516

! TOP OF CALICO HILLS (n2)

H130 V9300 D1.88 X0 Z1440 X3917 Z1894
H131 V9300 D1.88 X3917 Z1894 * X3935 Z1829 *
H132 V9300 D1.88 X3935 Z1829 X4345 Z1869
H133 V9300 D1.88 X4345 Z1869 * X4357 Z1822 *
H134 V9300 D1.88 X4357 Z1822 X4690 Z1867
H135 V9300 D1.88 X4690 Z1867 * X4700 Z1828 *
H136 V9300 D1.88 X4700 Z1828 X5152 Z1898
H137 V9300 D1.88 X5152 Z1898 * X5168 Z1850 *
H138 V9300 D1.88 X5168 Z1850 X5273 Z1870
H139 V9300 D1.88 X5273 Z1870 * X5284 Z1838 *
H140 V9300 D1.88 X5284 Z1838 X5700 Z1967
H141 V9300 D1.88 X5700 Z1967 * X5710 Z1940 *
H142 V9300 D1.88 X5710 Z1940 X6769 Z2212
H143 V9300 D1.88 X6769 Z2212 * X6779 Z2179 *
H144 V9300 D1.88 X6779 Z2179 X7761 Z2574
H145 V9300 D1.88 X7761 Z2574 * X7782 Z2489 *
H146 V9300 D1.88 X7782 Z2489 X8128 Z2618
H147 V9300 D1.88 X8128 Z2618 * X8151 Z2544 *
H148 V9300 D1.88 X8151 Z2544 X9125 Z2806

! FOURTH SET OF FAULTS
```

```
H160 V9300 D1.88 X3729 Z2629 X3917 Z1894
H161 V9300 D1.88 X4162 Z2628 X4345 Z1869
H162 V9300 D1.88 X4505 Z2642 X4690 Z1867
H163 V9300 D1.88 X4962 Z2672 X5152 Z1898
H164 V9300 D1.88 X5089 Z2653 X5273 Z1870
H165 V9300 D1.88 X5510 Z2743 X5700 Z1967
H166 V9300 D1.88 X6570 Z2993 X6769 Z2212
H167 V9300 D1.88 X7582 Z3298 X7761 Z2574
H168 V9300 D1.88 X7943 Z3360 X8151 Z2544

! TOP OF BULLFROG MEMBER, CRATER FLAT TUFF (Tcbw)

H180 V12900 D2.32 X0 Z2293 X3712 Z2692
H181 V12900 D2.32 X3712 Z2692 * X3729 Z2629 *
H182 V12900 D2.32 X3729 Z2629 X4147 Z2677
H183 V12900 D2.32 X4147 Z2677 * X4162 Z2628 *
H184 V12900 D2.32 X4162 Z2628 X4492 Z2682
H185 V12900 D2.32 X4492 Z2682 * X4505 Z2642 *
H186 V12900 D2.32 X4505 Z2642 X4945 Z2711
H187 V12900 D2.32 X4945 Z2711 * X4962 Z2672 *
H188 V12900 D2.32 X4962 Z2672 X5075 Z2690
H189 V12900 D2.32 X5075 Z2690 * X5089 Z2653 *
H190 V12900 D2.32 X5089 Z2653 X5498 Z2782
H191 V12900 D2.32 X5498 Z2782 * X5510 Z2743 *
H192 V12900 D2.32 X5510 Z2743 X6556 Z3026
H193 V12900 D2.32 X6556 Z3026 * X6570 Z2993 *
H194 V12900 D2.32 X6570 Z2993 X7555 Z3392
H195 V12900 D2.32 X7555 Z3392 * X7582 Z3298 *
H196 V12900 D2.32 X7582 Z3289 X7924 Z3418
H197 V12900 D2.32 X7924 Z3418 * X7943 Z3360 *
H198 V12900 D2.32 X7943 Z3360 X9125 Z3674

! FIFTH SET OF FAULTS

H210 V12900 D2.32 X3668 Z2967 X3712 Z2692
H211 V12900 D2.32 X4103 Z2864 X4147 Z2677
H212 V12900 D2.32 X4449 Z2875 X4492 Z2682
H213 V12900 D2.32 X4904 Z2913 X4945 Z2711
H214 V12900 D2.32 X5033 Z2888 X5075 Z2690
H215 V12900 D2.32 X5449 Z2975 X5498 Z2782
H216 V12900 D2.32 X6512 Z3226 X6556 Z3026
H217 V12900 D2.32 X7521 Z3535 X7555 Z3392
H218 V12900 D2.32 X7879 Z3598 X7924 Z3418

! TOP OF INTRA BULLFROG/TRAM NONWELDED UNIT (n3)

H230 V11100 D2.07 X0 Z2510 X3649 Z2928
H231 V11100 D2.07 X3649 Z2928 * X3668 Z2867 *
```

```
H232 V11100 D2.07 X3668 Z2867 X4087 Z2914
H233 V11100 D2.07 X4087 Z2914 * X4103 Z2864 *
H234 V11100 D2.07 X4103 Z2864 X4437 Z2918
H235 V11100 D2.07 X4467 Z2918 * X4449 Z2875 *
H236 V11100 D2.07 X4449 Z2875 X4892 Z2942
H237 V11100 D2.07 X4892 Z2942 * X4904 Z2913 *
H238 V11100 D2.07 X4904 Z2913 X5019 Z2932
H239 V11100 D2.07 X5019 Z2932 * X5033 Z2888 *
H240 V11100 D2.07 X5033 Z2888 X5438 Z3015
H241 V11100 D2.07 X5438 Z3015 * X5449 Z2975 *
H242 V11100 D2.07 X5449 Z2975 X6501 Z3260
H243 V11100 D2.07 X6501 Z3260 * X6512 Z3226 *
H244 V11100 D2.07 X6512 Z3226 X7498 Z3625
H245 V11100 D2.07 X7498 Z3625 * X7521 Z3535 *
H246 V11100 D2.07 X7521 Z3535 X7866 Z3651
H247 V11100 D2.07 X7866 Z3651 * X7879 Z3598 *
H248 V11100 D2.07 X7879 Z3598 X9125 Z3933

! SIXTH SET OF FAULTS

H260 V11100 D2.07 X3529 Z3417 X3649 Z2928
H261 V11100 D2.07 X3965 Z3420 X4087 Z2914
H262 V11100 D2.07 X4315 Z3428 X4437 Z2918
H263 V11100 D2.07 X4767 Z3467 X4892 Z2942
H264 V11100 D2.07 X4895 Z3442 X5019 Z2932
H265 V11100 D2.07 X5312 Z3535 X5438 Z3015
H266 V11100 D2.07 X6375 Z3773 X6501 Z3260
H267 V11100 D2.07 X7384 Z4093 X7498 Z3625
H268 V11100 D2.07 X7741 Z4145 X7866 Z3651

! TOP OF TRAM MEMBER, CRATER FLAT TUFF (Tctw)

H280 V12700 D2.27 X0 Z3104 X3509 Z3479
H281 V12700 D2.27 X3509 Z3479 * X3529 Z3417 *
H282 V12700 D2.27 X3529 Z3417 X3948 Z3464
H283 V12700 D2.27 X3948 Z3646 * X3965 Z3420 *
H284 V12700 D2.27 X3965 Z3420 X4299 Z3472
H285 V12700 D2.27 X4299 Z3472 * X4315 Z3428 *
H286 V12700 D2.27 X4315 Z3428 X4753 Z3499
H287 V12700 D2.27 X4753 Z3499 * X4767 Z3467 *
H288 V12700 D2.27 X4767 Z3467 X4886 Z3484
H289 V12700 D2.27 X4886 Z3484 * X4895 Z3442 *
H290 V12700 D2.27 X4895 Z3442 X5300 Z3568
H291 V12700 D2.27 X5300 Z3568 * X5312 Z3535 *
H292 V12700 D2.27 X5312 Z3535 X6362 Z3811
H293 V12700 D2.27 X6362 Z3811 * X6375 Z3773 *
H294 V12700 D2.27 X6375 Z3773 X7364 Z4172
H295 V12700 D2.27 X7364 Z4172 * X7384 Z4093 *
```

```
H296 V12700 D2.27 X7384 Z4093 X7725 Z4209
H297 V12700 D2.27 X7725 Z4209 * X7741 Z4145 *
H298 V12700 D2.27 X7741 Z4145 X9125 Z4515

! SEVENTH SET OF FAULTS

H310 V12700 D2.27 X3508 Z3502 X3509 Z3479
H311 V12700 D2.27 X3943 Z3498 X3948 Z3464
H312 V12700 D2.27 X4297 Z3509 X4299 Z3472
H313 V12700 D2.27 X4748 Z3541 X4753 Z3499
H314 V12700 D2.27 X4877 Z3528 X4886 Z3484
H315 V12700 D2.27 X5252 Z3614 X5300 Z3568
H316 V12700 D2.27 X6351 Z3867 X6362 Z3811
H317 V12700 D2.27 X7363 Z4182 X7364 Z4172
H318 V12700 D2.27 X7723 Z4231 X7725 Z4209

! TOP OF INTRA TRAM/LITHIC RIDGE NONWELDED UNIT (n4)

H330 V11700 D2.21 X0 Z3181 X3493 Z3552
H331 V11700 D2.21 X3493 Z3552 * X3508 Z3502 *
H332 V11700 D2.21 X3508 Z3502 X3929 Z3547
H333 V11700 D2.21 X3929 Z3547 * X3943 Z3498 *
H334 V11700 D2.21 X3943 Z3498 X4283 Z3548
H335 V11700 D2.21 X4283 Z3548 * X4297 Z3509 *
H336 V11700 D2.21 X4297 Z3509 X4736 Z3575
H337 V11700 D2.21 X4736 Z3575 * X4748 Z3541 *
H338 V11700 D2.21 X4748 Z3541 X4865 Z3562
H339 V11700 D2.21 X4865 Z3562 * X4877 Z3528 *
H340 V11700 D2.21 X4877 Z3528 X5279 Z3655
H341 V11700 D2.21 X5279 Z3655 * X5292 Z3614 *
H342 V11700 D2.21 X5292 Z3614 X6340 Z3899
H343 V11700 D2.21 X6340 Z3899 * X6351 Z3867 *
H344 V11700 D2.21 X6351 Z3867 X7340 Z4269
H345 V11700 D2.21 X7340 Z4269 * X7363 Z4182 *
H346 V11700 D2.21 X7363 Z4182 X7707 Z4294
H347 V11700 D2.21 X7707 Z4294 * X7723 Z4231 *
H348 V11700 D2.21 X7723 Z4231 X9125 Z4608

! EIGHTH SET OF FAULTS

H360 V11700 D2.21 X3158 Z4876 X3493 Z3552
H361 V11700 D2.21 X3603 Z4879 X3929 Z3547
H362 V11700 D2.21 X3964 Z4896 X4283 Z3548
H363 V11700 D2.21 X4405 Z4920 X4736 Z3575
H364 V11700 D2.21 X4548 Z4896 X4865 Z3562
H365 V11700 D2.21 X4952 Z4980 X5279 Z3655
H366 V11700 D2.21 X6012 Z5217 X6340 Z3899
H367 V11700 D2.21 X7010 Z5580 X7340 Z4269
```

```
H368 V11700 D2.21 X7373 Z5628 X7707 Z4294

! TOP OF LITHIC RIDGE UNIT, CRATER FLAT TUFF (Tlrw)

H380 V13100 D2.23 X0 Z4574 X3139 Z4933
H381 V13100 D2.23 X3139 Z4933 * X3158 Z4876 *
H382 V13100 D2.23 X3158 Z4876 X3589 Z4926
H383 V13100 D2.23 X3589 Z4926 * X3603 Z4879 *
H384 V13100 D2.23 X3603 Z4879 X3954 Z4926
H385 V13100 D2.23 X3954 Z4926 * X3964 Z4896 *
H386 V13100 D2.23 X3964 Z4896 X4394 Z4955
H387 V13100 D2.23 X4394 Z4955 * X4405 Z4920 *
H388 V13100 D2.23 X4405 Z4920 X4537 Z4941
H389 V13100 D2.23 X4537 Z4941 * X4548 Z4896 *
H390 V13100 D2.23 X4548 Z4896 X4938 Z5024
H391 V13100 D2.23 X4938 Z5024 * X4952 Z4980 *
H392 V13100 D2.23 X4952 Z4980 X5998 Z5257
H393 V13100 D2.23 X5998 Z5257 * X6012 Z5217 *
H394 V13100 D2.23 X6012 Z5217 X7002 Z5653
H395 V13100 D2.23 X7002 Z5653 * X7010 Z5580 *
H396 V13100 D2.23 X7010 Z5580 X7358 Z5705
H397 V13100 D2.23 X7358 Z5705 * X7373 Z5628 *
H398 V13100 D2.23 X7373 Z5628 X9125 Z6053

! NINTH SET OF FAULTS

H410 V13100 D2.23 X3120 Z5014 X3139 Z4933
H411 V13100 D2.23 X3569 Z5019 X3589 Z4926
H412 V13100 D2.23 X3932 Z5031 X3954 Z4926
H413 V13100 D2.23 X4371 Z5062 X4394 Z4955
H414 V13100 D2.23 X4514 Z5039 X4537 Z4941
H415 V13100 D2.23 X4913 Z5128 X4938 Z5024
H416 V13100 D2.23 X5972 Z5381 X5998 Z5257
H417 V13100 D2.23 X6988 Z5716 X7002 Z5653
H418 V13100 D2.23 X7336 Z5745 X7358 Z5705

! BASE OF LITHIC RIDGE MEMBER, CRATER FLAT TUFF (n5)

H430 V12500 D2.26 X0 Z4734 X3107 Z5068
H431 V12500 D2.26 X3107 Z5068 * X3120 Z5014 *
H432 V12500 D2.26 X3120 Z5014 X3554 Z5064
H433 V12500 D2.26 X3554 Z5064 * X3569 Z5019 *
H434 V12500 D2.26 X3569 Z5019 X3921 Z5064
H435 V12500 D2.26 X3921 Z5064 * X3932 Z5031 *
H436 V12500 D2.26 X3932 Z5031 X4361 Z5096
H437 V12500 D2.26 X4361 Z5094 * X4371 Z5062 *
H438 V12500 D2.26 X4371 Z5062 X4502 Z5083
H439 V12500 D2.26 X4502 Z5083 * X4514 Z5039 *
```

```
H440 V12500 D2.26 X4514 Z5039 X4900 Z5166
H441 V12500 D2.26 X4900 Z5166 * X4913 Z5128 *
H442 V12500 D2.26 X4913 Z5128 X5960 Z5411
H443 V12500 D2.26 X5960 Z5411 * X5972 Z5381 *
H444 V12500 D2.26 X5972 Z5381 X6965 Z5755
H445 V12500 D2.26 X6965 Z5755 * X6988 Z5716 *
H446 V12500 D2.26 X6988 Z5716 X7313 Z5804
H447 V12500 D2.26 X7313 Z5804 * X7336 Z5745 *
H448 V12500 D2.26 X7336 Z5745 X9125 Z6250

! TENTH SET OF FAULTS

H460 V12500 D2.26 X2884 Z6000 X3107 Z5068
H461 V12500 D2.26 X3326 Z6000 X3554 Z5064
H462 V12500 D2.26 X3693 Z6000 X3921 Z5064
H463 V12500 D2.26 X4109 Z6000 X4361 Z5094
H464 V12500 D2.26 X4245 Z6000 X4502 Z5083
H465 V12500 D2.26 X4714 Z6000 X4900 Z5166
H466 V12500 D2.26 X5813 Z6000 X5960 Z5411
H467 V12500 D2.26 X6900 Z6000 X6965 Z5755
H468 V12500 D2.26 X7260 Z6000 X7313 Z5804

EOD
EOJ
```